Over the Air Testing of MIMO Capable Terminals

Fan, Wei

Publication date:
2014

Document Version
Early version, also known as pre-print

Over the Air Testing of MIMO Capable Terminals

Ph.D. Dissertation

Wei Fan

Aalborg University
Department of Electronic Systems
Fredrik Bajers Vej 7B
DK-9220 Aalborg

Abstract

This thesis focuses on multi-probe anechoic chamber testing, which is a promising over the air (OTA) testing method to evaluate multiple-input multiple-output (MIMO) capable terminals. With MIMO technology being adopted by new wireless technologies, mobile manufacturers and cellular operators need standard test methods to evaluate MIMO device performance. Due to its capability to reproduce radio multipath environments in a shielded laboratory, the multi-probe anechoic chamber method has attracted great research attention.

This thesis addresses various aspects related to OTA testing of MIMO capable devices, where the focus is on techniques to emulate radio channels in multi-probe setups with a limited number of probes. Several channel emulation techniques are proposed to create realistic 2D and 3D spatial channel models in the thesis. A novel method to calculate probe weights for the prefaded signal synthesis (PFS) technique is proposed to reproduce geometry-based stochastic channel models (GBSMs) in the multi-probe anechoic chamber setup. Plane wave synthesis technique for channel emulation purpose is investigated theoretically and experimentally in the thesis as well.

The required number of probes is a key issue, as it directly determines the test system costs. In the thesis, the relationship between the test zone size in terms of figure of merits e.g. spatial correlation and capacity, and the required number of probes has been investigated in detail. Further investigation demonstrated that the DUT antenna radiation pattern is relevant to test zone size. As an extension to work in the literature limited to emulate Rayleigh fading channels, a technique to emulate Rician channel model, with a specular component of arbitrary impinging angles is proposed. To reduce the test system cost, a probe selection method and a flexible probe configuration concept are proposed. Experimental verifications of the proposed algorithms and measurement uncertainties in practical setups are investigated and results are included in the thesis.

Resumé

Denne afhandling fokuserer på brug af multiple prober i et radiodødt rum i forbindelse med en lovende metode til trådløst (*over the air (OTA)*) at evaluere *multiple-input multiple-output (MIMO)* mobile terminaler.

MIMO-teknologi indføres i nye trådløse teknologier og fabrikanter af mobile enheder og mobiloperatører har brug for standard testmetoder til at vurdere MIMO enhedernes ydeevne radiomæssigt. På grund af sin evne til at reproducere den mobile radiokanal i et afskærmet laboratorie, har metoden med brug af multiple prober tiltrukket sig stor forskningsmæssig opmærksomhed. Denne afhandling behandler forskellige aspekter i forbindelse med OTA afprøvning af MIMO kompatible enheder, hvor der er fokus på teknikker til at efterligne de ønskede radiokanaler med at begrænset antal prober.

Med henblik på at gengive radiokanaler med et vilkårligt antal klynger (*clusters*), hver beskrevet ved et vinkel-effektspektrum (*power angular spectrum (PAS)*), foreslås i afhandlingen en ny metode baseret på konveks optimering. I metoden tilnærmes den ønskede rumlige korrelation under hensyntagen til begrænsninger på den maksimale afvigelse mellem ønsket og emuleret PAS.

Udstrålingsdiagrammerne for enhedens antenner har i litteraturen generelt været betragtet som irrelevante for nøjagtigheden i kanalemuleringen. Udstrålingsdiagrammernes inflydelse undersøges i afhandlingen teoretisk og eksperimentelt, og resultaterne viser, at for at teste realistiske enheder med direktivitet er det nødvendigt med flere prober for at opretholde samme nøjagtighed i kanalemuleringen som i tilfældet med omni-direktionelle antenner.

For at reducere systemets omkostninger, foreslås i afhandlingen en metode til probevalg og et koncept for fleksible probekonfigurationer. Eksempler viser, at med et lille antal prober i disse systemer kan der opnås en nøjagtig kanalemulering i testzonen på niveau med den som kan opnås i systemer med et større antal prober fordelt jævnt vinkelmæssigt.

En 2D-kanalmodel er ikke generelt anvendelig. Målinger omtalt i litteraturen har vist, at spredning i vinkelelevation ikke kan ignoreres i mange udbredelsesmiljøer. Med henblik på disse miljøer præsenteres i afhandlingen algoritmer til emulering af kanalmodeller baseret på 3D-geometri og adskillige 3D probekonfigurationer evalueres.

Det krævede antal prober er et centralt spørgsmål i forbindelse med multi-probe løsningen, da antallet direkte bestemmer systemets pris. Sammenhængen mellem testzone størrelse og det krævede antal prober er blevet undersøgt i detaljer i afhandlingen. Rumlig korrelation, der anvendes til at bestemme, hvor godt det emulerede PAS tilnærmer det ønskede, er valgt som et godhedstal (*figure of merit (FOM)*) til bestemmelse af testzonestørrelse. Endvidere undersøges forholdet mellem kapacitetsemuleringsnøjagtighed og størrelsen af testområdet i detaljer både teoretisk og eksperimentelt i afhandlingen. Det undersøges også, både teoretisk og eksperimentelt, hvor godt plane bølger med vilkårlige retninger kan gengives med et begrænset antal prober.

Rayleigh-fading kanalmodelelen er ikke generelt gyldig. Ofte eksisterer en direkte vej imellem sender og modtager. Derfor foreslås en teknik til at skabe Rician-fading kanalmodeller i multiprobe opstillinger. De foreslåede algoritmer verificeres eksperimentielt og måleusikkerheder i praktiske opstillinger undersøges.

Contents

Preface

This thesis is submitted as partial fulfillment of the requirements for the degree of Doctor of Philosophy at Aalborg University, Denmark. The thesis addresses over the air (OTA) testing of multiple-input multiple output (MIMO) capable terminals with multi-probe anechoic chamber based methods. The main part of the thesis is a collection of papers published in or submitted to peer-reviewed conferences and journals. It is the results of three years research at the Antennas, Propagation and Radio Networking (APNet) section, Department of Electronic Systems, Aalborg University, in the period of November 2011 - Octorber 2014. The thesis was prepared under the supervision of Professor Gert F. Pedersen and Associate Professor Jesper Ø. Nielsen, and funded by the 4th Generation Mobile Communication and Test Platform (4GMCT) project.

The thesis is comprised by ten publications in total, where eight addresses radio channel emulation in the multi-probe anechoic chamber setup, and two on measurement uncertainty investigations in practical setups.

All publications are enclosed as the latest version, i.e. the final version of the accepted paper. Two papers (Paper D and Paper H), however, are enclosed as the latest revised versions, they are currently in the review process. The page layout also varies between papers depending on the publication channels. References are listed with numbers in the order they are cited in the text, and each enclosed paper has its individual reference list.

Acknowledgements

During this Ph.D., I have had many discussions with, and received many suggestions from colleagues and friends from Aalborg University and from the industry. Their support has been a great help in the process of the Ph.D. work presented in the thesis.

First of all, I would like to express my sincere gratitude to my supervisors Gert F. Pedersen and Jesper Ø. Nielsen. I want to thank Gert for offering me this wonderful Ph.D. project. I am also very grateful to his encouragement, unconditional support throughout my study; He has always been supportive when I need his help. Without his support and guidance, I am sure this Ph.D. thesis will not be possible in my opinion. I want to thank Jesper, with whom I work everyday, for valuable guidance and numerous discussions throughout the last three years. He spent a lot of time teaching me the basic knowledge, correcting my papers and discussing with me. He is very easygoing and optimistic. It has been an enjoyable experience for me to work with him.

I want to thank Intel mobile communications, Denmark. Their co-funding in the 4GMCT project made this thesis possible. Especially, I want to acknowledge the continuous and strong support of their team, Mikael B. Knudsen, now with Aarhus University, for ensuring the good collaboration between Aalborg University and Intel, Christian Rom for his confidence in me and his recommendation for the Ph.D. application, Xavier Carreño for the numerous technical discussions, Jagjit S. Ashta for his valuable help on automation tools and support for the time-consuming practical measurements, Günter Krenz and Tommy Nielsen for their help in the project. A special acknowledgment goes to Xavier, for his help for the past four years.

I conducted a three-month internship at Anite telecoms oy, Finland. I want to thank COST IC1004 for supporting the abroad study. I would like to thank Pekka Kyösti, Lassi Hentilä and Tommi Jämsä for our fruitful collaborations and many interesting discussions. A special acknowledgment goes to Pekka, for his generous help with the channel modeling, ideas for OTA testing and many interesting discussions we had. It was a very enjoyable experience for me, despite the white frozen winter in Oulu.

I conducted a one month exchange study in Motorola Mobility, Libertyville and in ETS-Lindgren, Cedar Park, US. I want to thank COST IC1004 again for supporting the trip. I thank Dr. Istvan Szini and Dr. Michael D. Foegelle for arranging my visit,

and helping me with the practical measurements during the stay.

I am very grateful to APNet section, which provided me with a wonderful working environment. I was free to follow my ideas and arrange my tasks. I owe many thanks to all my colleagues in APNet who could help me with the questions I had. I especially want to mention Ondrej Franek, for his technical discussions and guidance on research topics related to antennas. Fan Sun, for introducing me into the interesting convex optimization field and sharing valuable ideas with me; Kim Olesen and Kristian Bank for their support and discussions in the practical measurements; Section secretary Charlotte K. Madsen for her continuous assistance with management and administrative issues. Many thanks go to my other colleagues in APNet section, who are very friendly, helpful and making my study enjoyable.

I would like to thank Prof. Michael A. Jensen, Prof. Jun-ichi Takada and Assoc. Prof. Troels B. Sørensen for being my committee members of my defense and taking the time to read my dissertation.

I want to thank my family and my friends. Special thanks go to my parents who unconditionally supported me in every way possible, for which I am immensely and forever grateful. Finally, I want to thank my beloved wife, Shujin, who is now expecting our first child, for being extremely patient and supportive for my Ph.D. work.

Wei Fan
Aalborg University,

Thesis Details

Thesis Title:	Over the Air Testing of MIMO capable terminals
Ph.D. Student:	Wei Fan
Supervisors:	Prof. Gert F. Pedersen, Aalborg University
	Assoc. Prof. Jesper Ø. Nielsen, Aalborg University

The main body of this thesis consists of the following papers:

[A] Wei Fan, Xavier Carreño, Fan Sun, Jesper Ø. Nielsen, Mikael B. Knudsen and Gert F. Pedersen, "Emulating Spatial Characteristics of MIMO Channels for OTA Testing ," *IEEE Transactions on Antennas and Propagation*, vol. 61, no. 8, pp. 4306–4314, August, 2013.

[B] Wei Fan, Jesper Ø. Nielsen, Ondrej Franek, Xavier Carreño, Jagjit S. Ashta, Mikael B. Knudsen and Gert F. Pedersen, "Antenna Pattern Impact on MIMO OTA Testing," *IEEE Transactions on Antennas and Propagation*, vol. 61, no. 11, pp. 5714–5723, November, 2013.

[C] Wei Fan, Fan Sun, Jesper Ø. Nielsen, Xavier Carreño, Jagjit S. Ashta, Mikael B. Knudsen and Gert F. Pedersen, "Probe Selection in Multi-probe OTA Setups," *IEEE Transactions on Antennas and Propagation*, vol. 62, no. 4, pp. 2109–2120, April, 2014.

[D] Wei Fan, Pekka Kyösti, Jesper Ø. Nielsen, and Gert F. Pedersen, "Wideband MIMO Channel Capacity Analysis in Multi-probe Anechoic Chamber Setups," resubmitted after major revision to *IEEE Transactions on Antennas and Propagation*, August. 2014.

[E] Wei Fan, Fan Sun, Pekka Kyösti, Jesper Ø. Nielsen, Xavier Carreño, Mikael B. Knudsen and Gert F. Pedersen, "3D Channel Emulation in a Multi-probe Setup," *Electronics Letters*, vol. 49, no. 9, pp. 623–625, April, 2013. (Featured Article)

[F] Wei Fan, Jesper Ø. Nielsen, and Gert F. Pedersen, "Estimating Discrete Power Angular Spectra in Multi-probe OTA Setups," *IEEE Antennas and Wireless Propagation Letters*, vol. 13, pp. 349–352, February, 2014.

[G] Wei Fan, Istvan Szini, Jesper Ø. Nielsen, and Gert F. Pedersen, "Channel Spatial Correlation Reconstruction in Flexible Multiprobe Setups," *IEEE Antennas and Wireless Propagation Letters*, Special Cluster on Terminal Antenna Systems for 4G and Beyond, vol. 12, pp. 1724–1727, January, 2014.

[H] Wei Fan, Pekka Kyösti, Lassi Hentilä, Jesper Ø. Nielsen, and Gert F. Pedersen, "Rician Channel Modeling for Multi-probe Anechoic Chamber Setups," accepted to *IEEE Antennas and Wireless Propagation Letters*, July, 2014.

[I] Wei Fan, Xavier Carreño, Jagjit S. Ashta, Jesper Ø. Nielsen, Gert F. Pedersen and Mikael B. Knudsen, "Channel Verification Results for the SCME models in a Multi-Probe Based MIMO OTA Setup," *IEEE* 78^{th} *Vehicular Technology Conference (VTC Fall)*, pp. 1–5, September, 2013.

[J] Wei Fan, Istvan Szini, Michael D. Foegelle, Jesper Ø. Nielsen, Gert F. Pedersen, "Measurement Uncertainty Investigation in the Multi-probe OTA Setups," 8^{th} *European Conference on Antennas and Propagation (EuCAP)*, pp. 1–5, April, 2014.

In addition to the main papers, I have been involved in the following publications during the Ph.D. project. Their full contents are not included in the dissertation, as some of the results are covered in papers listed above. They addresses other challenges related to over the air testing of MIMO capable terminals with multi-probe anechoic chamber methods.

[1] Elpiniki Tsakalaki, Osama N. Alrabadi, Wei Fan and Gert F. Pedersen, "Covariance-Based Spatial Channel Structure Emulation for MIMO OTA Testing," *IEEE Communications Letters*, vol. 18, no. 2, pp. 205-208, February, 2014.

[2] Wei Fan, Pekka Kyösti, Fan Sun, Jesper Ø. Nielsen, Xavier Carreño, Mikael B. Knudsen and Gert F. Pedersen, "3D Channel Model Emulation in a MIMO OTA Setup," *IEEE* 78^{th} *Vehicular Technology Conference (VTC Fall)*, pp. 1–5, September, 2013.

[3] Wei Fan, Jesper Ø. Nielsen, Xavier Carreño, Jagjit S. Ashta, Gert F. Pedersen and Mikael B. Knudsen, "Impact of Non-Ideal System on Spatial Correlation in a Multi-Probe Based MIMO OTA Setup," 7^{th} *European Conference on Antennas and Propagation (EuCAP)*, pp. 97–101, April, 2013.

[4] Wei Fan, Jesper Ø. Nielsen, Xavier Carreño, Ondrej Franek, Mikael B. Knudsen and Gert F. Pedersen, "Impact of probe placement error on MIMO OTA test zone

performance," *Antennas and Propagation Conference Loughborough (LAPC)*, pp. 1–4, November, 2012.

[5] Wei Fan, Xavier Carreño, Jesper Ø. Nielsen, Kim Olesen, Mikael B. Knudsen and Gert F. Pedersen, "Measurement Verification of Plane Wave Synthesis Technique Based on Multi-probe MIMO-OTA Setup," *IEEE* 76^{th} *Vehicular Technology Conference (VTC Fall)*, pp. 1–5, September, 2012.

[6] Wei Fan, Xavier Carreño, Jesper Ø. Nielsen, Jagjit S. Ashta, Gert F. Pedersen and Mikael B. Knudsen, "Verification of Emulated Channels in Multi-Probe Based MIMO OTA Testing Setup," 7^{th} *European Conference on Antennas and Propagation (EuCAP)*, pp. 97–101, April, 2013.

[7] Wei Fan, Tommi Jämsä, "Some investigations on angular sampling method for 3D spatial cluster," *COST IC1004 Temporary Document*, pp. 1–7, May, 2014.

[8] Jesper Ø. Nielsen, Gert F. Pedersen and Wei Fan, "Characterization of Interference for Over the Air Terminal Testing," *COST IC1004 Temporary Document*, pp. 1–6, May, 2013.

[9] Xavier Carreño, Wei Fan, Jesper Ø. Nielsen, Jagjit S. Ashta, Gert F. Pedersen and Mikael B. Knudsen, "Test Setup for Anechoic Room based MIMO OTA Testing of LTE Terminals," 7^{th} *European Conference on Antennas and Propagation (EuCAP)*, pp. 97–101, April, 2013.

[10] Jesper Ø. Nielsen, Osama Alrabadi, Wei Fan, Atsushi Yamamoto and Gert F. Pedersen, "Testing MIMO Devices Over the Air," *Proceedings of the 2012 IEEE International Symposium on Antennas and Propagation (APSURSI)*, pp. 1–2, July, 2012.

[11] Wei Fan, Jesper Ø. Nielsen and Gert F. Pedersen, "Estimating Power Angular Spectra in Multi-probe Setups for Terminal Testing," *Proceedings of the 2014 IEEE International Symposium on Antennas and Propagation (APSURSI)*, pp. 1–2, July, 2014.

In addition to the academic papers, the following patents have been made and filed during the Ph.D. project as well. Their full content is not included in the dissertation.

[1] Wei Fan, Pekka Kyösti and Lassi Hentilä, "Over-the-air Test," *Patent*, pending, May. 2014.

[2] Anatoliy Ioffe, Jagjit Singh Ashta, Xavier Carreño, Tommy Nielsen, Mikael Knudsen, Guenter Krenz, Wei Fan, Jesper Ø. Nielsen, Gert F. Pedersen and Ondrej Franek, "Advanced Wireless Communication Systems and Techniques," *Patent*, Application Number: U.S. 61/821,634, filed, May. 2013.

[3] Jagjit Singh Ashta, Mikael Knudsen, Xavier Carreño, Bent Kristensen, Anatoliy Ioffe, Gert F. Pedersen, Wei Fan, Ondrej Franek, and Kristian Bank, "Advanced Wireless Communication Systems and Techniques," *Patent*, Application Number: U.S. 61/859,125, filed, July, 2013.

[4] Jagjit Singh Ashta, Anatoliy Ioffe, Xavier Carreño, Tommy Nielsen, Mikael Knudsen, Guenter Krenz, Wei Fan, Jesper Ø. Nielsen, Gert F. Pedersen and Ondrej Franek, "Throughput Charaterization," *Patent*, pending, May, 2014

This thesis has been submitted for assessment in partial fulfillment of the PhD degree. The thesis is based on the submitted or published scientific papers which are listed above. Parts of the papers are used directly or indirectly in the extended summary of the thesis. As part of the assessment, co-author statements have been made available to the assessment committee and are also available at the Faculty. The thesis is not in its present form acceptable for open publication but only in limited and closed circulation as copyright may not be ensured.

Part I

Introduction

1 Background of the thesis

Due to the ever growing demand for higher data rate and more reliable communication, the performance requirements of the mobile terminals continues to increase dramatically. To meet this increased performance requirement, new wireless technologies such as Long-Term Evolution (LTE), LTE-Advanced and Worldwide Interoperability for Microwave Access (WiMAX) employ multiple antennas both at the mobile terminal and base station (BS) sides. Multiple-input multiple-output (MIMO) technique is an attractive and promising technology to improve the performance of wireless communication systems [1]. With MIMO technologies being adopted in the commercial LTE systems, mobile network operators and manufactures urgently require standard test methods which are suitable to test the MIMO device radio performance. Accurate evaluation of MIMO capable terminals is critical both for network operators and mobile manufacturers. A poor terminal performance may result in reduced coverage and low data rate connections, which will force network operators to install more base stations. Performance testing is a mandatory step for mobile manufactures in the research and design stages before massive roll-out for the device. This thesis focuses on testing methods for MIMO capable terminals.

1.1 Testing MIMO capable terminals

SISO conducted testing

Testing for a single-input signal-output (SISO) device is typically done in a conducted way, where the test system consists of a BS, a device under test (DUT) and a wireless channel emulator directly cabled to the DUT, i.e. with the DUT antenna bypassed. These test systems are thus suitable for characterizing the SISO device without considering the antenna impact.

SISO OTA

Over-the-air (OTA) testing of the radio performance of mobile terminals has the advantage, compared to conducted test methods, of not needing to break or otherwise modify the mobile device. Furthermore, all parts of the device design (antennas, RF front end, baseband processing) are thoroughly and simultaneously evaluated with OTA testing. OTA testing of SISO devices has been standardized in both CTIA (International Association for the Wireless Telecommunication Industry) and 3rd Generation Partnership Project (3GPP), where two figures of merit (FoMs) were chosen [2, 3]:

- Total radiated power (TRP), a measure of how much power is radiated by the mobile terminal when it is connected to an active BS.

- Total isotropic sensitivity (TIS), which determines the lowest received power necessary to achieve a given bit error rate (BER) performance.

Alternatively, the mean effective gain (MEG), which is another power measure to describe the impact of the antenna on the link budget, is considered to evaluate SISO device as well [4]. TRP and TIS are parameters directly related to the antenna radiation efficiency, while MEG also includes the impact of the propagation channel on the overall antenna performance.

In the recent years, MIMO technology has been extensively used in new wireless technologies. MIMO device performance depends directly on the propagation channel and its interaction with the antennas [5]. SISO OTA is intended to evaluate mobile terminal antenna gain related parameters only, and hence it is not sufficient for characterizing performance of MIMO capable terminals.

Traditional MIMO testing

Conducted testing Often, a MIMO device is tested in a conducted way, as illustrated in Figure 1. Antennas are disconnected and replaced with coaxial cables, which guide the signals directly to the DUT. Conducted testing is useful during the research and design phase of the device. For example, the baseband and parts of the radio frequency (RF) chains can be evaluated. Though it is able to provide repeatable measurements, it is not adequate in the final evaluation stage of the product. There are some shortcomings. First, some devices typically have integrated antennas that are impractical to access and remove for testing. Second, conducted testing is incapable of including the impact of antenna effects e.g., user impact, antenna mismatch, and etc. Moreover, antennas play a significant and integral role to the MIMO capable device performance. MIMO device might pass the conducted testing, but results might not be consistent with field results in real world. It would be desirable that all critical parts of the device (antennas, RF front end and baseband processing) are tested together.

Field drive testing Field drive testing is another alternative to evaluate MIMO capable device, where MIMO device performance is measured in the fields using different driving routes and different radio channel environments. It has always been a “necessary evil”. It presents many drawbacks such as high cost and complexity. It is also very time-consuming and labour-intensive to perform massive measurement campaigns in different scenarios. Moreover, field testing may not be repeatable and hard to control due to the open testing environment. Some initial LTE field measurement results were reported in [6].

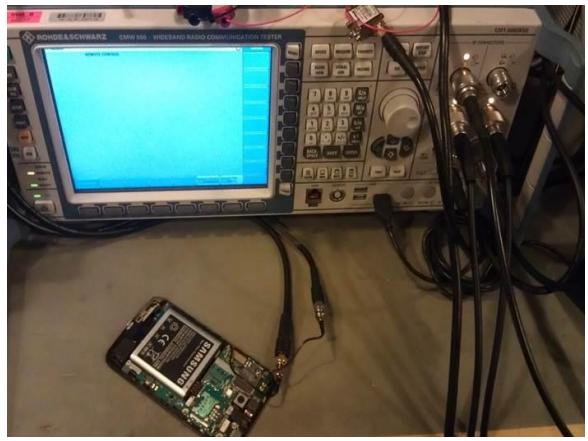

Fig. 1: An illustration of conducted testing for MIMO devices.

1.2 MIMO OTA testing

Field testing is performed "over the air". However, MIMO OTA testing in the thesis specifically refers to testing a wireless device without any connected cables in the laboratory, where the external interferences and noises are not present.

The most realistic way to account for MIMO antennas is to test them as they are used in the final product, meaning that no modifications are made to the phones. There is a strong need to perform proper MIMO OTA testing. MIMO OTA can truly evaluate the final product under realistic conditions. Standardization work for the development of the MIMO OTA test methods is currently ongoing. Several approaches for standardizing the MIMO terminal evaluation are under investigation in 3GPP Radio Access Network Work Group 4 (RAN WG4), European Cooperation in Science and Technology (COST) IC 1004 and CTIA. The ultimate goal of MIMO OTA testing is to rank MIMO devices as either good, fair or poor in a reliable, repeatable, efficient and cost-effective manner.

Many different MIMO OTA test methods have been proposed, which differs significantly in terms of emulated propagation channel characteristics, test setup size, and cost [7]. These methods mainly fall into three categories: the multi-probe anechoic chamber based method, the reverberation chamber based method and the two-stage method [8], as summarized below. The thesis focuses on the multi-probe anechoic chamber based methods.

Multi-probe anechoic chamber based method

An illustration of the multi-probe anechoic chamber based methods is shown in Figure 2. Multiple antennas (called probe antennas in the thesis) are located around the DUT.

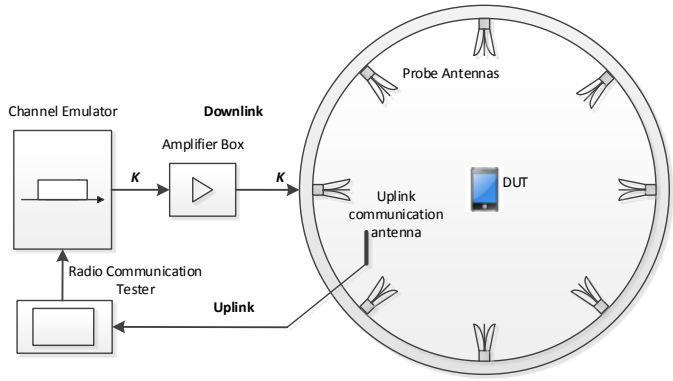

Fig. 2: An illustration of the multi-probe anechoic chamber based method. The test system consists of a BS emulator, one or several channel emulators, an anechoic chamber, multiple probes, a DUT, a turntable, cables and power amplifiers.

Radio propagation environments are reproduced in the laboratory by transmitting appropriately controlled signals, by use of the radio channel emulators and the multiple probes [7]. As the testing is done in an shielded anechoic chamber, there will be no external interferences. Anechoic chambers are free from reverberation, and hence target multipath propagation environments and intended interferences can be created in a controlled and repeatable manner. The multi-probe anechoic chamber method has been a promising candidate due to its capability to physically synthesize the multipath channel, with desired temporal and spatial characteristics, yet the cost is high due to the need of an anechoic chamber and possibly multiple fading emulators. A literature review on the research topics in the multi-probe anechoic chamber method is detailed in Section 3.

Reverberation chamber based method

A reverberation chamber is a highly conductive enclosed cavity, which is typically equipped with metallic paddles (mode stirrers) and turntables [9, 10]. A reverberation chamber is considered as a useful tool to emulate rich multipath environments [10]. With the reverberation chamber method, the spatial richness is created by reflections from the metallic walls of the chamber, which are further randomized by mode stirrers and turntable inside the chamber. Over a long period of time, the created field approaches a statistically isotropic Rayleigh fading environment around the DUT. Note that the field around DUT is instantaneously directive. Reverberation chamber based methods vary from a simple single chamber to more complex multiple chambers with or without the addition of a fading emulator [9]. The reverberation chamber method

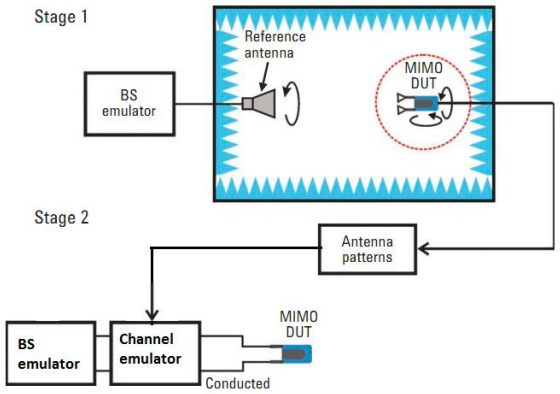

Fig. 3: An illustration of two stage method (Figure by courtesy of Agilent technology).

is cost-effective and 3D channels are intrinsic with the methods. However, it is limited to channels with the isotropic power angular distribution, 0-dB cross polarization ratio (XPR), and limited temporal characteristics (unless an additional fading emulator is used) [7]. Realistic propagation scenarios experienced by end-users are rarely with isotropic incoming power spectrum. An overview of the recent advances in mode-stirred reverberation chamber used for MIMO OTA testing is given in [9].

Two stage method

The two stage method was proposed in [11]. In the first stage, the complex antenna patterns of the DUT are measured by a traditional anechoic chamber-based antenna measurement system. The second stage combines the antenna pattern information and the channel model to calculate the MIMO correlation matrices and antenna power imbalances, which are implemented in a channel emulator allowing a conducted measurement. An illustration of the two stage method is shown in Figure 3.

The two-stage method is capable of modelling the 2D and 3D spatial channels with relatively low cost. Unfortunately, it requires a cable connection to the device under test (DUT). Hence, it cannot evaluate the DUT's self-interference. Self-interference in a DUT could significantly reduce receiver sensitivity. In [12], a so-called radiated two-stage method was proposed to eliminates the problems of connecting an RF cable directly to the DUT in the second stage. However, a non-intrusive measurement of the complex patterns of the antennas on the DUT in the first stage is still challenging. Furthermore, more work on the concept verification is required for the practical setups.

Other methods

Some other methods exist as well for OTA testing of MIMO devices. In [13], an idea of using an electronically reconfigurable reverberation chamber to support OTA testing in a compact and cost-effective way is introduced. Desired channel characteristics could be obtained by varying reconfigurable loads placed on the walls of the chamber. More investigation and practical implementations are required for this method. In [14], a so-called decomposition method was described for OTA testing. It is cost-efficient, as channel emulation is not required. However, it is not capable of emulating standard fading channel models adopted in MIMO OTA standardizations.

2 Aim Of Work

The ultimate goal of the project is to rank MIMO capable terminals. The present work mainly investigates how to conduct OTA testing of the MIMO terminals in a radio anechoic chamber setup. The project focuses on the new mobile standard LTE and the coming LTE-A system for mobile phones, tablets and laptops. The work is limited to emulate downlink channel models (i.e. from BS to mobile station). The main goals of the Ph.D. projects are listed and explained as follows.

- Radio channel emulation
  The main objective of the work is to investigate techniques to reproduce realistic electromagnetic fields with the aid of an anechoic room, channel emulators and multiple probe antennas located around the DUT. In this way the actual antenna system of the device is used and aspects such as self-interference is also included in the analysis. Emulation techniques of desired channels for evaluating MIMO device performance in an anechoic chamber are fundamental for the investigation.

- Test zone size investigation
  The test zone is a physical area where the DUT is located during testing. It is required that the desired channel should be approximated over the test zone accurately, and hence the DUT would experience the same radio propagation channels as it would in the real field.

- Required number of probes investigation
  The cost of the multi-probe anechoic chamber setup mainly depends on the channel emulators and the number of probes required for reproducing the desired channel models. Also, the test zone size depends directly on the number of probes utilized for synthesizing the radio channels.

- Design of the multi-probe anechoic chamber setups
  The purpose is to find the key aspects related to the design of the setups. Open

questions, e.g. the physical dimensions of the OTA ring, the antenna design for probe antennas, the size of the anechoic chamber, probe placement, and etc. have to be addressed.

- Emulation of arbitrary spatial channel models
  Measurements have demonstrated that elevation spread can not be ignored in many propagation environments, see. e.g. [4, 15]. It would be desirable to emulate realistic 3D models with the multi-probe setups. Appropriate 3D probe configurations have to be investigated as well.

- Measurement uncertainty investigation in the setups
  As a mandatory step for standardization, it is required to analyse the sources of errors and uncertainties in the measurements. Impact of system nonidealities (e.g. reflections inside the chamber, power coupling between the OTA probes, calibration of the OTA setups, cable reflections and etc.) on the testing results have to be investigated.

- Validation of the emulated channels
  The desired channel models should be correctly implemented inside the test zone. And hence channel verification measurements are necessary.

- Cost reduction of the setup
  The main disadvantage with the multi-probe anechoic chamber methods is the cost of the setups. It would be desirable to reduce the number of probes (consequently the channel emulator output ports) to the minimum necessary to generate the desirable spatial channel models.

3 State of the Art

The multi-probe anechoic chamber method has attracted huge attention both from industry and academia in recent years, due to its capability to physically reproduce realistic multipth environments in the laboratory. The objective is to reproduce the radio propagation environments as it would be experienced by the DUT in the intended environment, but in a repeatable and controllable manner.

Various contributions on different aspects of the multi-probe anechoic chamber method have been published in the literature. One fundamental question is how to reproduce arbitrary target channel models with limited number of probes. Mainly two channel emulation techniques are proposed in the literature.

- One technique is the plane wave synthesis (PWS) technique. The basic idea is to create static plane waves with arbitrary impinging angles of arrival (AoAs) by allocating appropriate complex weights to the probes. Different techniques have

been proposed to obtain the complex weights for the probes, see e.g. spherical wave expansion techniques addressed in [16–20], least squares technique [21–23], convex optimizations in Paper B and a closed-form technique based on trigonometric interpolation in Paper B. This idea was briefly addressed in [24,25] as well, though details on how to reproduce static plane waves were missing. In Paper B, techniques based on convex optimization are introduced to emulate vertically or horizontally polarized plane waves. Simulation results show that the difference between the complex weights for the two polarizations depends on the ratio between test area radius and OTA ring radius, and the complex weights are practically the same for large ring radius cases. Two channel emulation schemes based on the PWS technique have been proposed in the literature, as summarized below:

  - In one channel modeling scheme, a channel with a given incoming power angular spectrum (PAS) is modeled by a collection of plane waves. Each of the plane waves impinging the test area with a specific AoA and power can be approximated by allocating appropriate complex weights to the probes. A Doppler shift can then be introduced to each static plane wave to enable time variant channels. Note that the target channel model is essentially a stationary channel model with fixed AoAs, as the incoming cluster has a specified PAS shape. This idea is proposed in [21, 22]. Note that both magnitude and phase calibration of the probes are required to synthesize fields with desired impinging AoAs. This idea is further addressed in [26].
  - In another channel modeling scheme proposed in [20], each snapshot of the time-varying channel is considered static. The snapshots are characterized by the AoAs, complex amplitudes, and polarizations of all waves, and hence can be reproduced by allocating appropriate complex weights to the multiple probes. The static plane waves are approximated from the spherical wave theory point of view. Arbitrary multipath environments (e.g. channels with time-varying mean angles of arrival) can be reproduced using this channel modeling scheme, unlike the first method.

- Another technique named the pre-faded signal synthesis (PFS) technique was proposed in [21, 27] for the 2D multiprobe setup and was extended to the 3D multi-probe setup in Paper C and Paper E. As detailed in [21], the focus is on reproducing the channel spatial characteristics in the test volume at the receiver (Rx). The basic idea is that by allocating appropriate power weights to the OTA probes, we can reproduce the incoming PAS of the channel in the test volume. Different clusters are modeled independently and each cluster is mapped to the probes, based on the cluster PAS and the angular locations of the probes. The spatial correlation is used as a figure of merit (FoM) to determine how accurately the spatial characteristics of the cluster at the Rx side (e.g. the impinging PAS shape of the cluster) are reproduced. The target spatial correlation is determined

by the target PAS shape, while the emulated spatial correlation depends on the created discrete PAS shape. Note that only magnitude calibration of the probes is required. This technique has been implemented in several commercial channel emulators, see e.g. [27–29]. Different techniques have been proposed in the literature to obtain appropriate power weights, see e.g. several numerical optimization techniques mentioned in [29], least squares in [27] and convex optimization in Paper A. In Paper A, it was illustrated that the optimization problem can be expressed as a convex optimization problem, which can be solved efficiently. The proposed optimization algorithm in Paper A is compared with results achieved by two commercial channel emulators for the spatial channel extended model (SCME) urban macro (Uma) tapped delay line (TDL) channel model and better emulation accuracy was achieved.

Various research topics based on the above mentioned two techniques have been addressed in recent years, as summarized below:

- Relationship between test zone size and required number of probes investigation. The test zone is the geometrical area inside which the DUT is located during the measurement. Acceptable channel emulation error levels are defined to ensure that the target propagation environment is reproduced around the DUT with certain accuracy. The required number of probes is a key issue related to the multi-probe anechoic chamber solution, as it directly determines the test system costs.

  - For channels emulated with the PWS technique, the field synthesis error (named equivalent reflectivity level in [16–20]) is often selected as the FoM. It has been demonstrated that the equivalent reflectivity level depends on the number of probes, the test area size, the center frequency, impinging angles and the OTA probe angular locations [16, 17, 20–24, 26, 30]. In [30], it was demonstrated the difference between target received voltage, assuming ideal impinging plane waves with arbitrary AoAs, and the induced received voltage, with waves radiated from the multiple probes impinging the DUT, depends on the DUT radiation pattern as well.
  - For channels emulated with the PFS technique, spatial correlation is often selected as the FoM. Conclusions similar to those for the PWS were drawn for the relationship between test zone size and number of probes, as detailed in [17, 21], Paper A-C and Paper E. The impact of the antenna pattern on emulation accuracy for spatial correlation of the received signals in the PFS method is demonstrated by simulation and measurement results in Paper B.
  - Paper D investigates wideband MIMO channel capacity in multi-probe anechoic chamber setups, with emphasis on the relationship between capacity emulation accuracy and test area size. The capacity emulation accuracy has been shown to be a valid measure to determine the test area size.

- Emulation of 3D channel models in multi-probe setups. The 2D channel model is not generally valid. Measurements have demonstrated that elevation spread can not be ignored in many propagation environments, and thus emulation of 3D models is required [4, 15]. In [31], it was briefly mentioned that probes in a 3D setup were used to emulate 3D channel models, but no algorithm description is given. In Paper E, a technique to emulate 3D geometry-based channel models in a multi-probe over the air test setup is presented. The proposed technique provides a general emulation framework for any spherical incoming power spectrum. This work is further extended in [32]. Some 3D probe configurations to emulate 3D channel models were proposed in [16, 33, 34], Paper C and Paper E.
- Design of multi-probe test setups. Some papers have investigated the key aspects related to the multi-probe system setup design. One key part of the multi-probe test systems is probe antennas located around the DUT. Several probe designs were proposed in the literature, see, e.g. horn antennas in [35] and Vivaldi antennas in [36]. These two probe prototypes are widely used in current multi-probe setups, as reported in the open literature. The OTA ring physical dimension is another critical aspect of the test system. There is concern on the physical dimension requirement of the OTA ring to measure a given DUT with certain accuracy. In [37], criteria for physical dimensions are developed based on field strength stability and phase stability across the test zone. In Paper J, uncertainty measurements were performed in three different labs equipped with different multi-probe anechoic chamber setups to show key aspects related to the multi-probe system setup design.
- Verification of emulated channel models. The objective of the measurements is to ensure that desired channel models are correctly implemented inside the test area, i.e. the approximation is acceptable.
  - Verification results of the PWS technique were reported in [23, 38] and Paper G. In Paper G, good agreement were obtained between the measured fields and the target target fields both for the vertical and horizontal polarizations.
  - Verification results of the PFS technique were reported in [38–41]. It was concluded that all the key parameters of the target channel models (i.e. the SCME models), i.e., power delay profile, temporal correlation, spatial correlation and cross polarization ratio, can be accurately reproduced in a multi-probe anechoic chamber based setup.
  - In Paper F, a technique to estimate the discrete PASs modeled in multi-probe setups is proposed. The discrete PAS can be used to verify how well the channels are implemented in the laboratory.
- Cost reduction of multi-probe setups. The cost of the multi-probe anechoic chamber setup mainly depends on the channel emulators and the number of probes required for reproducing the desired channel models.

  - Finding ways to limit the number of probes while still approximating the target channels sufficiently accurately could make the test system cheaper. Several ideas were proposed to address this challenge. Paper C proposed a probe selection mechanism, which basically selected a subset of probes from a large set of available probes according to the directivity of the target channel models. A flexible multi-probe setups were proposed in Paper G, where the number of probes (consequently the channel emulator output ports) are optimized to the minimum necessary to generate the desirable spatial channel models.
  - In some contributions, the expensive commerical channel emulators were avoided. In [42], instead of using commercial channel emulators, phase shifters and programmable attenuators are utilized to control radio signals transmitted from the probes. In [43], a custom-made fading emulator was proposed.
  - In [44], small anechoic chambers equipped with a set of probes for evaluating DUT with PWS techniques were proposed. It is concluded that it is possible to perform tests in a small anechoic chamber that previously required a large anechoic chamber, e.g., MIMO OTA testing and antenna-pattern measurements.

- Reference antenna concept. The reference antenna concept was created based on the need to eliminate the unknown antenna patterns of the MIMO capable devices for radiated data throughput measurements [45, 46]. The reference antenna can help minimize the measurement uncertainty, and used to validate test methods. Note that the investigation in [45, 46] has been carried out for the special case of isotropic incoming power distribution only.

- Modeling Rician channel in multi-probe setups. The focus in MIMO OTA standards and literature is on modeling Rayleigh fading channel models. Rician scenarios are expected to be more likely, as future cell sizes will further decrease. Paper H proposed a method to create a Rician fading channel model with a line of sight (LOS) component with an arbitrary polarization and direction.

- Reproducing field measurement results in the laboratory. Work in the literature has been focused on reproducing synthesized radio channels. However, it would be desirable to replay the field recorded channels in the laboratory. In [20], an idea based on the PWS technique is proposed to reproduce arbitrary multipath environments in the multi-probe anechoic chamber setups. The impact of limited number of probes and noise on the received signal and the channel capacity are demonstrated. In [47], the idea of replaying recorded channels in the laboratory is mentioned, though no results were provided.

- Throughput measurements in the multi-probe setups. Currently, there is a great interest in conducting throughput measurements of LTE devices. Throughput measurement results of live LTE devices were reported in several contributions, see e.g. [48, 49]. However, due to the lack of throughput prediction model, the throughput results are hard to interpret in practice. Potential systematic errors in measurements, which might impact the throughput measurement results, are hard to identify in practical measurements.
- Other new applications. Besides utilized for evaluating LTE devices, the multi-probe anechoic chamber methods have been used for other new applications. see e.g. car to car and car to infrastructure communications [50, 51], cognitive radio [51], etc.

4 Contributions in This Thesis

The papers included in this thesis are briefly summarized in this chapter. The motivation for each individual contributions is described along with their main results and how they are linked to the other contributions.

Paper A

Emulating Spatial Characteristics of MIMO Channels for OTA Testing
Wei Fan, Xavier Carreño, Fan Sun, Jesper Ø. Nielsen, Mikael B. Knudsen and Gert F. Pedersen
Published in the *IEEE Transactions on Antennas and Propagation.*

Motivation

The concept of clusters has been widely adopted to model the multipath phenomenon based on extensive measurements. This paper addresses the technique to generate an arbitrary number of clusters, each associated with an arbitrary mean Angle of Arrival (AoA) and Azimuth Spread (AS), impinging the test zone with a limited number of probes. It has been shown that the essence is to find proper power weightings for each probe such that channel PAS can be approximated. Several optimization techniques are briefly discussed in patents to obtain probe power weightings. However, most techniques are very computationally inefficient and detailed explanations are not available. Furthermore, spatial correlation has been selected as the main figure of merit to characterize the channel spatial information, while cluster PAS shape parameters including AS and mean AoA are often ignored in the literature. Channel profiles with the same spatial correlation may present very different PAS shapes when the spatial sampling points for spatial correlation calculation are limited. A novel technique to obtain optimum power weights for the OTA probes based on convex optimization is proposed. The

proposed technique emulates spatial correlation as well as introduces constraints on the maximum deviation between the target PAS and the emulated PAS in terms of mean AoA and AS.

Paper content

In the paper, we first form the channel emulation problem with constraints on the resulting discrete PAS shape such as AS and mean AoA, when angular locations of OTA probes are fixed. The discrete PAS is characterized by the angular locations and power weights for the probes. We further illustrate the problem can be expressed as a convex optimization problem, which can be solved efficiently. The discussions are first limited to single cluster PAS and then extended to multi-cluster PAS. The proposed optimization algorithm is compared with results achieved by two commercial channel emulators for the SCME Uma TDL channel model. Research topics, e.g. impact of channel models on optimization results, required number of probes, are investigated based on the proposed algorithms. The proposed optimization algorithm is compared with a reference algorithm implemented in the commercial channel emulator in the practical multi-probe anechoic chamber setups.

Main Results

We have introduced an novel algorithm to determine probe power weights for a multi-probe anechoic chamber setup utilizing the prefaded signal synthesis method. The proposed algorithm outperforms the algorithms implemented in the commercial channel emulators in several aspects. By employing convex optimization framework into channel emulation algorithm, computational complexity is reduced dramatically compared to other numerical optimization techniques. Better optimization accuracy is achieved both for the multi-cluster PAS and each individual PAS within the multi-cluster. Another advantage with the proposed algorithm is that the error tolerance for the emulated PAS in terms of mean AoA and AS can be predefined in the optimization. Smaller errors in terms of mean AoA and AS are achieved for the proposed algorithm as well. Measurement results are consistent with the simulation results and better emulation accuracy of the proposed algorithm is demonstrated in a practical setup.

Paper B

Antenna Pattern Impact on MIMO OTA Testing
Wei Fan, Jesper Ø. Nielsen, Ondrej Franek, Xavier Carreño, Jagjit S. Ashta, Mikael B. Knudsen and Gert F. Pedersen
Published in the *IEEE Transactions on Antennas and Propagation.*

Motivation

One major challenge for multi-probe anechoic chamber method is to emulate a realistic environment which accurately reflects the real wireless propagation environment. An optimization algorithm to obtain power weights for the PFS technique is proposed in Paper A. In paper A, and also in other papers in the literature, the DUT antenna pattern has been considered irrelevant to test area size. DUT Antennas with omnidirectional antenna patterns are generally assumed, as the DUT antenna pattern is typically not known beforehand. Furthermore, if some antenna patterns are embedded to the channel model, the OTA performance will depend on both the DUT antenna pattern embedded in the channel as well as antenna pattern in the DUT. For the PWS technique, the work in the literature is limited to create plane wave impinging the test area with arbitrary directions. However, the difference between the target received voltage, assuming ideal impinging plane waves with arbitrary AoAs, and the induced received voltage, with waves radiated from the multiple probes impinging the DUT, has not been investigated. For the PFS technique, the work in the literature is limited to investigate the difference between the target spatial correlation and the emulated spatial correlation, assuming two omnidirectional antenna elements. However, the spatial correlation of the received signals at the antenna output with realistic antenna patterns has not been investigated.

Paper content

In the paper, we first form the optimization techniques to generate a vertically polarized or horizontally polarized static plane wave with an arbitrary direction impinging the test area with convex optimization problems. A closed-form technique based on trigonometric interpolation technique is then proposed to investigate the DUT antenna pattern impact on induced received voltage accuracy. The impact of DUT pattern on the received voltage accuracy is demonstrated with the proposed technique. The relationship between the PWS technique and the proposed technique is summarized in the paper. After that, the impact of DUT antenna pattern on antenna correlation accuracy in the PFS technique is investigated. Three different DUTs (i.e. a DUT with two practical dipoles, CTIA band 7 good antenna and CTIA band 7 nominal antenna) and four different test scenarios are selected to demonstrate the impact of DUT pattern in a practical multi-probe anechoic chamber setup.

Main Results

The main contribution of the PWS section lies in two aspects: the optimization problem is formed as a convex optimization problem, which gives optimal results and low complexity; an optimization technique for PWS of the horizontal polarization is introduced. Simulation results show that the difference between the complex weights for the two polarizations depends on the ratio between test area radius and OTA ring radius and

the complex weights are practically the same for large R cases. A novel closed form technique to reproduce the target received voltage based on trigonometric interpolation is presented. The closed form technique gives practically the same complex weights as the PWS optimization technique for large ring radius case. The proposed technique shows that the impact of the antenna pattern on the received voltage accuracy is ruled by Nyquist sampling theory. The impact of the antenna pattern on emulation accuracy for spatial correlation of the received signals in the PFS method is demonstrated by simulation and measurement results. We show that to test realistic DUTs with higher variations in directivity, we need more probes to maintain the same received voltage and spatial correlation accuracy level, as when an omnidirectional antenna is assumed.

Paper C

Probe Selection in Multi-probe OTA Setups
Wei Fan, Fan Sun, Jesper Ø. Nielsen, Xavier Carreño, Jagjit S. Ashta, Mikael B. Knudsen and Gert F. Pedersen
Published in the *IEEE Transactions on Antennas and Propagation.*

Motivation

The cost of the multi-probe anechoic chamber setup mainly depends on the channel emulators and the number of probes required for reproducing the desired channel models. It has been demonstrated that a large number of probes is required to create a large test area in the chamber, as in Paper A. As the number of available output ports of the channel emulator is limited, several channel emulators are often required, which will dramatically increase the setup cost. Setting up a 3D multi-probe configuration is even more costly, so finding ways to limit the number of probes while still approximating the target channels sufficiently accurately could make the test system both cheaper and simpler to implement. Radio channel models are generally directional in real world scenarios, which has been widely studied in the literature and adopted in the standard channel models. However, a uniform configuration of the OTA probes over the azimuth plane is often adopted in the multi-probe setup. The discussions in Paper A are limited to a 2D uniform configuration as well. As a consequence, contributions from some probes might be dominant, while negligible from other probes when synthesizing the target radio channels. Hence a probe selection mechanism has potential to save cost, via reducing the required number of fading channels. The basic idea is to select an optimal subset of probes from a large set of probes. The selected probes are connected to the power amplifiers and the channel emulators and hence are used for reproducing the target channels in the test zone, while the other probes are disconnected from the channel emulator and properly terminated.

Paper content

The paper starts with presenting a summary of the two channel emulation techniques in the literature, i.e. the PFS technique and the PWS technique. After that, the general probe selection framework both for the PFS and the PWS techniques are formed. Probe selection for single cluster and multi-cluster channels are discussed as well. Then the focus of the paper is on presenting four different probe selection algorithms. Pros and cons of the four proposed algorithms are summarized. The proposed techniques provide a probe selection framework for the two channel emulation techniques. A measurement campaign was carried out in a practical setup to verify the proposed probe selection algorithms.

Main Results

In this paper, the probe selection in a 3D multi-probe OTA setup is addressed, where the probes are selected based on channel emulation accuracy in terms of either field synthesis error or spatial correlation error, which are selected as the FoM in the PWS and the PFS technique, respectively. This paper presents three probe selection algorithms for 3D multi-probe based setups. Simulation results show that good channel emulation accuracy can be achieved with the selected subset of probes for the considered target channel models. The probe selection algorithm for the SCME urban micro (UMi) TDL model is supported by measurements in a practical 2D multiprobe setup. The measurement results show that the channel emulation accuracy achieved with 8 selected probes is only slightly worse compared to that achieved with 16 uniformly placed probes.

Paper D

Wideband MIMO Channel Capacity Analysis in Multi-probe Anechoic Chamber Setups
Wei Fan, Pekka Kyösti, Jesper Ø. Nielsen, and Gert F. Pedersen
Accepted with major revision to *IEEE Transactions on Antennas and Propagation.*

Motivation

In the literature, to appropriately assess how accurately the emulated power angle spectrum (PAS) approximates the target PAS, the difference between the emulated spatial correlation and the target spatial correlation is chosen and used as a measure to determine the test zone size, see, e.g. Paper A and Paper C. However, there is a concern whether th correlation coefficient error $|\rho - \hat{\rho}|$ is the optimal figure of merit (FoM) to determine the test area size, as the ultimate goal is to investigate whether performance of MIMO capable terminals, e.g. data throughput, can be accurately evaluated in the laboratory. Intuitively, $|\rho - \hat{\rho}|$ is more critical when $|\rho|$ is high, as MIMO performance (e.g.

MIMO capacity) is highly sensitive to correlation at high correlation region ($|\rho| > 0.5$), while $|\rho - \hat{\rho}|$ is less critical with small $|\rho|$, as the performance reduction is negligible. The MIMO channel capacity in a particular environment depends highly on its propagation characteristics. Since the channels emulated in the multi-probe setup are only approximations, it is necessary to investigate how the capacity of the emulated channels matches with that of the target channel models.

Paper content

The paper investigates the MIMO capacities of the emulated channels in the multi-probe anechoic chamber setups and compares the results with the capacities of the target channel models. Channel capacity, spatial correlation and singular value distributions of the emulated and target channel models are investigated and compared in the paper. The impact of spatial correlation at the Tx side and at the Rx side on MIMO channel capacity is shown for the two representative channel models: 1) the SCME Urban micro (Umi) Tap delay line (TDL) model and 2) the SCME Urban macro (Uma) TDL model. Three different Tx and Rx configurations are investigated for the considered two channel models. A measurement campagin was carried out in a practical setup to verify the capacity analysis results.

Main Results

This paper investigates wideband MIMO channel capacity in multi-probe anechoic chamber setups, with emphasis on the relationship between capacity emulation accuracy and test area size. The investigation is based on the well accepted channel models in the standards for over the air testing of MIMO capable terminals, i.e. the SCME Umi TDL and SCME Uma TDL models. For these models, the simulation results show that it is irrelevant how well the spatial characteristics at the Rx side are reproduced when the spatial correlation at the Tx side is in the high region (e.g. $\rho > 0.7$), as both the emulated capacity and target capacity will be equally low. When the correlation at the Tx side is low, the Rx correlation deviation $|\rho^{Rx} - \hat{\rho}^{Rx}|$ is highly critical with high $|\rho^{Rx}|$. The capacity emulation accuracy is less sensitive to spatial correlation emulation error at the Rx with small correlation at the Rx side. Simulation results have shown that the capacity deviation $|C - \hat{C}|$ is negligible up to 1λ wavelength for the Umi channel models with eight uniformly located probes, as $|\rho^{Rx} - \hat{\rho}^{Rx}|$ is less critical when $|\rho^{Rx}|$ is small ($|\rho^{Rx}| = 0.3$). The simulation results are further supported by measurements in a practical multi-probe anechoic chamber setup.

Paper E

3D Channel Emulation in a Multi-probe Setup
Wei Fan, Fan Sun, Pekka Kyösti, Jesper Ø. Nielsen, Xavier Carreño, Mikael B. Knud-

sen and Gert F. Pedersen
Published in the *Electronics Letters.*

Motivation

Paper A, Paper B and Paper D have discussed OTA testing setups for MIMO devices with emphasis on channel modeling, where the goal is to accurately reproduce realistic 2D channels in the test area with a limited number of OTA probes. However, the 2D channel models are not generally applicable. Measurements have demonstrated that elevation spread can not be ignored in many propagation environments, and thus emulation of 3D models is required. Very few contributions have addressed this issue. The 3D channel emulation technique has been implemented in a commercial channel emulator, the Elektrobit Propsim F8, where the Laplacian distributions are defined for the power azimuth spectrum and the power elevation spectrum. However, a description of the implemented channel emulation algorithm is not available. This letter presents a new channel emulation technique for arbitrary 3D channel models.

Paper content

A technique to emulate 3D geometry-based channel models in a multiprobe over the air test setup is presented. The proposed technique provides a general emulation framework for any spherical incoming power spectrum. The emulation method results in two optimization objectives, which are both convex. One objective is to minimize the summation over the total emulation error and the other is to minimize the maximum emulation error. They give optimal emulation accuracy and allow relatively low computational complexity. Different ways to sample the test volume are discussed in the paper. An example 3D channel model and three different probe configurations are assessed in the simulations.

Main Results

This letter presents a channel emulation technique for 3D geometry-based channel models for a multi-probe based setup. The proposed methods provides a general emulation framework for all spherical power spectrums and offers globally optimal emulation accuracy with low computational complexity.

Paper F

Estimating Discrete Power Angular Spectra in Multi-probe OTA Setups
Wei Fan, Jesper Ø. Nielsen, and Gert F. Pedersen
Published in the *IEEE Antennas and Wireless Propagation Letters.*

Motivation

The spatial correlation, which is a statistical measure of the similarity between received signals at different Rx antennas, has been used to represent the channel spatial characteristics at the Rx side, as discussed in Paper A-C and E. However, the PAS itself is interesting. The PAS of the channel at the Rx side modeled with the multiple probes is discrete, characterized by the angular locations and power weights of the active probes. The discrete PAS directly represent the directivity of the created channels and is preferable to the spatial correlation for certain channel models, e.g. the Rician fading channel models and the constant non-fading channel models. In practical multi-probe setups, knowledge on how the channel is emulated in commercial channel emulators is very limited. Estimation of the discrete PAS can be used to verify how well the target channel is implemented in the test area. Unlike previous work that merely rely on the spatial correlation to model and estimate the channel spatial characteristics created at the Rx side, this paper intends to estimate the discrete PAS using the antenna array theory. While DoA estimation using antenna arrays have been well studied in the literature, the discrete PAS estimation in multi-probe based anechoic chamber setup has not been reported in the literature.

Paper content

A technique based on a virtual uniform circular array (UCA) to estimate discrete PAS modeled in multi-probe setups is proposed in the paper. Measurement results based on a virtual UCA in a preliminary 3D multi-probe setup show that the techniques are useful in practice. Previous measurement results were mainly based on 2D multi-probe setups. However, elevation spread can not be ignored in many propagation environments. Possible reasons for the deviation between the measurement and simulation results are given as well in the paper.

Main Results

Two techniques to estimate discrete power angular spectrum in the multi-probe based anechoic chamber setups, i.e. the beamforming and the Multiple signal classification (MUSIC) technique with power estimation. The beamforming technique provides consistent AoA and power estimates, which are prone to inaccuracy due to low spatial resolution and sidelobes. The MUSIC algorithm presents AoA estimates with high resolution. The power estimates based on AoA estimates match well with the target in the measurements. To improve accuracy and robustness in elevation DoA estimation, a virtual array with large aperture in elevation is suggested in measurements.

Paper G

Channel Spatial Correlation Reconstruction in Flexible Multiprobe Setups
Wei Fan, Istvan Szini, Jesper Ø. Nielsen, and Gert F. Pedersen
Published in the *IEEE Antennas and Wireless Propagation Letters.*

Motivation

One major challenge with the multi-probe method is the cost of the system and the setup complexity. Each probe is typically connected to an expensive channel emulator. The cost will likely increase dramatically for 3D probe configurations, as shown in Paper E. The fixed multi-probe setup may not be cost effective, as often many probes are not actually used in synthesizing the radio channels. If the probes can be placed according to the channel spatial characteristics in a flexible manner, a larger test area can be created compared with the fixed probe setups with the same number of probes. Hence, a flexible setup mechanism has the potential to save cost of the system, via reducing the number of required active probes and respective hardware. In one possible installation discussed in Paper C, a large number of probes are installed with fixed locations, and a switch box drives a subset of probes based on the target channel models. To reduce mutual coupling and reflection between probes, a minimum separation between probes is required. Fixing the probe locations in the chamber may result in suboptimal probe locations for a given channel model. In this paper, we propose a flexible system arrangement, where the number of probes (consequently the channel emulator output ports) are optimized to the minimum necessary to generate the desirable spatial channel model. The probe placement is flexible in both the elevation and azimuth angles, enabling the placement on optimal location defined by the proposed algorithm.

Paper content

Compared to the work in Paper A, Channel emulation for the flexible setup with a small number of probes is more challenging as both the probe weights and the probe angular locations are to be optimized. In this paper, two algorithms, namely the genetic algorithm and the so-called multi-shot algorithm, are proposed to emulate channel spatial correlation in flexible setups. Three channel models, i.e. single cluster, SCME Umi TDL and SCME Uma TDL are considered for the flexible setups in the simulations and the results are compared with the reference setups.

Main Results

This paper discusses OTA testing for MIMO capable terminals in flexible multi-probe setups. Two techniques to obtain weights as well as angular locations for the OTA probes are proposed for accurate reconstruction of the channel spatial correlation at the

receiver side. Examples show that with a small number of probes in a flexible setup, accurate spatial correlation can still be achieved within the test zone.

Paper H

Rician Channel Modeling for Multi-probe Anechoic Chamber Setups
Wei Fan, Pekka Kyösti, Lassi Hentilä, Jesper Ø. Nielsen, and Gert F. Pedersen
Submitted to *IEEE Antennas and Wireless Propagation Letters.*

Motivation

The work in the literature (see, e.g. Paper A-G) is so far limited to model the Rayleigh fading channel models so far. The discussions on channel models in MIMO OTA standards are limited to Rayleigh fading channel models as well. However, as shown in numerous contributions in the literature, the Rayleigh fading channel model is not generally valid. Often a specular path exists between the transmitter (Tx) and the Rx. The time varying envelope of the received signal in the multipath environment is often modeled by a Rician distribution, characterized by the K factor. Furthermore, Rician scenarios are expected to be more likely, as future cell sizes will further decrease. To test MIMO capable terminals in realistic environments in the lab, there is a strong need to model Rician channel models in the multi-probe setups.

Paper content

In this paper, a novel technique is proposed to model the Rician fading channel models in the multi-probe setup, where the LOS path with an arbitrary incident direction is possible and a non-LOS (NLOS) component with arbitrary power angular spectrum (PAS) shape can be modeled. More specifically, the specular path is modeled using the so-called plane wave synthesis (PWS) technique, while the scattering NLOS component can be modeled with the PFS technique. Simulations to demonstrate how accurately the emulated Rician channel approaches the target channel models in terms of field envelope distribution, K factor Doppler power spectrum and spatial correlation at the Rx side are carried out.

Main Results

A method to create Rician fading channel model with a LOS component with arbitrary polarization and direction is proposed. Both phase and amplitude calibration are required to model the LOS component. Simulation results show that the field envelope distribution, K factor, and Doppler spectrum of the emulated channels match well with the target. The emulated spatial correlation at the Rx side follows the target well up to 0.7λ and deviates after that due to the fact that the test area size, inside which

the spatial characteristics of the channel are accurately modeled, is limited with eight probes.

Paper I

Channel Verification Results for the SCME models in a Multi-Probe Based MIMO OTA Setup

Wei Fan, Xavier Carreño, Jagjit S. Ashta, Jesper Ø. Nielsen, Gert F. Pedersen and Mikael B. Knudsen

Presented in the *IEEE* 78^{th} *Vehicular Technology Conference (VTC Fall)*, Las Vegas, USA, 2013.

Motivation

The CTIA MIMO OTA Sub Group (MOSG) has been investigating aspects related to MIMO OTA performance evaluation and an inter-lab/inter-technique OTA performance comparison testing campaign was started in 2012, where the focus is on comparing results of the same methods in different labs and results between different methods. In order to ensure different MIMO OTA techniques render comparable testing results, test prerequistes are defined in detail. That is, ENodeB configuration, MIMO channel models used for evaluation of MIMO devices, emulated base station (BS) setup, device under test (DUT) and DUT orientation are specified. One prerequisite is that target channel models should be correctly implemented inside the test area for all techniques. And hence channel verification measurements are necessary in the test campaign.

Paper content

In the paper, we first describe the multi-probe anechoic chamber setup used for channel verification measurements and then we present the channel verification results and possible causes for the deviations found in the results..

Main Results

This paper describes the multi-probe anechoic chamber setup used to perform the Inter-lab/inter-technique measurements and presents the channel verification results. Good match between measurements and target has been achieved in terms of PDP, temporal correlation, spatial correlation and cross polarization ratio of the channel. This paper shows that the all the key parameters of the SCME models can be accurcately reproduced in a multi-probe anechoic chamber based MIMO OTA setup.

Paper J

Measurement Uncertainty Investigation in the Multi-probe OTA Setups
Wei Fan, Istvan Szini, Michael D. Foegelle, Jesper Ø. Nielsen, Gert F. Pedersen
Presented in the 8^{th} *European Conference on Antennas and Propagation (EuCAP)*, The Hague, The Netherlands, 2014.

Motivation

As a mandatory step for standardization, it is required to analyze the sources of errors and uncertainties in the measurements. Very few contributions have addressed the measurement uncertainties in a multi-probe OTA system. This paper attempts to compare and understand measurement uncertainty levels with different labs, i.e. at Aalborg university, Denmark, Motorola Mobility, USA and ETS-Lindgren, USA, thus to show key aspects related to the multi-probe system setup design.

Paper content

The paper started by first presenting the multi-probe anechoic chamber setup and the measurement items related to system uncertainty levels. Detailed measurement procedure and measurement results are reported for each measurement item.

Main Results

In this contribution, we presented the uncertainty measurements performed in three different multi-probe setups. Main findings of the work are: 1). Cable effects will distort the radiation pattern of the DUT and hence affect the results of the measurements. By use of a choke cartridge or Ferrite loaded cable, the cable effect can be minimized. Field synthesis measurements demonstrated the improved results with chokes/cartridges and Ferrite loaded cables. 2). Polystyrene that used to support the DUT in the AAU setup introduces instability after movement. Turntables used in the MM and ETS setup are more stable. 3). Unflat frequency response of the OTA system can be introduced by the channel emulator, termination of the cables (probe antenna) and mismatch between the components. 3). Good agreement between the measured plane wave and the target plane wave both for the vertical and horizontal polarizations is obtained in the MM and ETS setup.

5 Summary and Future Work

The main objective in the thesis throughout contributions is to reproduce desired radio channels in the multi-probe anechoic chamber setups with limited number of probes for testing MIMO capable terminals. The link between the papers are described, along

with their perspective and consequences in this part. Several remaining challenges are discussed as well for the future work.

5.1 Summary

Techniques to reproduce desired radio channels are investigated theoretically and experimentally in the thesis. In Paper A, the objective is to reproduce an multipath channels with an arbitrary number of clusters, each associated with an arbitrary mean AoA and AS impinging the test zone. Simulation results show that the proposed emulation technique presents better performance compared with existing commercial techniques. This improvement is further demonstrated by measurement results in a practical MIMO OTA setup. Paper A is limited to model 2D channel models with multiple probes uniformly located on a 2D MIMO OTA ring. Paper E extended the technique to model 3D channel models. The DUT radiation pattern is assumed irrelevant for channel emulation accuracy in Paper A and Paper E. In Paper B, a detailed investigation on the DUT radiation pattern impact is carried out theoretically and experimentally. Results have demonstrated that to test realistic DUTs with higher variations in directivity, we need more probes to maintain the same received voltage and spatial correlation accuracy level. To reduce the system cost, a probe selection mechanism and a flexible probe configuration concept are proposed in Paper D and G, respectively, based on the techniques proposed in Paper A and Paper E. In Paper A, B, C, E and G, spatial correlation is selected as FoM to determine the test zone size. However, there is a concern whether it is optimal, as the ultimate goal is to investigate whether performance of MIMO capable terminals, e.g. data throughput, can be accurately evaluated in the laboratory. And hence, a detailed investigation on the relationship between capacity emulation accuracy and test area size is performed in Paper D, theoretically and experimentally. In Paper F, a technique based on a virtual UCA to estimate discrete PAS modeled in multi-probe setups is proposed, unlike work limited to spatial correlation in the other papers. This technique is useful to verify how well the channels are implemented in the lab. In Paper H, a technique to create Rician channel models in the multiprobe anechoic chamber setups is proposed, while the discussions in other papers in the thesis are limited to model Rayleigh fading channel models. The focus of Paper I and Paper J is on experimental verification of techniques addressed in Paper A, where sources of uncertainties in practical multi-probe setups are identified.

5.2 Future work

Though extensive efforts have been made to the standardization of evaluating MIMO capable terminals, some research challenges still exist in the multi-probe anechoic chamber based methods. Some examples are mentioned below:

- Throughput prediction model for MIMO OTA testing. Data throughput has been

selected as the FoM in MIMO OTA standards to rank MIMO capable terminals. Extensive measurement campaigns have been performed in different laboratories and numerous measurement results have been reported in the literature, see e.g. [39]. Inter-lab OTA performance comparison testing campaign was started in 2012, where the focus is on comparing results of the same methods in different labs. However, deviations in measurement results still exist among laboratories and exact causes are still missing. There is a strong need to develop a throughput simulation model with reasonable accuracies. A sound simulation model is desired, as it can help eliminate potential systematic errors in measurements and it would enable more insight into the test results.

- Full duplex channel modeling for MIMO OTA testing. Research work in multi-probe based systems has been focused on emulating realistic downlink (communication from BS to MS) channel models, where the uplink channel is generally realized through a single communication antenna and a cable. Emulating of realistic full duplex channel models (i.e. both downlink and uplink) is becoming more and more important. The uplink channel state information can be critical for downlink performance in some closed loop communication systems with adaptive modulation, coding and MIMO transmission modes. Furthermore, to reduce the difference in peak data rate on the uplink and downlink, uplink with up to 4 transmission antennas (i.e. 4 antennas on mobile terminals are used for transmission) is introduced in LTE-Advanced (Release 10 and beyond). Realistic channel models have to be emulated for the uplink as well to evaluate the uplink MIMO performance.

- Testing of larger devices, e.g. cars. More and more wireless systems have been included in modern vehicles in automobile industry. Besides cellular service, car to car and car to infrastructure communications have attracted great attention as well. There is a need to test the performance of these wireless systems in real environments [50]. Compared with mobile handset testing, testing wireless systems in the cars is more challenging due to requirement of much larger test zone.

- Testing MIMO terminals with adaptive radiation patterns. MIMO terminals with steerable radiation patterns have been proposed in many contributions. Unlike conventional handsets with fixed radiation pattern, terminals equipped with steerable antenna patterns can adapt to the propagation environments, to achieve better performance. Multi-probe anechoic chamber based method is applicable for evaluating smart MIMO terminals as well. However, many open issues still remain and more investigation is required.

- Virtual drive testing. There is a strong need to replay the field recorded radio channels in the laboratory. Research work in the literature has been focused on

reproducing synthesized standard radio channels (e.g. SCME channel models) in the laboratory. Virtual drive testing (VDT), which targets to reproduce practical recorded channels in the anechoic chamber, has attracted great research attention recently. In [47], the idea of VDT was presented, without showing any result in the anechoic chamber, though.

6 Conclusion

In addition to the individual conclusions in the papers comprising the main part of the thesis, it is now possible to take a step back and draw some overall conclusions. The thesis mainly addresses techniques to reproduce radio propagation channels in the anechoic chamber with limited number of probes. Both the PFS and PWS technique can be utilized to emulate stationary channel models with specified PASs. The PWS technique can be used to reproduce arbitrary channel models (e.g. channels with time-varying angles of arrival). Both Rayleigh and Ricean fading channel models are considered in the thesis. It has been shown that, with a limited number of probes, the test zone where the channel can be accurately reproduced is limited. The test zone size depends on the probe configuration, frequency, number of probes, target channel models, acceptable error level and DUT radiation patterns. Both the PFS and PWS techniques are extended for modeling 3D radio channels. To reduce the system cost, a probe selection algorithm and flexible probe setup concepts are proposed. Results have demonstrated that compared with fixed setups, accurate channel emulation results can still be achieved within the test zone with a smaller number of probes in a flexible setup. Most algorithms and concepts proposed in the thesis are supported with measurement results in practical setups. It has been shown that the simulation results can be well reproduced in the laboratory. Measurement uncertainties in practical are investigated, where sources of errors, e.g. cable connection, turntable stability, cable reflection, etc. are identified. It has been demonstrated theoretically and experimentally that radio propagation environments with desired channel characteristics can be accurately reproduced with within a test zone with limited number of probes.

References

[1] A. Paulraj, D. Gore, R. Nabar, and H. Bolcskei, "An overview of MIMO communications - a key to gigabit wireless," *Proceedings of the IEEE*, vol. 92, no. 2, pp. 198–218, Feb 2004.

[2] CTIA, "Method of measurement for radiated RF power and receiver performance," CTIA certification program, test plan for mobile station over the air performance, January 2011.

[3] 3GPP, "User equipment (UE) / mobile station (MS) over the air (OTA) antenna performance," 3GPP, TR TS 34.114 V11.1.0, Jun. 2013.

[4] T. Taga, "Analysis for mean effective gain of mobile antennas in land mobile radio environments," *Vehicular Technology, IEEE Transactions on*, vol. 39, no. 2, pp. 117–131, 1990.

[5] M. Jensen and J. Wallace, "A review of antennas and propagation for MIMO wireless communications," *Antennas and Propagation, IEEE Transactions on*, vol. 52, no. 11, pp. 2810–2824, Nov 2004.

[6] R. Irmer, H. P. Mayer, A. Weber, V. Braun, M. Schmidt, M. Ohm, N. Ahr, A. Zoch, C. Jandura, P. Marsch, and G. Fettweis, "Multisite field trial for LTE and advanced concepts," *Communications Magazine, IEEE*, vol. 47, no. 2, pp. 92–98, February 2009.

[7] 3GPP, "Verification of radiated multi-antenna reception performance of User Equipment," 3GPP, TR 37.977 V1.0.0, Sep. 2013.

[8] M. Rumney, R. Pirkl, M. H. Landmann, and D. A. Sanchez-Hernandez, "MIMO Over-The-Air Research, Development, and Testing," *International Journal of Antennas and Propagation*, vol. 2012, 2012.

[9] M. Garcia-Fernandez, J. Valenzuela-Valdes, and D. Sanchez-Hernandez, "Latest advances in mode-stirred reverberation chambers for MIMO OTA evaluation of wireless communications devices," in *Antennas and Propagation (EUCAP), Proceedings of the 5th European Conference on*, April 2011, pp. 2427–2431.

[10] P. S. Kildal, C. Orlenius, and J. Carlsson, "OTA Testing in Multipath of Antennas and Wireless Devices With MIMO and OFDM," *Proceedings of the IEEE*, vol. 100, no. 7, pp. 2145–2157, July 2012.

[11] Y. Jing, X. Zhao, H. Kong, S. Duffy, and M. Rumney, "Two-Stage Over-the-Air (OTA) Test Method for LTE MIMO Device Performance Evaluation," *International Journal of Antennas and Propagation*, vol. 2012, 2012.

[12] W. Yu, Y. Qi, K. Liu, Y. Xu, and J. Fan, "Radiated Two-Stage Method for LTE MIMO User Equipment Performance Evaluation," no. 99, 2014, pp. 1–6.

[13] J. W. Wallace, R. Mehmood, and M. A. Jensen, "Electronically Reconfigurable Reverberation Chambers," in *Antennas and Propagation (EUCAP), Proceedings of the 8th European Conference on.* IEEE, 2014.

[14] T. Adam and G. Christoph, "On Spatial Characteristics of the Decomposition Method in MIMO OTA Testing ," in *Antennas and Propagation (EUCAP), Proceedings of the 8th European Conference on.* IEEE, 2014.

[15] M. B. Knudsen and G. F. Pedersen, "Spherical outdoor to indoor power spectrum model at the mobile terminal," *Selected Areas in Communications, IEEE Journal on*, vol. 20, no. 6, pp. 1156–1169, 2002.

[16] T. Laitinen and P. Kyösti, "On appropriate probe configurations for practical MIMO over-the-air testing of wireless devices," in *Antennas and Propagation (EUCAP), 2012 6th European Conference on*, 2012, pp. 1544–1548.

[17] A. Khatun, H. Laitinen, V.-M. Kolmonen, and P. Vainikainen, "Dependence of Error Level on the Number of Probes in Over-the-Air Multiprobe Test Systems," *International Journal of Antennas and Propagation*, vol. 2012, 2012.

[18] P. Kyösti and A. Khatun, "Probe configurations for 3D MIMO Over-the-Air testing," in *Antennas and Propagation (EuCAP), 2013 7th European Conference on*, April 2013, pp. 1421–1425.

[19] T. Laitinen, P. Kyösti, J. P. Nuutinen, and P. Vainikainen, "On the number of OTA antenna elements for plane-wave synthesis in a MIMO-OTA test system involving a circular antenna array," in *Antennas and Propagation (EuCAP), 2010 Proceedings of the Fourth European Conference on*, April 2010, pp. 1–5.

[20] J. Toivanen, T. Laitinen, V. Kolmonen, and P. Vainikainen, "Reproduction of Arbitrary Multipath Environments in Laboratory Conditions," *Instrumentation and Measurement, IEEE Transactions on*, vol. 60, no. 1, pp. 275–281, 2011.

[21] P. Kyösti, T. Jämsä, and J. Nuutinen, "Channel modelling for multiprobe over-the-air MIMO testing," *International Journal of Antennas and Propagation*, 2012.

[22] P. Kyösti, J. Nuutinen, and T. Laitinen, "Over the air test," Patent WO 2012/117 147 A1, Sep. 7, 2012.

[23] W. Fan, X. Carreño, J. Ø. Nielsen, K. Olesen, M. Knudsen, and G. Pedersen, "Measurement Verification of Plane Wave Synthesis Technique Based on Multi-Probe MIMO-OTA Setup," in *Vehicular Technology Conference (VTC Fall), 2012 IEEE*, 2012, pp. 1–5.

[24] W. A. T. Kotterman, A. Heuberger, and R. Thoma, "On the accuracy of synthesised wave-fields in MIMO-OTA set-ups," in *Antennas and Propagation (EUCAP), Proceedings of the 5th European Conference on*, April 2011, pp. 2560–2564.

[25] W. A. T. Kotterman, M. Landmann, A. Heuberger, and R. Thoma, "New laboratory for Over-The-Air testing and Wave Field Synthesis," in *General Assembly and Scientific Symposium, 2011 XXXth URSI*, Aug 2011, pp. 1–4.

[26] T. Laitinen, P. Kyösti, T. Jämsä, and P. Vainikainen, "Generation of a field with a Laplacian-distributed power azimuth spectrum scattered by a single cluster in a MIMO-OTA test system based on multiple probe antennas," in *Microwave Conference Proceedings (APMC), 2010 Asia-Pacific*, Dec., pp. 2127–2130.

[27] P. Kyösti and J. Nuutinen, "Over the air test," Patent US 20 110 189 962, Aug. 4, 2011.

[28] M. A. Mow, B. Niu, R. W. Schlub, and R. Caballero, "Tools for design and analysis of over-the-air test systems with channel model emulation capabilities," Patent US 20 110 270 567, Nov. 3, 2011.

[29] J. D. Reed, "Emulation and controlled testing of MIMO OTA channels," Patent US 20 110 299 570, Dec. 8, 2011.

[30] W. Fan, J. Nielsen, O. Franek, X. Carreño, J. Ashta, M. Knudsen, and G. Pedersen, "Antenna Pattern Impact on MIMO OTA Testing," *Antennas and Propagation, IEEE Transactions on*, vol. 61, no. 11, pp. 5714–5723, Nov 2013.

[31] L. Hentila, P. Kyösti, and J. Meinila, "Elevation extension for a geometry-based radio channel model and its influence on MIMO antenna correlation and gain imbalance," in *Antennas and Propagation (EUCAP), Proceedings of the 5th European Conference on.* IEEE, 2011, pp. 2175–2179.

[32] W. Fan, P. Kyösti, S. Fan, J. Nielsen, X. Carreño, G. Pedersen, and M. Knudsen, "3D Channel Model Emulation in a MIMO OTA Setup," in *Vehicular Technology Conference (VTC Fall), 2013 IEEE 78th*, Sept 2013, pp. 1–5.

[33] M. A. Mow, R. W. Schlub, and R. Caballero, "System for testing multi-antenna devices," Patent US 2011/0 084 887 A1, Apr. 14, 2011.

[34] P. Kyösti and A. Khatun, "Probe Configurations for 3D MIMO Over-the-Air Testing," in *Antennas and Propagation (EUCAP), Proceedings of the 7th European Conference on.* IEEE, 2013.

[35] O. Franek and G. Pedersen, "Spherical horn array for wideband propagation measurements," *Antennas and Propagation, IEEE Transactions on*, vol. 59, no. 7, pp. 2654–2660, July 2011.

[36] M. Sonkki, V. Hovinen, and E. Salonen, "Scattering Properties of Wideband Dual-Polarized Vivaldi Antenna for MIMO OTA," in *XXXIII Finnish URSI Convention on Radio Science and SMARAD Seminar*, April 2013.

[37] P. Kyösti and L. Hentilä, "Criteria for physical dimensions of MIMO OTA multi-probe test setup," in *Antennas and Propagation (EUCAP), 2012 6th European Conference on.* IEEE, 2012, pp. 2055–2059.

[38] Wei Fan and Carreño, X. and Nielsen, J.Ø. and Ashta, J.S. and Pedersen, G.F. and Knudsen, M.B., "Verification of Emulated Channels in Multi-Probe Based MIMO OTA Testing Setup," in *Antennas and Propagation (EUCAP), Proceedings of the 7th European Conference on*. IEEE, 2013.

[39] A. Scannavini, F. Chauvet, and N. Gross, "MIMO OTA measurement with anechoic chamber method," in *Antennas and Propagation (EUCAP), 2013 7th European Conference on*. IEEE, April 2013.

[40] W. Fan, X. Carreño, J. Ø. Nielsen, M. B. Knudsen, and G. F. Pedersen, "Channel Verification Results for the SCME models in a Multi-Probe Based MIMO OTA Setup," in *Vehicular Technology Conference (VTC Fall)*. IEEE, September 2013, pp. 1–5.

[41] P. Kyösti, J.-P. Nuutinen, and T. Jämsä, "MIMO OTA test concept with experimental and simulated verification," in *Antennas and Propagation (EuCAP), Proceedings of the Fourth European Conference on*. IEEE, 2010, pp. 1–5.

[42] H. Iwai, A. Yamamoto, T. Sakata, K. Ogawa, K. Sakaguchi, and K. Araki, "Spatial fading emulator for handset antennas," in *Antennas and Propagation Society International Symposium, 2005 IEEE*, vol. 1A, July 2005, pp. 218–221 Vol. 1A.

[43] S. Pasisingi, K. Nakada, A. Kosako, and Y. Karasawa, "Performance evaluation of a mimo channel model for simplified ota test systems," *EURASIP Journal on Wireless Communications and Networking*, vol. 2013, no. 1, 2013. [Online]. Available: http://dx.doi.org/10.1186/1687-1499-2013-285

[44] T. Hansen, "Plane wave generation within a small volume of space for evaluation of wireless devices," Patent, feb, 2013, US Patent App. 13/569,518.

[45] I. Szini, G. Pedersen, A. Scannavini, and L. Foged, "MIMO 2×2 reference antennas concept," in *Antennas and Propagation (EUCAP), 2012 6th European Conference on*, March, pp. 1540–1543.

[46] S. Zhang, K. Zhao, B. Zhu, Z. Ying, and S. He, "MIMO reference antennas for OTA applications," in *Antennas and Propagation (EuCAP), 2013 7th European Conference on*, April 2013, pp. 2556–2557.

[47] P. Kyösti, P. Kemppainen, and T. Jämsäs, "Radio Channel Measurements in Live LTE Networks for MIMO Over-the-Air Emulation," in *Antennas and Propagation (EUCAP), 2014 8th European Conference on*, 2014.

[48] I. Szini, G. F. Pedersen, S. Del Barrio, and M. Foegelle, "LTE Radiated Data Throughput Measurements, Adopting MIMO 2x2 Reference Antennas," in *Vehicular Technology Conference (VTC Fall), 2012 IEEE*, Sept 2012, pp. 1–5.

[49] I. Szini, M. Foegelle, D. Reed, T. Brown, and G. Pedersen, "On Antenna Polarization Discrimination, Validating MIMO OTA Test Methodologies," *Antennas and Wireless Propagation Letters, IEEE*, vol. 13, pp. 265–268, 2014.

[50] M. Nilsson, P. Hallbjorner, N. Araback, B. Bergqvist, and F. Tufvesson, "Multipath propagation simulator for v2x communication tests on cars," in *Antennas and Propagation (EuCAP), 2013 7th European Conference on*, April 2013, pp. 1342–1346.

[51] S. Rajesh, K. Wim, L. Markus, and el., "Over-the-Air Testing of Cognitive Radio Nodes in a Virtual Electromagnetic Environment," *International Journal of Antennas and Propagation*, vol. 2013, 2013.

Part II

Papers

Paper A

Emulating Spatial Characteristics of MIMO Channels for OTA Testing

Wei Fan, Xavier Carreño, Fan Sun, Jesper Ø. Nielsen, Mikael B. Knudsen and Gert F. Pedersen

The paper has been published in the
IEEE Transactions on Antennas and Propagation vol. 61, no. 8, pp. 4306–4314, Aug. 2013.

The layout has been revised.

Emulating Spatial Characteristics of MIMO Channels for OTA Testing

Wei Fan, Xavier Carreño, Fan Sun, Jesper Ø. Nielsen, Mikael B. Knudsen and Gert F. Pedersen

***Abstract*—This paper discusses over the air (OTA) testing for multiple input multiple output (MIMO) capable terminals with emphasis on channel spatial characteristics emulation. A novel technique to obtain optimum power weights for the OTA probes based on convex optimization is proposed. The proposed technique emulates spatial correlation as well as introduces constraints on the maximum deviation between the target power azimuth spectrum (PAS) and the emulated PAS in terms of mean angle of arrival (AoA) and azimuth spread (AS). Simulation results show that the proposed emulation technique present better performance compared with existing techniques in the literature. This improvement is further demonstrated by measurement results in a practical MIMO OTA setup.**

***Index Terms*—Channel emulation, MIMO OTA, anechoic chamber, power azimuth spectrum, spatial correlation, convex optimization.**

I. Introduction

The Multiple Input Multiple Output (MIMO) technique is an attractive and promising technology to improve performance of wireless communication systems. With MIMO technology being adopted by new wireless technologies such as LTE, LTE-Advanced and WIMAX, mobile network operators and manufactures urgently require standard test methods which are suitable to test the MIMO device performance. MIMO Over The Air (OTA) testing, which is considered a promising solution to evaluate devices in realistic situations, has attracted huge interest from both industry and academia. Many different MIMO test methods have been proposed which vary widely in how they emulate the propagation channel. An overview was presented in [1].

One promising approach is a multi-probe anechoic chamber based method. With this method, multipath environments in which the performance of the device is evaluated can be physically emulated in a controllable manner. The focus is on reproducing spatial aspects of the channel, which is new and critical as we extend Single Input Single Output (SISO) OTA to MIMO OTA testing.

The concept of clusters has been widely adopted to model the multipath phenomenon based on extensive measurements. A cluster has a specific Power Azimuth Spectrum (PAS) shape. For MIMO OTA testing, it is desirable that with a limited number of probes we should generate an arbitrary number of clusters, each associated with an arbitrary mean Angle of Arrival (AoA) and Azimuth Spread (AS) impinging the test zone. It has been shown that the essence is to find proper power weightings for each probe such that channel spatial characteristics can be recreated [2]–[5]. This idea was named prefaded signal synthesis technique and was detailed in [4]. Several optimization techniques are proposed to obtain optimum probe power weightings. However, most techniques, which are based on numerical optimization, can be very computationally inefficient.

The PAS is of great importance for multiple antenna techniques with spatial treatment of the incoming signals. The spatial correlation between the waves impinging on two antenna elements depends on the PAS and on the radiation pattern of the antenna elements. Spatial correlation has been selected as the main figure of merit to characterize the channel spatial information, while cluster PAS shape parameters including AS and mean AoA are often ignored [2], [3], [5]. Channel profiles with the same spatial correlation may present very different PAS shapes when the spatial sampling points for spatial correlation calculation are limited, e.g. on a line [3], [4] or on a circle [6]. To solve the problem, a new way to select spatial samples for optimization is proposed in this paper. Also, to obtain an accurate resulting PAS shape in terms of AoA and AS, constraints are introduced for spatial correlation emulation. Note that emulation accuracy in this paper denotes the difference between emulated spatial correlation resulting from the discrete PAS composed by the probe power weights and target spatial correlation resulting from the continuous PAS. To the best of our knowledge, the proposed spatial sample selection method and the spatial correlation emulation with constraints on the resulting discrete PAS have not been achieved in the literature so far. In [3]–[6], spatial correlation was selected as the objective function without constraints on the resulting discrete PAS shape, although the possibility of joint optimizing cluster mean AoA and spatial correlation was briefly mentioned in [3].

In this paper, we first form the channel emulation problem with constraints on the resulting discrete PAS shape such as AS and mean AoA, when angular locations of OTA probes are fixed. We further illustrate the problem can be expressed as a convex optimization problem [7], which can be solved efficiently. The main contributions of this work are two-fold: the proposed emulation problem with constraints on the resulting discrete PAS shape gives a more realistic characterization; employing convex optimization framework into channel emulation can greatly reduce the computational complexity compared to known results based on numerical optimizations. Furthermore, the relationship between the required number of

Wei Fan, Fan Sun, Jesper Ø. Nielsen, and Gert F. Pedersen are with the Antennas, Propagation and Radio Networking section at the Department of Electronic Systems, Faculty of Engineering and Science, Aalborg University, Denmark (email: {wfa, fs, jni, gfp}@es.aau.dk).

Xavier Carreño and Mikael B. Knudsen are with Intel Mobile Communications, Denmark (email: {xavier.carreno, mikael.knudsen}@intel.com).

probes and test area size is derived based on the proposed optimization technique. Also, the impact of channel models on the emulation accuracy has been investigated. In the end the proposed optimization algorithm is compared with the algorithm implemented in a commercial channel emulator in a practical MIMO OTA setup and better emulation accuracy is demonstrated by the measurement results.

Notations: $||\cdot||_1$ and $||\cdot||_2$ denote the first order norm and the second order norm, respectively. $vec()$ is vectorization operator which converts a matrix into a column vector.

II. Method

A. Configuration of MIMO OTA setup and problem statement

Figure 1 illustrates a general setup for the multi-probe anechoic chamber based method. Probes are located on a horizontally oriented ring and a Device Under Test (DUT) is placed at the center of the anechoic chamber. To alleviate the complexity and cost of 3D multi-probe setup, the simpler 2D configurations are considered in this work.

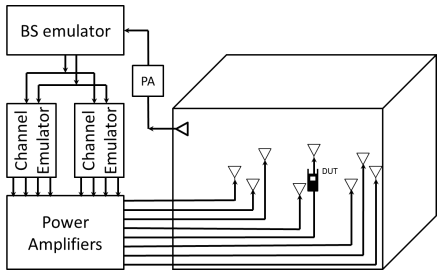

Fig. 1. An illustration of the MIMO OTA setup. The measurement system consists of a Base Station (BS) emulator, one or several channel emulators, an anechoic chamber, probes, a DUT, a turntable, cables and power amplifiers. Test area defines the maximum dimension of the DUT and is an area where target channel characteristics are reproduced with certain accuracy requirement.

The idea of prefaded signal synthesis technique is to radiate independent fading signals from multiple probes on the basis of power weights determined by the emulated channel [2], [4], [5]. In order to reconstruct the PAS of each cluster, a single cluster should be mapped to several OTA probes depending on the PAS shape and OTA probe angular locations. For each cluster, receiver side spatial characteristics are reconstructed by allocating appropriate average power weights to the associated OTA probes. The focus of this paper is to obtain optimum power weightings to recreate the target channel spatial characteristics.

B. Channel PAS model

PAS shape of clusters have been widely studied in the literature. Several PAS models, namely wrapped Gaussian [8], uniform, truncated Laplacian [9] and Von Mises distribution [10] have been proposed based on extensive measurements in various scenarios. For the sake of simplicity, we assume each cluster is defined with an interval of $[\phi_p - \pi, \phi_p + \pi]$ centered at AoA ϕ_p. Figure 2 illustrates several different PAS distributions.

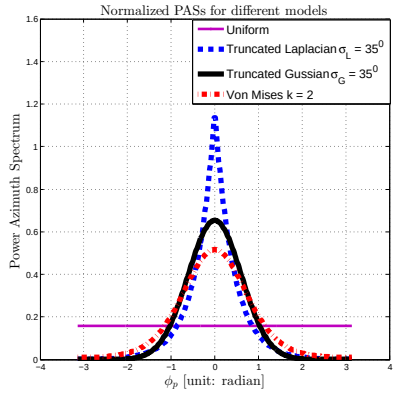

Fig. 2. Normalized PASs. For the 4 different PASs, the clusters have the same mean angle of incidence $\overline{\phi_p} = 0^o$. σ_G and σ_L are standard deviations of wrapped Gaussian and truncated Laplacian distribution respectively. k in Von Mises distribution controls the angle spread.

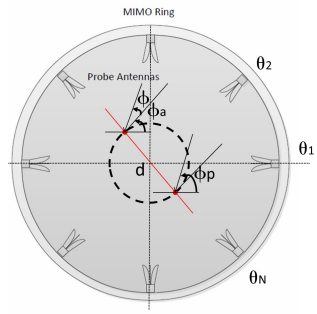

Fig. 3. An illustration of the OTA probe setup. θ_i is angular location of the ith probe.

C. Criterion to model channel spatial characteristics

The spatial correlation has been selected as a main criterion to model spatial characteristics of the channel [2], [4], [5]. Spatial correlation is a statistical measure of the similarity of the received signals. The angle notations are illustrated in Figure 3. A plane wave with AoA ϕ_p impinges on an array with two antenna elements separated by a distance d, the direction of the array boresight is ϕ_a. ϕ is the angle of the plane wave with respect to the boresight of the antenna elements. As detailed in [11], the spatial correlation can be written as:

$$\rho = \frac{\int_{-\pi}^{\pi} G_1(\phi) G_2^*(\phi) p(\phi) d\phi}{\sqrt{\int_{-\pi}^{\pi} p(\phi)|G_1(\phi)|^2 d\phi} \sqrt{\int_{-\pi}^{\pi} p(\phi)|G_2(\phi)|^2 d\phi}} \quad (1)$$

where G_1 and G_2 are the complex radiation patterns of antenna element 1 and 2, respectively, with a common phase center. $p(\phi)$ is the PAS. In order to be used as an angular power density function, the $p(\phi)$ needs to satisfy $\int_{-\pi}^{\pi} p(\phi) d\phi = 1$.

As stated in [4], the antenna pattern is usually assumed omnidirectional for channel emulation purpose since the DUT

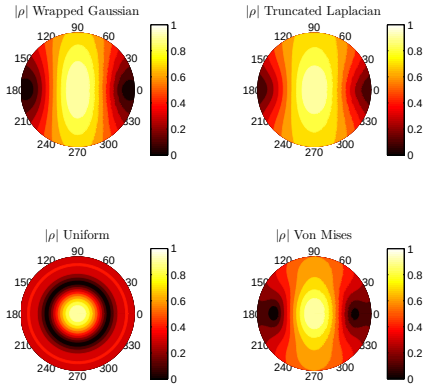

Fig. 4. Theoretical spatial correlation $|\rho|$ for the PASs shown in Figure 2. Test area size: 0.7λ.

antenna pattern is typically unknown. Using this property, we can rewrite (1) as

$$\rho(d,\phi_a) = \int_{-\pi}^{\pi} \exp(-j2\pi\frac{d}{\lambda}\sin(\phi_p-\phi_a))p(\phi_p)d\phi_p. \quad (2)$$

A specific PAS can be formed by introducing a number of plane waves each with an appropriate AoA and power value. Two different methods to discretize the PAS were discussed in the literature. One method allocates the same power to each ray while arranging the plane wave angles in a non-uniform manner. In the other method, the power of the rays follows the PAS distribution with their angles uniformly distributed.

The mean AoA $\overline{\phi_p}$ and AS σ_p are also used to model the PAS, which are defined according to the definition in the Annex A of [12]. Note that circular AS is introduced to solve the ambiguity problem for the AS of the PAS.

As illustrated in Figure 4, spatial correlation is a function of the normalized antenna distance d and antenna orientation ϕ_a. Each sub-figure corresponds to one PAS shown in Figure 2. The radius and polar angle of each point on the plots correspond to the value at distance d and antenna orientation ϕ_a. Maximum radius of the circle corresponds to the test area size. The correlation globally decreases with increasing distance for all PASs, as expected.

D. Optimal Probe Power Weights

As detailed below, the goal is to obtain the optimum OTA probe power weights so as to:

- Minimize the deviation between the theoretical spatial correlations resulting from a target PAS and the correlation resulting from a discrete PAS characterized by power weights of the probes.
- Constrain the maximum deviation between the target PAS and a discrete PAS characterized by power weights of the probes in terms of AS and mean AoA.

Several contributions in literature have addressed this issue. In [5], several exhaustive search techniques are used to obtain optimum angular location and power weight for each of the probes. In [2], the angular location of probe is considered as a factor to be optimized in order to build the optimum test system. However, such flexible setup might not be practical in an actual setup. It is desirable that the probes are fixed on the OTA ring where frequent probe location adjustment may pose a huge challenge on system calibration. Given this practical issue, OTA setups with flexible probe locations are not considered in this paper.

1) Emulated spatial correlation: The probe angular locations are depicted in Figure 3. $\boldsymbol{\theta} = [\theta_1, ..., \theta_N]^T$ is the vector containing the fixed angular locations of the probes with $\theta_n \in [0, 2\pi]$ and N is the number of OTA probes. $\boldsymbol{w} = [w_1, ..., w_N]^T$ is the vector containing the power allocated for probes. A location pair (d, ϕ_a) is used to represent the locations of two spatial samples with distance d and orientation ϕ_a, and there are in total M location pairs. The spatial correlation for an antenna pair with antenna separation d and array orientation ϕ_a can be calculated based on the discrete PAS characterized by N probes as:

$$\hat{\rho}(d,\phi_a) = \boldsymbol{w}^T \cdot \boldsymbol{a}(d,\phi_a) \quad (3)$$

where $\boldsymbol{a}(d,\phi_a) = [a_1(d,\phi_a), ..., a_N(d,\phi_a)]^T$ with $a_n(d,\phi_a) = \exp(-j2\pi\frac{d}{\lambda}\sin(\theta_n - \phi_a))$.

2) Practical constraints: An important contribution of this paper is to introduce constraints on the PAS shape for the optimization. Two completely different PASs may result in similar spatial correlations if limited spatial samples are selected for the spatial correlation calculation. Thus, we need to consider the PAS shape as constraints for optimization. It is desirable that the mean AoA $\overline{\phi}^{OTA}$ and AS σ^{OTA} resulting from a discrete PAS should be close to those from the target PAS. In addition, from a realistic point of view, probes with smaller angular distance to the PAS cluster mean AoA $\overline{\phi_p}$ should be allocated with more power, which can be mathematically expressed as $w_i \geq w_j$ for $|\theta_i - \overline{\phi_p}| \leq |\theta_j - \overline{\phi_p}|\,(i \neq j)$. One more constraint with the practical system is that probe weights are limited, as the output gain of typical channel emulators is limited to 0 dB.

3) Objective function: Let us denote $\hat{\boldsymbol{\rho}}$ and $\boldsymbol{\rho}$ to be the emulated spatial correlation and target spatial correlation vectors with each element corresponding to the spatial correlation between two isotropic antennas at a certain location pair. The objective function is evaluated over M location pairs, and hence ρ and $\hat{\rho}$ are $M\times 1$ vectors:

$$\begin{aligned} &\min_{\boldsymbol{w}} \|\hat{\boldsymbol{\rho}}(\boldsymbol{w}) - \boldsymbol{\rho}\|_2^2 \quad (4)\\ &\text{s. t. } \|\boldsymbol{w}\|_1 = 1,\ \ 0 \leq w_i \leq 1\ \ (\forall i \in [1, N])\\ &\quad \left|\mathbf{b}^T\boldsymbol{w} - \overline{\phi_p}\right| \leq \epsilon_{AoA}\\ &\quad \mathbf{c}^T\boldsymbol{w} \leq (\epsilon_{AS} + \sigma_p)^2,\ \mathbf{c}^T\boldsymbol{w} \geq (\epsilon_{AS} - \sigma_p)^2\\ &\quad w_i \geq w_j,\ \ \text{if } |\theta_i - \overline{\phi_p}| \leq |\theta_j - \overline{\phi_p}|\,(i \neq j) \end{aligned}$$

where the mean AoA and AS of the resulting discrete PAS is

$$\overline{\phi}^{OTA} = \sum_{i=1}^{N} \chi_i w_i = \mathbf{b}^T \boldsymbol{w} \tag{5}$$

$$\sigma^{OTA} = \sqrt{\sum_{i=1}^{N} (\chi_i - \overline{\phi_p})^2 w_i} = \sqrt{\mathbf{c}^T \boldsymbol{w}} \tag{6}$$

with

$$\chi_i = \begin{cases} \theta_i - 2\pi & \text{if } \theta_i - \overline{\phi_p} > \pi \\ \theta_i & \text{if } -\pi < \theta_i - \overline{\phi_p} < \pi \\ \theta_i + 2\pi & \text{if } \theta_i - \overline{\phi_p} < -\pi \end{cases}$$

ϵ_{AoA} and ϵ_{AS} are the error tolerance for the emulated PAS in terms of mean AoA and AS respectively. $\mathbf{b}$ and $\mathbf{c}$ being two known $N \times 1$ vectors defined in (5) and (6), repectively. $\boldsymbol{w}$ can be obtained by solving the objective function, which is a quadratic programming problem with linear constraints when the probe positions are fixed. Therefore, we can easily solve the problem in (4) via a popular convex problem solver CVX in [7].

E. Selecting spatial samples inside the test area

1) State of the art: In the following, we first summarize two existing ways to select spatial samples inside the test area in the literature:

- One option is that we can fix ϕ_a while varying d to obtain spatial samples. That is, the spatial samples are selected on a line. d linearly steps from 0 to the test area size D. In [3], the objective function used minimize deviations for a fixed orientation. Also, it is mentioned that cluster AoA can be considered for the joint optimization, but it is not specified further.
- The other option is that we can fix d while varying ϕ_a for optimization. That is, spatial samples are selected on a circle. ϕ_a linearly steps from 0 to 2π. In [5], the optimization was done for a fixed distance.

2) Proposed spatial sample point selection: The above-mentioned two ways to obtain spatial samples will give optimum results at a certain fixed orientation ϕ_a or a certain fixed separation d. However, they might not give optimum emulation results for all orientations and separations within the test area and emulation accuracy might be critically bad at some orientations or separations. As for the new proposal, samples are covering the whole test area. d is swept linearly from 0 to the test area size D and ϕ_a is swept linearly from 0 to 2π for the optimization.

Note that for limited spatial sample points cases, e.g. spatial samples are selected on a line or on a circle, constraints on discrete resulting PAS shape have to be added for spatial correlation optimization. Otherwise the resulting discrete PAS might be very different from the target PAS. Similarly, if other objective functions, e.g. $||\rho| - |\hat{\rho}||$ in [6] is selected, adding the constraint on the resulting PAS shape will also be beneficial to obtain accurate resulting PAS shape. With the proposed technique to select spatial samples, the resulting discrete PAS will be close to the target continuous PAS shape and the constraints on the PAS shape are not critical. Usually the constraints on resulting PAS shape will be automatically satisfied. An accurate resulting PAS shape can be obtained by adding the constraints in the optimization, with a slight degradation for spatial correlation optimization if the constraints on resulting discrete PAS are necessary. Below in the simulation the error tolerance ϵ_{AS} and ϵ_{AoA} are selected to be 1^o to obtain accurate AoA and AS of the resulting PAS.

F. Emulation for multi-cluster PAS

The radio waves could gather in several clusters distributed over the space domain. In standard channel models, i.e. SCME [9], clusters are with different delays. Techniques to emulate the multi-cluster PAS are discussed in [6]. In order to preserve the delay information, each cluster is emulated individually with the probes. The SCME Urban macro (UMA) TDL model (six Laplacian shaped clusters) from [9] has been selected as the target channel model for emulation in this paper. The normalized power weights for each cluster in the SCME UMA TDL model are shown in Figure 5. Note that the power weights need to be scaled according to the power per cluster as specified in the SCME UMA TDL model. Extensive measurements on the channel emulator uncertainty level have been performed previously, e.g. [13]. Measurement results have shown that the power weight information can be accurately generated in the channel emulator. Spatial correlation $|\rho|$ for the SCME UMA TDL model are shown in Figure 6.

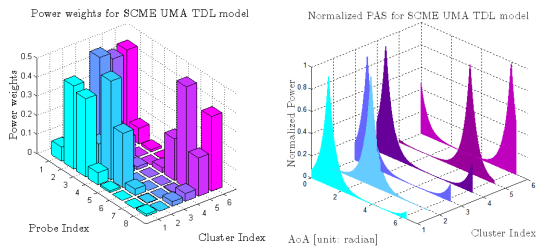

Fig. 5. Normalized power weights for each cluster in the SCME UMA TDL model obtained with the proposed technique.

III. Simulation Results

The emulation results for different PASs are firstly shown in this part. After that, several algorithms in the literature are compared with the proposed solution in terms of spatial correlation error. Furthermore, the impact of cluster PAS on the correlation error has been investigated. In the end of this part, the relationship between the required number of probes and test area size is shown for the proposed optimization technique. For the possibility to recreate any spatial channel model without relocation of the probes, the configuration where all the probes are equally spaced on an OTA ring is considered in the simulation. The number of probes N is selected to be 8 unless otherwise stated.

A. Spatial correlation for different PASs

As we can see in Figure 7, correlation error depends on the the channel model and generally gets worse as the normalized distance increases. Wrapped Gaussian and truncated Lapacian distributions shown in Figure 2 present similar correlation error.

The correlation error $|\hat{\rho} - \rho|$ for SCME UMA TDL model with the proposed algorithm is shown in Figure 6. Maximum deviation of 0.03 is achieved over the test area size 0.5λ.

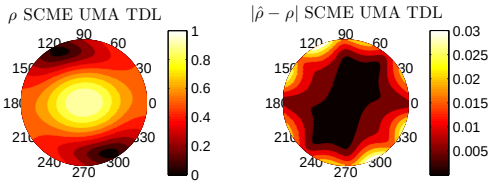

Fig. 6. $|\rho|$ and correlation error $|\hat{\rho} - \rho|$ for SCME UMA TDL model. Test area size: 0.5λ.

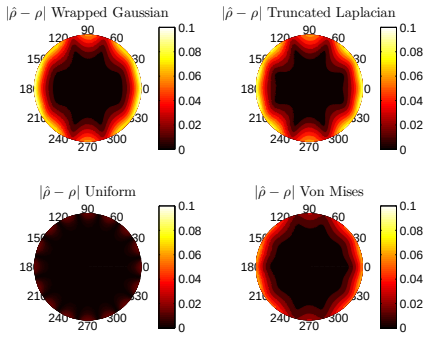

Fig. 7. Correlation error $|\hat{\rho} - \rho|$ for PASs shown in Figure 2. Test area size: 0.7λ.

B. Comparison of correlation error for different algorithms in literature

In this section, the proposed optimization algorithm is compared with the results published in [6] and the algorithm implemented in a commercial channel emulator from Elektrobit (EB). The SCME UMA TDL model is chosen for illustration and the test area size is selected to 0.5λ. In [6] and [5], the probe power weights are optimized for a fixed antenna separation without considering the PAS shape such as AoA and AS. The objective function is to minimize the absolute spatial correlation error $||\rho| - |\hat{\rho}||$. The optimization algorithm used in the EB channel emulator is briefly discussed in [3]. The probe power weights are obtained by optimizing for one or several fixed antenna orientations. The Least Square Error (LSE) technique was used to obtain the power weightings. It is mentioned in [3] that cluster mean AoA could be jointly considered when optimizing the power weightings, but the detailed algorithm is not given. For the sake of simplicity, the algorithm implemented in the EB channel emulator is named here after as the reference method [3], [4]. Here we will show the main advantages of our proposed algorithm through simulation results.

One advantage with the proposed algorithm is that by employing convex optimization framework into channel emulation, computational complexity is reduced dramatically compared to other numerical optimization techniques [5].

The correlation error for the multi-cluster SCME UMA TDL model is improved. The proposed algorithm presents maximum deviation of 0.03 over the test area, as shown in Figure 6. The correlation error for the SCME UMA TDL model based on power weights from [6] and the reference method is shown in Figure 8. Maximum deviation over the test area is 0.07 and 0.06, respectively.

The correlation error for each individual cluster of the SCME UMA TDL model is also improved. The correlation error $||\rho| - |\hat{\rho}||$ for the 6th cluster of the SCME UMA TDL model based on [6] is shown in Figure 9. At the antenna distance $d = 0.5\lambda$ selected for optimization, maximum deviation $||\rho| - |\hat{\rho}||$ is 0.01. However, correlation error at other antenna distances can be much worse. Maximum deviation $||\rho| - |\hat{\rho}||$ at antenna distance $d = 0.25\lambda$ is around 0.12. For the reference method, correlation error at some antenna orientations are worse (i.e. $\phi_a = 120^0$) than the other orientations. This is expected from the description in [3]. The proposed algorithm gives better correlation results for all antenna orientation and antenna separation within the test area.

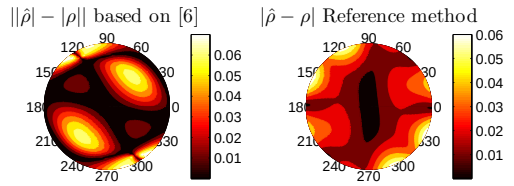

Fig. 8. Correlation error for SCME UMA TDL model based on [6] and the reference method.

The maximum correlation error $|\rho - \hat{\rho}|$ for each cluster in SCME UMA TDL model based on power weights from the reference method and the proposed algorithm is shown in Table I. The proposed algorithm generally present better correlation error.

TABLE I
MAXIMUM CORRELATION ERROR $|\rho - \hat{\rho}|$ FOR SCME UMA TDL MODEL

Cluster index	1	2	3	4	5	6	SCME
Reference method	0.12	0.08	0.04	0.10	0.05	0.14	0.06
Proposed algorithm	0.06	0.04	0.02	0.05	0.03	0.06	0.03

Another advantage coming from the proposed algorithm is that the error tolerance for the emulated PAS in terms of mean AoA and AS can be predefined in the optimization.

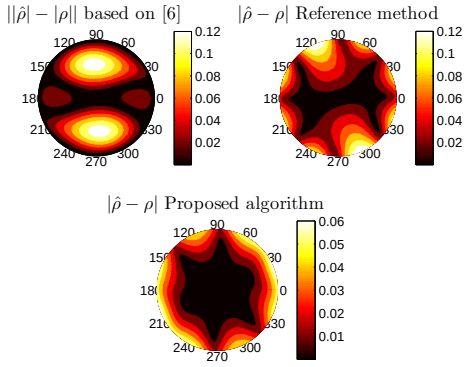

Fig. 9. Correlation error for the 6th cluster of the SCME UMA TDL model for the three algorithms.

Comparison results for the 1st cluster is shown in Table II. As we can see, compared with the algorithm implemented in the channel emulator, better correlation results in terms of mean AoA and AS can be obtained with the proposed optimization algorithm. The emulated PAS matches quite well with the target PAS in terms of AoA and AS.

TABLE II
COMPARISON RESULTS FOR CLUSTER ONE (TARGET AS = 35 AND AOA = 65.7489)

Cluster 1	AS (degree)	AoA (degree)
Reference method	36.4	64.1
Results from [6]	52.7	71.5
Proposed algorithm	35.0	66.0

C. Impact of channel model on correlation error

It is known that correlation error is dependent on the target channel. As shown in Figure 7, a uniform PAS generally gives better correlation error compared to the other PASs. Even for clusters with same PASs distribution but various ASs and AoAs, the correlation error is expected to be different. As shown in Table I, the correlation error for the 6 clusters with the same Laplacian PAS shape but diverse AoAs is different.

Emulation accuracy for a single Laplacian shaped cluster with different ASs will also be different. One critical scenario is that the convex optimization problem might be unsolvable when AS is too small for an arbitrary AoA since the optimization constraints on ϵ_{AoA} and ϵ_{AS} will never be satisfied. As discussed in [4], prefaded signal synthesis technique does not support for creating the LOS paths between OTA antennas.

D. Required number of probes

One important issue that needs to be addressed in anechoic chamber based multi-probe systems is the relationship between number of required probes and test area size. A comparison of the results for the required number of probes as a function of test area size obtained by different methods is given in [14]. It is not practical to have a large number of probe antennas since the output ports of the channel emulator are limited. Furthermore, due to possible additional reflections introduced by the multiple probes, the characteristics of the anechoic chamber can be degraded. Figure 10 illustrates the test area size as a function of the number of OTA probes for a truncated Laplacian cluster with AS = 35^o. Here the emulation accuracy threshold $|\rho - \hat{\rho}| < 0.1$ is defined to determine the size of the test area. For a given emulation accuracy level, as explained in Section III-C, the test area size will depend on the channel models. Simulation results show that if the cluster is arriving to the test area from the direction where one of the OTA antennas are located, the test area performance is better than from other directions. The worst case is the cluster impinging from an angle exactly in the middle of two adjacent OTA probes. The test area size for the best scenario will be larger than that for the worst scenario. One criterion we should follow is that inside the test area, emulation accuracy should be sufficiently good even for the worst channel case. A similar trend can be observed when compared with the results reported in [14]. However, it is difficult to directly compare the results, as the acceptable error levels and methods are different. Note that the probes are assumed uniformly distributed on a circle and the error tolerance is 1 degree on AoA and AS of the cluster in the simulation.

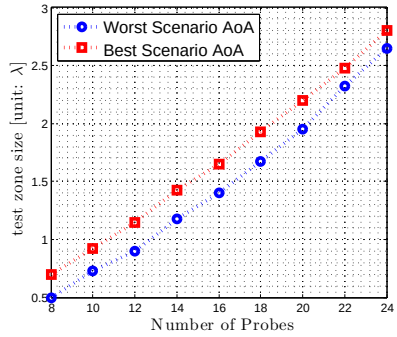

Fig. 10. The test area size as a function of number of OTA probes for a target truncated Laplacian cluster with AS = 35^o.

IV. MEASUREMENT VERIFICATION

In this section, the proposed optimization algorithm is compared with the reference algorithm implemented in the EB channel emulator in a practical MIMO OTA setup. First, the measurement system is briefly presented. After that, the settings and specifications of each of the component in the system are shown. The measurement procedure and results are given in the end.

A. Measurement setup

The measurement system is illustrated in Figure 1. Figure 11 shows the practical measurement system. 16 dual polarized horn antennas are equally spaced and fixed on a metallic OTA

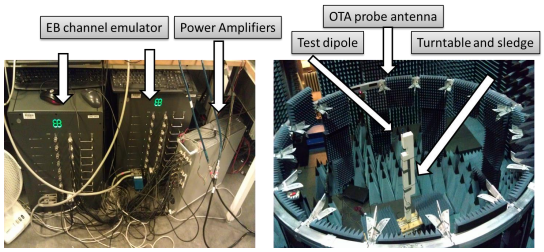

Fig. 11. EB channel emulator used in the measurement (left) and anechoic chamber setup in the measurement system (right).

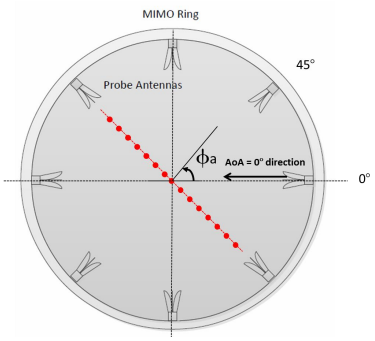

Fig. 12. Test antenna positions.

ring. The OTA ring is covered by absorbers to avoid reflections during the test. Two EB channel emulators are connected through power amplifiers to feed the probes. The measurement setup is summarized in Table III. Although the presented algorithm presents better accuracy for a test area size of 0.5λ with 8 probes, both the proposed technique and the technique implemented in the channel emulator present good emulation accuracy. To better demonstrate the accuracy improvement in the measurement, a test area of 0.8λ is selected. Note that the emulation accuracy threshold $|\rho - \hat{\rho}|$ for a test area of 0.8λ could be larger than 0.1.

B. Measurement procedure

Phase and amplitude calibrations are performed for each probe before the measurements. The goal of the calibration is to compensate errors caused by the non-idealities of the measurement setup, i.e. probe placement and orientation error, etc. The target is that equal field response at the center is obtained for all the probes. The measurement procedure is detailed in [16]. As a summary, the channel emulator is stopped every 10 CIRs and the field is measured with the network analyzer and saved for post-processing. The test antenna is then moved to next antenna position, and the sweep of the same 1000 CIR values is repeated for this new position. This procedure is repeated 15 times until all the test antenna positions are covered for the specified antenna orientation ϕ_a.

The measured spatial correlation between antenna test position m and n is calculated according to definition:

TABLE III
SETUP AND SPECIFICATIONS OF EACH COMPONENT IN THE OTA SYSTEM

Component	Setup and specifications
Network Analyzer	Center frequency at 2450MHz with a span of 10MHz
EB emulator	A radio channel (implementation method detailed in [4]) with following parameters set: • Carrier frequency: 2450MHz • Mobile speed: 30km/h • Direction of travel: 0^0 • Cluster PAS shape: one Laplacian PAS with mean AoA 22.5^0 and AS 35^0 • 4 samples per wavelength is selected to sample the channel and 10000 channel impulse responses (CIRs) are stored. • The CIRs are mapped to the OTA probes with the proposed optimization algorithm or the algorithm implemented in the EB channel emulator. • Test area size is selected to be 0.8λ.
Test antenna	Satimo electric sleeve dipole at 2450MHz.
Turntable	• The sledge and turntable support radial and rotational movement of the test antenna with respect to the ring center. • As shown in Figure 12, 15 test antenna positions sample a segment of line of length 15cm (around 1.15λ) with sampling interval of 1cm are selected for each antenna orientation ϕ_a.
Power Amplifiers	16 power amplifiers were used to improve the dynamic range.
OTA probes	• Horn antennas are designed by Aalborg University [15]. • Only 8 uniformly equally spaced with 45^0 angular separation on an OTA ring with radius 2m. • Only vertical polarization is considered

$$\rho_{meas}(m,n) = \frac{\sum_i (s_m(i) - \overline{s}_m)(s_n(i) - \overline{s}_n)}{\sqrt{\sum_i (s_m(i) - \overline{s}_m)^2 \cdot \sum_i (s_n(i) - \overline{s}_n)^2}} \quad (7)$$

where $s_m(i)$ and $s_n(i)$ are the complex signals received at antenna test position m and n at the ith CIR value, respectively, and $i = 1, ..., 1000$. $\overline{s}_m$ and $\overline{s}_n$ are the mean received signal over time at test position m and n, respectively.

C. Measurement results

The CIRs measured at each antenna position generally follow a Rayleigh distribution. The measured spatial correlation for antenna orientation $\phi_a = 30^0$, 60^0, and 150^0 are shown in Figure 13, Figure 14 and Figure 15, respectively. In (1), (2) and (3), the waves impinging the test area are assumed plane for the spatial correlation calculation. The impact of physical limitation of the OTA ring on errors caused by a difference between the plane and spherical waves is considered negligible

in this paper, according to the results in [17]. This is also supported by the fact that the measured spatial correlations generally match very well with the emulation results.

The deviations between emulated and target spatial correlation are due to the limited number of OTA probes we used for a test area size of 0.8λ. The proposed algorithm and the reference algorithm present similar performance at $\phi_a = 150^0$. However, at $\phi_a = 30^0$ and $\phi_a = 60^0$, the proposed algorithm shows better emulation accuracy. As found previously, the emulation error increases as the test size gets larger in the proposed algorithm, which is not always the case in the reference algorithm.

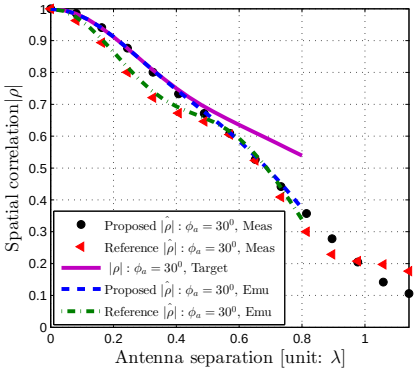

Fig. 13. Comparison between target, emulated and measured spatial correlation for antenna orientation $\phi_a = 30^0$.

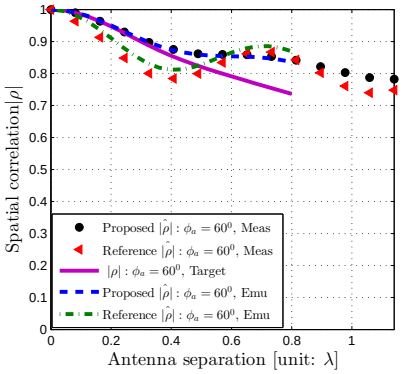

Fig. 14. Comparison between target, emulated and measured spatial correlation for antenna orientation $\phi_a = 60^0$.

V. Conclusions

We have introduced an improved algorithm to determine probe power weights for a MIMO OTA setup utilizing the prefaded synthesis method. Spatial correlation is selected as the emulation target and we further introduce constraints on PAS shape in terms of AS and AoA. The problem is expressed as a convex optimization problem, which can be solved efficiently. Simulation results show that with 8 OTA probes and a test area size of 0.5λ, the emulation error is 0.03 for the SCME UMA TDL model with the proposed algorithm with error tolerance of 1 degree on AoA and AS of each cluster, compared with emulation error 0.07 and no constraint on PAS shape found in the literature. The proposed algorithm is compared with the algorithm implemented in an commercial channel emulator in a practical MIMO OTA setup. Measurement results are consistent with the simulation results and better emulation accuracy of the proposed algorithm is demonstrated in practice.

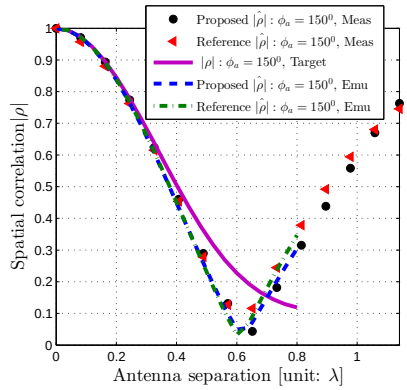

Fig. 15. Comparison between target, emulated and measured spatial correlation for antenna orientation $\phi_a = 150^0$.

References

[1] M. Rumney, R. Pirkl, M. H. Landmann, and D. A. Sanchez-Hernandez, "MIMO over-the-air research, development, and testing," *International Journal of Antennas and Propagation*, vol. 2012, pp. 1–8, 2012.

[2] M. A. Mow, B. Niu, R. W. Schlub, and R. Caballero, "Tools for design and analysis of over-the-air test systems with channel model emulation capabilities," Patent US 20 110 270 567, Nov. 3, 2011.

[3] P. Kyösti and J. Nuutinen, "Over the air test," Patent US 20 110 189 962, Aug. 4, 2011.

[4] P. Kyösti, T. Jämsä, and J. Nuutinen, "Channel modelling for multiprobe over-the-air MIMO testing," *International Journal of Antennas and Propagation*, vol. 2012, pp. 1–11, 2012.

[5] J. D. Reed, "Emulation and controlled testing of mimo ota channels," Patent US 20 110 299 570, Dec. 8, 2011.

[6] D. Reed, "Experiments with spatial correlation for evaluating ota techniques," no. TD (09)856. COST2100, May 2009, pp. 1–4. [Online]. Available: http://www.COST2100.org/.

[7] S. Boyd and L. Vandenberghe, *Convex Optimization*. Cambridge University Press, 2004.

[8] L. Hentilä, P. Kyösti, M. Käske, M. Narandzic, and M. Alatossava, "Matlab implementation of the winner phase ii channel model ver1. 1," *Online: https://www. ist-winner. org/phase_2_model. html*, 2007.

[9] D. Baum, J. Hansen, and J. Salo, "An interim channel model for beyond-3G systems: extending the 3GPP spatial channel model (SCM)," in *Vehicular Technology Conference, 2005. VTC 2005-Spring. 2005 IEEE 61st*, vol. 5, 2005, pp. 3132–3136 Vol. 5.

[10] J. Guillet, "Measurement-based statistical model and simulation of mobile station anisotropic power angular spectrum," *Electronics Letters*, vol. 42, no. 12, pp. 671–673, 2006.

[11] R. Vaughan, J. Bach-Anderson, and J. B. Andersen, "Channels, propagation and antennas for mobile communications." Institution of Electrical Engineers, 2003.

[12] "Spatial channel model for Multiple Input Multiple Output (MIMO) simulations (Release 11)," 3GPP/3GPP2, TR 25.996 V11.0.0, Sep. 2012.

[13] W. Fan, X. Carreno, J. O. Nielsen, J. S. Ashta, G. F. Pedersen, and M. B. Knudsen, "Verification of emulated channels in multi-probe based MIMO OTA testing setup," in *Antennas and Propagation (EuCAP), 2013 7th European Conference on*, 2013, pp. 97–101.
[14] A. Khatun, T. Laitinen, V.-M. Kolmonen, and P. Vainikainen, "Dependence of error level on the number of probes in over-the-air multiprobe test systems," *International Journal of Antennas and Propagation*, vol. 2012, pp. 1– 6, 2012.
[15] O. Franek and G. F. Pedersen, "Spherical horn array for wideband propagation measurements," *Antennas and Propagation, IEEE Transactions on*, vol. 59, no. 7, pp. 2654–2660, 2011.
[16] "Verification of radiated multi-antenna reception performance of User Equipment," 3GPP, TR 37.977 V0.2.0, May. 2012.
[17] P. Kyosti and L. Hentila, "Criteria for physical dimensions of mimo ota multi-probe test setup," in *Antennas and Propagation (EUCAP), 2012 6th European Conference on*. IEEE, 2012, pp. 2055–2059.

Wei Fan received his Bachelor of Engineering degree in electrical engineering from Harbin Institute of technology, China, in 2009 and Master's double-degree with highest honors from Politecnico di Torino, Italy, and Grenoble Institute of Technology, France, in electronic engineering in 2011. From February 2011 to August 2011, he was with Intel Mobile Communications, Denmark. He is currently a Ph.D. candidate at Department of Electronic Systems at Aalborg University, Denmark. His main areas of research are over the air testing of MIMO terminals and radio channel modeling.

Xavier Carreo Bautista de Lisbona received his Masters degree from Escola Tcnica Superior de Enginyeria de Telecomunicacions de Barcelona UPC in 2011. At UPC he was deeply involved in baseband signal processing algorithms and MIMO OTA research topics within Intel Mobile Communications, where he currently has a leading role in the MIMO OTA development team as system engineer. He is involved in the standardization of MIMO OTA methods and has coauthored several 3GPP, CTIA and IC1004 contributions and several conference and journal papers on the subject. His primary interests are within the area of MIMO OTA testing techniques, MIMO channel modeling and LTE platform testing.

Fan Sun received the B.Eng. degree in telecommunication engineering with highest honors from Beijing University of Aeronautics and Astronautics (now renamed as Beihang University), China, in 2007, and the M.S. degree in wireless systems from Royal Institute of Technology (KTH), Sweden, in 2009, respectively. From November 2008 to September 2009, he was with Ericsson Research, Sweden. From September 2009 to September 2010, he was with Nokia Siemens Network Research, Denmark. He is now pursuing his Ph.D. degree in wireless communications at Aalborg University, Denmark. His research interests include multiple antenna techniques, cooperative communication, cross-layer design, and signal processing for communication systems.

Jesper Ødum Nielsen received his master's degree in electronics engineering in 1994 and a PhD degree in 1997, both from Aalborg University, Denmark. He is currently employed at Department of Electronic Systems at Aalborg University where main areas of interests are experimental investigation of the mobile radio channel and the influence mobile device users have on the channel. He has been involved in MIMO channel sounding and modeling, as well as measurements using live GSM and LTE networks. In addition he has been working with radio performance evaluation, including over the air testing of active wireless devices.

Mikael Bergholz Knudsen (S99M01) was born in 1964. He received the B.S. degree in electrical engineering from Aarhus Teknikum, Denmark, in 1989, and the M.S. and Ph.D. degrees from Aalborg University, Denmark, in 1992 and 2001, respectively. In 1993, he joined Maxon Telecom A/S, Aalborg, Denmark, where he designed RF circuitry for both analog and digital mobile phones. From 1998 to 2001, he worked as an industrial Ph.D. student for Siemens Mobile Phones A/S, Denmark, while he at the same time studied at Aalborg University. He is now with Intel Mobile Communications Denmark, where he is the project manager for the 4th Generation Mobile Communication and Test platform (4GMCT) and also the chairman of the steering committee for the Smart Antenna Front End (SAFE) projects; both sponsored by the Danish National Advanced Technology Foundation. His areas of interest include RF system design and handset antenna performance including more than one antenna. In the resent years one of his focus areas has been how to utilize the unique possibilities in the cooperation between university researchers and private companies. To support this effort he pursued and obtained an Executive-MBA in 2012 with focus on inter-organizational research strategies.

Gert Frølund Pedersen was born in 1965 and married to Henriette and have 7 children. He received the B.Sc. E. E. degree, with honour, in electrical engineering from College of Technology in Dublin, Ireland in 1991, and the M.Sc. E. E. degree and Ph. D. from Aalborg University in 1993 and 2003. He has been with Aalborg University since 1993 where he is a full Professor heading the Antenna, Propagation and Networking LAB with 36 researcher. Further he is also the head of the doctoral school on wireless communication with some 100 phd students enrolled. His research has focused on radio communication for mobile terminals especially small Antennas, Diversity systems, Propagation and Biological effects and he has published more than 175 peer reviewed papers and holds 28 patents. He has also worked as consultant for developments of more than 100 antennas for mobile terminals including the first internal antenna for mobile phones in 1994 with lowest SAR, first internal triple-band antenna in 1998 with low SAR and high TRP and TIS, and lately various multi antenna systems rated as the most efficient on the market. He has worked most of the time with joint university and industry projects and have received more than 12 M$ in direct research funding. Latest he is the project leader of the SAFE project with a total budget of 8 M$ investigating tunable front end including tunable antennas for the future multiband mobile phones. He has been one of the pioneers in establishing Over-The-Air (OTA) measurement systems. The measurement technique is now well established for mobile terminals with single antennas and he was chairing the various COST groups (swg2.2 of COST 259, 273, 2100 and now ICT1004) with liaison to 3GPP for over-the-air test of MIMO terminals. Presently he is deeply involved in MIMO OTA measurement.

Paper B

Antenna Pattern Impact on MIMO OTA Testing

Wei Fan, Jesper Ø. Nielsen, Ondrej Franek, Xavier Carreño, Jagjit S. Ashta, Mikael B. Knudsen and Gert F. Pedersen

The paper has been published in the
IEEE Transactions on Antennas and Propagation, vol. 61, no. 11, pp.5714–5723, Nov. 2013.

The layout has been revised.

Antenna Pattern Impact on MIMO OTA Testing

Wei Fan, Jesper Ø. Nielsen, Ondrej Franek, Xavier Carreño, Jagjit S. Ashta, Mikael B. Knudsen and Gert F. Pedersen

***Abstract*—This paper investigates the impact of the DUT antenna pattern on the test area performance for multi-probe based MIMO OTA setup in terms of received voltage and spatial correlation. The plane wave synthesis (PWS) technique has been proposed for vertical polarization in the literature, where the goal is to approximate plane waves with arbitrary directions. The received voltage at the antenna terminal depends on the antenna radiation pattern and the impinging plane waves. A novel closed form technique to reproduce the received voltage with arbitrary incoming plane waves based on trigonometric interpolation is presented. The proposed technique provides a closed form solution for the PWS when the probe ring radius is infinite. The proposed technique shows that the impact of the antenna pattern on the induced received voltage accuracy is ruled by Nyquist sampling theory. Furthermore, the impact of the antenna pattern on spatial correlation accuracy for prefaded signal synthesis (PFS) technique is investigated as well. Simulation and measurement results show that the number of required probes depend directly on the DUT antenna pattern. To test realistic DUTs with higher variations in directivity, we need more probes to maintain the same received voltage and spatial correlation accuracy level.**

I. Introduction

Multiple-input multiple-output (MIMO) technology is a key factor for achieving high data rate for wireless technologies such as LTE and LTE-Advanced. Mobile manufacturers and cellular operators are pushing for standard test methods to evaluate MIMO device performance. As a promising solution to evaluate MIMO device performance in realistic conditions in the lab, MIMO over the air (OTA) testing has attracted huge attention from both industry and academia [1]. Standardization work for the development of the MIMO OTA test methods is ongoing in CTIA, 3GPP and COST IC1004 [1]. One promising candidate is the multi-probe anechoic chamber based method.

The major challenge for MIMO OTA testing with the multi-probe method is to emulate a realistic environment which accurately reflects the real wireless propagation environment. Mainly two channel emulation techniques have been proposed for multi-probe based MIMO OTA setups. One technique is the plane wave synthesis (PWS) technique reported in [2]–[6]. The basic idea of the PWS technique is that static plane waves with arbitrary impinging angle of arrivals (AoAs) can be created inside the test area by selecting appropriate complex weights for the probes. Desired radio channels inside the test area can be formed based on superposition of a plurality of plane waves as detailed in [2], [3]. The other technique is named the prefaded signal synthesis (PFS) technique [2] and has been adopted in several commercial tools [7]–[9]. The essence of this technique is to allocate proper power weights to the probes to reproduce the channel desired spatial characteristics at the receiver (Rx) side [7].

The test area is the geometrical area inside which the DUT is located during the measurement. Acceptable error levels are defined for the channel emulation to ensure that the target propagation environment is reproduced around the DUT with certain accuracy. The required number of probes is a key issue related to the multi-probe anechoic chamber solution. It is generally assumed that the number of probes depends on the test area size, the center frequency, the channel model, the OTA probe angular locations, and the acceptable error level [2], [6], while the DUT antenna pattern has been considered irrelevant. The above-mentioned two techniques generally assume that:

- For the PWS technique, the goal is to approximate plane waves inside the test area. However, what matters is whether we can reproduce the desired received voltage with the multiple probes. The difference between target received voltage, assuming ideal impinging plane waves with arbitrary AoAs, and the induced received voltage, with waves radiated from the multiple probes impinging the DUT, has not been investigated. The resulting received voltage accuracy depends on the antenna pattern, as demonstrated in this paper.
- For the PFS technique, the difference between the target spatial correlation and the emulated spatial correlation of the ideal omnidirectional antennas are used to determine the number of required probes. However, what matters is whether we can reproduce the spatial correlation of the received signals at the antenna output.

The main contributions of this paper lie in the following aspects:

- An optimization technique for PWS of horizontal polarization is introduced. Simulation results show that the difference between the complex weights for the two polarizations depends on the ratio between test area radius and OTA ring radius r/R and the complex weights are practically the same for large R cases.
- A novel closed form technique to reproduce the target received voltage based on trigonometric interpolation (TI) is presented. The closed form technique gives practically the same complex weights as the PWS optimization technique for large ring radius case. The proposed technique shows that the impact of the antenna pattern on the received voltage accuracy is ruled by Nyquist sampling

Wei Fan, Jesper Ø. Nielsen, Ondrej Franek, and Gert F. Pedersen are with the Antennas, Propagation and Radio Networking section at the Department of Electronic Systems, Faculty of Engineering and Science, Aalborg University, Denmark (email: {wfa, fs, jni, gfp}@es.aau.dk).

Xavier Carreño, Jagjit S. Ashta, and Mikael B. Knudsen are with Intel Mobile Communications, Denmark (email: {xavier.carreno, jagjitx.singh.ashta, mikael.knudsen}@intel.com).

theory.

- The impact of the antenna pattern on emulation accuracy for spatial correlation of the received signals in the PFS method is demonstrated by simulation and measurement results.
- We show that to test realistic DUTs with higher variations in directivity, we need more probes to maintain the same received voltage and spatial correlation accuracy level.

II. Method

A. Plane wave synthesis technique

In this section, we describe the optimization techniques to generate a single static plane wave with an arbitrary direction impinging the test area for both vertical and horizontal polarization. Note that the PWS technique for vertical polarization has been addressed in several contributions and the same notations as in [2] has been adopted in this paper. The main contribution of this part lies in two aspects: the optimization problem is formed as a convex optimization problem, which gives optimal results and low complexity; an optimization technique for PWS of the horizontal polarization is introduced.

1) Vertical polarization : As shown in Figure 1, a target plane wave is with an arbitrary direction $\overline{\beta}_{AoA}$ impinging the test area. $\overline{\beta}_{AoA}$ is a wave vector with $\parallel \overline{\beta}_{AoA} \parallel = \frac{2\pi}{\lambda}$. We approximate the target plane wave inside the test area by superposing the radiated fields from each of the OTA probes. Complex weights are obtained by minimizing the difference between the target field and the synthesized field within the test area. One constraint with the practical system is that probe weights are limited, as the output gain of typical channel emulators is limited to 0 dB. The weighting vector $\boldsymbol{g_\theta}$ for a vertically polarized single plane wave can be obtained by solving the optimization problem as follows:

$$\begin{aligned} &\min_{\boldsymbol{g_\theta}} \ \|\mathbf{F}_\theta \boldsymbol{g_\theta} - \boldsymbol{t}_\theta\|_2^2 \\ &\text{s.t.} \quad 0 \le |g_{\theta,k}| \le 1 \ \forall k \in [1, K] \end{aligned} \tag{1}$$

where

- $||\cdot||_2$ denotes the second order norm.
- $\boldsymbol{g_\theta} = \{g_{\theta,k}\} \in \mathbb{C}^{K\times 1}$ is a vector of the complex weights for vertically polarized probes. K is the number of probes.
- $\boldsymbol{t}_\theta = \{e(\overline{r}_m)\} \in \mathbb{C}^{M\times 1}$ is a vector of vertically polarized complex target field samples. M is the total number of sample points. $\overline{r}_m$ is a position vector of sample point m.
- $\mathbf{F}_\theta = \{f(m,k) \in \mathbb{C}^{M\times K}\}$ is a transfer matrix of known gains from the probes to the sample points.

The target field for an ideal plane wave is with uniform power distribution and linear phase front along the propagation direction, that is,

$$e(\overline{r}_m) = E_0 \exp(-j\overline{\beta}_{AoA} \cdot \overline{r}_m), \tag{2}$$

where the field strength E_0 is assumed constant and $(\cdot)$ is the dot product operator. The transfer coefficient from the kth OTA antenna to the mth location $\overline{r}_m$ is:

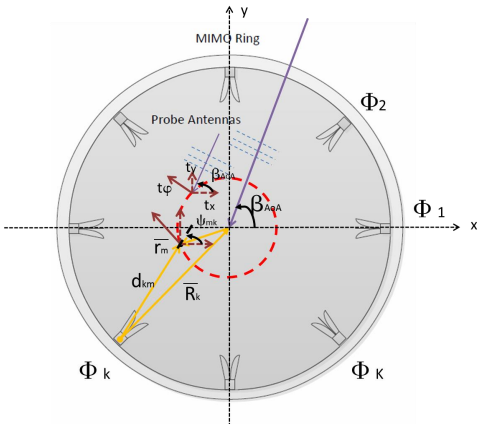

Figure 1. A single plane wave with AoA β_{AoA} impinging the test area.

$$f(m,k) = A(d_{km}) \cdot \exp(-j\frac{2\pi}{\lambda} d_{km}), \tag{3}$$

where $d_{km} = \parallel \overline{d}_{km} \parallel = \parallel \overline{R}_k + \overline{r}_m \parallel$ is the distance from the kth OTA antenna to the mth location. $A(d_{km})$ is the free space path loss factor. $\overline{R}_k$ is a position vector of the kth probe.

2) Horizontal polarization: The same principle can be applied for the horizontal polarization:

$$\min_{\boldsymbol{g_\varphi}} \ \|\mathbf{F}_\varphi \boldsymbol{g_\varphi} - \boldsymbol{t}_\varphi\|_2^2, \tag{4}$$

where $\boldsymbol{g_\varphi} = \{g_{\varphi,k}\} \in \mathbb{C}^{K\times 1}$, $\boldsymbol{t}_\varphi \in \mathbb{C}^{M\times 1}$ and $\mathbf{F}_\varphi \in \mathbb{C}^{M\times K}$ are defined similarly to the vertical polarization.

The PWS technique for vertical and horizontal polarizations is addressed in [4], [10], [11]. In a 2D MIMO OTA setup as illustrated in Figure 1, the direction of the vertically polarized field will be perpendicular to the xy (azimuth) plane both for the emulated and target fields. However, for the horizontally polarized field, the direction of the target field is on xy plane and perpendicular to the AoA of the target plane wave, while the direction of the radiated field from a horizontally polarized probe is on the xy plane and perpendicular to the AoA from where the probe is located. That is, the direction of the target field and emulated field might be different. In order to ensure that the emulated field matches with the target field in terms of magnitude, phase, and polarization for the sample points inside test zone, decomposition into the two orthogonal axises x and y is required for the horizontal polarization. This effect is, however, not considered in the literature so far.

We can decompose the target field and the transfer matrix into x and y orthogonal components, as:

- $\mathbf{F}_x = \{f_x(m,k)\} \in \mathbb{C}^{M\times K}$ with $f_x(m,k) = -f(m,k) \cdot \sin(\psi_{mk})$
- $\mathbf{F}_y = \{f_y(m,k)\} \in \mathbb{C}^{M\times K}$ with $f_y(m,k) = f(m,k) \cdot \cos(\psi_{mk})$
- $\boldsymbol{t}_x = \{e_x(\overline{r}_m)\} \in \mathbb{C}^{M\times 1}$ with $e_x(\overline{r}_m) = -e(\overline{r}_m) \cdot \sin(\beta_{AoA})$

- $\boldsymbol{t}_y = \{e_y(\overline{r}_m)\} \in \mathbb{C}^{M\times 1}$ with $e_y(\overline{r}_m) = e(\overline{r}_m) \cdot \cos(\beta_{AoA})$

where β_{AoA} is the AoA of the target plane wave and ψ_{mk} is angle between $\overline{d}_{km}$ and x axis, as illustrated in Figure 1.

Then the objective function to obtain the optimal weights for horizontal polarization can be rewritten as:

$$\min_{\mathbf{g}_{\boldsymbol{\varphi}}} \left\| \begin{bmatrix} \mathbf{F}_x \\ \mathbf{F}_y \end{bmatrix} \boldsymbol{g}_{\boldsymbol{\varphi}} - \begin{bmatrix} \boldsymbol{t}_x \\ \boldsymbol{t}_y \end{bmatrix} \right\|_2^2 \quad \text{s.t.} \quad 0 \le |g_{\varphi,k}| \le 1 \; \forall k \in [1, K] \tag{5}$$

Both objective functions in equation (1) and (5) are quadratic programming problems with linear constraints. This standard convex optimization problem can then be solved using the cvx package in Matlab with high efficiency [12].

B. Equivalent induced voltage (EIV) technique

For the PWS technique, the goal is to generate the plane waves with arbitrary AoAs impinging the test area. However, what matters is the difference between the induced received voltage, with waves radiated from the probes and the target received voltage, with ideal impinging plane waves. The induced received voltage accuracy will depend on the field synthesis accuracy and the DUT antenna pattern. The goal of the EIV technique is to obtain the complex weights such that the target received voltage with an arbitrary impinging plane wave can be reproduced with the multiple probes.

The antenna radiation pattern is defined as a complex function of direction, whose value gives the intensity of the radiated field in the far field area. Due to the reciprocity theorem, the same complex function gives us the voltage on the antenna terminals depending on from which direction an ideal plane wave is impinging to the antenna. The received voltage can be represented as

$$V = E_0 \cdot L(\alpha). \tag{6}$$

If the electric intensity of the incident field E_0 is constant, then the induced voltage V varies with the AoA α of the plane wave according to the radiation pattern L. L also represents the effective length of an antenna.

In a multi-probe anechoic chamber OTA setup as shown in Figure 1, the OTA ring radius $R = ||\overline{R}_k||$ is much larger than the DUT and ideal plane waves radiating from the probes are assumed. The resulting received voltage at the antenna terminal will be given by the superposition of the partial voltages which corresponds to antenna pattern sampled at the discrete angles in which the OTA probes are placed:

$$\hat{V} = \sum_{k=1}^{K} V_k = E_0 \cdot \sum_{k=1}^{K} g_k(\alpha) L(\Phi_k) = E_0 \cdot \hat{L}(\alpha), \tag{7}$$

where $g_k(\alpha)$ is the complex weight assigned for the kth probe. Φ_k is the angular location of kth probe. $\hat{L}(\alpha)$ is the resulting value of the antenna pattern at arbitrary direction α, given by a summation of the samples of antenna pattern at the directions of the probes, weighted by the complex weights. To ensure to we obtain $\hat{V} = V$, we need to find $\boldsymbol{g}(\boldsymbol{\alpha})$ so that we have $L(\alpha) = \hat{L}(\alpha)$ for an arbitrary direction α. This can be seen as an antenna pattern interpolation problem, where we need to reconstruct the antenna pattern $L(\alpha)$ from K discrete periodic samples $L(\Phi_k)$.

We assume the probes are located on the OTA ring with equal spacing between them,

$$\Phi_{K,k} = \frac{360^o}{K}(k-1). \tag{8}$$

The antenna pattern $L(\alpha)$ sampled by K equidistant probes is a periodic (with the period 2π) sequence. The EIV problem can be solved by TI, as stated below.

1) Trigonometric interpolation: Let us describe the interpolation of the radiation pattern as

$$\hat{L}(\alpha) = \sum_{k=1}^{K} g_k(\alpha) L(\Phi_k) \tag{9}$$

where α is the azimuth angle of the plane wave. The weights of the probes $g_k(\alpha)$ can then be expressed, using trigonometric interpolation [13], as

$$g_k(\alpha) = \frac{1}{K} \sum_{i=1}^{K} \cos m(\alpha - \Phi_k), \tag{10}$$

with $m = i - \lceil N/2 \rceil$, where $\lceil\rceil$ is the ceiling operator which rounds up the number inside the bracket to the next higher integer.

If the phase at the ring center is set to 0. The complex weights for interpolation is:

$$g_{TI,k}(\alpha) = g_k(\alpha) \exp(-j\beta R) \tag{11}$$

where β is the wave number. Note that the complex weights are independent of the antenna pattern samples $L(\Phi_k)$ and plane wave polarizations.

In this part, ideal plane waves radiating from the probes are assumed. Also, uniform probe configuration on the OTA ring is assumed for the sake of simplicity. The TI used for EIV technique detailed here can be extended to the case where OTA probes are not uniformly located on the OTA ring [13]. The TI can also be extended to 3D MIMO OTA configurations.

2) Antenna pattern impact on the EIV technique: According to the Nyquist sampling criterion, the number of probes K for complete reconstruction of the antenna pattern $L(\alpha)$ must exceed two times the highest harmonics in the spatial frequency spectrum of the antenna pattern. We expect to have certain conditions on smoothness of the antenna pattern versus density of number of probes. That is, if the antenna pattern variation is too high with respect to the number of probes, K will not satisfy the Nyquist criterion. As a result, the resulting interpolated values will present aliasing. An example is shown in Figure 2, where $K = 8$ uniformly located probes are used to sample the antenna pattern. However, since the antenna pattern variation is too high with respect to the number of probes, the interpolated antenna pattern $\hat{L}$ is different from the original antenna pattern L. As a result, the resulting received voltage $\hat{V}$ will not be the same as the target received voltage V for some AoAs. More probes are required to obtain the correct induced received voltage.

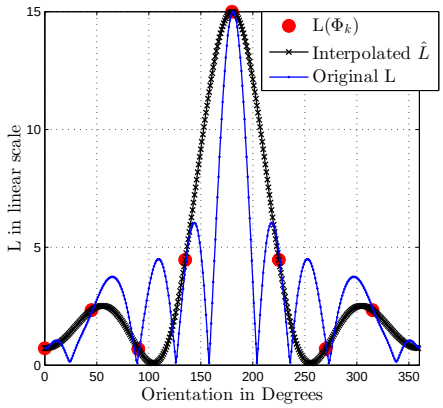

Figure 2. An illustration of inaccurate interpolated antenna pattern.

3) Required number of probes for the EIV technique : The antenna radiation pattern of any antenna with a fixed size (inside a limited test volume) can be described with a finite series of spherical wave functions [14]. That is, the highest harmonics in the spatial frequency spectrum of the antenna pattern is limited. The antenna pattern $L(\alpha)$ is thus a band-limited periodic function, which can be perfectly reconstructed with a finite number of probes. The highest significant wave mode present is given by [14],

$$K_{mode} = \lceil kr_t + 10 \rceil, \tag{12}$$

where r_t is the radius of the minimum spherical volume that contains the DUT. The minimum number of required probes for the complete reconstruction of $L(\alpha)$, according to Nyquist criterion is [14]:

$$K_{min}^{2D} = 2K_{mode} + 1, \tag{13}$$

where the superscript $2D$ refers to the 2D MIMO OTA configurations.

C. Prefaded signal synthesis technique

A channel model specifies a certain continuous power azimuth spread (PAS) at the Rx. However, with a limited number of probes, we can only approximately reproduce the PAS inside the test area. Spatial correlation has been selected as the main figure of merit (FoM) to characterize the channel spatial information at receiver side [2], [6]–[9], [15]. Omnidirectional antenna patterns are used for the channel emulation purpose as the DUT antenna pattern is typically not known beforehand. Furthermore, if some antenna patterns are embedded to the channel model, the channel model itself will assume some DUT antennas. Thus, it is not realistic to use the emulated channel to evaluate the DUT performance [7], [8].

As explained in [2], The PFS technique works the same for both vertically and horizontally polarized PAS. The theoretical spatial correlation between a pair antenna elements can be determined according to [16]:

$$\rho_a = \frac{\int_{-\pi}^{\pi} G_u(\phi) G_v^{\star}(\phi) p(\phi) d\phi}{\sqrt{\int_{-\pi}^{\pi} p(\phi)|G_u(\phi)|^2 d\phi}\sqrt{\int_{-\pi}^{\pi} p(\phi)|G_v(\phi)|^2 d\phi}} \tag{14}$$

where G_u and G_v are the complex radiation patterns of antennas u and v, respectively, with a common phase center. $p(\phi)$ is the PAS. In order to be used as an angular power density function, the $p(\phi)$ needs to satisfy $\int_{-\pi}^{\pi} p(\phi)d\phi = 1$. Using this property and the omnidirectional antenna pattern assumption, we can rewrite (14) as:

$$\rho = \int_{-\pi}^{\pi} \exp(j\beta(\overline{r}_u - \overline{r}_v) \cdot \overline{\phi}) p(\phi) d\phi \tag{15}$$

where $\overline{r}_u$ and $\overline{r}_v$ are vectors containing the position information of antenna u and v, respectively. $\overline{\phi}$ is an unit vector corresponding to the azimuth angle ϕ.

The goal is to obtain OTA probe power weights which minimize the deviation between the theoretical spatial correlation resulting from the target continuous PAS, and the emulated correlation resulting from the discrete PAS characterized by the power weights of the probes. Similar to (15), the emulated spatial correlation can be calculated based on the discrete PAS as:

$$\hat{\rho} = \sum_{k=1}^{K} w_k \exp(j\beta(\overline{r}_u - \overline{r}_v) \cdot \overline{\Phi}_k), \tag{16}$$

where w_k is the power weight for the kth probe. $\overline{\Phi}_k$ is a unit position vector of the kth probe. Optimization techniques to obtain power weights $\boldsymbol{w} = \{w_k\} \in \mathbb{R}^{K\times 1}$ have been discussed in [2], [7], [8] and results from [7] are used here.

Once the optimal power weights vector $\boldsymbol{w}$ is found, the resulting spatial correlation with antenna pattern $\hat{\rho}_a$ can be written as:

$$\hat{\rho}_a = \frac{\sum_k G_u(\theta_k) \cdot G_v^*(\Phi_k) \cdot w_k}{\sqrt{\sum_k \mid G_u(\Phi_k) \mid^2 w_k \cdot \sum_k \mid G_v(\Phi_k) \mid^2 w_k}}, \tag{17}$$

where G_u and G_v can be obtained through electromagnetic antenna simulations or measurements in an anechoic chamber.

The deviation between $\hat{\rho}$ and ρ shows how well the channel PAS is reconstructed, and hence it is generally selected as FoM to investigate the relationship between the number of required probes and test area size [2], [7]–[9], [17]. However, this does not take into account the DUT antenna pattern and what really matters is the deviation between target correlation ρ_a and emulated spatial correlation $\hat{\rho}_a$ with antenna patterns. In this paper, the focus is on the impact of antenna pattern on deviation between ρ_a and $\hat{\rho}_a$.

III. MIMO OTA MEASUREMENT

A. Introduction

An illustration of a general multi-probe anechoic chamber setup is shown in Figure 3. In the measurement of

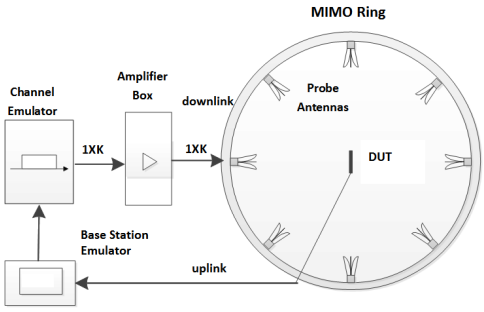

Figure 3. An illustration of the multi-probe based MIMO OTA setup. The main components are a base station emulator (BSE), one or several radio channel emulators, an anechoic chamber, OTA probe antennas, power amplifiers (PAs) and an DUT.

the current work, the BSE is replaced by a vector network analyzer (VNA). Figure 4 shows the multi-probe setup used for measurements at Aalborg University. 16 dual polarized horn antennas are equally spaced and fixed on an aluminum OTA ring with radius $R = 2$ meters.

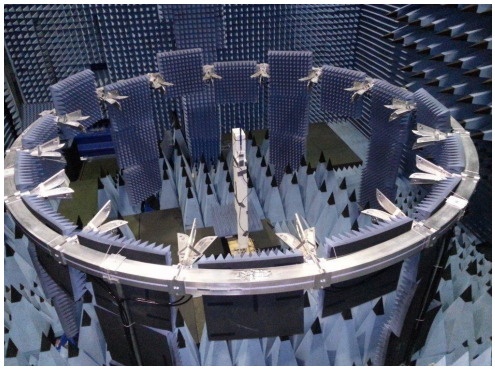

Figure 4. An illustration of the practical anechoic chamber setup in the measurement system.

B. Measurement setup for PFS

1) System setup : The PFS measurement setup is summarized in Table I.

2) Test DUTs and test channel scenarios: Since the paper aims at investigating the antenna pattern impact, special attention has been paid to selecting DUTs.

a) Test DUTs: Three test DUTs were used for the measurements: a pair of practical dipoles with antenna separation 0.525λ (at frequency 2100MHz) (shown in Figure 5(a)), the CTIA band 7 good antenna (shown in Figure 5(b)) and the CTIA band 7 nominal antenna (shown in Figure 5(c)) both with antenna separation 0.5λ (at frequency 2655MHz). The CTIA reference antennas are used to rule out the measurement uncertainty introduced by antenna patterns between different labs [18]. The so-called "good" antennas were designed

Table I
SETUP AND SPECIFICATIONS FOR THE PFS MEASUREMENTS

Component	Setup and specifications
VNA	Sweep time: 4.803s Number of sweeps per DUT orientation: 13 Number of samples per sweep: 1601
Channel emulator	A radio channel (implementation method detailed in [2]) with following parameter sets: • 10000 channel impulse responses (CIRs) are created and stored. • The CIRs are mapped to the OTA probes with the PFS algorithm implemented in the Elektrobit Propsim channel emulator.
Turntable	The DUT is rotated 360^o with 4^o step size for test scenario A and B and 5^o step size for test scenario C and D listed in Table II.
OTA probes	Only vertical polarization is considered.

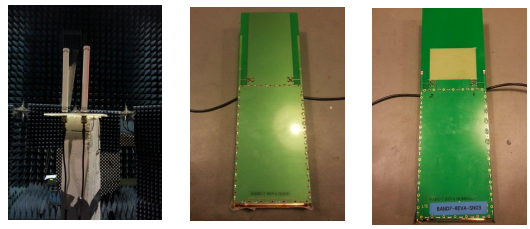

(a) Two practical dipoles (b) CTIA band 7 good (c) CTIA band 7 nominal

Figure 5. DUTs used in the measurements

to emulate good MIMO antenna systems that present low correlation coefficient, high total antenna efficiency and low gain imbalance, while the "nominal" antennas present median correlation coefficient, median total antenna efficiency and low gain imbalance. Note that the CTIA reference antennas were designed for the isotropic incoming power distribution only. The correlation coefficient in this work will depend on how the antennas are placed and the specific incoming power distribution. All three DUTs are vertically placed with respect to the OTA ring (as shown in Figure 5(a) and Figure 6(a)).

Mobile terminals could be arbitrarily positioned by the end users in real life and the antenna pattern in certain orientations can be critical compared to that in vertical positions. CTIA antennas are slanted 45^o in the measurements as well, as shown in Figure 6(b). Note that the DUT positions were carefully calibrated to ensure that the center of the two antennas on the DUT match with the center of the OTA ring and the rotation center of the turntable for all the measurements as shown in Figure 6(a) and Figure 6(b).

b) Test Scenarios: For the sake of simplicity, single clusters with Laplacian shaped PAS are considered as the target channels. Various AoAs and azimuth spread (AS) of 35^o are used to characterize the considered target clusters. AS = 35^o is selected as the standard channel models, e.g. the 3GPP spatial channel model extended (SCME) models, which have been considered as the target channel models in the MIMO OTA setup, are with AS = 35^o for the clusters [1],

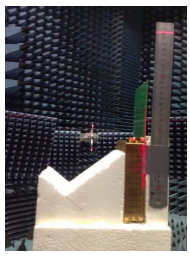

(a) Vertically positioned CTIA anenna

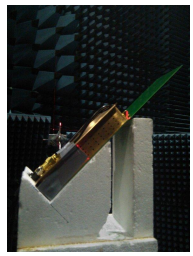

(b) 45 degrees slanted CTIA anenna

Figure 6. An illustration of DUT position calibrations with a laser positioner

Table II
TEST SCENARIOS

Scenario	Comments
A	AoA = 0^o and AS = 35^o Number of probes: 8
B	AoA = 22.5^o and AS = 35^o Number of probes: 8
C	AoA = 0^o and AS = 35^o Number of probes: 16
D	AoA = 22.5^o and AS = 35^o Number of probes: 16

[19], [20]. Four test scenarios are emulated with the channel emulators as listed in Table II. One channel emulator and 8 probes were used to emulate scenario A and B, while two channel emulators and 16 probes were used for scenario C and D. Only vertical polarization is considered.

3) Measurement procedure: For each DUT, complex radiation patterns of the two antenna elements are measured with the VNA at the same time with 1 degree resolution. Correlation measurements are performed for each test scenario with the same setup just after the antenna pattern measurements to ensure that the radiation patterns of the DUT remain unchanged for the correlation measurements. The VNA sweep time is selected according to the maximum Doppler shift defined in the test scenarios to meet the Nyquist sampling criterion.

The measured spatial correlation at DUT orientation ϕ_a is calculated according to the correlation definition:

$$\rho_m(\phi_a) = \frac{\sum_{i=1}^{I}(s_u(i) - s_{u,m})(s_v(i) - s_{v,m})}{\sqrt{\sum_{i=1}^{I}(s_u(i) - s_{u,m}).\sum_{i}^{I}(s_v(i) - s_{v,m})}} \quad (18)$$

where $s_u(i)$ and $s_v(i)$ are the ith complex signals received at antenna element u and v , respectively, at the antenna orientation index ϕ_a. $s_{u,m}$ and $s_{v,m}$ are the mean received signal over all measured samples for the two antennas, respectively.

IV. RESULTS AND DISCUSSION

A. Comparison between the PWS and the EIV technique

As mentioned previously, the goal of the PWS technique is to obtain complex weights to create plane waves impinging the test area, while the EIV technique is used to obtain complex weights to reproduce the target received voltage with arbitrary impinging plane waves. In this part, we will first show the complex weights obtained by the two techniques. After that the relationship between the two techniques is described. In the end, we will show the pros and cons of each technique.

The real and imaginary part of the complex weighting matrix $\boldsymbol{G}_{TI}$ obtained with the EIV technique with $R = 2$m and $f = 2.45$GHz is shown in Figure 7. The plots show the real and imaginary parts of a 360×8 complex weighting matrix with the ith row containing the 8 complex weights for the EIV at angle $\alpha = (i-1)^o$. The periodic pattern observed in Figure 7 is with period 45^o due to the symmetry of the probe configuration. The complex weighting matrix $\mathbf{G}_{\theta,op}$ and $\boldsymbol{G}_{\phi,op}$ are used to represent the complex weighting matrix obtained for vertically and horizontally polarized plane waves with AoA ranges from 0^o to 359^o with 1^o step, respectively. The difference between $G_{\theta,op}$ and $G_{\phi,op}$ for $R = 0.5$m, $R = 2$m, $R = 1000$m is shown in Figure 8 (figures on the left). The difference depends on the ratio between test area radius and ring radius r/R. Simulation results show that complex weights for the two polarizations are practically the same for $R \geqslant 2$ meters, which is consistent with the fact that the complex weights obtained with the EIV technique is independent of polarizations.

The difference between $\mathbf{G}_{TI}$and $\boldsymbol{G}_{\phi,op}$ for $R = 0.5$m, $R = 2$m, $R = 1000$m is shown in Figure 8 (figures on the right). The difference between the two complex weighting matrix is due to the limited ring radius. As explained in Section II-B, ideal plane waves radiating from the probes are assumed. The complex weighting matrix obtained with the EIV technique is practically the same as the weights obtained with the PWS optimization technique for large R case. The conclusion for relationship between test area size and number of probes is consistent for the PWS and the EIV techniques. For the PWS technique, the smaller the test area, the smaller number of required probes we need to maintain the field synthesized accuracy. For the EIV technique, the smaller the test area, the smaller number of required probes we need to reconstruct the received voltage. Note that for a multi-probe setup with $R \geqslant 2$m, complex weighting matrix $\mathbf{G}_{TI}$, $\boldsymbol{G}_{\phi,op}$ and $\mathbf{G}_{\theta,op}$ are practically the same.

Depending on the number of samples selected for field synthesis and the number of plane waves for optimization, the PWS can be computationally heavy. While the EIV technique offer a closed form solution for large R case. However, for small R cases, the PWS technique offer better accuracy. Furthermore, accurate field synthesis is not sufficient to guarantee accurate resulting received voltage. The received voltage accuracy depends on the DUT antenna pattern, which can not be demonstrated by the PWS technique.

Measurement verification of the PWS technique is given in [5]. Good agreement between measurements and simulations has been achieved in terms of the received voltage, as an omnidirectional Satimo calibration dipole was used as the DUT.

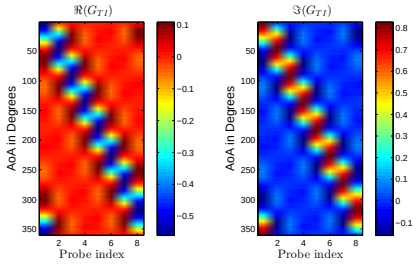

Figure 7. Real and imaginary part of the complex weighting matrix G_{TI} with TI technique for $R = 2$m. The phase at the ring center is set to 0 the frequency is set to 2.45GHz.

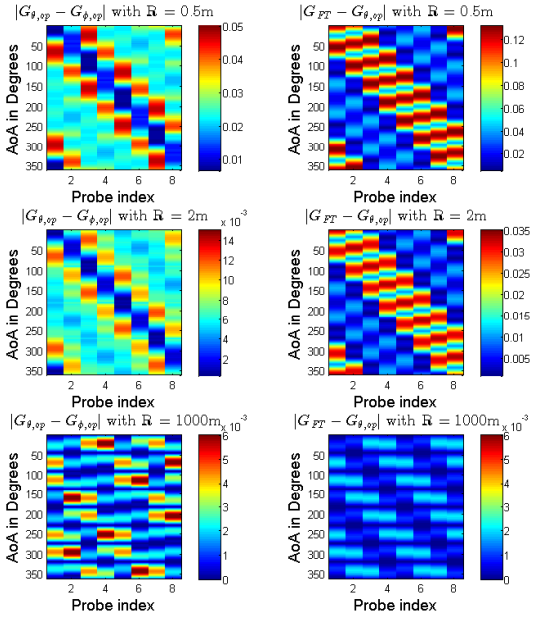

Figure 8. Difference between $G_{\theta,op}$ and $G_{\phi,op}$ and difference between $G_{\theta,op}$ and G_{TI} for $R = 0.5$m, $R = 2$m, $R = 1000$m respectively. The phase at the ring center is set to 0. The frequency is set to 2.45GHz and test area radius $r = 0.35\lambda$ is selected for the PWS optimization.

B. Results for prefaded signal synthesis (PFS)

1) Measured radiation pattern results: The measured radiation patterns of the DUTs are shown in Figure 9 and Figure 10. Due to the close-by antenna coupling impact, the dipole gain patterns are not omnidirectional. The measured phase patterns of the practical dipoles, vertically placed CTIA good and nominal antennas over DUT orientation follow sinusoidal curves quite well, as shown in Figure 9. However, the measured phase patterns of 45^o slanted CTIA good and nominal antennas do not follow sinusoid curves at all (not shown). Phase patterns are quite inaccurate when the gain patterns are in deep fades. Deep nulls are present in the

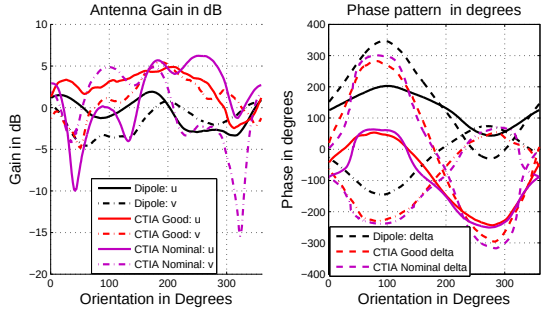

Figure 9. Measured antenna patterns for practical dipoles, vertically placed CTIA good and nominal antennas. Legend delta in the phase pattern curves corresponds to the phase difference between u and v. Note that the power amplifier gain, cable and free space propagation attenuation are not normalized in the results.

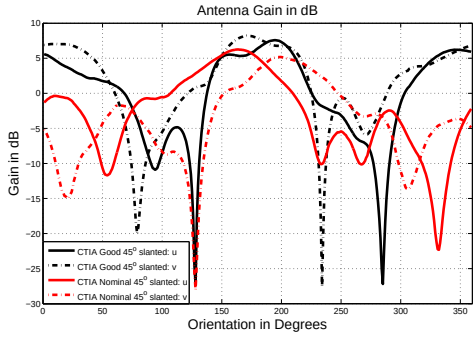

Figure 10. Measured antenna patterns for the 45^o slanted CTIA good and nominal antennas.

gain patterns for the two DUTs, as shown in Figure 10. The measured antenna pattern are used to calculate ρ_a and $\hat{\rho}_a$ as specified in (14) and (17), respectively.

2) Emulated spatial correlation results: Table III summarizes the spatial correlation emulation error $|\rho_a - \hat{\rho}_a|$ for all the DUTs in the four test scenarios. The ideal DUT denotes two omnidirectional antennas with 0.5λ antenna separation. $|\rho_a - \hat{\rho}_a|$ for the practical dipoles present comparable accuracy when compared with ideal DUT case for all the test scenarios. However, the relative error level is higher for practical dipoles, as correlation over orientations for the ideal DUT ranges from 0.25 to 0.8, compared with from 0.45 to 0.7 for the practical dipoles, as shown in Figure 11.

$|\rho_a - \hat{\rho}_a|$ in the test scenario A present better accuracy than in B for all the DUTs. This is expected since the test area performance is the best if the cluster is arriving to the test area from the direction where one of the OTA antennas are located (Scenario A), while the worst case is the cluster impinging from an angle exactly in the middle of two adjacent OTA probes (Scenario B). Emulation results in test scenario C and D present comparable accuracy. Test area emulation accuracy highly depends on the number of probes used in the setup.

Table III
STATISTICS OF SPATIAL CORRELATION EMULATION ERROR $|\rho_a - \hat{\rho}_a|$ AND STATISTICS OF MEASURED CORRELATION DEVIATION FROM EMULATED CORRELATION $|\rho_m - \hat{\rho}_a|$ FOR ALL TEST SCENARIOS

Test DUT	A				B				C				D			
	$\lvert\rho_a - \hat{\rho}_a\rvert$		$\lvert\rho_m - \hat{\rho}_a\rvert$		$\lvert\rho_a - \hat{\rho}_a\rvert$		$\lvert\rho_m - \hat{\rho}_a\rvert$		$\lvert\rho_a - \hat{\rho}_a\rvert$		$\lvert\rho_m - \hat{\rho}_a\rvert$		$\lvert\rho_a - \hat{\rho}_a\rvert$		$\lvert\rho_m - \hat{\rho}_a\rvert$	
	rms	max	rms	max	rms	max	rms	max	rms	max	rms	max	rms	max	rms	max
Ideal DUT	0.03	0.05			0.10	0.15			0.01	0.01			0.01	0.01		
Dipoles	0.04	0.07	0.04	0.06	0.09	0.14	0.05	0.08	0.01	0.02	0.02	0.05	0.01	0.02	0.03	0.04
Nominal	0.11	0.18	0.02	0.05	0.22	0.33	0.03	0.05	0.01	0.03	0.04	0.08	0.02	0.04	0.04	0.08
Good	0.16	0.28	0.03	0.05	0.29	0.45	0.06	0.14	0.02	0.04	0.05	0.10	0.02	0.05	0.08	0.20
Nominal slanted	0.20	0.44	0.09	0.34	0.30	0.53	0.08	0.15	0.02	0.03	0.07	0.11	0.03	0.05	0.11	0.32
Good slanted	0.29	0.61	0.09	0.18	0.38	0.71	0.05	0.12	0.02	0.04	0.08	0.15	0.04	0.08	0.07	0.13

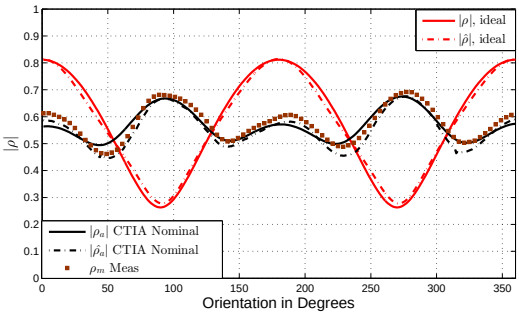

Figure 11. Target $|\rho_a|$, emulated $|\hat{\rho}_a|$ and measured $|\rho_m|$ spatial correlation for practical dipoles for test scenario A.

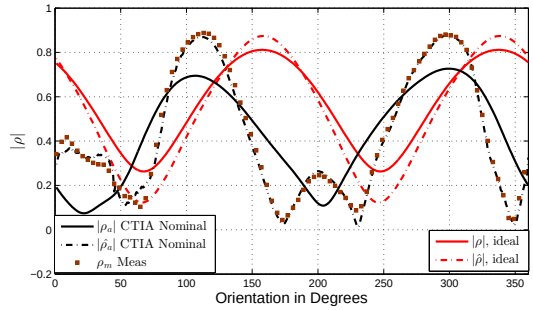

Figure 12. Target $|\rho_a|$, emulated $|\hat{\rho}_a|$ and measured $|\rho_m|$ spatial correlation for the vertically placed CTIA good antenna for test scenario B.

Therefore, emulation accuracy results in scenario C and D are much better than in A and B for all the DUTs, respectively.

For test scenario A and B, the antenna patterns have a great impact on emulation accuracy. Maximum emulation error is 0.15 for the ideal DUT for test scenario B and up to 0.71 for the 45^o slanted CTIA good antenna. Figure 12 shows the target, emulated and measured spatial correlation for the vertically placed CTIA good antenna for test scenario B. The root mean square (RMS) emulation error $|\rho_a - \hat{\rho}_a|$ is 0.29, although $|\hat{\rho}_a|$ follows the tendency of $|\rho_a|$ very well over orientations. Figure 13 shows the real and imaginary part of the target, emulated and measured spatial correlation for the 45^o slanted CTIA good antenna for test scenario B. Although both the real and imaginary part of $\hat{\rho}_a$ follow the tendency of ρ_a, big deviations exist. If the antenna pattern variation is too high with respect to the number of probes, $\hat{\rho}_a$ will be inaccurate. The antenna pattern hence have to be considered when investigating the required number of OTA probes. The antenna pattern impact on spatial correlation emulation accuracy in test scenario C and D is negligible. As shown in Figure 14, both the real and imaginary parts of $\hat{\rho}_a$ follow ρ_a accurately for the 45^o slanted CTIA nominal antenna for test scenario C.

3) Measurement results: Statistics of the deviation between the measured correlations from the emulated correlations $|\rho_m - \hat{\rho}_a|$ for all the DUTs in all test scenarios are shown in Table III. Measurement verification of the ideal DUT with a virtual uniform linear array (ULA) can be found [17]. Measured spatial correlation ρ_m for all scenarios generally matches

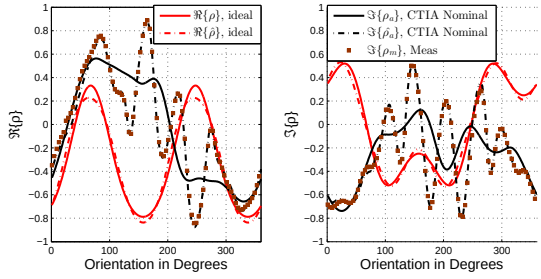

Figure 13. Real and imaginary part of the target ρ_a, emulated $\hat{\rho}_a$ and measured ρ_m spatial correlation for the 45^o slanted placed CTIA good antenna for test scenario B.

$\hat{\rho}_a$ accurately, as shown in Figure 11-14. RMS deviations of up to 0.05 can be found for the practical dipoles while the RMS deviation is up to 0.08 for vertically placed for the CITA good and nominal antennas. When placed 45^o slanted, very few big deviations can be found in some orientations for the CTIA antennas while the RMS deviation levels are only slightly higher than the vertically placed cases. Deviations are likely due to the cable movement. During the antenna pattern and correlation measurements, the cables that connect the DUT to the VNA are moving and bending around the turntable. Different cable movements may happen during the antenna pattern and correlation measurements, and hence the measured antenna patterns might be different from the antenna patterns that the DUT presents during the correlation measurements.

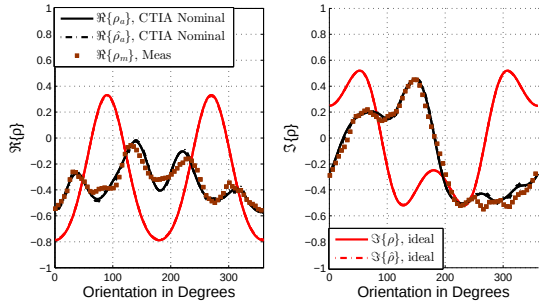

Figure 14. Real and imaginary part of the target ρ_a, emulated $\hat{\rho}_a$ and measured ρ_m spatial correlation for the 45^o slanted placed CTIA nominal antenna for test scenario C.

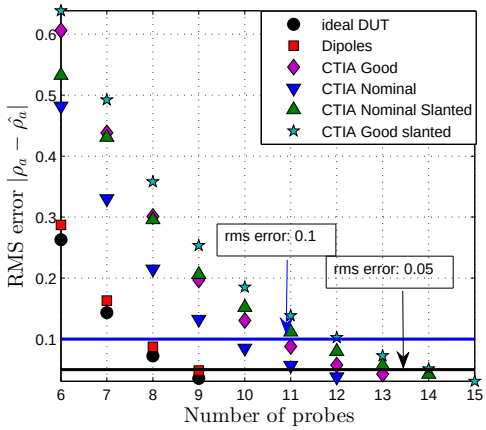

Figure 15. Number of required probes for realistic DUTs. Test zone size: 0.5λ.

4) Number of required probes for accurate spatial correlation reconstruction: Results have shown $|\rho_a - \hat{\rho}_a|$ depends on the target channel model. One criterion we should follow is that inside the test area, emulation accuracy should be sufficiently good even for the worst channel case. Figure 15 shows the number of required probes for realistic DUTs for a Laplacian shaped PAS with AoA =$180^o/K$ and AS = 35^o. The measured DUT radiation patterns are used to calculate $|\rho_a - \hat{\rho}_a|$ for a given number of probes. Figure 15 shows that we need only 8 probes for the dipoles within a test area size of 0.5λ with 0.05 rms error accuracy requirement. However, to obtain the same test area performance, we need as many as 14 probes for the 45^o slanted CTIA good antenna. The number of probes, which is considered enough to obtain accurate $|\rho - \hat{\rho}|$ for ideal DUTs [2], [7]–[9], [17], is generally not sufficient for realistic DUTs.

V. Conclusion

This paper investigates the impact of the antenna pattern on test zone performance for multi-probe based MIMO OTA setup from the received voltage and spatial correlation point of view. The PWS technique for horizontal polarization is introduced, and simulation results show that complex weights for the two polarizations are practically the same for large R. A novel closed form technique named the EIV technique to reproduce received voltage with arbitrary plane waves based on trigonometric interpolation is presented. The EIV technique presents practically the same complex weights as the PWS techniques for large R MIMO OTA setups. We have shown that the received voltage accuracy depends not only on the field synthesis accuracy, but also on the DUT radiation pattern. The impact of the antenna pattern on the received voltage accuracy is ruled by the Nyquist sampling theory. We show that more probes are required for DUTs with bigger variation in the antenna pattern to obtain accurate received voltage. Furthermore, in the PFS method, the impact of the antenna pattern on spatial correlation accuracy is investigated. Simulation and measurement results show that the number of probes, which is considered enough to obtain accurate spatial correlation $|\rho - \hat{\rho}|$ for ideal DUTs, is generally not sufficient for realistic DUTs with higher variation in the antenna pattern. For example, RMS emulation error for test scenario A with 8 uniformly spaced probes is 0.03 for the ideal DUTs for a test area of 0.5λ, while up to 0.29 for the 45^o slanted CTIA good antenna. We show that only 8 probes are sufficient to achieve 0.05 rms error accuracy for the dipoles within a test area size of 0.5λ. However, to obtain the same test area performance, we need as many as 14 probes for the 45^o slanted CTIA good antenna.

Wei Fan received his Bachelor of Engineering degree in electrical engineering from Harbin Institute of technology, China, in 2009 and Master's double-degree with highest honors from Politecnico di Torino, Italy, and Grenoble Institute of Technology, France, in electronic engineering in 2011. From February 2011 to August 2011, he was with Intel Mobile Communications, Denmark. He is currently a Ph.D. candidate at Department of Electronic Systems at Aalborg University, Denmark. His main areas of research are over the air testing of MIMO terminals and radio channel modeling.

Jesper Ødum Nielsen received his master's degree in electronics engineering in 1994 and a PhD degree in 1997, both from Aalborg University, Denmark. He is currently employed at Department of Electronic Systems at Aalborg University where main areas of interests are experimental investigation of the mobile radio channel and the influence mobile device users have on the channel. He has been involved in MIMO channel sounding and modeling, as well as measurements using live GSM and LTE networks. In addition he has been working with radio performance evaluation, including over the air testing of active wireless devices.

Ondrej Franek was born in 1977. He received the M.Sc. (Ing., with honors) and Ph.D. degrees in electronics and communication from Brno University of Technology, Czech Republic, in 2001 and 2006, respectively. Currently, he is working at the Department of Electronic Systems, Aalborg University, Denmark, as an associate research professor. Since 2012, he has also been employed as an external consultant for antenna topics at Intel Mobile Communications in Aalborg, Denmark. His research interests include computational electromagnetics with focus on fast and efficient numerical methods, especially the finite-difference time-domain method. He is involved in research on antennas, biological effects of non-ionizing electromagnetic radiation, indoor and outdoor radiowave propagation, and electromagnetic compatibility.

Dr. Franek was the recipient of the Seventh Annual SIEMENS Award for outstanding scientific publication.

Xavier Carreño received his Master degree from 'Escola Tènica Superior d'Enginyeria de Telecomunicació de Barcelona' (UPC) in 2011. At UPC he was deeply involved in baseband signal processing algorithms and MIMO OTA research topics within Intel Mobile Communications, where he currently has a leading role in the MIMO OTA development team as system engineer. He is involved in the standardization of MIMO OTA methods and has coauthored several 3GPP, CTIA and IC1004 contributions and several conference and journal papers on the subject. His primary interests are within the area of MIMO OTA testing techniques, MIMO channel modeling and LTE platform testing.

Jagjit Singh Ashta born in 1988, obtained a Master Degree in Telecommunications in the 'Escola Tènica Superior d'Enginyeria de Telecomunicació de Barcelona' (UPC) in 2012. In the same year he completed with honours his Master Thesis on MAC layer improvements for IEEE 802.11 networks (WLAN) at Aalborg University (AAU) in collaboration with Nokia Solutions and Networks (NSN). Currently he develops his career as a Wireless Communications Engineer at Xtel ApS and is employed as an external software consultant at Intel Mobile Communications, Denmark. His research interests cover the MAC and PHY layers of the RANs and the development of software solutions required to study them.

Mikael Bergholz Knudsen was born in 1964. He received the B.S. degree in electrical engineering from Aarhus Teknikum, Denmark, in 1989, and the M.S. and Ph.D. degrees from Aalborg University, Denmark, in 1992 and 2001, respectively. In 1993, he joined Maxon Telecom A/S, Aalborg, Denmark, where he designed RF circuitry for both analog and digital mobile phones. From 1998 to 2001, he worked as an industrial Ph.D. student for Siemens Mobile Phones A/S, Denmark, while he at the same time studied at Aalborg University. He is now with Intel Mobile Communications Denmark, where he is the project manager for the 4th Generation Mobile Communication and Test platform (4GMCT) and also the chairman of the steering committee for the Smart Antenna Front End (SAFE) projects; both sponsored by the Danish National Advanced Technology Foundation. His areas of interest include RF system design and handset antenna performance including more than one antenna. In the resent years one of his focus areas has been how to utilize the unique possibilities in the cooperation between university researchers and private companies.

Gert Frølund Pedersen was born in 1965 and married to Henriette and have 7 children. He received the B.Sc. E. E. degree, with honour, in electrical engineering from College of Technology in Dublin, Ireland in 1991, and the M.Sc. E. E. degree and Ph. D. from Aalborg University in 1993 and 2003. He has been with Aalborg University since 1993 where he is a full Professor heading the Antenna, Propagation and Networking LAB with 36 researcher. Further he is also the head of the doctoral school on wireless communication with some 100 phd students enrolled. His research has focused on radio communication for mobile terminals especially small Antennas, Diversity systems, Propagation and Biological effects and he has published more than 175 peer reviewed papers and holds 28 patents. He has also worked as consultant for developments of more than 100 antennas for mobile terminals including the first internal antenna for mobile phones in 1994 with lowest SAR, first internal triple-band antenna in 1998 with low SAR and high TRP and TIS, and lately various multi antenna systems rated as the most efficient on the market. He has worked most of the time with joint university and industry projects and have received more than 12 M$ in direct research funding. Latest he is the project leader of the SAFE project with a total budget of 8 M$ investigating tunable front end including tunable antennas for the future multiband mobile phones. He has been one of the pioneers in establishing Over-The-Air (OTA) measurement systems. The measurement technique is now well established for mobile terminals with single antennas and he was chairing the various COST groups (swg2.2 of COST 259, 273, 2100 and now ICT1004) with liaison to 3GPP for over-the-air test of MIMO terminals. Presently he is deeply involved in MIMO OTA measurement.

REFERENCES

[1] M. Rumney, R. Pirkl, M. H. Landmann, and D. A. Sanchez-Hernandez, "MIMO Over-The-Air Research, Development, and Testing," *International Journal of Antennas and Propagation*, vol. 2012, 2012.

[2] P. Kyösti, T. Jämsä, and J. Nuutinen, "Channel modelling for multiprobe over-the-air MIMO testing," *International Journal of Antennas and Propagation*, 2012.

[3] P. Kyösti, J. Nuutinen, and T. Laitinen, "Over the air test," Patent WO 2012/117 147 A1, Sep. 7, 2012.

[4] T. Laitinen, P. Kyösti, J.-P. Nuutinen, and P. Vainikainen, "On the number of OTA antenna elements for plane-wave synthesis in a MIMO-OTA test system involving a circular antenna array," in *Antennas and Propagation (EuCAP), 2010 Proceedings of the Fourth European Conference on*. IEEE, 2010, pp. 1–5.

[5] W. Fan, X. Carreño, J. Ø. Nielsen, K. Olesen, M. B. Knudsen, and G. F. Pedersen, "Measurement Verification of Plane Wave Synthesis Technique Based on Multi-probe MIMO-OTA Setup," in *Vehicular Technology Conference (VTC Fall), 2012 IEEE*. IEEE, 2012, pp. 1–5.

[6] A. Khatun, H. Laitinen, V.-M. Kolmonen, and P. Vainikainen, "Dependence of Error Level on the Number of Probes in Over-the-Air Multiprobe Test Systems," *International Journal of Antennas and Propagation*, vol. 2012, 2012.

[7] P. Kyösti and J. Nuutinen, "Over the air test," Patent US 20 110 189 962, Aug. 4, 2011.

[8] J. D. Reed, "Emulation and controlled testing of MIMO OTA channels," Patent US 20 110 299 570, Dec. 8, 2011.

[9] M. A. Mow, B. Niu, R. W. Schlub, and R. Caballero, "Tools for design and analysis of over-the-air test systems with channel model emulation capabilities," Patent US 20 110 270 567, Nov. 3, 2011.

[10] J. Toivanen, T. Laitinen, V. Kolmonen, and P. Vainikainen, "Reproduction of Arbitrary Multipath Environments in Laboratory Conditions," *Instrumentation and Measurement, IEEE Transactions on*, vol. 60, no. 1, pp. 275–281, 2011.

[11] T. Laitinen and P. Kyösti, "On appropriate probe configurations for practical MIMO over-the-air testing of wireless devices," in *Antennas and Propagation (EUCAP), 2012 6th European Conference on*, 2012, pp. 1544–1548.

[12] S. Boyd and L. Vandenberghe, *Convex Optimization*. Cambridge University Press, 2004.

[13] G. Giacaglia, "Trigonometric interpolation," *Celestial mechanics*, vol. 1, pp. 360–367, 1970. [Online]. Available: http://dx.doi.org/10.1007/BF01231141

[14] J. E. Hansen, *Spherical near-field antenna measurements*. Peter Peregrinus Ltd, 1988, vol. 26.

[15] Y. Okano, K. Kitao, and T. Imai, "Impact of number of probe antennas for MIMO OTA spatial channel emulator," in *Antennas and Propagation (EuCAP), 2010 Proceedings of the Fourth European Conference on*. IEEE, 2010, pp. 1–5.

[16] R. Vaughan, J. Bach-Anderson, and J. B. Andersen, "Channels, propagation and antennas for mobile communications." Institution of Electrical Engineers, 2003.

[17] P. Kyosti, J.-P. Nuutinen, and T. Jamsa, "MIMO OTA test concept with experimental and simulated verification," in *Antennas and Propagation (EuCAP), 2010 Proceedings of the Fourth European Conference on*. IEEE, 2010, pp. 1–5.

[18] I. Szini, G. Pedersen, A. Scannavini, and L. Foged, "MIMO 2×2 reference antennas concept," in *Antennas and Propagation (EUCAP), 2012 6th European Conference on*, March, pp. 1540–1543.

[19] "Measurement of Radiated Perfromances for MIMO and Multi-antenna reception for HSPA, and LTE terminals," 3GPP/3GPP2, TR 37.976 v11.1.0, April. 2012.

[20] "Verification of radiated multi-antenna reception performance of User Equipment," 3GPP, TR 37.977 V0.2.0, May. 2012.

Paper C

Probe Selection in Multi-probe OTA Setups

Wei Fan, Fan Sun, Jesper Ø. Nielsen, Xavier Carreño, Jagjit S. Ashta, Mikael B. Knudsen and Gert F. Pedersen

The paper has been published in the
IEEE Transactions on Antennas and Propagation, vol. 62, no. 4, pp. 2109–2120, April, 2014.

The layout has been revised.

Probe Selection in Multi-probe OTA Setups

Wei Fan, Fan Sun, Jesper Ø. Nielsen, Xavier Carreño, Jagjit S. Ashta, Mikael B. Knudsen and Gert F. Pedersen

***Abstract*—Standardization work for over-the-air (OTA) testing of multiple input multiple output (MIMO) capable terminals is currently ongoing in COST IC1004, 3GPP and CTIA, where a multi-probe anechoic chamber based method is a promising candidate. Setting up a multi-probe configuration with channel emulators is costly, so finding ways to limit the number of probes while still reproducing the target channels accurately could make the test system both cheaper and simpler to implement. Several probe selection algorithms are presented in this paper to address this issue. The proposed techniques provide a probe selection framework for the channel emulation techniques published in the literature. Simulation results show that good channel emulation accuracy can be achieved with the selected subset of probes for the considered target channel models. The probe selection algorithm is further supported by measurement results in a practical multi-probe setup.**

I. Introduction

Over-the-air (OTA) testing of the radio performance of mobile terminals has the advantage of not needing to break or otherwise modify the mobile device. OTA testing for mobile terminals with a single antenna was standardized by CTIA and 3GPP about ten years ago, but these standards cannot be used directly for evaluating multiple input multiple output (MIMO) capable devices [1]. OTA testing for MIMO capable terminals is mandatory as traditional conductive tests bypass the antennas and thus results in unrealistic performance evaluation results. There are three main types of OTA test methods for MIMO devices: multi-probe anechoic chamber-based methods, reverberation chamber-based methods and two-stage methods [1]. All currently have their limitations: there is limited temporal and spatial control of the reproduced channel in the reverberation chamber-based method; practical issues such as including self-interference still exist in the two-stage method; and the cost of the setup is the main issue with the multi-probe anechoic chamber-based method [1].

Several papers have addressed OTA testing for MIMO devices in multi-probe anechoic chamber setups with emphasis on channel modeling, where the goal is to accurately reproduce realistic channel models in the test volume. Two channel emulation techniques have been proposed in the literature. One technique is the plane wave synthesis (PWS) technique reported in [2]–[4]. The other technique is named the prefaded signal synthesis (PFS) technique [2] and has been adopted in several commercial channel emulators, e.g. Anite Propsim channel emulation solutions and Spirent VR5 [5], [6]. Verification measurements of the two techniques in a two dimensional (2D) multi-probe setup have been reported in many contributions, see e.g. [7]–[10]. It has been shown that the channels reproduced in the test area match well with the target. To emulate a realistic environment which can accurately reflect the real wireless propagation environment in the anechoic chamber, 3D channel model emulation with the multi-probe setup in an anechoic chamber has attracted interest as well [4], [11]–[13].

The cost of the multi-probe anechoic chamber setup mainly depends on the channel emulators and the number of probes required for reproducing the desired channel models. It has been demonstrated that a large number of probes is required to create a large test area in the chamber [11], [12], [14]. As the number of available output ports of the channel emulator is limited, several channel emulators are often required, which will dramatically increase the setup cost. Setting up a 3D multi-probe configuration is even more costly, so finding ways to limit the number of probes while still approximating the target channels sufficiently accurately could make the test system both cheaper and simpler to implement. Radio channel models are generally directional in real world scenarios, which has been widely studied in the literature and adopted in the standard channel models, see e.g. [15]–[18]. However, a uniform configuration of the OTA probes over the azimuth plane is often adopted in the multi-probe setup [1]. As a consequence, contributions from some probes might be dominant, while negligible from other probes when synthesizing the target radio channels. Hence a probe selection mechanism has potential to save cost, via reducing the required number of fading channels.

Figure 1 shows an illustration of a practical 3D multi-probe setup, where a probe selector is used to select the optimal subset of probes for reproducing the desired channels. The basic idea is to select an optimal subset of probes of size N from K total available probes ($N \leq K$). The N selected probes are connected to the PAs and the channel emulators and hence are used for reproducing the target channels in the test zone, while the other probes are disconnected from the channel emulator and properly terminated.

The probe selection technique for 2D single cluster spatial channel models has been implemented in a commercial channel emulator, the Anite Propsim channel emulator. In [19], the probe selection algorithm in 2D multi-probe setups was briefly described for the PFS technique, although no results were given.

In this paper, the probe selection in a 3D multi-probe OTA setup is addressed, where the probes are selected based on channel emulation accuracy in terms of either field synthesis error or spatial correlation error, which are selected as the figure of merit (FoM) in the PWS and the PFS technique,

Wei Fan, Fan Sun, Jesper Ø. Nielsen, and Gert F. Pedersen are with the Antennas, Propagation and Radio Networking section at the Department of Electronic Systems, Faculty of Engineering and Science, Aalborg University, Denmark (email: {wfa, fs, jni, gfp}@es.aau.dk).

Xavier Carreño, Jagjit S. Ashta, and Mikael B. Knudsen are with Intel Mobile Communications, Denmark (email: {xavier.carreno, jagjitx.singh.ashta, mikael.knudsen}@intel.com).

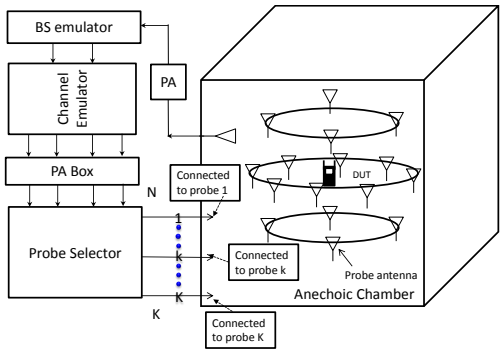

Figure 1. An illustration of the probe selection in a multi-probe setup. The system consists of a base station (BS) emulator, one or several radio channel emulators, an anechoic chamber, OTA probe antennas, a power amplifier (PA) box, a probe selector and a device under test (DUT). K and N denote the number of available OTA probes and the number of active OTA probes that are connected to the channel emulator, respectively.

respectively [2], [20]. The main contributions of this work are:

- We form the probe selection algorithms both for the PWS and the PFS techniques.
- The probe selection algorithm for multi-cluster channel models is proposed.
- We propose the probe selection algorithm for 3D multi-probe setups with arbitrary probe configurations.
- Three different probe selection algorithms are proposed and evaluated.
- The probe selection algorithm for a multi-cluster channel model is supported by measurements in a practical 2D multi-probe setup.

II. Channel Emulation Techniques

A. Prefaded signal synthesis (PFS)

The PFS technique was proposed in [2] for the 2D multi-probe setup and was extended to the 3D multi-probe setup in [11]. As detailed in [11], the focus is on reproducing the channel spatial characteristics in the test volume at the receiver (Rx). The basic idea is that by allocating appropriate power weights to the OTA probes, we can reproduce the incoming spherical power spectrum (SPS) of the channel in the test volume. The goal is to minimize the deviation between the theoretical spatial correlation resulting from the target continuous SPS, and the emulated spatial correlation resulting from the discrete SPS, with its shape characterized by the discrete angular positions of the probes and the power weights.

A location pair is used to represent the locations of two spatial samples where the two isotropic antennas u and v are placed [11], [21]. The two spatial samples are selected to be directly opposite to each other w.r.t the test volume center and the distance between them is the test volume size. It is desirable that the spatial correlation error $|\rho - \hat{\rho}|$ should be smaller than the predefined emulation accuracy requirement for all the location pairs. The DUT should be smaller than the test volume size to ensure that the target propagation environment is accurately reproduced around the DUT. As explained in [2], [11], the polarization is omitted from the described PFS method, as the SPS of target channel models for different polarizations can be reproduced applying the same PFS technique. Probe selection for the dual polarized channel models should be based on the cross polarization ratio (XPR) of the channel models.

The spatial correlation for the mth location pair can be determined according to [11], for a single polarization, as:

$$\rho(m) = \oint \exp(ja(\overline{r}_{u,m} - \overline{r}_{v,m}) \cdot \overline{\Omega}) p(\Omega) d\Omega, \qquad (1)$$

where $\overline{r}_{u,m}$ and $\overline{r}_{v,m}$ are vectors containing the position information of antenna u and v at the mth location pair, respectively. $\overline{\Omega}$ is an unit vector corresponding to the solid angle Ω. a is the wave number. $p(\Omega)$ is the SPS satisfying $\oint p(\Omega) d\Omega = 1$. $(\cdot)$ is the dot product operator. Similar to (1), the emulated spatial correlation for the mth location pair can be calculated based on the discrete SPS characterized by K probes as:

$$\hat{\rho}(m) = \sum_{k=1}^{K} w_k \exp(ja(\overline{r}_{u,m} - \overline{r}_{v,m}) \cdot \overline{\Phi}_k), \qquad (2)$$

where $\boldsymbol{w} = [w_1, ..., w_K]^T$ is a power weighting vector to be optimized. $\overline{\Phi}_k$ is a unit position vector of the kth probe.

To minimize the emulation error over M location pairs, the following objective function is used:

$$\min_{\boldsymbol{w}} \ \|\mathbf{F}_S \boldsymbol{w} - \boldsymbol{\rho}\|_2^2, \qquad (3)$$
$$\text{s.t. } 0 \le w_k \le 1, \ \forall k \in [1, K]$$

where $\mathbf{F}_S \boldsymbol{w} = \hat{\boldsymbol{\rho}}$ and $\boldsymbol{\rho}$ are the emulated spatial correlation and target spatial correlation vectors of size M, respectively, with the mth element corresponding to the spatial correlation between two isotropic antennas at the mth location pair. The M location pairs are selected on the surface of the test volume, as in [11]. Other ways to select location pairs, e.g. throughout the test volume, might give better emulation accuracy. However, they are not considered in this paper due to the computation complexity. $\mathbf{F}_S \in \mathbb{C}^{M \times K}$ is the transfer matrix whose elements are, according to (2), given by:

$$(\mathbf{F}_S)_{m,k} = \exp(ja(\overline{r}_{u,m} - \overline{r}_{v,m}) \cdot \overline{\Phi}_k), \quad 1 \le m \le M \quad (4)$$

B. Plane wave synthesis (PWS)

Two channel modeling schemes based on the PWS techniques have been proposed in the literature as summarized below:

- In one channel modeling scheme [2], [3], a channel with a given incoming SPS is modeled by a collection of plane waves. Each of the plane waves impinging the test area with a specific angle-of-arrival can be approximated by allocating appropriate complex weights to the probes. The weights are obtained using optimization techniques, e.g. least mean square. A Doppler shift can then be introduced to each static plane wave to enable time variant channels.

Note that the complex weights to create each of the plane waves have to be determined only once and the temporal behavior is generated by multiplying the fixed weight with a rotating phasor. Also note that this is essentially a stationary channel model with fixed angles of arrival, as the incoming SPS has a specified shape.

- In another channel modeling scheme proposed in [4], each snapshot of the time-varying channel is considered static. The snapshots are characterized by the angles-of-arrivals, complex amplitudes, and polarizations of all waves, and hence can be reproduced by allocating appropriate complex weights to the multiple probes. The static plane waves are approximated from the spherical wave theory point of view. Arbitrary multipath environments (e.g. channels with time-varying angles of arrival) can be reproduced using this channel modeling scheme, unlike the first method. Note that the complex weights are calculated for each snapshot of the channel.

The basis for both channel modeling schemes is to obtain optimal complex weights for creating static plane waves with arbitrary angles-of arrivals for θ and φ polarizations. Note that same notations as [2] have been adopted in this paper. In order to ensure the emulated field approximates the target field in terms of magnitude, phase and polarization for all the samples inside the test volume, decomposition into three orthogonal axes x, y and z is required. The weighting vector $\boldsymbol{g_\theta}$ for a θ polarized plane wave can be obtained by solving the optimization problem as follows:

$$\min_{\mathbf{g}_{\boldsymbol{\theta}}} \left\| \begin{bmatrix} \mathbf{F}_{\theta,x} \\ \mathbf{F}_{\theta,y} \\ \mathbf{F}_{\theta,z} \end{bmatrix} \boldsymbol{g_\theta} - \begin{bmatrix} \boldsymbol{t}_{\theta,x} \\ \boldsymbol{t}_{\theta,y} \\ \boldsymbol{t}_{\theta,z} \end{bmatrix} \right\|_2^2 \quad \text{s.t. } 0 \leq |g_{\theta,k}| \leq 1 \; \forall k \in [1, K] \tag{5}$$

where

- $\mathbf{g}_{\boldsymbol{\theta}} = \{g_{\theta,k}\} \in \mathbb{C}^{K\times 1}$ is a vector of the complex weights for θ polarized probes.
- $\boldsymbol{t}_{\theta,x}$, $\boldsymbol{t}_{\theta,y}$, and $\boldsymbol{t}_{\theta,z} \in \mathbb{C}^{M\times 1}$ are vectors of θ polarized complex target fields projected to the x, y and z axes, respectively. M is the total number of samples.
- $\mathbf{F}_{\theta,x}$, $\mathbf{F}_{\theta,y}$ and $\mathbf{F}_{\theta,z} \in \mathbb{C}^{M\times K}$ are transfer matrices of known field propagation coefficients from the K probes to the M sample points for the θ polarization projected to the x, y and z axes, respectively.

The same principle can be applied for the φ polarization.

III. Probe selection algorithm

A. General formulation

Without the explicit constraints for each element of the weighting vector, the objective functions (3) and (5) can be written in a generic format as:

$$\min_{\mathbf{c}} \|\mathbf{F}\mathbf{c} - \boldsymbol{t}\|_2^2 \tag{6}$$

where $\mathbf{F}$ and $\boldsymbol{t} \in \mathbb{C}^{M\times 1}$ are the transfer matrix and the target as specified in Sec. II. $\boldsymbol{c} = [c_1, ..., c_K]$ is the weighting vector to be optimized for the K probes. Note that the constraint for $\boldsymbol{c}$ is different for the PWS and the PFS technique. All the constraints documented in the previous section are convex constraints. Therefore, the formulation in (6) with additional convex constraints is a convex problem in this study. For simplicity, the constraints are omitted in the following problem formulation for the probe selection.

Then, the objective of the probe selection is to reproduce the channel models in the test volume with N OTA probes selected from the available K probes, i.e. to select N probes for channel emulation and disconnect the remaining probes from the channel emulator. The problem formulation for the probe selection is as follows:

$$\min_{\mathbf{c}} \; \|\mathbf{F}\mathbf{c} - \boldsymbol{t}\|_2^2 \quad \text{s.t. } \|\mathbf{c}\|_0 = N \tag{7}$$

where the norm-0 operation $\|\cdot\|_0$ is defined to be the number of nonzero entries in the vector. The problem in (7) is non-convex and NP-hard due to the norm-0 constraint.

After knowing locations of the nonzero entries, the optimization is simplified to be a convex optimization problem as:

$$\min_{\mathbf{c}_{sel}} \|\mathbf{F}_{sel}\mathbf{c}_{sel} - \boldsymbol{t}\|_2^2$$

where $\mathbf{F}_{sel}$ is the $M \times N$ matrix with N selected columns from $\mathbf{F}$, and $\mathbf{c}_{sel}$ is the $N \times 1$ vector with N selected probe locations.

B. Probe selection for the single cluster and multi-cluster channels

The concept of clusters has been widely adopted to model the multipath phenomenon based on extensive measurements. The radio waves could gather in one cluster or several clusters distributed over the space domain, see e.g. the SCME models [22]. Different clusters have different delays, thus making the channel wideband. Single cluster channel models and multi-cluster channel models have to be treated in a different manner in the probe selection process. In order to preserve the delay information of the channel, each cluster should be emulated individually with the multiple probes [21]. However, this is problematic with the probe selections. If each cluster is emulated independently, different sets of probes may be selected for different clusters, and the total number of selected probes might be larger than the number of available channel emulator output ports.

We propose to perform one probe selection optimization for the combined clusters, i.e. without delay discrimination and thus essentially a narrowband channel, instead of performing a probe selection optimization for each cluster. After knowing N probes for the narrow-band multi-cluster channel models, each cluster of the wideband channel can be then emulated individually with the same selected N probes.

C. Probe selection for different channel modeling schemes based on PWS technique: angular static and dynamic

If the target channel model consists of only static plane waves, the target field will be the sum of the static fields.

The probe selection process can be directly applied. For time varying channels modeled with the two channel modeling schemes based on the PWS techniques mentioned in Sec.II-B, two different probe selection processes should be considered.

- For channels emulated with the channel modeling scheme as described in [2], [3], the probe selection should be based on the SPS of the target channels, as the target is to form a channel with the target incoming SPS shape [2]. Hence the probe selection algorithm should be based on spatial correlation error. After selecting the optimal N probes for the target channel models, each of the different plane waves that are used to form the SPS is emulated individually with the same selected N probes. As explained in [2], complex weights for the PWS are function of angle-of-arrival of the plane wave and the probe configuration only. Even though the complex weights are time dependent for time-varying channels, the angle-of-arrival dependent part has to be determined only once. Temporal behavior is generated by multiplying the fixed weights with a rotating phasor. It is possible to precalculate the complex weights for each plane wave synthesis, which would reduce the computing time significantly during emulation.
- For channels emulated with channel modeling scheme detailed in [4], the time-varying channel at a time moment (each snapshot) can be represented by a collection of static plane waves. At each snapshot, since the target channel is static plane waves, the probe selection process can be directly applied. Different snapshots may present different target plane waves, and thus a different set of N probes might be selected for different snapshots of the channel. Note that probe switching from snapshot to snapshot is required, and the probe-switching time has to be shorter than the required channel update rate.

D. Probe selection algorithms

Different probe selection algorithms are detailed in the following part to deal with the non-convex problem explained in (7). As a benchmark, we perform the channel emulation with all the available K probes to evaluate the performance deterioration when less probes are used. This channel emulation with all available probes can be simply treated as a performance upper bound. It worth mentioning here that the probe selection algorithm is similar to the antenna selection process in MIMO communication systems [23], [24].

1) Brute force algorithm: A straightforward way to select probes is to use the brute force method where the optimization is performed for each possible combination of the N probes out of K probes. Then weights which result in the best fit in terms of spatial correlation accuracy or field synthesis accuracy using N probes will be selected. Therefore, the total number of combinations is $\begin{pmatrix} K \\ N \end{pmatrix}$. When we go over all the possible combinations, the combination which gives the minimum emulation error can be obtained. However, the number of combinations to be tested becomes huge when K is large. Other alternatives have to be considered as the computation time for the probe selection is crucial.

Algorithm 1 Multi-shot algorithm

Set $n = 0$ and $k_0 = 0$

Iterate

Update $n = n + 1$ until $K - \sum_{m=0}^{n-1} k_m = N$

1. Build $\mathbf{F}_n$ based on $K - \sum_{m=0}^{n-1} k_m$ active probes
2. Optimize for $K - \sum_{m=0}^{n-1} k_m$ active probes

$$\min_{\mathbf{c}_n} \|\mathbf{F}_n \mathbf{c}_n - \boldsymbol{t}\|_2^2 .$$

3. In $\mathbf{c}_n$, remove k_n probes with least power values.

Return $N \times 1$ vector $\mathbf{c}_n$ based on $\min_{\mathbf{c}_n} \|\mathbf{F}_n \mathbf{c}_n - \boldsymbol{t}\|_2^2$ and the corresponding N probe index numbers

2) Multi-shot algorithm: Alternatively, probes can be selected in a sequential manner in the multi-shot algorithm. In this multi-shot algorithm, we will remove a certain number of probes at each iteration ("shot"). Basically, in each iteration the probes with least contributions are removed. Note that the number of probes removed in each iteration is not necessarily constant. We denote by k_n the number of probes we remove in the nth iteration and $\mathbf{F}_n$ is the matrix associated with the selected $K - \sum_{m=0}^{n-1} k_m$ probes in the nth iteration.

In the multi-shot algorithm, we first perform the power optimization for K probes. In the nth iteration, based on the individual probe power values in $\mathbf{c}_n$, we remove k_n probes with the least contributions. We repeat the probe removal process until only $K - \sum_{m=0}^{n-1} k_m = N$ probes are left. In the end, we return both the final probe weights and the corresponding probe index numbers. The detailed process is summarized in Algorithm 1.

3) Successive probe cancellation (SPC) algorithm: In the multi-shot algorithm, we are removing probes with least power values and form a new optimization with less probes in an iterative manner. In contrast, for the SPC algorithm we select probes with largest power values in a sequentially manner. This probe selection algorithm adopts the idea of successive interference cancellation (SIC) technique, which is a popular technique in wireless communications.

The key idea is to find the probes with most contributions in each iteration. Then the contributions of the selected dominant probes are removed in the target and the consequent probe power optimizations. In each iteration, we target to find a certain number of dominant probes and the number of probes selected does not need to remain the same across the iterations.

In this algorithm, we still perform the probe power optimization for K probes at first. In each iteration, we will select a certain number of active probes with largest power contributions and store the probe index numbers and the corresponding angular locations. To differentiate from the k_n used in the multi-shot algorithm, we denote p_n to be the number of probes we select in the nth iteration and $\mathbf{F}_n$ to be the matrix associated with the remaining non-selected $K - \sum_{m=0}^{n-1} p_m$ probes in the nth iteration. In the beginning of each iteration, we update $\mathbf{F}_n$ according to the current remaining non-selected probes. Then to prepare for the subsequent optimization, we remove the contributions of the selected probes by modifying the target $\boldsymbol{t}_{n+1} = \boldsymbol{t}_n - \mathbf{F}_n \hat{\mathbf{c}}_n$, where $\hat{\mathbf{c}}_n$ is the weighting

Algorithm 2 Successive probe cancellation (SPC) algorithm

Set $n = 0$ and $p_0 = 0$

Iterate

Update $n = n + 1$ until $\sum_{m=0}^{n-1} p_m = N$

1. Build $\mathbf{F}_n$: $K - \sum_{m=0}^{n-1} p_m$ non-selected probes
2. Optimize for $K - \sum_{m=0}^{n-1} p_m$ active probes

$$\min_{\mathbf{c}_n} \|\mathbf{F}_n \mathbf{c}_n - \boldsymbol{t}_n\|_2^2 .$$

3. Select p_n probes with largest power values in $\mathbf{c}_n$
4. Compute $\hat{\mathbf{c}}_n$ and update $\boldsymbol{t}_{n+1} = \boldsymbol{t}_n - \mathbf{F}_n \hat{\mathbf{c}}_n$

Return the selected N probe index numbers and derive the power weights based on $\min_{\mathbf{c}_{spc}} \|\mathbf{F}_{spc}\mathbf{c}_{spc} - \boldsymbol{t}\|_2^2$

vector obtained from $\mathbf{c}_n$, and $\hat{\mathbf{c}}_n$ consists of the weights for the p_n selected probes from $\mathbf{c}_n$ in the nth iteration and the rest entries set to zero. This probe contribution cancellation process carried out in the end of each iteration, is analogous to the SIC technique. We continue the iteration until $\sum_{m=0}^{n-1} p_m = N$ probes are selected. In the end, based on the selected probes, we build $\mathbf{F}_{spc}$ and perform a final optimization to find the power weights $\mathbf{c}_{spc}$. The successive probe cancellation (SPC) algorithm is detailed in Algorithm 2.

The main difference from the multi-shot algorithm lies in that the contributions of the removed probes are also removed from the target, whereas in the multi-shot algorithm the target stays the same throughout all the iterations.

4) One-shot algorithm: A simple way to select probes is to use the one-shot method where the convex optimization is performed with K probes for $\min_{\mathbf{c}} \|\mathbf{F}\mathbf{c} - \boldsymbol{t}\|_2^2$. Based on the individual probe power values $|c_{index}|$ $(1 \leq index \leq K)$, $(K - N)$ probes with least power values are removed.

We denote $\mathbf{F}_{one}$ to be the matrix associated with the selected N probes of dimension $M \times N$. Then we perform the optimization for the remaining N probes with $\mathbf{c}_{one}$ being the $N \times 1$ vector

$$\min_{\mathbf{c}_{one}} \|\mathbf{F}_{one}\mathbf{c}_{one} - \boldsymbol{t}\|_2^2 .$$

5) Algorithm Summary: In the multi-shot algorithm, we can remove different number of probes in each iteration, $k_n \neq k_m\,(m \neq n)$. If we set $k_n = k_m = k\,(m \neq n)$, we need to apply the convex optimization $\frac{K-N}{k} + 1$ times to accomplish the probe selection process. The previous one-shot algorithm is an extreme case of the multi-shot algorithm where $k = K - N$ is used. Also, if we set $p_n = p_m = p\,(m \neq n)$ for the SPC algorithm, we need to apply the convex optimization $\frac{N}{p} + 1$ times. Notice that the one-shot algorithm is also an extreme case of the SPC algorithm where $p = N$ is used. A summary of different algorithms is given in Table I.

As described above, different k_m and p_m can be used in simulations. In the following numerical evaluations, $k_n = k_m = 1\,(m \neq n)$ and $p_n = p_m = 1\,(m \neq n)$ are chosen for the multi-shot algorithm and the SPC algorithm, unless otherwise stated. Further investigations are needed to find the tradeoff between computation complexity and accuracy for various target channel models and probe configurations.

Table I
ALGORITHM COMPARISON (SELECTION: N OF K PROBES)

Algorithm	Number of convex optimizations	Emulation performance
Brute force	$\binom{K}{N} = \frac{K!}{(K-N)!N!}$	Best performance
One-shot	2	Worst performance
Multi-shot	$\frac{K-N}{k} + 1$	No worse than one-shot
Successive probe cancellation	$\frac{N}{p} + 1$	No worse than one-shot
No probe selection (benchmark)	1	Performance bound

Table II
PROBE CONFIGURATIONS. ($K = 48$)

Case	Probe Setup
P1	$\theta_1 = -30^o\ \phi_{1i} = -180^o + i \cdot 30^o, i \in [1, ..., 12]$
	$\theta_2 = 0^o\ \phi_{2i} = -180^o + i \cdot 15^o, i \in [1, ..., 24]$
	$\theta_3 = 30^o\ \phi_{3i} = -180^o + i \cdot 30^o, i \in [1, ..., 12]$
P2	$\theta_1 = -45^o\ \phi_{1i} = -180^o + i \cdot 45^o, i \in [1, ..., 8]$
	$\theta_2 = -10^o\ \phi_{2i} = -180^o + i \cdot 22.5^o, i \in [1, ..., 16]$
	$\theta_3 = 10^o\ \phi_{3i} = -180^o + i \cdot 22.5^o, i \in [1, ..., 16]$
	$\theta_4 = 45^o\ \phi_{4i} = -180^o + i \cdot 45^o, i \in [1, ..., 8]$

IV. SIMULATION RESULTS

The probe configurations and the target channel models are firstly described in this part. After that, the simulation results with different probe selection algorithms are shown. The total number of available probes is $K = 48$, and the number of output ports of the channel emulator N is set to 16. The test volume size is selected to be one wavelength. Vertical polarization is assumed for all the target channel models, for the sake of simplicity.

A. Probe configuration

Two different probe configurations are assessed for the probe selection algorithm, as detailed in Table II. The probes are placed on a sphere, and the elevation angle θ and the azimuth angle φ are specified for each probe. The probes are organized on several elevation rings. θ_l denotes the elevation angle for all the probes on the lth elevation ring. ϕ_{lj} is the azimuth angle of the jth probe on the lth elevation ring. Figure 2(a) and Figure 2(b) illustrate the probe configuration P1 and P2, respectively.

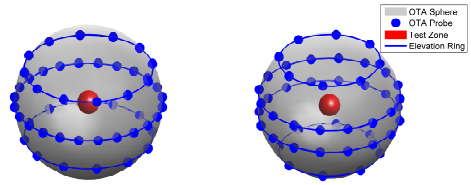

(a) Probe setup P1 (b) Probe setup P2

Figure 2. An illustration of probe configuration P1 (a) and P2 (b), detailed in Table II.

Table III
TARGET SINGLE CLUSTERS

Target Case	Target Spherical Power Spectrum		
	PAS shape	PES shape	Comment
A	AoA = 0^o ASA = 35^o	EoA = 0^o ESA = 10^o	Laplacian shaped PAS and PES, as shown in Figure 4
B	AoA = 15^o ASA = 35^o	EoA = 15^o ESA = 10^o	Gaussian shaped PAS and PES
C	Uniform	EoA = 0^o ESA = 10^o	Uniform shaped PAS and Laplacian shaped PES, as shown in Figure 3

Table IV
TEST CASE D FOR THE ALGORITHM COMPARISON

Cluster Index	Cluster info	1	2	3	4	5	6
PAS	AoA [^{o}]	66	46	143	33	-91	-19
	ASA [^{o}]	35	35	35	35	35	35
PES	EoA [^{o}]	0	-10	0	10	0	15
	ESA [^{o}]	10	10	10	10	10	10
Power [dB]		0	-2.2	-1.7	-5.2	-9.1	-12.5

B. Probe selection simulation results for the PFS technique

Three target single cluster channel models are considered, as detailed in Table III. The SPS is modeled independently by the power azimuth spectrum (PAS) characterized by the azimuth angle of arrival (AoA) and azimuth spread of arrival (ASA), and the power elevation spectrum (PES) characterized by the elevation angle of arrival (EoA) and elevation spread of arrival (ESA) [15]. Several different PAS and PES models are considered for the target channel models. A multi-cluster channel model is considered as well, as described in Table IV. The considered model is the SCME UMa TDL model extended to 3D. The SCME models are defined only on the azimuth plane and with no spread over the elevation dimension. Here a Laplacian shaped PES is introduced to each of the clusters. Note that the proposed algorithms are not restricted to any model, and SPS based on measurements can be reproduced as well.

Figure 3 and Figure 4 shows the emulated and target SPS for target channel case C with no probe selection and case A with the one-shot algorithm, respectively. As discussed previously, the emulated discrete SPS is characterized by power weights of the probes. The shape of the emulated discrete SPSs match well visually with the shape of the continuous target PASs for both cases. The target SPS for case D is shown in Figure 5 (below). As we can see in Figure 5 (top), no probes corresponding to the 5th and 6th cluster are selected, as the probe selection optimization is based on the SPS of the multi-cluster model (without delay discrimination). The selected probes are favoring the dominant clusters, so the emulation accuracy for individual clusters might be bad. The target spatial correlation $|\rho|$ for case D and associated correlation error $|\rho - \hat{\rho}|$ associated with no probe selection, the one-shot and the multi-shot algorithm are shown in Figure 6. The spatial correlation between the antennas u and v varies with the location pair position. The distance between the location pair is the test volume size, i.e. 1λ, and the location pair position is characterized by the elevation and azimuth angle.

The root mean square (RMS) values of the correlation error $|\rho - \hat{\rho}|$ with different algorithms for the considered target channel models are shown in Table IV-B. The deviation between the theoretical spatial correlation of the target continuous SPS, and the emulated correlation of the discrete SPS depends on the channel models and probe configurations. Note that generally the correlation error $|\rho - \hat{\rho}|$ increases as we increase the test volume size [2], [11], [21]. That is, the correlation

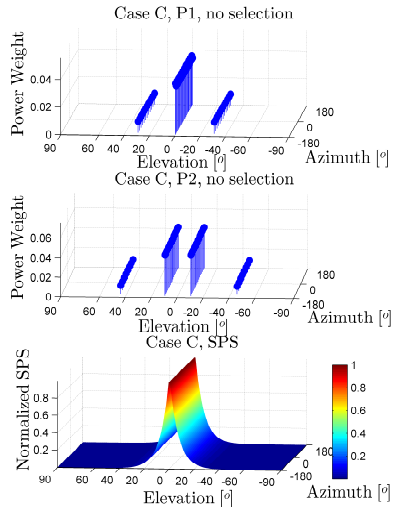

Figure 3. Emulated and target SPS for case C and using all probes for the two probe configurations.

error with antenna separation smaller than test volume size will be smaller than the values presented in Table IV-B.

The performance deterioration when less probes are used is quite small for case A, case C and case D, which is expected as the cluster is arriving to the test zone from the direction where the probes are located. For case B, the emulation accuracy is worse as the cluster is impinging from an angle between the probes. The no probe selection case provides the best emulation accuracy for all the cases, as expected. The one-shot algorithm provides slightly worse or the same performance as the multi-shot algorithm, as all the probes with high weights are selected both for the one-shot algorithm and the multi-shot algorithm, and only a few probes with small weights are selected differently, as shown in Figure 5 and Figure 6 for case D, as an example. The same probes are selected for the one-shot algorithm and the SPC algorithm for all the considered scenarios. All the proposed probe selection algorithms work well, as the correlation error is only slightly worse than the case with no probe selection.

The RMS of the correlation error $|\rho - \hat{\rho}|$ as a function of number of selected probes for the two probe configurations with the one-shot and the multi-shot algorithm is shown in Figure 7. The more probes selected, the better channel emulation accuracy we can achieve for all scenarios, as expected. This improvement, however, saturates at a certain number

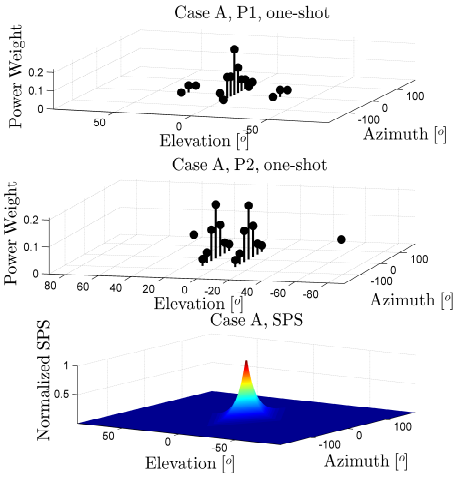

Figure 4. Emulated and target SPS for case A with the one-shot algorithm for the two probe configurations.

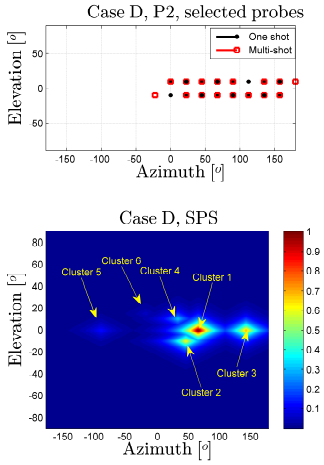

Figure 5. The target SPS and selected probes with the one-shot and the multi-shot algorithm for case D.

Table V
RMS OF THE EMULATION ERROR $|\rho - \hat{\rho}|$ WITH DIFFERENT ALGORITHMS FOR DIFFERENT TARGET MODELS. $N = 16$

Method	Probe Setup	A	B	C	D
No probe selection	P1	0.028	0.278	0.018	0.019
	P2	0.047	0.16	0.025	0.009
One-shot	P1	0.031	0.281	0.029	0.024
	P2	0.06	0.16	0.061	0.023
Multi-shot	P1	0.03	0.28	0.029	0.023
	P2	0.057	0.16	0.036	0.02
SPC	P1	0.031	0.281	0.029	0.024
	P2	0.06	0.16	0.061	0.023

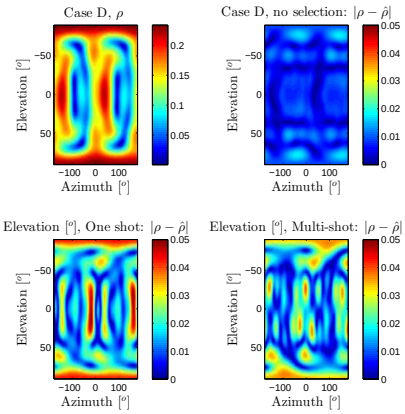

Figure 6. The target spatial correlation $|\rho|$ and the associated correlation error $|\rho - \hat{\rho}|$ with no probe selection, the one-shot and the multi-shot algorithm for case D.

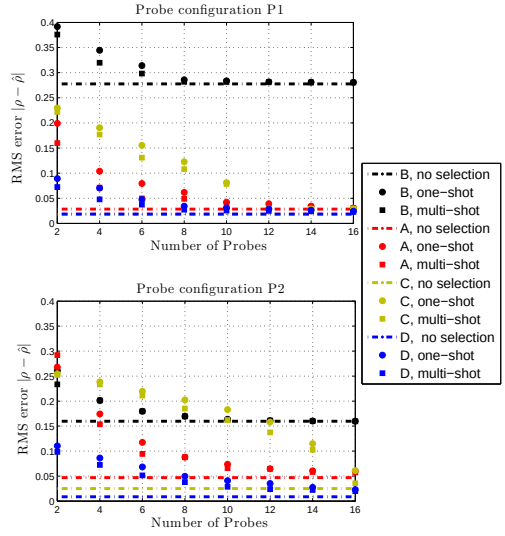

Figure 7. The RMS error $|\rho - \hat{\rho}|$ as a function of the number of selected probes for the two probe configurations. Note that for probe configuration P1, the curve with no probe selection for channel model C is on top of the curve with no probe selection for channel model D.

of selected probes, depending on the target channel models and probe configuration. The multi-shot algorithm generally outperforms, though marginally, the one-shot algorithm. This is due to the fact that only a few probes with small weights are selected differently in the two algorithms.

C. Probe selection for the PWS technique

As explained in Section II-B, the basis for radio channel emulation with the PWS techniques is to reproduce the static plane waves. Three static scenarios are considered as examples

Table VI
TARGET STATIC PLANE WAVES

Target case	E	F	G
AoA [^{o}]	0	100	Two static plane waves detailed in case E and F, respectively.
EoA [^{o}]	0	15	
Target field at test volume	Phase 0^o at center		
	Uniform magnitude of 1 over test volume		
Comment	Vertically polarized	Vertically polarized	

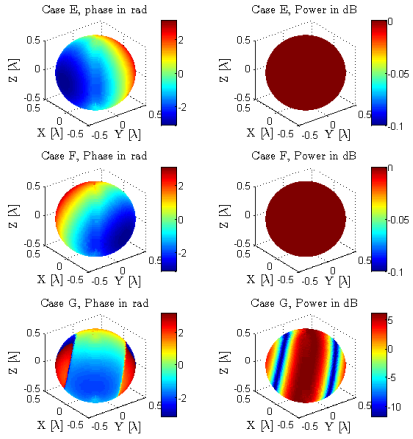

Figure 8. The phase and power distribution over test volume of target scenario E (top), F (middle) and G (bottom), respectively.

for the target scenarios, as detailed in Table VI. The impinging angle of each plane wave is characterized by the AoA and EoA. A single static plane wave is considered in case E and in case F, respectively. Case F represents a critical scenario where the target plane wave is impinging from between the probes, while case E is expected to offer better emulation accuracy. A multi-static plane wave case is considered in case G. Figure 8 illustrates the phase and power distribution over the test volume of target scenario E, F, and G, respectively. Linear phase fronts along the propagation direction and uniform power distribution over the test volume can be observed for scenario E and F. For scenario G, the fades in power are caused by the destructive superposition of two static plane waves with different propagation directions. To characterize the deviation between the target field and synthesized field, the maximum of the error vector magnitude in dB among all the sample points on the surface of the test volume ϵ is defined as follows:

$$\epsilon = \max\{10\lg(|\mathbf{F}_{\xi,x}\boldsymbol{g}_{\boldsymbol{\xi}} - \boldsymbol{t}_{\xi,x}|^2 + |\mathbf{F}_{\xi,y}\boldsymbol{g}_{\boldsymbol{\xi}} - \boldsymbol{t}_{\xi,y}|^2 + |\mathbf{F}_{\xi,z}\boldsymbol{g}_{\boldsymbol{\xi}} - \boldsymbol{t}_{\xi,z}|^2)\},$$

where ξ denotes either θ or φ polarization. The maximization is performed over M sample points.

A summary of field synthesis error ϵ with different algorithms is shown in Table VII. The polarization of the target

Table VII
FIELD SYNTHESIS ERROR ϵ [dB] WITH DIFFERENT ALGORITHMS. N = 16

Method	Probe Setup	E	F	G
No probe selection	P1	-28.72	-13.28	-13
	P2	-23.1	-22.1	-20.2
One-shot/SPC	P1	-28.58	-13.39	-9.95
	P2	-22.31	-21.24	-19.23
Multi-shot	P1	-28.57	-13.31	-9.96
	P2	-22.30	-21.11	-19.17

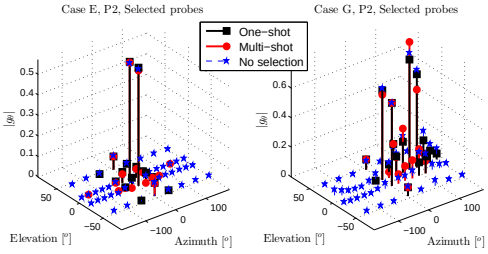

Figure 9. Magnitude of the complex weights for the selected probes with the one-shot and the multi-shot algorithm for case E (left) and case G, respectively.

channel models E, F, and G are detailed in Table VI. The same probes are selected for the SPC algorithm as the one-shot algorithm and the results are not shown. ϵ depends on the target channel models and probe configurations, as previously discussed. The performance deterioration when less probes are used is marginal. This is due to the fact that only a few probes are dominant when synthesizing the target channel models, as shown in Figure 9, for example. Also, as all the probes with high weights are selected both for the one-shot algorithm and the multi-shot algorithm, the two probe selection algorithms present similar performance.

D. A critical probe configuration for the one-shot algorithm

In the previously considered cases, the one-shot algorithm presents only slightly worse results than the multi-shot algorithm. This is due to the fact that the number of selected probes N is sufficiently large that all dominant probes are selected with the one-shot and the multi-shot algorithm. To better demonstrate the difference between the two algorithms for the scenarios where the number of selected probes N is smaller than the number of dominant probes, a simple 2D probe configuration and a 2D target channel model are considered, as detailed in Table VIII. Note this probe configuration with $K = 360$ might be practically unrealistic due to the issues such as the power coupling between probes, reflections and physical size. This case is included only to illustrate the problems with the one-shot algorithms.

The target spatial correlation $|\rho|$ and the associated emulated spatial correlation $|\hat{\rho}|$ with no probe selection, the multi-shot algorithm and the one-shot algorithm with $N = 5$ for the case H is shown in Figure 10 (top). As we can see, the multi-shot algorithm works well and the correlation error $|\rho - \hat{\rho}|$ is quite small. However, the one-shot algorithm presents

Table VIII
A CRITICAL PROBE CONFIGURATION.

Target Channel Case:H	Probe configuration P3	Test area size
Laplacian shaped PAS with AoA = 22.5^o and ASA = 35^o	$K = 360$ uniformly distributed probes on the azimuth plane	0.7λ

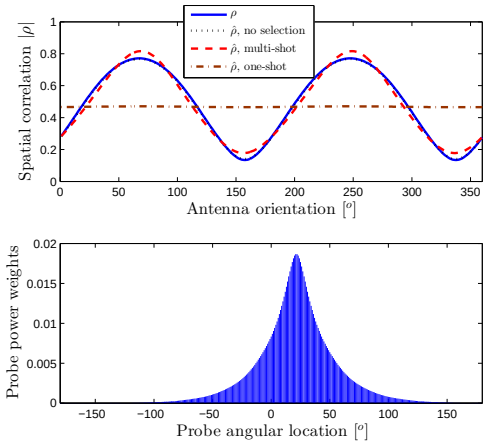

Figure 10. The target spatial correlation $|\rho|$ and the associated emulated spatial correlation $|\hat{\rho}|$ with no probe selection, the multi-shot and the one-shot algorithms for case H (top). The probe weights with no probe selection is shown in the figure as well (bottom). The selected number of probes is $N = 5$.

large deviations. The probe weights for the probes selected with the one-shot algorithm and the multi-shot algorithm are shown in Figure 11. The probes around AoA = 22.5^o are selected for the one-shot algorithm, as the probes with high weights concentrate around AoA = 22.5^o, as shown in the Figure 10 (bottom). However, these selected probes will be incapable of creating the azimuth spread of target channels. The power weights of the $N = 5$ selected probes are shown in Figure 11 (left). The zeros for the middle probes are due to the convex optimization after the probe selection. As the optimization attempts to create the azimuth spread of the channel, effectively only two probes with larger angular distance to AoA = 22.5^o are used to synthesize the channel. With the multi-shot algorithm, the emulated PAS follows well the target PAS, as shown in the Figure 11 (right).

The RMS error $|\rho - \hat{\rho}|$ as a function of the number of selected probes for the target channel H with the one-shot and the multi-shot algorithm is shown in Figure 12. The multi-shot algorithm clearly outperforms the one-shot algorithm. The SPC algorithm presents the same results as the one-shot algorithm, as the same probes are always selected.

V. MEASUREMENT VERIFICATION

A measurement campaign was carried out in a practical setup at Aalborg University to verify the proposed probe

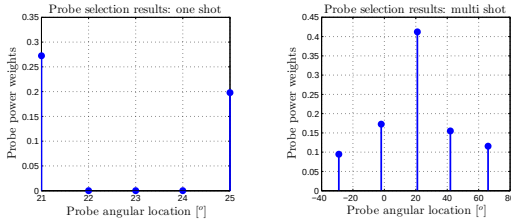

Figure 11. The probe weights for the probes selected with the one-shot algorithm (left) and the multi-shot algorithm (right) with $N = 5$.

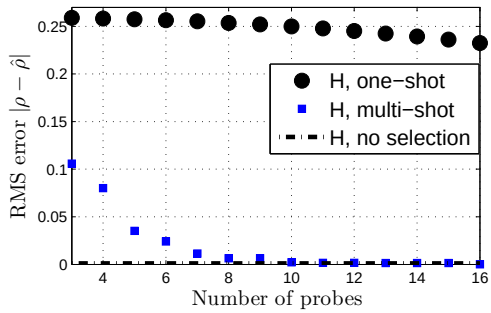

Figure 12. The RMS error $|\rho - \hat{\rho}|$ as a function of number of selected probes for target channel H with the probe configuration P3.

selection algorithm. Figure 13 shows the practical multi-probe setup inside the anechoic chamber. A small choke is used on the test dipole to minimize cable effects. The measurement setup and the spatial correlation measurement procedure were described in section IV of [21] and not detailed here. A summary of the measurement setup is given in Table IX. As detailed in Table X, three test cases are considered for the measurement campaign. The total available number of probes is $K = 16$ and the number of selected probes is $N = 8$. It is desirable that with the selected subset of probes ($N = 8$), we can emulate the SCME UMi TDL model with comparable channel emulation accuracy achieved with 16 uniformly placed probes (i.e. with no probe selection). The multi-shot algorithm is used to select the subset of probes. Figure 14 illustrates the probe configurations for the three cases. The angular locations of the selected probes match well with the AoAs of the SCME UMa TDL model, as expected.

In [2], it is concluded that both channel emulation techniques are capable of creating spatial radio channel characteristics according to the target model. However, the PWS technique requires accurate phase calibration of the setup and hence the PFS technique is considered for the channel emulation in the measurements.

The simulation results of the spatial correlation $|\rho|$ for the SCME UMi TDL model and correlation error $|\hat{\rho} - \rho|$ with the three setups are shown in Figure 15. The radius d and polar angle ϕ_a of each point on the plots correspond to the value at antenna separation d and antenna orientation ϕ_a [21]. Given the error criteria $|\hat{\rho} - \rho|$, the corresponding radius of the

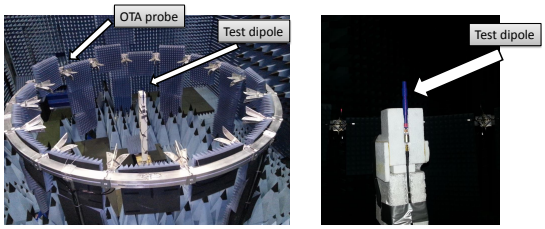

Figure 13. An illustration of the multi-probe setup (left) and the dipole setup (right) in the anechoic chamber.

Table IX
MEASUREMENT SETUP SUMMARY

	Setup and specifications
Target channel model	SCME urban micro (UMi) TDL model as detailed in [25] with carrier frequency $f_c = 1900$ MHz.
Test antenna	Satimo electric sleeve dipole at 1900MHz.
Test antenna position	25 test antenna positions sample a segment of line of length 24cm (around 1.5λ) with sampling interval of 1cm and with antenna orientation $\phi_a = 0^o$ and $\phi_a = 90^o$.
OTA probes	Three configurations as detailed in Table X and shown in Figure 14.

circle, which corresponds to the test area size, can be found. The antenna separation d and the antenna orientation ϕ_a are used to characterize the position of the location pair in 2D setup. Maximum deviation of 0.06 is achieved over the test area size of 1.5λ for the setup II with 16 probes. With 8 uniformly spaced probes, the test area is much smaller. With the setup III, a test area size of 1.5λ can be achieved with slight performance deterioration compared with setup II with 16 probes.

The target $|\rho|$, emulated $|\hat{\rho}|$ and measured $|\rho_{meas}|$ spatial correlation of the SCME UMi TDL model for the three setups for antenna orientation $\phi_a = 0^o$ and $\phi_a = 90^o$ are

Table X
TEST CASES FOR THE MEASUREMENTS

Setup	No. of Probe	Test area	probe configuration
I	8	0.7λ	uniformly spaced with 45^o angular separation
II	16	1.5λ	uniformly spaced with 22.5^o angular separation
III	8	1.5λ	8 probes selected from 16 uniformly placed probes

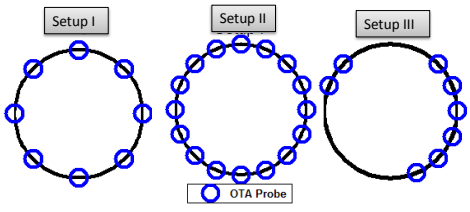

Figure 14. An illustration of the probe configurations for the three cases.

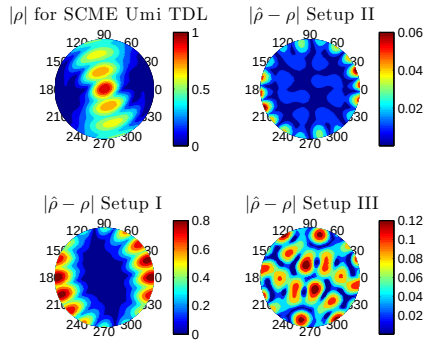

Figure 15. $|\rho|$ and spatial correlation error $|\rho - \hat{\rho}|$ for the SCME UMi TDL model for the three setups. Test area size: 1.5λ.

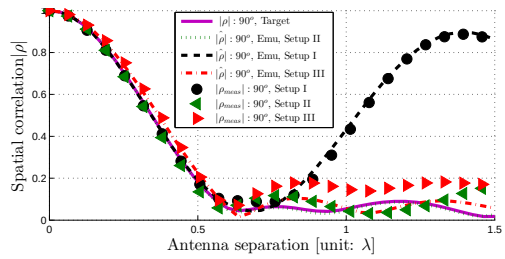

Figure 16. Comparison between target, emulated and measured spatial correlation for antenna orientation $\phi_a = 0^o$ for the three setups.

shown in Figure 16 and Figure 17, respectively. The deviations between $|\hat{\rho}|$ and $|\rho|$ depend on the probe configuration and the number of OTA probes [2], [21]. The measured spatial correlations $|\rho_{meas}|$ generally match well with the emulated spatial correlations $|\hat{\rho}|$ for the three setups.

The deviation caused by a difference between the plane and spherical waves due to the physical limitation of the OTA ring is negligible, according to the results in [26]. One possible reason for the deviation between measurements and simulations is that the radiation pattern of the test dipole presents around 1.5 dB variation due to the cable effect, although a small choke was used. As shown in the results, the channel emulation accuracy achieved with 8 selected probes is only slightly worse than that achieved with 16 uniformly placed probes.

VI. CONCLUSION

This paper presents three probe selection algorithms for 3D multi-probe based setups. The proposed techniques provide a probe selection framework for the two channel emulation techniques, i.e. the plane wave synthesis technique and the prefaded signal synthesis techniques. Simulation results show that good channel emulation accuracy can be achieved with the selected subset of probes for the considered target channel models. The one-shot algorithm presents lowest computation complexity and only slight performance deterioration compared with the multi-shot algorithm for the scenarios where

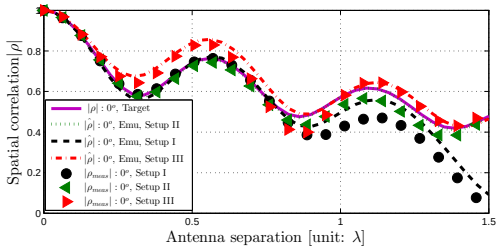

Figure 17. Comparison between target, emulated and measured spatial correlation for antenna orientation $\phi_a = 90^o$ for the three setups.

the number of selected probes is sufficiently large that all dominant probes are selected with the one-shot algorithm. For the scenarios where the number of selected probes is smaller than the number of dominant probes, the multi-shot algorithm generally outperforms the one-shot algorithm significantly. The probe selection algorithm for the SCME UMi TDL model is supported by measurements in a practical 2D multi-probe setup. The measurement results show that the channel emulation accuracy achieved with 8 selected probes is only slightly worse compared to that achieved with 16 uniformly placed probes for a test area of 1.5λ.

REFERENCES

[1] M. Rumney, R. Pirkl, M. H. Landmann, and D. A. Sanchez-Hernandez, "MIMO Over-The-Air Research, Development, and Testing," *International Journal of Antennas and Propagation*, vol. 2012, 2012.

[2] P. Kyösti, T. Jämsä, and J. Nuutinen, "Channel modelling for multiprobe over-the-air MIMO testing," *International Journal of Antennas and Propagation*, 2012.

[3] P. Kyösti, J. Nuutinen, and T. Laitinen, "Over the air test," Patent WO 2012/117 147 A1, Sep. 7, 2012.

[4] J. Toivanen, T. Laitinen, V. Kolmonen, and P. Vainikainen, "Reproduction of Arbitrary Multipath Environments in Laboratory Conditions," *Instrumentation and Measurement, IEEE Transactions on*, vol. 60, no. 1, pp. 275–281, 2011.

[5] P. Kyösti and J. Nuutinen, "Over the air test," Patent US 20 110 189 962, Aug. 4, 2011.

[6] J. D. Reed, "Emulation and controlled testing of MIMO OTA channels," Patent US 20 110 299 570, Dec. 8, 2011.

[7] W. Fan, X. Carren, J. Nielsen, K. Olesen, M. Knudsen, and G. Pedersen, "Measurement Verification of Plane Wave Synthesis Technique Based on Multi-Probe MIMO-OTA Setup," in *Vehicular Technology Conference (VTC Fall), 2012 IEEE*, 2012, pp. 1–5.

[8] W. Fan, X. Carreño, J. Ø. Nielsen, M. B. Knudsen, and G. F. Pedersen, "Channel Verification Results for the SCME models in a Multi-Probe Based MIMO OTA Setup," in *Vehicular Technology Conference (VTC Fall)*. IEEE, September 2013, pp. 1–5.

[9] S. Alessandro, F. C., and N. G., "MIMO OTA measurement with anechoic chamber method," in *Antennas and Propagation (EUCAP), 2013 7th European Conference on*. IEEE, April 2013.

[10] P. Kyosti, J.-P. Nuutinen, and T. Jamsa, "MIMO OTA test concept with experimental and simulated verification," in *Antennas and Propagation (EuCAP), Proceedings of the Fourth European Conference on*. IEEE, 2010, pp. 1–5.

[11] W. Fan, F. Sun, P. Kyösti, J. Nielsen, X. Carreño, M. Knudsen, and G. Pedersen, "3D channel emulation in multi-probe setup," *Electronics Letters*, vol. 49, pp. 623–625(2), April 2013.

[12] P. Kyösti and A. Khatun, "Probe Configurations for 3D MIMO Over-the-Air Testing," in *Antennas and Propagation (EUCAP), Proceedings of the 7th European Conference on*. IEEE, 2013.

[13] M. A. Mow, R. W. Schlub, and R. Caballero, "System for testing multi-antenna devices," Patent US 2011/0 084 887 A1, Apr. 14, 2011.

[14] T. Laitinen, P. Kyösti, J.-P. Nuutinen, and P. Vainikainen, "On the number of OTA antenna elements for plane-wave synthesis in a MIMO-OTA test system involving a circular antenna array," in *Antennas and Propagation (EuCAP), 2010 Proceedings of the Fourth European Conference on*. IEEE, 2010, pp. 1–5.

[15] M. B. Knudsen and G. F. Pedersen, "Spherical outdoor to indoor power spectrum model at the mobile terminal," *Selected Areas in Communications, IEEE Journal on*, vol. 20, no. 6, pp. 1156–1169, 2002.

[16] T. Taga, "Analysis for mean effective gain of mobile antennas in land mobile radio environments," *Vehicular Technology, IEEE Transactions on*, vol. 39, no. 2, pp. 117–131, 1990.

[17] "Spatial channel model for Multiple Input Multiple Output (MIMO) simulations (Release 11)," 3GPP/3GPP2, TR 25.996 V11.0.0, Sep. 2012.

[18] L. Hentilä, P. Kyösti, M. Käske, M. Narandzic, and M. Alatossava, "MATLAB implementation of the WINNER Phase II Channel Model ver1. 1," 2007.

[19] P. Kyösti, J. Nuutinen, and J. Malm, "Over the air test," Patent US 20 130 059 545 A1, Mar. 7, 2013.

[20] A. Khatun, H. Laitinen, V.-M. Kolmonen, and P. Vainikainen, "Dependence of Error Level on the Number of Probes in Over-the-Air Multiprobe Test Systems," *International Journal of Antennas and Propagation*, vol. 2012, 2012.

[21] W. Fan, X. de Lisbona, F. Sun, J. Nielsen, M. Knudsen, and G. Pedersen, "Emulating spatial characteristics of mimo channels for ota testing," *Antennas and Propagation, IEEE Transactions on*, vol. 61, no. 8, pp. 4306–4314, 2013.

[22] D. Baum, J. Hansen, and J. Salo, "An interim channel model for beyond-3G systems: extending the 3GPP spatial channel model (SCM)," in *Vehicular Technology Conference, 2005. IEEE 61st*, vol. 5, 2005, pp. 3132–3136 Vol. 5.

[23] Y.-P. Zhang, P. Wang, Q. Li, and P. Zhang, "Hybrid Transform Coding for Channel State Information in MIMO-OFDM Systems," in *Communications (ICC), 2011 IEEE International Conference on*, 2011, pp. 1–6.

[24] Y.-P. Zhang, P. Wang, S. Feng, P. Zhang, and S. Tong, "On the efficient channel state information compression and feedback for downlink MIMO-OFDM systems," *accepted by IEEE Trans. Vehicular Technology*, 2013.

[25] "Verification of radiated multi-antenna reception performance of User Equipment," 3GPP, TR 37.977 V1.0.0, Sep. 2013.

[26] P. Kyosti and L. Hentila, "Criteria for physical dimensions of MIMO OTA multi-probe test setup," in *Antennas and Propagation (EUCAP), 2012 6th European Conference on*. IEEE, 2012, pp. 2055–2059.

Wei Fan received his Bachelor of Engineering degree in electrical engineering from Harbin Institute of technology, China, in 2009 and Master's double-degree with highest honors from Politecnico di Torino, Italy, and Grenoble Institute of Technology, France, in electronic engineering in 2011. From February 2011 to August 2011, he was with Intel Mobile Communications, Denmark. He is currently a Ph.D. candidate at Department of Electronic Systems at Aalborg University, Denmark. His main areas of research are over the air testing of MIMO terminals and radio channel modeling.

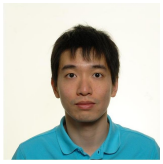

Fan Sun received the B.Eng. degree in telecommunication engineering with highest honors from Beijing University of Aeronautics and Astronautics (BUAA, now renamed as Beihang University), China, in 2007, the M.S. degree in wireless systems with highest honors from Royal Institute of Technology (KTH), Sweden, in 2009, the PhD degree from Aalborg University, Denmark, in 2013. From November 2008 to September 2009, he was with Ericsson Research, Sweden. From September 2009 to September 2010, he was with Nokia Siemens Network Research, Denmark. From June 2012 to December 2013, he was with Stanford University as a visiting student. He is currently a postdoc scholar in wireless communications at Stanford University. His research interests include multiple antenna techniques, cooperative communication, cross-layer design, and signal processing for communication systems.

Jesper Ødum Nielsen received his master's degree in electronics engineering in 1994 and a PhD degree in 1997, both from Aalborg University, Denmark. He is currently employed at Department of Electronic Systems at Aalborg University where main areas of interests are experimental investigation of the mobile radio channel and the influence mobile device users have on the channel. He has been involved in MIMO channel sounding and modeling, as well as measurements using live GSM and LTE networks. In addition he has been working with radio performance evaluation, including over the air testing of active wireless devices.

Xavier Carreño received his Master degree from 'Escola Tènica Superior d'Enginyeria de Telecomunicació de Barcelona' (UPC) in 2011. At UPC he was deeply involved in baseband signal processing algorithms and MIMO OTA research topics within Intel Mobile Communications, where he currently has a leading role in the MIMO OTA development team as system engineer. He is involved in the standardization of MIMO OTA methods and has coauthored several 3GPP, CTIA and IC1004 contributions and several conference and journal papers on the subject. His primary interests are within the area of MIMO OTA testing techniques, MIMO channel modeling and LTE platform testing.

Jagjit Singh Ashta born in 1988, obtained a Master Degree in Telecommunications in the 'Escola Tènica Superior d'Enginyeria de Telecomunicació de Barcelona' (UPC) in 2012. In the same year he completed with honours his Master Thesis on MAC layer improvements for IEEE 802.11 networks (WLAN) at Aalborg University (AAU) in collaboration with Nokia Solutions and Networks (NSN). Currently he develops his career as a Wireless Communications Engineer at Xtel ApS and is employed as an external software consultant at Intel Mobile Communications, Denmark. His research interests cover the MAC and PHY layers of the RANs and the development of software solutions required to study them.

Mikael Bergholz Knudsen was born in 1964. He received the B.S. degree in electrical engineering from Aarhus Teknikum, Denmark, in 1989, and the M.S. and Ph.D. degrees from Aalborg University, Denmark, in 1992 and 2001, respectively. In 1993, he joined Maxon Telecom A/S, Aalborg, Denmark, where he designed RF circuitry for both analog and digital mobile phones. From 1998 to 2001, he worked as an industrial Ph.D. student for Siemens Mobile Phones A/S, Denmark, while he at the same time studied at Aalborg University. He is now with Intel Mobile Communications Denmark, where he is the project manager for the 4th Generation Mobile Communication and Test platform (4GMCT) and also the chairman of the steering committee for the Smart Antenna Front End (SAFE) projects; both sponsored by the Danish National Advanced Technology Foundation. His areas of interest include RF system design and handset antenna performance including more than one antenna. In the resent years one of his focus areas has been how to utilize the unique possibilities in the cooperation between university researchers and private companies. To support this effort he pursued and obtained an Executive-MBA in 2012 with focus on inter-organizational research strategies.

Gert Frølund Pedersen was born in 1965 and married to Henriette and have 7 children. He received the B.Sc. E. E. degree, with honour, in electrical engineering from College of Technology in Dublin, Ireland in 1991, and the M.Sc. E. E. degree and Ph. D. from Aalborg University in 1993 and 2003. He has been with Aalborg University since 1993 where he is a full Professor heading the Antenna, Propagation and Networking LAB with 36 researcher. Further he is also the head of the doctoral school on wireless communication with some 100 phd students enrolled. His research has focused on radio communication for mobile terminals especially small Antennas, Diversity systems, Propagation and Biological effects and he has published more than 175 peer reviewed papers and holds 28 patents. He has also worked as consultant for developments of more than 100 antennas for mobile terminals including the first internal antenna for mobile phones in 1994 with lowest SAR, first internal triple-band antenna in 1998 with low SAR and high TRP and TIS, and lately various multi antenna systems rated as the most efficient on the market. He has worked most of the time with joint university and industry projects and have received more than 12 M$ in direct research funding. Latest he is the project leader of the SAFE project with a total budget of 8 M$ investigating tunable front end including tunable antennas for the future multiband mobile phones. He has been one of the pioneers in establishing Over-The-Air (OTA) measurement systems. The measurement technique is now well established for mobile terminals with single antennas and he was chairing the various COST groups (swg2.2 of COST 259, 273, 2100 and now ICT1004) with liaison to 3GPP for over-the-air test of MIMO terminals. Presently he is deeply involved in MIMO OTA measurement.

Paper D

Wideband MIMO Channel Capacity Analysis in Multi-probe Anechoic Chamber Setups

Wei Fan, Pekka Kyösti, Jesper Ø. Nielsen, and Gert F. Pedersen

The paper has been resubmitted after major revision to
IEEE Transactions on Antennas and Propagation, August. 2014.

The layout has been revised.

Wideband MIMO Channel Capacity Analysis in Multi-probe Anechoic Chamber Setups

Wei Fan, Pekka Kyösti, Jesper Ø. Nielsen, and Gert F. Pedersen

***Abstract*—This paper discusses over the air (OTA) testing for multiple input multiple output (MIMO) capable terminals with emphasis on wideband MIMO channel capacity analysis in multi-probe anechoic chamber setup. In the literature, the spatial correlation emulation accuracy at the receiver (Rx) side has been used to determine the test area size for a limited number of probes. However, it is desirable that the test area size is defined in terms of data rate deviation for the emulated channel in the laboratory from that of the target channel model. This paper reports the MIMO capacity analysis results for wideband spatio-temporal channel models, with emphasis on the impact of spatial correlation at the transmit (Tx) side, the channel model, and the spatial correlation at the Rx side on the capacity emulation accuracy. Simulation results show that the number of probes is irrelevant to capacity emulation accuracy when the spatial correlation at the Tx side is in the high region (e.g. $\rho > 0.7$). Furthermore, when correlation at the Tx side is low, the spatial correlation accuracy is less critical with small correlation at the Rx side. The simulation results are further supported by measurements in a practical multi-probe anechoic chamber setup. The capacity emulation accuracy has been shown to be a valid measure to determine the test area size.**

***Index Terms*—MIMO OTA testing, multi-probe, anechoic chamber, wideband channel capacity, test area size**

I. Introduction

The capacity of wireless systems can be enhanced by the use of multiple antennas at both the transmitter (Tx) and the receiver (Rx) ends [1]. New wireless standards such as LTE and LTE advanced have adopted multiple antenna technology. Over the air (OTA) testing methods of multiple-input multiple-output (MIMO) capable terminals have been actively discussed in standardization recently [2]. Due to its capability to physically synthesize electromagnetic fields in a shielded laboratory, the multi-probe anechoic chamber method has attracted great research attention. With the multi-probe anechoic chamber method, the radio propagation environment is reproduced as it would be experienced by the device under test (DUT) in the intended environment, but in a repeatable and controllable manner.

One major challenge with the multi-probe method is to create a realistic multipath environment around the test device in the laboratory. The test area is a geometrical area inside which the DUT is located. Acceptable error levels are defined for the channel emulation to ensure that the target propagation environment is reproduced accurately inside the test area. The test area size depends directly on the number of probes used for synthesizing the radio channel [3], [4]. Many measurements have been performed to verify how well the emulated channel models follow the target models in terms of channel parameters such as power delay profile, power Doppler spectrum, cross polarization ratio (XPR) and spatial correlation at the Rx side, see e.g., [5], [6]. In the literature, to appropriately assess how accurately the emulated power angle spectrum (PAS) approximates the target PAS, the difference between the emulated spatial correlation and the target spatial correlation $|\rho - \hat{\rho}|$ is chosen and used as a measure to determine the test zone size [3], [4], [7]. However, there is a concern whether $|\rho - \hat{\rho}|$ is the optimal figure of merit (FoM) to determine the test area size, as the ultimate goal is to investigate whether performance of MIMO capable terminals, e.g. data throughput, can be accurately evaluated in the laboratory. Intuitively, $|\rho - \hat{\rho}|$ is more critical when $|\rho|$ is high, as MIMO performance (e.g. MIMO capacity) is highly sensitive to correlation at high correlation region ($|\rho| > 0.5$), while $|\rho - \hat{\rho}|$ is less critical with small $|\rho|$, as the performance reduction is negligible [8].

The MIMO channel capacity in a particular environment depends highly on its propagation characteristics [8]. The effect of fading correlation on MIMO channel capacity has been investigated based on existing spatio-temporal wideband propagation channel models and extensive measurements in the literature [9]. Since the channels emulated in the multi-probe setup are only approximations, it is necessary to investigate how the capacity of the emulated channels matches with that of the target channel models. This paper reports MIMO capacity analysis results for wideband spatio-temporal channel models in the multi-probe anechoic chamber setup for the first time in the literature, to the best of our knowledge. Unlike previous work limited to spatial correlation emulation accuracy at the Rx side, the impact of the Tx side antenna arrays and the propagation environments are considered as well in this study. The main contributions of the paper are:

- The MIMO capacities of the emulated channels in the multi-probe anechoic chamber setup is investigated and compared with the capacities of the target channel models.
- The impact of spatial correlation at the Tx side and at the Rx side on MIMO channel capacity is shown for the two representative channel models that are used in the standard for the MIMO OTA testing [2]. The models are the SCME Urban micro (Umi) Tap delay line (TDL)

Wei Fan, Jesper Ø. Nielsen, and Gert F. Pedersen are with the Antennas, Propagation and Radio Networking section at the Department of Electronic Systems, Faculty of Engineering and Science, Aalborg University, Denmark (email: {wfa, jni, gfp}@es.aau.dk).

Pekka Kyösti is with Anite Telecoms Oy, Oulu, Finland (email: {pekka.kyosti}@anite.com).

model (six Laplacian shaped clusters) and the SCME Urban macro (Uma) TDL model from [10].
- The test zone size in terms of MIMO capacity accuracy of the emulated channel and target channel is discussed for the two representative wideband channel models.
- Measurement results from a practical multi-probe anechoic chamber setup further support the capacity analysis results.

II. Capacity Evaluation for Multi-probe Anechoic Chamber Setups

A. Channel Models

1) Target channel model: The target channel models adopted in this study are geometry-based stochastic channel models. The widely approved MIMO channel models like SCME, WINNER, and IMT-Advanced models belong to this family [10]–[12]. Geometry-based modelling enables separation of channel propagation and antennas at the Rx and the Tx side [3]. A geometry-based channel model is composed of multiple clusters, each of which is modelled by the cluster power, delay, nominal angle of arrival (AoA), nominal angle of departure (AoD), angle spread of arrival (ASA), angle spread of departure (ASD), and cluster cross-polarization power ratio (XPR).

For N_t Tx antennas and N_r Rx antennas, the MIMO channel $\mathbf{H} \in \mathbb{C}^{N_r \times N_t \times N_{ir} \times N_{taps}}$ can be represented by:

$$H(t,\tau) = \begin{bmatrix} h_{1,1}(t,\tau) & \cdots & h_{1,N_t}(t,\tau) \\ \vdots & \ddots & \vdots \\ h_{N_r,1}(t,\tau) & \cdots & h_{N_r,N_t}(t,\tau) \end{bmatrix}, \quad (1)$$

where $\{h_{n_r,n_t}(t,\tau)\} \in \mathbb{C}^{N_{ir} \times N_{taps}}$ represents the time-variant channel impulse responses (CIRs) between the input of the n_t-th Tx antenna and output of the n_r-th Rx antenna with $t = 1, ..., N_{ir}$ and $\tau = 1, ..., N_{taps}$. N_{ir} and N_{tap} are the maximum number of time samples and maximum number of delays (resolvable paths), respectively. Note that each CIR contains the cascaded effect of a Tx antenna, the propagation environment and a Rx antenna. In this study, two representative channel models: a) the SCME Umi TDL and b) the SCME Uma TDL are selected as the target channel models. Several Tx antenna arrays are considered. For the sake of simplicity, the discussion in this paper is limited to a single polarization. Similar to [3], [7], an omnidirectional antenna pattern is assumed for each antenna element at the Rx side. The MIMO channel in the frequency domain $\mathbf{H}_F = \{h_F(n_r, n_t, t, n_f)\} \in \mathbb{C}^{N_r \times N_t \times N_{ir} \times N_f}$ is obtained by performing the Fourier transform of $\{h_{n_r,n_t}(t,\tau)\}$ in the delay domain, where N_f is the number of sub-carriers. N_f has to be large enough to ensure that each sub-channel is flat fading, i.e. sub-channel bandwidth is much smaller than channel coherence bandwidth.

2) Emulated Channel models in the multi-probe setup: The channel emulation method for multi-probe anechoic chamber setups, named as the prefaded signal synthesis (PFS) method, is detailed in [3]. The basic idea of the PFS technique is to transmit fading signals separately from the multiple probes. Different clusters are modeled independently. Each cluster is mapped to the probes based on the cluster PAS and probe angular locations. Each probe associated with the cluster transmits weighted independent fading sequences with identical statistics.

Table I
Target channel model for idea illustration

Cluster index	Power [dB]	Delay [ns]	AoA	AS
1	0	0	0^o	35^o
2	-3	1000	45^o	35^o

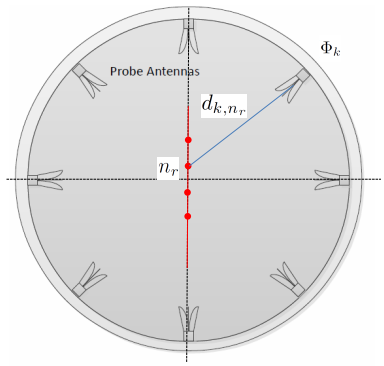

Figure 1. An illustration of the multi-probe setup. $K = 8$ OTA probes are uniformly located on the OTA ring. A uniform linear array (ULA) with 4 elements is used as the Rx.

A simple channel model that consists of two clusters as described in Table I is selected as an example to demonstrate the idea of the PFS technique. Eight uniformly located probes on an OTA ring are utilized to synthesize the target channel models, as illustrated in Figure 1. The weighted CIRs (originating from a single Tx antenna) that are transmitted from all the eight probes are shown in Figure 2. Each cluster is mapped to several OTA probes. Probe 1 (with angular location 0^o) is dominant in synthesizing cluster 1, while probe 5 (with angular location 180^o) does not contribute to cluster 1. This is expected, as the AoA of cluster 1 is 0^o. Similar observations can be made for cluster 2. Optimization techniques to obtain power weights $\omega = \{w_k\} \in \mathbb{R}^{K \times 1}$ have been discussed in [3], [13] and results from [13] are used here.

As detailed in [3], the CIRs from N_t Tx antennas to the k-th probe over time are $\{h_k^{ota}(n_t, t, \tau)\} \in C^{N_t \times N_{ir} \times N_{taps}}$ with $k \in [1, K]$ and K is the total number of probes. The CIRs from the n_t-th Tx antenna to the n_r-th Rx antenna over time are $\{\hat{h}_{n_r}(n_t, t, \tau)\} \in \mathbb{C}^{N_t \times N_{ir} \times N_{taps}}$ with:

$$\hat{h}_{n_r}(n_t, t, \tau) = \sum_{k=1}^{K} G_{n_r}(\Phi_k) \cdot h_k^{ota}(n_t, t, \tau) \cdot \alpha_{k,n_r} \quad (2)$$

where Φ_k denotes the angular location for the k-th probe. G_{n_r} is the complex radiation pattern of the n_r-th Rx antenna and we have amplitude of $G_{n_r}(\Phi)$ equal to 1 for $n_r \in [1, N_r]$, as omnidirectional antenna pattern is assumed for all the Rx

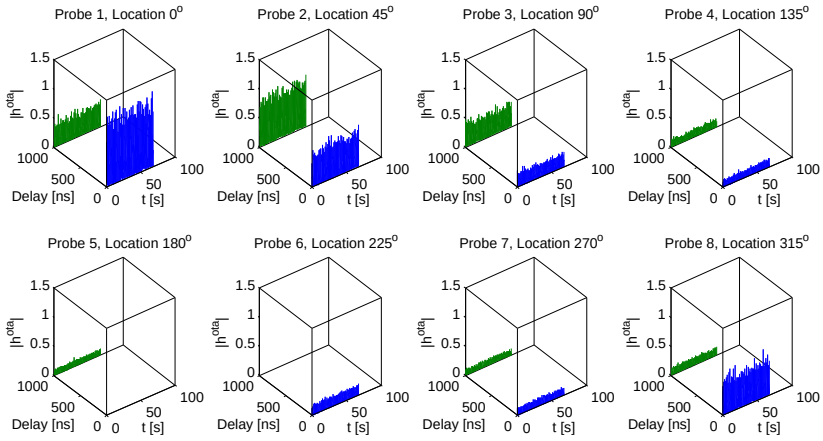

Figure 2. An illustration of CIRs for the target channel model detailed in Table I. Eight uniformly located OTA probes are used. Plots in blue corresponds to the CIRs associated with cluster 1 and plots in green denote the CIRs associated with cluster 2.

antennas. α_{k,n_r} is the transfer coefficient from k-th OTA probe to the n_r-th Rx antenna:

$$\alpha_{k,n_r} = L(d_{k,n_r}) \cdot \exp(-j\frac{2\pi}{\lambda} d_{k,n_r}), \tag{3}$$

where $L(\cdot)$ is the pathloss term and d_{k,n_r} is the distance from the k-th OTA probe to the n_r-th Rx antenna element. The probe radiation pattern is assumed constant, as the test zone is much smaller than the OTA ring size in the study. The variation of the radiation patterns of the probes over the small angles, which corresponds to the test area, can hence be ignored. We can denote the emulated channel in multi-probe setups as $\hat{\mathbf{H}} = \{\hat{h}_{n_r}(n_t, t, \tau)\} \in \mathbb{C}^{N_r \times N_t \times N_{ir} \times N_{taps}}$. Similarly we can obtain the emulated channel for multi-probe setups in frequency domain $\hat{\mathbf{H}}_F \in \mathbb{C}^{N_r \times N_t \times N_{ir} \times N_f}$.

B. Capacity Evaluation and Spatial Correlation

1) Capacity Evaluation:

a) Target channel capacity: In this paper, we assume that the channel knowledge is not available at the Tx side, and hence MIMO capacity is evaluated by assuming equal power allocation among the Tx antennas. The MIMO channel matrices are normalized in two ways in the literature [14]. One way is to ensure constant Tx power over the whole simulation period. Another way is ensure constant instantaneous SNR, which corresponds to perfect power control at the Tx side. Note that similar conclusions can be drawn for the two normalizations, and the first normalization is used for the results presented in this work. The channel normalization factor η for the target channel model is:

$$\eta = \frac{1}{N_r N_t N_{ir} N_f} \sum_{n_r=1}^{N_r} \sum_{n_t=1}^{N_t} \sum_{t=1}^{N_{ir}} \sum_{n_f=1}^{N_f} |h_F(n_r, n_t, t, n_f)|^2 \tag{4}$$

The instantaneous channel capacity of the target channel model can be computed as [9]:

$$C(t) = \frac{1}{N_f} \sum_{n_f=1}^{N_f} \log_2 \det(\mathbf{I} + \frac{\sigma}{N_t \cdot \eta} \cdot H_F(t, n_f) \cdot H_F(t, n_f)^H), \tag{5}$$

where $\mathbf{I}$ is the identity matrix, and $H_F(t, n_f) \in \mathbb{C}^{N_r \times N_t}$ is the channel matrix of the n_f-th sub-carrier at time instant t. σ is the received SNR. $(\cdot)^H$ denotes the Hermitian transpose. An average SNR of 15dB is assumed in the simulations and measurements unless otherwise stated.

Similar to the analysis performed in [9], we can obtain two kinds of statistics for the instantaneous capacity: a) capacity in the narrowband case (with $N_f = 1$) and b) capacity in the wideband case with a sufficiently large N_f using Eq. (5). In [9], it was concluded that the wideband capacity results present similar mean and smaller variance as a result of averaging compared with the narrowband capacity.

b) Emulated channel capacity: The channel normalization factor for the emulated channel model $\hat{\eta}$ is defined similarly as in Eq (4), with $\mathbf{H}_F$ replaced by $\hat{\mathbf{H}}_F$. Similarly, the instantaneous channel capacity of the emulated channel model $\hat{C}(t)$ is calculated similarly as in Eq (5), with $\mathbf{H}_F$ replaced by $\hat{\mathbf{H}}_F$.

2) Spatial Correlation :

a) Target spatial correlation: The correlation coefficient at the Tx and the Rx can be obtained from the wideband MIMO channel matrices detailed in Section II-A. The spatial correlation ρ_{ij}^{Tx} between a pair of channels from the i-th and the j-th Tx antennas, both arriving to the n_r-th Rx antenna is:

$$\begin{aligned} \rho_{ij}^{Tx} &= corr\left[\sum_{\tau=1}^{N_{tap}} \mathbf{h}_{n_r,i}(\tau), \sum_{\tau=1}^{N_{tap}} \mathbf{h}_{n_r,j}(\tau)\right] \\ &= \frac{\sum_{t=1}^{N_{ir}} [\sum_{\tau=1}^{N_{tap}} h_{n_r,i}(t,\tau) \cdot \sum_{\tau=1}^{N_{tap}} h_{n_r,j}^*(t,\tau)]}{\sqrt{\sum_{t=1}^{N_{ir}} |\sum_{\tau=1}^{N_{tap}} h_{n_r,i}(t,\tau)|^2 \cdot \sum_{t=1}^{N_{ir}} |\sum_{\tau=1}^{N_{tap}} h_{n_r,j}(t,\tau)|^2}} \end{aligned} \tag{6}$$

where $corr()$ is the correlation operator. $\mathbf{h}_{n_r,n_t}(\tau) = \{h_{n_r,n_t}(t,\tau)\} \in C^{N_{ir} \times 1}$ denotes the CIRs associated with delay τ between the n_r-th Rx antenna and the n_t-th Tx

antenna. In Eq. (6), the spatial correlation of the composite of all clusters is calculated. Cluster-wise spatial correlation can be calculated as well.

Similarly, the coefficient ρ_{ij}^{Rx}, denoting the correlation for channels between the i-th and the j-th Rx antenna, both from the same n_t-th Tx antenna, is

$$\rho_{ij}^{Rx} = corr\left[\sum_{\tau=1}^{N_{tap}} \mathbf{h}_{i,n_t}(\tau), \sum_{\tau=1}^{N_{tap}} \mathbf{h}_{j,n_t}(\tau)\right] \quad (7)$$

Alternatively, the spatial correlation can be computed analytically, as detailed in [15]:

$$\rho_{ij} = \frac{\int_{-\pi}^{\pi} G_i(\phi) G_j^{\star}(\phi) p(\phi) d\phi}{\sqrt{\int_{-\pi}^{\pi} p(\phi)|G_i(\phi)|^2 d\phi}\sqrt{\int_{-\pi}^{\pi} p(\phi)|G_j(\phi)|^2 d\phi}}, \quad (8)$$

where G_i and G_j are the complex radiation patterns of antenna element i and j, respectively, with a common phase center. $p(\phi)$ is the PAS which satisfy $\int_{-\pi}^{\pi} p(\phi)d\phi = 1$. Eq. (8) can be used to calculate the spatial correlation based on the antenna configuration, antenna pattern and PAS defined in at the Tx and the Rx side.

b) Emulated spatial correlation: In the multi-probe anechoic chamber setup, the emulated spatial correlation at the Tx side $\hat{\rho}^{Tx}$ and the Rx side $\hat{\rho}^{Rx}$ can be calculated directly based on Eq (6) and Eq (7), with $\mathbf{H}$ replaced by $\hat{\mathbf{H}}$. From Eq. (8), the emulated spatial correlation at the Tx side $\hat{\rho}^{Tx}$ can be directly calculated as well, as the same continuous PAS as the target channel model is used for emulation at the Tx side [3]. However, at the Rx side, what the DUT sees is essentially a discrete PAS, characterized by the angular locations and power weights of the active probes. The emulated spatial correlation between the i-th and j-th element at the Rx side is:

$$\hat{\rho}_{ij}^{Rx} = \frac{\sum\limits_{k} G_i(\Phi_k) \cdot G_j^{*}(\Phi_k) \cdot w_k}{\sqrt{\sum\limits_{k} \mid G_i(\Phi_k) \mid^2 w_k \cdot \sum\limits_{k} \mid G_j(\Phi_k) \mid^2 w_k}} \quad (9)$$

where w_k is the power weight for the k-th probe.

The emulated spatial correlation at the Tx $\hat{\rho}^{Tx}$ will always match the target ρ_{ij}^{Tx}, as the same continuous PAS is used. However, due to the limitation in the number of probes, a deviation between emulated spatial correlation and target spatial correlation at the Rx side exists, as discussed in [3], [7].

Note that the correlation at the Tx side is assumed independent from the considered Rx antenna. Similarly, correlation at the Rx side are assumed independent from the considered Tx antenna. This assumption is valid if the spatial stationarity regions are larger than the array sizes at the Tx and the Rx side, as explained in [16]. In our study, the array dimensions at the Tx and the Rx are not unreasonably large and hence the assumption is valid in our investigation.

Table II
THREE SIMULATION SCENARIOS FOR CAPACITY ANALYSIS

	Tx configuration	Channel model	Rx configuration
A	2 co-located elements with X configuration, as detailed in [2]	Umi/Uma model	A 2 antenna element ULA with 0.5λ spacing
B	A 2 antenna element ULA with 10λ spacing	Umi/Uma model	A 2 antenna element ULA with 0.5λ spacing
C	A 4 antenna element ULA with 10λ spacing	Umi/Uma model	A 4 antenna element ULA with 0.5λ spacing

III. SIMULATION RESULTS

A. Simulation Scenarios

To understand the impact of the Tx antenna array, the propagation environment and the Rx antenna array on MIMO capacity and the emulated capacity accuracy, three scenarios are selected for the capacity analysis, as detailed in Table II. Antenna elements on the Tx side are dipoles without considering the mutual coupling effect between them. The ULA broadsight direction is 0^o for all the three scenarios in the Rx configuration. The ULAs consisting of vertical polarized ideal dipoles are considered. Note that any other polarized array can be assumed for the Rx as well. As the channel polarizations are independent and treated individually in the channel emulation [3], similar simulation results can be obtained for other polarizations. Omnidirectional antenna patterns are used, as the DUT antenna pattern is typically not known beforehand. Furthermore, if some antenna patterns are embedded in the channel model, the OTA performance will depend on both the antenna pattern embedded in the channel as well as antenna pattern in the DUT itself, which is obviously undesirable. In scenario A, two $\pm 45^o$ cross polarized dipoles are used at the Tx side. Again, any antenna array can be used for simulation in the Tx configuration. The Tx configurations in scenario A, B and C consisting of ideal dipoles are used for the sake of simplicity. Similar setups are adopted in standardization for MIMO OTA testing [2]. In [2], channel models with XPR = 9dB are used, while only vertically polarized channel models are considered in this study for the sake of simplicity. In scenario C, a 4×4 MIMO system is evaluated, with antenna spacing 0.5λ, i.e, a maximal separation of 1.5λ among antenna elements at the Rx side. The probe setup used in the simulation is illustrated in Figure 1. Note that the two SCME channel models are selected, as they have been standardized and adopted in MIMO OTA standards as well [2], [11]. Hence, the results shown in this paper could be directly used for standards. The discussion in this paper is limited to the standard channel models. Virtual drive testing (VDT), which targets to reproduce practical recorded channels in the anechoic chamber, has attracted great research attention recently. In [17], the idea of VDT was presented, without showing any result in the anechoic chamber, though. Replaying field recorded channels in the laboratory is currently a challenging task and not the focus of this paper.

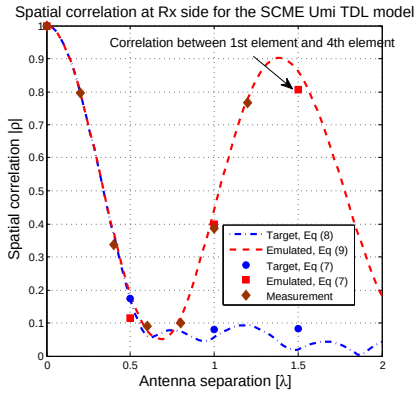

Figure 3. Spatial correlation at the Rx side for the SCME Umi TDL model for scenario C.

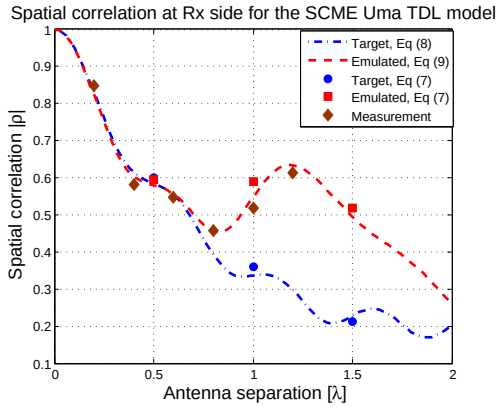

Figure 4. Spatial correlation at the Rx side for the SCME Uma TDL model for scenario C.

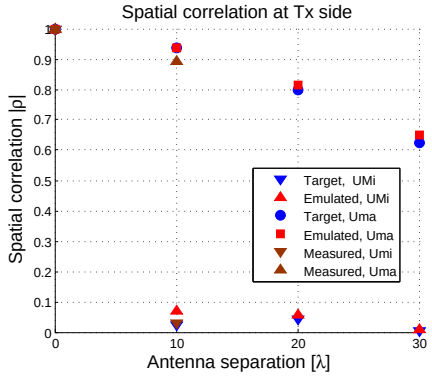

Figure 5. Spatial correlation at the Tx side for the SCME Umi TDL model and SCME Uma TDL model for scenario C.

B. Spatial Correlation

1) Spatial correlation at the Rx side: Spatial correlation results at the Rx side for the Umi and the Uma channel models for scenario C are shown in Figure 3 and Figure 4, respectively. Spatial correlation results at the Rx side for scenario A and B can be obtained from scenario C directly. The spatial correlation between the two Rx antennas in scenario B is the same as the spatial correlation between two neighboring Rx antennas in scenario C, since the same antenna element and antenna separation are used in the simulation for the two scenarios. As we can see, the spatial correlation depends highly on the channel models. The spatial correlations calculated from Eq. (7) match well with the analytical formula results detailed in Section II-B both for the target and emulated spatial correlation. Generally, the emulated spatial correlation at the Rx side $\hat{\rho}^{Rx}$ match well with the target ρ^{Rx}, when the Rx maximum antenna separation is smaller than 0.7λ. When the antenna separation exceeds 0.7λ, the emulated spatial correlation will be larger than the target for both channel models, as a result of the limited number of probes. Note that spatial correlation results at the Rx side have been reported in the literature, see, e.g. [2], [6], [13], and is included here to explain the capacity results in the following sections.

2) Spatial correlation at the Tx side: As the channel models are vertically polarized, the spatial correlation between two co-located (i.e. with antenna separation 0λ) dipoles at the Tx side for scenario A will be 1 for both channel models. Spatial correlation results at the Tx side for the Umi and Uma channel models in scenario C are shown in Figure 5. As we can see, the emulated spatial correlation results match very well with the target correlation, independent of the antenna separation, as expected. The Tx antennas are de-correlated for the UMi channel model, with correlation dramatically falling to 0 at antenna separation 10λ. However, for the Uma channel model, the Tx antennas are highly correlated, with $\rho_{14}^{Tx} > 0.6$ for an antenna separation of 30λ. Spatial correlation results at the Tx side for scenario B can be obtained from scenario C directly as well. The correlation at the Tx side, as shown in Eq. (8), depends both on the antenna array configuration at the Tx side and the channel spatial profile at the Tx side. For scenario B and C, the high Tx correlation observed for the Uma channel model is due to the fact that the AoDs of the dominant clusters are concentrated around the Tx array boresight direction [18]. The two channel models, i.e. the Umi channel model with low Tx correlation and the Uma channel model with high Tx correlation, are considered in the paper to demonstrate the impact of Tx correlation on test zone size. The Tx antennas in real sites are generally not highly correlated. However, high Tx correlation might be present in some scenarios as well, as shown in the measurement results in [19].

C. Capacity Analysis

1) Eigenvalue analysis: The cumulative distribution functions (CDFs) of the ordered singular values are shown for scenario A (left) and B (right) in Figure 6. For scenario A, only one dominant singular value is present due to the high Tx

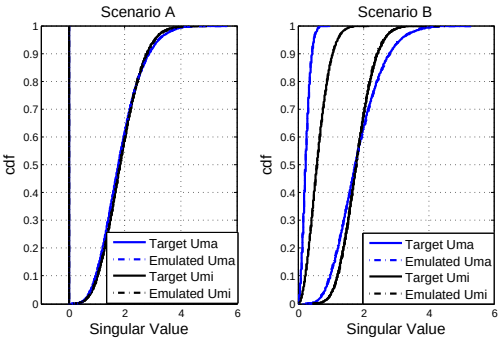

Figure 6. CDF of the singular values for scenario A (left) and scenario B (right). Note that the plots for the emulated channels are on top of the plots for target channel models.

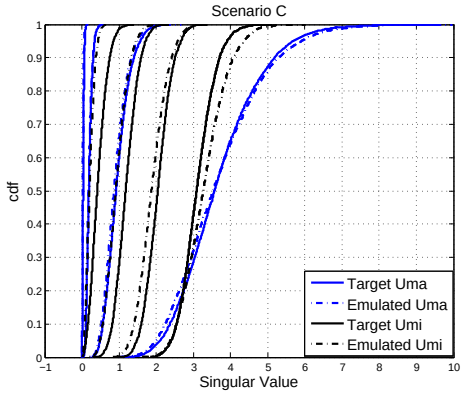

Figure 7. CDF of the singular values for scenario C

correlation ($\mid \rho^{Tx} \mid = 1$) for both channel models, and hence spatial multiplexing is not supported. For scenario B, two dominant singular values are present for both channel models. However, the Uma channel model is worse-conditioned due to the high Tx correlation. The CDF of the emulated channel models match well with the target channel models for scenario A and scenario B, as expected.

The CDFs of the ordered singular values are shown for scenario C in Figure 7. For the Uma channel models, the most dominant singular value is much larger the other three singular values. The CDFs of the emulated channel match well with the target for the Uma channel model due to the high Tx correlation. As for the Umi channel model, deviations between the CDFs of the emulated channel and target channel exists, as a result of limited number of probes.

2) Capacity in narrowband and wideband case: Capacity results in the narrowband case (with $N_f = 1$) and in the wideband case (with $N_f = 201$ and bandwidth 20MHz in the simulations) are compared for all the scenarios. The difference between the mean of the wideband capacity and the mean of the narrowband capacity is negligible for all cases. The capacity variance is smaller in the wideband case compared

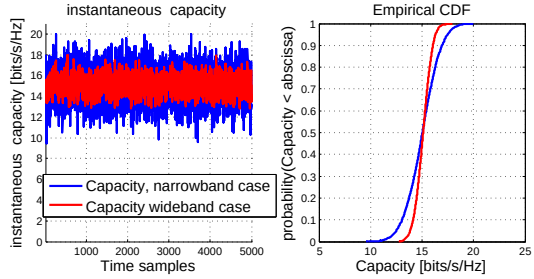

Figure 8. The instantaneous capacity in narrowband and wideband case for the emulated SCME Umi TDL channel models for scenario C (left) and their cumulative distribution function (CDF) plots. The SNR SNR σ is 15dB.

with the narrowband case for all the scenarios, as a result of averaging. Figure 8 shows the instantaneous capacity in narrowband and wideband cases for the emulated Umi channel models for scenario C, where the mean capacity difference is less than 0.1 bits/s/Hz. The standard deviation of the wideband instantaneous capacity is 0.75 bits/s/Hz, compared with 1.5 bits/s/Hz in the narrowband case. Wideband capacity results are shown in the following simulations unless otherwise stated.

3) Capacity Simulation results: CDF plots of the capacity results for scenario A, B and C are shown in Figure 9, 10 and 11, respectively.

In scenario A, although the spatial correlation results at the Rx side for the Umi model and for the Uma models are different (as shown in Figure 3 and Figure 4), the capacity difference is negligible. This is due to the fact the Tx antennas are fully correlated for both channel models and spatial multiplexing is not supported. Therefore the capacity results are equally low for both channel models. In scenario B, the capacity for the Umi model is higher than the capacity for the Uma model. The capacity gain for the Umi channel model, compared to scenario A, is a result of low spatial correlation both at the Tx and at the Rx side. However, for the Uma channel model, the capacity gain compared with scenario A is negligible, as the spatial correlation at the Tx side and the Rx side are still high, with $\rho^{Tx} = 0.9$ and $\rho^{Rx} = 0.6$. In scenario C, the capacity for the Umi model is higher than for the Uma model, as the spatial correlation correlation at Tx side for the Uma model is always above 0.6, where the Tx side correlation is 0 for the Umi model, as shown in Figure 5.

The emulated capacity results match very well with the target capacity results for both channel models in scenario A and scenario B. The maximum antenna spacing at the Rx is 0.5λ for scenario A and B. As shown in Figure 3 and Figure 4, the Rx side channel spatial characteristics can be accurately modeled in a test area of 0.7λ with eight OTA probes. The emulated capacity results are smaller than the target capacity results for scenario C for both channel models. For the Uma channel model, the deviation in capacity is negligible. This is due to the fact that the emulated and target spatial correlation at the Tx side are equally high, which will cause dramatic capacity reduction and both C and $\hat{C}$ are equally low. For the Umi channel model, the capacity

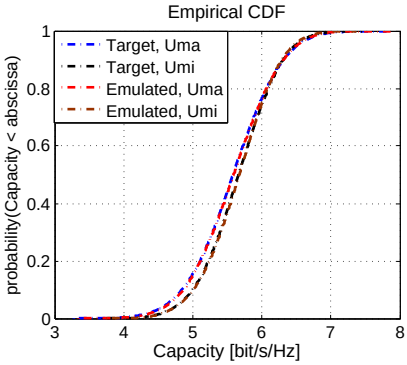

Figure 9. CDF plots of the capacity results for scenario A with average SNR $\sigma = 15$ dB.

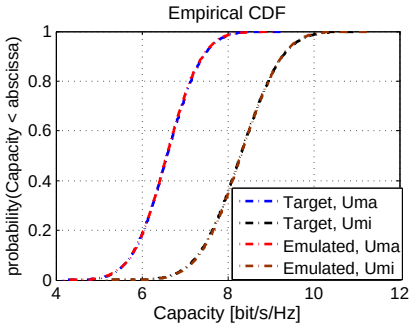

Figure 10. CDF plots of the capacity results for scenario B with average SNR $\sigma = 15$ dB.

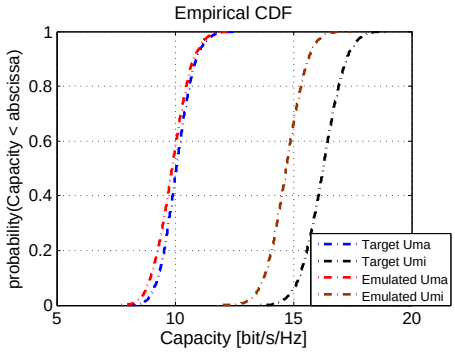

Figure 11. CDF plots of the capacity results for scenario C with average SNR $\sigma = 15$ dB.

difference is substantial. As the spatial correlation at the Tx side is equally low (close to 0), the difference is caused by deviation between target and emulated channel at the Rx side. The maximum antenna spacing at the Rx is 1.5λ in scenario C, while the Rx side channel spatial correlation can only be modeled accurately when the antenna separation is smaller than about 0.7λ, as shown in Figure 3. For the emulated channels, the spatial correlation at the Rx side for antenna elements with antenna separation 1.0λ and 1.5λ are 0.4 and 0.8, respectively, compared with values lower than 0.1 for the target curve. Therefore, we see a difference between the capacity of the emulated channel $\hat{C}$ and the capacity of the target channel C.

As a summary, if the Tx correlation is high, the channel emulation accuracy at the Rx side is irrelevant to the capacity, as the channel is ill-conditioned and the capacity results will be equally low for the emulated and target channel model. Anyhow, the number of probes may affect the Rx power level in emulation with practical DUT antennas, and thus the throughput results might be affected by the number of probes in the measurements. The impact is not present in the capacity simulation results in this paper, as channel normalization and omnidirectional DUT antennas at the Rx are assumed. However, for practical OTA measurements (e.g. throughput measurement), absolute power without normalization is used. When the spatial correlation at the Tx side is low, the capacity of the emulated channels will follow that of the target channels within the test area where $|\rho^{Rx} - \hat{\rho}^{Rx}|$ is small. When the DUT is outside the test zone area, we might see a difference between C and $\hat{C}$, as explained in Section III-D. Note that in reality, a Tx correlation ρ^{Tx} close to 1 is not very likely with practical antennas for realistic channels. It is selected in the paper for some scenarios to emphasize the importance of Tx correlation impact in channel emulation, which has not been considered in the literature.

D. Test zone size analysis

As explained earlier, it is desirable that the test zone size is defined in terms of data rate deviation of the emulated channel in the laboratory compared to the target channel model. Channel capacity is the theoretical upper bound on the data rate that can be reliably transmitted over a communications channel. We can express the test zone size in terms of how accurate the capacity of the emulated channel model $\hat{C}$ match with that of the target channel model C. As shown earlier, the Rx side spatial characteristics emulation accuracy become irrelevant when correlation at the Tx side is high. To ensure that the capacity results are sensitive to spatial characteristics at the Rx side in the example, the spatial correlation at the Tx side is selected to be low. In the following, the settings of scenario C for the Tx antenna array and the Umi channel model are selected. At the Rx side, the ULA antenna element spacing ranges from 0.1λ to 0.5λ with a step of 0.1λ, which corresponds to maximum antenna separation from 0.3λ to 1.5 λ with 0.3λ step for a 4 element ULA. The CDF plots of the capacity results for various antenna spacings for the Umi channel model are shown in Figure 12. The mean capacity of the target and emulated channel models for the 4×4 MIMO system with different maximum antenna separations among elements in the Rx are shown in Table III. As we can see, the capacity deviation $|C - \hat{C}|$ is very small when the maximal

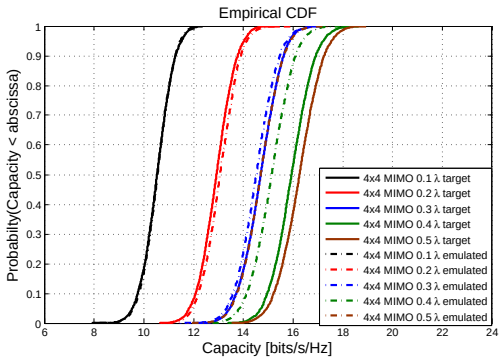

Figure 12. CDF plots of the capacity results for scenario C with different antenna spacing for the Rx ULA with average SNR $\sigma = 15$ dB. The antenna element spacing in the ULA is shown in the legend for each curve.

Table III
MEAN CAPACITY FOR THE 4×4 MIMO SYSTEM WITH DIFFERENT ANTENNA SPACING [UNIT: BITS/S/HZ].

Maximum antenna separation	0.3λ	0.6λ	0.9λ	1.2λ	1.5λ
C	10.5	12.9	14.7	16.0	16.3
$\hat{C}$	10.5	13.1	14.5	15.1	14.7
$\lvert C - \hat{C} \rvert$	0	0.2	0.2	0.9	1.6

antenna separation is smaller than 0.9λ. Although $|\rho^{Rx} - \hat{\rho}^{Rx}|$ is around 0.25 at 0.9λ maximum antenna separation, as shown in Figure 3, the capacity deviation $|C - \hat{C}|$ is negligible. This is due to the fact that $|\rho - \hat{\rho}|$ is less critical with small $|\rho|$ ($|\rho| = 0.3$). At maximal antenna separation 1.2λ, the capacity deviation $|C - \hat{C}|$ is 0.9 bits/Hz/s, as ρ^{Rx} is close to 0, compared with $\hat{\rho}^{Rx}$ in the high correlation region ($\hat{\rho}^{Rx} = 0.8$).

IV. MEASUREMENT VERIFICATION

A measurement campaign was carried out in a practical setup at Anite Telecoms Oy, Finland to verify the capacity analysis results. Figure 13 illustrates the test setup. Figure 14 shows parts of the practical probe configuration in the anechoic chamber. Eight uniformly located probes on the azimuth ring were connected to an Anite Propsim F32 to synthesize the channel (with only 8 channel emulator output ports connected), while the rest of the probes on the other rings were not connected. A sledge and turntable that support radial and rotational movement respectively of the calibration dipole were used in the measurements.

Phase and amplitude calibrations are performed for each probe before the measurements. Although the phase calibration is not required with the PFS technique, as explained in [3]. The basic idea is to record the channel matrices using the calibration dipole in several positions and calculate the capacity based on Eq. (5). The measurement procedure is similar to the spatial correlation measurements detailed in [2]. As a summary, for CIRs that are associated with each Tx antenna, the channel emulator is stopped every 10 CIRs (with

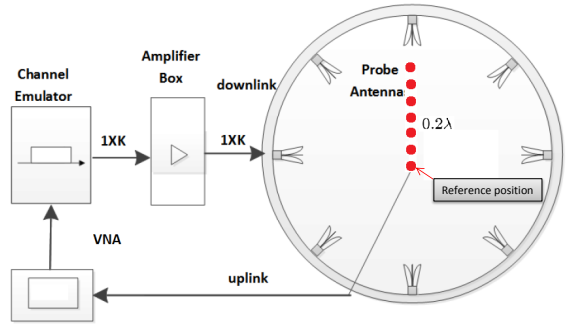

Figure 13. An illustration of the test setup. Red dots denote the positions for the calibration dipole during measurements.

4 CIRs per wavelength) to satisfy the Nyquist criteria and the field is measured with the network analyzer and saved for post-processing. 2000 CIRs were recorded in the measurements. The sweep of the same CIRs is repeated for all the seven test positions, as shown in Figure 13. Then the same procedure is repeated for the CIRs associated with other Tx antennas in a sequential manner. Note that narrowband measurements were performed to save measurement time. As shown in the simulation results in Section III-C2, the difference between wideband and narrowband mean capacity is negligible. The frequency responses were recorded at frequency $f = 2.14$ GHz. One important aspect related to practical measurements is that we should ensure that the absolute power levels associated with different Tx antennas in the calibration are the same (or at least known). Note that no interference or noise were emulated in the measurements. Only the frequency responses measured at a single frequency were recorded. The capacity of the measured channels is calculated assuming an average SNR $\sigma = 15$ dB.

In the measurements, the settings of scenario B for the Tx antenna array was selected, and both the Uma and Umi channel models are investigated. To understand capacity emulation accuracy as a function of antenna separation at the Rx side for both channel models, two antennas with different antenna spacing were used for the Rx. The CIRs recorded at the reference position (As shown in Figure 13) were used for the first Rx antenna, and CIRs recorded at other positions were used for the another Rx antenna. Hence, six 2×2 MIMO matrices with different antenna separations at the Rx side (from 0.2λ to 1.2λ with 0.2λ step) could be formed.

Mean capacity C results for the target channel model, mean capacity $\hat{C}$ for the emulated channel and mean capacity C_m for the measured channel for both the Umi and Uma channel models are shown in Figure 15. The spatial correlation at the Rx side and at the Tx side for the two channel models are shown in Figure 3, Figure 4 and Figure 5, respectively. The capacity for the Uma model is generally lower than for the Umi channel. The deviation $|C - \hat{C}|$ is generally small for the Uma channel model, as the correlation at the Tx side is high. For the Umi channel model, $|C - \hat{C}|$ is rather small when antenna separation is smaller than 1λ. Similar observations

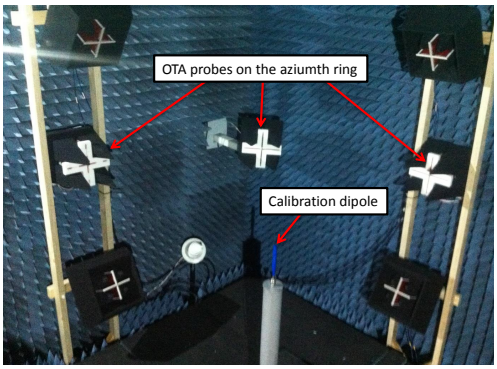

Figure 14. Illustration of part of the practical probe setup in the anechoic chamber. The measurement was done at $f = 2.14$ GHz

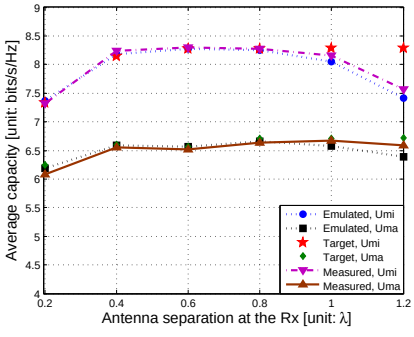

Figure 15. Mean capacity of the target channel model (C), mean capacity of the emulated channel ($\hat{C}$) and mean capacity of the measured channel (C_m) for the SCME UMi and SCME Uma TDL channel models.

have been made and explained for scenario B in section III-C3.

The measured spatial correlation matches very well with the emulated correlations at the Tx and Rx for both the Umi and Uma channel models, with a deviation between the measured and emulated correlation up to 0.03. The results for the measured spatial correlation at the Rx side are shown in Figure 3 and Figure 4 for the Umi and Uma channel models, respectively. The results for the measured spatial correlation at the Tx side are shown in Figure 5 for both channel models. As shown in Figure 15, and as expected, the measured mean capacity C_m matches very well with the emulated mean capacity $\hat{C}$ for both the Uma and Umi channel models,.

V. Conclusion

One of the key questions to be addressed in the multi-probe anechoic MIMO OTA testing is how large the test area can be supported with a limited number of probes. The current work investigates wideband MIMO channel capacity in multi-probe anechoic chamber setups, with emphasis on the relationship between capacity emulation accuracy and test area size. The investigation is based on the well accepted channel models in the standards for over the air testing of MIMO capable terminals, i.e. the SCME Umi TDL and SCME Uma TDL models. For these models, the simulation results show that it is irrelevant how well the spatial characteristics at the Rx side are reproduced when the spatial correlation at the Tx side is in the high region (e.g. $\rho > 0.7$), as both the emulated capacity and target capacity will be equally low. When the correlation at the Tx side is low, the Rx correlation deviation $|\rho^{Rx} - \hat{\rho}^{Rx}|$ is highly critical with high $|\rho^{Rx}|$. The capacity emulation accuracy is less sensitive to spatial correlation emulation error at the Rx with small correlation at the Rx side. Simulation results have shown that the capacity deviation $|C - \hat{C}|$ is negligible up to 1λ wavelength for the Umi channel models, as $|\rho^{Rx} - \hat{\rho}^{Rx}|$ is less critical when $|\rho^{Rx}|$ is small ($|\rho^{Rx}| = 0.3$). The simulation results are further supported by measurements in a practical multi-probe anechoic chamber setup.

Acknowledgment

The authors appreciate the help and discussions from colleagues in Anite Telecoms Oy, especially Mr. Lassi Hentilä and Mr. Jouni Uusimaa with the practical measurements.

References

[1] A. Paulraj, D. Gore, R. Nabar, and H. Bolcskei, "An overview of MIMO communications - a key to gigabit wireless," *Proceedings of the IEEE*, vol. 92, no. 2, pp. 198–218, Feb 2004.

[2] "Verification of radiated multi-antenna reception performance of User Equipment," 3GPP, TR 37.977 V1.0.0, Sep. 2013.

[3] P. Kyösti, T. Jämsä, and J. Nuutinen, "Channel modelling for multiprobe over-the-air MIMO testing," *International Journal of Antennas and Propagation*, 2012.

[4] A. Khatun, H. Laitinen, V.-M. Kolmonen, and P. Vainikainen, "Dependence of Error Level on the Number of Probes in Over-the-Air Multiprobe Test Systems," *International Journal of Antennas and Propagation*, vol. 2012, 2012.

[5] W. Fan, X. Carreño, J. Ø. Nielsen, M. B. Knudsen, and G. F. Pedersen, "Channel Verification Results for the SCME models in a Multi-Probe Based MIMO OTA Setup," in *Vehicular Technology Conference (VTC Fall)*. IEEE, September 2013, pp. 1–5.

[6] A. Scannavini, F. Chauvet, and N. Gross, "MIMO OTA measurement with anechoic chamber method," in *Antennas and Propagation (EUCAP), 2013 7th European Conference on*. IEEE, April 2013.

[7] W. Fan, F. Sun, P. Kyösti, J. Nielsen, X. Carreño, M. Knudsen, and G. Pedersen, "3D channel emulation in the multi-probe setup," *Electronics Letters*, vol. 49, pp. 623–625(2), April 2013.

[8] M. Chiani, M. Z. Win, and A. Zanella, "On the capacity of spatially correlated MIMO Rayleigh-fading channels," *Information Theory, IEEE Transactions on*, vol. 49, no. 10, pp. 2363–2371, 2003.

[9] V. Jungnickel, S. Jaeckel, L. Thiele, L. Jiang, U. Kruger, A. Brylka, and C. Von Helmolt, "Capacity measurements in a cooperative MIMO network," *Vehicular Technology, IEEE Transactions on*, vol. 58, no. 5, pp. 2392–2405, 2009.

[10] D. Baum, J. Hansen, and J. Salo, "An interim channel model for beyond-3G systems: extending the 3GPP spatial channel model (SCM)," in *Vehicular Technology Conference, 2005. IEEE 61st*, vol. 5, 2005, pp. 3132–3136 Vol. 5.

[11] "Spatial channel model for Multiple Input Multiple Output (MIMO) simulations (Release 11)," 3GPP/3GPP2, TR 25.996 V11.0.0, Sep. 2012.

[12] L. Hentilä, P. Kyösti, M. Käske, M. Narandzic, and M. Alatossava, "MATLAB implementation of the WINNER Phase II Channel Model ver1. 1," 2007.

[13] W. Fan, X. de Lisbona, F. Sun, J. Nielsen, M. Knudsen, and G. Pedersen, "Emulating Spatial Characteristics of MIMO Channels for OTA Testing," *Antennas and Propagation, IEEE Transactions on*, vol. 61, no. 8, pp. 4306–4314, 2013.

[14] N. Czink, "The random-cluster model: a stochastic mimo channel model for broadband wireless communication systems of the 3rd generation and beyond," *Available at: publik. tuwien. ac. at/files/PubDat_112121. pdf*, 2007.

[15] R. Vaughan and J. B. Andersen, "Channels, propagation and antennas for mobile communications." Institution of Electrical Engineers, 2003.

[16] C. Oestges, "Validity of the Kronecker Model for MIMO Correlated Channels," in *Vehicular Technology Conference, 2006. VTC 2006-Spring. IEEE 63rd*, vol. 6, May 2006, pp. 2818–2822.

[17] P. Kyösti, P. Kemppainen, and T. Jämsäs, "Radio Channel Measurements in Live LTE Networks for MIMO Over-the-Air Emulation," in *Antennas and Propagation (EUCAP), 2014 8th European Conference on*, 2014.

[18] "Spatial channel model for multiple input multiple output (MIMO) simulations," 3GPP/3GPP2, TR 25.996 V6.1.0, 2003.

[19] J. Nielsen, B. Yanakiev, S. Barrio, and G. Pedersen, "Channel statistics for mimo handsets in data mode," in *Antennas and Propagation (EuCAP), 2014 8th European Conference on*, 2014.

Paper E

3D Channel Emulation in a Multi-probe Setup

Wei Fan, Fan Sun, Pekka Kyösti, Jesper Ø. Nielsen, Xavier Carreño,
Mikael B. Knudsen and Gert F. Pedersen

The paper has been published in the
Electronics Letters, vol. 49, no. 9, pp. 623–625, April, 2013. (Featured Article)

The layout has been revised.

FURTHER READING

Page 623
'3D channel emulation in a multi-probe setup', W. Fan, F. Sun, P. Kyösti, J.Ø. Nielsen, X. Carreño, M.B. Knudsen and G.F. Pedersen

The first 3D channel emulation technique for testing MIMO devices in a more realistic environment

3: it's the magic number*

More realistic testing of mobile terminals is a step closer thanks to the first 3D channel emulation technique for use in multi-probe anechoic chamber-based testing, developed and implemented by collaborating researchers in Denmark and Finland.

"Mobile network operators and manufactures urgently require standard test methods to test MIMO device performance," said Wei Fan from Aalborg University, the first author of this work.

"Field testing and traditional conductive testing are not sufficient to truly evaluate MIMO device performance…there is a strong need to perform proper MIMO over-the-air testing. Our technique provides a general channel emulation framework for any incoming spherical, or 3D, power spectrum of the channel."

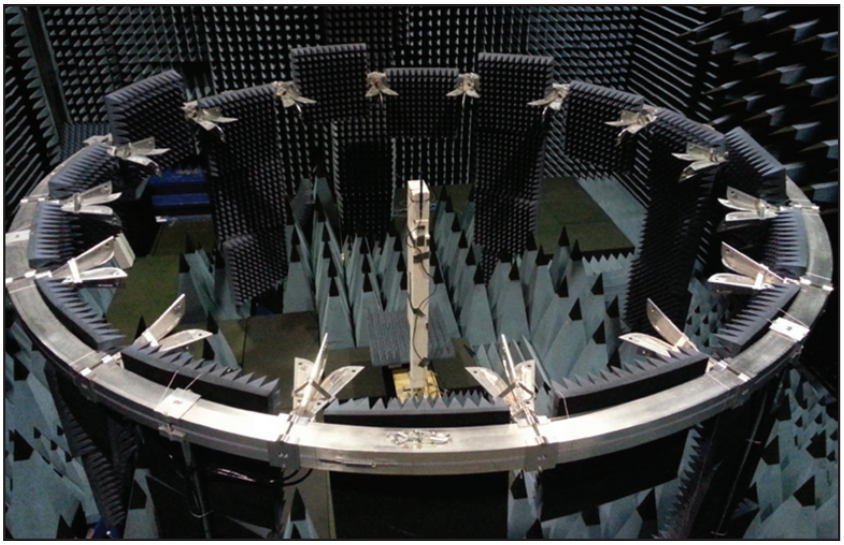

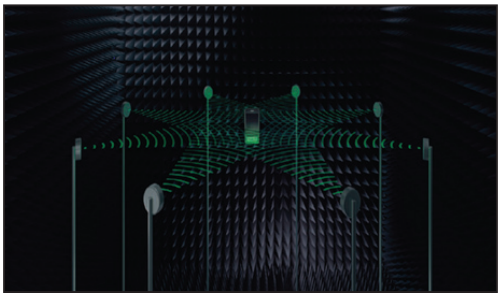

TOP: In this 2D MIMO over-the-air test system at Aalborg University, a mobile device sits in the centre of a ring of probe antennas. The new technique will also allow channel emulation in the vertical direction
BOTTOM: Plane waves inside the test zone can be approximated in a 2D setup (illustrated). Future work will include extending this to 3D

Nice and quiet

Over-the-air (OTA) testing of the radio performance of mobile terminals has the advantage, compared to other test methods, of not needing to break or otherwise modify the mobile device. OTA testing for mobile terminals with single antennas (SISO OTA) was standardised by CTIA and 3 GPP about ten years ago, but these methods cannot be used directly for MIMO technology. Testing methods for MIMO devices using an anechoic chamber were first introduced in CTIA, COST action 2100 and 3GPP in 2009.

There are three main types of test methods for MIMO devices: multi-probe anechoic chamber-based methods, reverberation chamber-based methods and two-stage methods. All currently have their limitations: there is limited temporal and spatial control of the reproduced channel in the reverberation chamber-based method; practical issues including self-interference still exist in the two-stage method; and the cost of the setup and the emulation of realistic channels with multi-probe and channel emulators are the main issues with the multi-probe anechoic chamber-based method.

Growing up...

Most of the standard channel models are 2D and MIMO over-the-air testing is currently limited to the use of these models which are defined only in the azimuth plane and assume that there is no spread over the elevation direction.

"The 2D channel model assumption is generally not valid," said Fan.

"Measurements have demonstrated that the channel elevation spread cannot be ignored in many propagation environments."

The idea and theory behind the 3D channel emulation model presented in this issue of *Electronics Letters* is a result of a collaboration between three organisations. The work was supported by the Danish National Advanced Technology Foundation via the 4th Generation Mobile Communication and Test Platform (4GMCT) project, of which two of the main partners are Intel Mobile Communications and Aalborg University. They worked with Anite who is the main developer and technology provider of the commercially available Propism radio channel emulators used in MIMO OTA. The implementation was carried out by the APNet section at Aalborg University which has been involved in radio propagation research for over 20 years, and also has extensive research expertise in electromagnetics, mobile devices and reliable radio networking.

...fast

The new technique is the first to emulate 3D channel models efficiently, allowing a more accurate reflection of a realistic wireless propagation environment inside an anechoic chamber. One of the next stages of development is to use the emulated 3D channels in some live phone testing with commercially available consumer devices.

Future work will also investigate several practical issues with the 3D multi-probe configuration. For a 3D MIMO OTA setup, the number of probes may be larger than the number of output ports of the emulator. Setting up a 3D multi-probe configuration is very costly, and so investigating properties such as the reflection and coupling can enable the system to be optimised. Finding ways to limit the number of probes while still approximating the target channels could make the test system both cheaper and simpler to implement as less calibration effort would be needed.

Other future developments will be focused on the relationship between the number of probes needed and the test volume size (for example the number needed for a MIMO device or a laptop), and to study ways to approximate plane waves inside the test zone.

doi: 10.1049/el.2013.1241

3D channel emulation in a multi-probe setup

W. Fan, F. Sun, P. Kyösti, J. Nielsen, X. Carreño, M. Knudsen and G. Pedersen

A technique to emulate 3D geometry-based channel models in a multi-probe over the air test setup is presented. The proposed technique provides a general emulation framework for any spherical incoming power spectrum. The emulation method results in two optimization objectives, which are both convex. They give optimal emulation accuracy and allow relatively low computational complexity.

Introduction: As a solution to evaluate multiple input multiple output (MIMO) device performance in realistic conditions in the lab, MIMO over the air (OTA) testing has attracted huge interest from both industry and academia, see e.g. [1]. One promising candidate is the multi-probe based anechoic chamber method. Several papers have discussed OTA testing setups for MIMO devices with emphasis on channel modeling, where the goal is to accurately reproduce realistic 2D channels in the test area with a limited number of OTA probes [1]. However, the 2D channel model is not generally valid. Measurements have demonstrated that elevation spread can not be ignored in many propagation environments, see e.g. [2, 3], and thus emulation of 3D models is required. Very few contributions have addressed this issue. In [4], it was briefly mentioned that probes in a 3D setup were used to emulate 3D channel models, but no algorithm description is given. The 3D channel emulation technique has also been implemented in a commercial channel emulator, the Elektrobit Propsim F8, where the Laplacian distributions are defined for the power azimuth spectrum (PAS) and the power elevation spectrum (PES). However, a description of the implemented channel emulation algorithm is not available. This letter presents a new channel emulation technique for arbitrary 3D channel models.

Method: The modeling of radio channel parameters such as delay, Doppler, channel polarization and transmitter (Tx) side spatial characteristics is detailed in [1] and can be easily modeled. Thus, the focus is on reproducing the channel in the test volume at the receiver (Rx). The device under test (DUT) should be smaller than the test volume to ensure that the target propagation environment is accurately reproduced around the DUT.

The spherical power spectrum (SPS) needs to be modeled as a function of both elevation angle (θ) and azimuth angle (ϕ). In [3], it is shown that PES and PAS are independent and the SPS can be expressed as:

$$p(\theta,\phi) = p(\theta)p(\phi) \tag{1}$$

where $p(\theta)$, $p(\phi)$ are the PES and PAS, respectively. In order to be used as an angular power density function, the SPS $p(\theta,\phi)$ needs to satisfy $\oint p(\Omega)d\Omega = \int_{-\pi}^{\pi}\int_{-\pi/2}^{\pi/2} p(\theta,\phi)\cos\theta d\theta d\phi = 1$ with Ω being the solid angle.

The spatial correlation is a statistical measure of the similarity of the received signals at different positions in space and it is selected as a figure of merit (FoM) to model 3D channel spatial characteristics at the Rx side, as adopted for the 2D case [1]. Isotropic antenna patterns are used for the 3D channel emulation, as the emulated channel model itself will assume some DUT antennas if antenna patterns are otherwise embedded for channel emulation. The polarizations are independent and can be treated individually and hence explained for any one polarization. The spatial correlation can be determined according to [5], for a single polarization, as:

$$\rho_a = \frac{\oint G_u(\Omega)G_v^*(\Omega)p(\Omega)d\Omega}{\sqrt{\oint |G_u(\Omega)|^2 p(\Omega)d\Omega}\sqrt{\oint |G_v(\Omega)|^2 p(\Omega)d\Omega}}, \tag{2}$$

where $()^\star$ denotes complex conjugate operation, G_u and G_v are the complex radiation patterns of antennas u and v, respectively, with a common phase center. Based on the assumption about the isotropic antenna pattern, we can rewrite equation (2) as:

$$\rho = \oint \exp(jk(\overline{r}_u - \overline{r}_v)\cdot\overline{\Omega})p(\Omega)d\Omega, \tag{3}$$

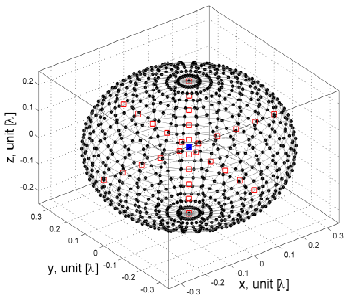

Fig. 1 *Different ways to sample the test volume: On line segments (squares) and on the surface of an ellipsoid (dots).*

where $\overline{r}_u$ and $\overline{r}_v$ are vectors containing the position information of antenna u and v, respectively. $\overline{\Omega}$ is an unit vector corresponding to space angle Ω. k is the wave number. $(\cdot)$ is the dot product operator.

The goal is to obtain OTA probe power weights which minimize the deviation between the theoretical spatial correlation of the target continuous SPS, and the emulated correlation of the discrete SPS characterized by power weights of the probes. Similar to (3), the emulated spatial correlation can be calculated based on the discrete spherical power spectrum characterized by M probes as:

$$\hat{\rho} = \sum_{m=1}^{M} w_m \exp(jk(\overline{r}_u - \overline{r}_v)\cdot\overline{\Phi}_m), \tag{4}$$

where w_m is the power weight for the mth probe. $\overline{\Phi}_m$ is a unit position vector of the mth probe. M is the number of probes. We will discuss two objective functions:

- Minimize the summation over the total emulation error (Min-Sum):

$$\min_{\boldsymbol{w}} \quad \|\hat{\boldsymbol{\rho}}(\boldsymbol{w}) - \boldsymbol{\rho}\|_2^2 \tag{5}$$
$$s.t. \quad 0 \le w_m \le 1,\ \forall m \in [1, M]$$

  where $\boldsymbol{w} = [w_1, ..., w_M]^T$ is a power weighting vector to be optimized. $\hat{\boldsymbol{\rho}}$ and $\boldsymbol{\rho}$ are the emulated spatial correlation and target spatial correlation vectors, respectively, with each element corresponding to the spatial correlation between two isotropic antennas at a certain location pair on the test volume.
- Minimize the maximum emulation error (Min-Max):

$$\min_{\boldsymbol{w}} \max_{i} |\hat{\rho}_i(\boldsymbol{w}) - \rho_i| \tag{6}$$
$$s.t.\ 0 \le w_m \le 1,\ \forall m \in [1, M].$$

  Through this objective function unacceptable high emulation errors are avoided, at the expense of larger total emulation error $\|\hat{\boldsymbol{\rho}}(\boldsymbol{w}) - \boldsymbol{\rho}\|_2^2$, as demonstrated below.

Eq. (5) is a convex problem and (6) can be easily converted to a convex problem, which can be handled efficiently.

In [4], the test volume is sampled by selecting locations for u and v from three orthogonal segments of line centered inside the sphere, as shown in Figure 1. This way of selecting all points within the test volume will give optimal results on the three axes. However, it might not present optimal emulation results for sample points within the entire test volume and emulation accuracy might be critically low in certain situations. To avoid this, samples on the surface of an oblate ellipsoid shaped test volume is proposed. The ellipsoid is chosen, since the number of OTA probes in the azimuth plane is likely different from that in the elevation plane. The sample locations for u and v ($\overline{r}_u$ and $\overline{r}_v$) are selected to be directly opposite to each other w.r.t the test volume center and are obtained by sweeping the location pairs over the whole surface of the ellipsoid.

Simulation results and discussions: An example target channel is considered with an azimuth angle of arrival (AoA) = 0^o and azimuth spread of arrival (ASA) = 35^o defined for the Laplacian shaped PAS; the elevation angle of arrival (EoA) = 15^o and elevation spread of arrival (ESA) = 10^o for the Laplacian shaped PES. Three different probe configurations are assessed for the target SPS, as detailed in Table 1. The probes are placed on

Table 1: Probe configurations. Value in () denotes the number of probes.

Case	Probe Setup	Test volume
A (16)	$\theta_1 = 0^o; \phi_{1i} = -180^o + i \cdot 90^o, i \in [1, \ldots, 4]$ $\theta_2 = 15^o; \phi_{2i} = -180^o + i \cdot 45^o, i \in [1, \ldots, 8]$ $\theta_3 = 30^o; \phi_{3i} = -180^o + i \cdot 90^o, i \in [1, \ldots, 4]$	major axis: 0.8λ minor axis: 0.9λ
B (32)	$\theta_1 = 0^o; \phi_{1i} = -180^o + i \cdot 45^o, i \in [1, \ldots, 8]$ $\theta_2 = 15^o; \phi_{2i} = -180^o + i \cdot 22.5^o, i \in [1, \ldots, 16]$ $\theta_3 = 30^o; \phi_{3i} = -180^o + i \cdot 45^o, i \in [1, \ldots, 8]$	major axis: 1.8λ minor axis: 0.9λ
C (48)	$\theta_1 = 0^o; \phi_{1i} = -180^o + i \cdot 30^o, i \in [1, \ldots, 12]$ $\theta_2 = 15^o; \phi_{2i} = -180^o + i \cdot 15^o, i \in [1, \ldots, 24]$ $\theta_3 = 30^o; \phi_{3i} = -180^o + i \cdot 30^o, i \in [1, \ldots, 12]$	major axis: 3λ minor axis: 0.9λ

Table 2: Statistics of the emulation results $|\rho - \hat{\rho}|$

Case	Channel emulator		Min-Sum		Min-Max	
	rms	max	rms	max	rms	max
A	0.07	0.16	0.07	0.23	0.08	0.10
B	0.07	0.19	0.05	0.18	0.06	0.09
C	0.07	0.21	0.05	0.14	0.05	0.08

a sphere, and the elevation angle θ and the azimuth angle ϕ are specified for each probe. The probes are organized on three elevation rings. θ_k denotes the elevation angle for all the probes on kth elevation ring. ϕ_{kj} is the azimuth angle of the jth probe on the kth elevation ring. The test volume is larger for case C than case A due to the larger number of probes.

The target spatial correlation $|\rho|$ for case C and emulation results with different algorithms are shown in Figure 2. The spatial correlation between the antennas on the surface of the test volume varies with locations of u and v. Statistics of the emulation results for all cases with different algorithms are summarized in Table 2. Generally, the Min-Sum algorithm presents the best performance for all scenarios in terms of rms error, while the Min-Max algorithm offers the smallest maximal error for all cases, as expected.

Target spatial correlations $|\rho|$ between antenna u and v and emulated spatial correlations $|\hat{\rho}|$ on two orthogonal axes (azimuth plane) for 3 cases are shown in Fig 3. A clear relation between the test volume and number of probes is shown.

Conclusion: This letter presents a channel emulation technique for 3D geometry-based channel models for a multi-probe based setup. The proposed methods provides a general emulation framework for all spherical power spectrums and offers globally optimal emulation accuracy with low computational complexity.

Acknowledgment: This work has been supported by the Danish National Advanced Technology Foundation via the 4GMCT project.

W. Fan, F. Sun, J. Nielsen, G. Pedersen (*Department of Electronic Systems, Faculty of Engineering and Science, Aalborg University, Denmark*)

E-mail: wfa@es.aau.dk

P. Kyösti (*Anite Telecoms Oy, Finland*)

X. Carreño and M. Knudsen (*Intel Mobile Communications, Denmark*)

References

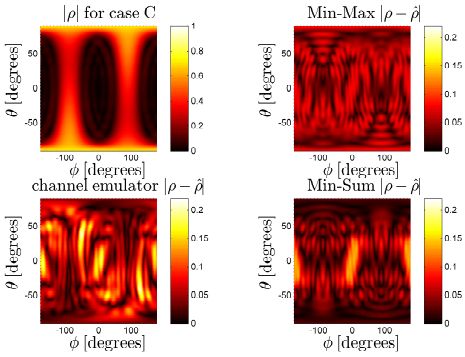

Fig. 2 *Target spatial correlation $|\rho|$ between antenna u and v on the surface of the test volume and the associated emulation results $|\rho - \hat{\rho}|$.*

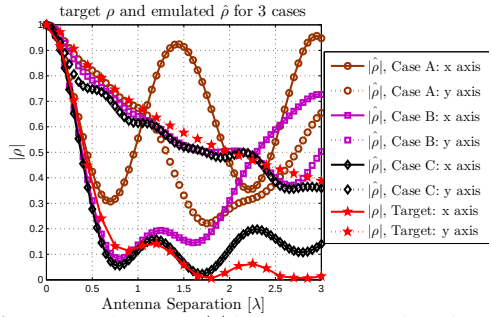

Fig. 3 *Target spatial correlation $|\rho|$ between antenna u and v and emulated spatial correlation $|\hat{\rho}|$ on two orthogonal axes (on azimuth plane) for the 3 cases detailed in Table 1. Axis x is along the AoA of the target channel. The power weights are obtained by the Min-Sum algorithm.*

1 Kyösti, P., Jämsä, T., and Nuutinen, J. P. :'Channel modelling for multiprobe over-the-air MIMO testing'. Int. Journal of Antennas and Propagation, 2012

2 Taga, T. :'Analysis for mean effective gain of mobile antennas in land mobile radio environments'. IEEE Trans. on Vehicular Technology, 1990, 39, (2), pp. 117-131

3 Knudsen MB, Pedersen GF.: 'Spherical Outdoor to Indoor Power Spectrum Model at the Mobile Terminal'. IEEE Journal on Selected Areas in Communications. 2002;20(6):1156-1169

4 Hentila, L., Kyösti, P., and Meinila, J. :'Elevation extension for a geometry-based radio channel model and its influence on MIMO antenna correlation and gain imbalance'. Proc. of the 5th European Conf. on Antennas and Propagation (EUCAP), 2011, pp. 2175-2179

5 Vaughan, R. and Bach-Anderson, J. :' Channels, Propagation and Antennas for Mobile Communications'. Institution of Electrical Engineers, 2003

Paper F

Estimating Discrete Power Angular Spectra in Multi-probe OTA Setups

Wei Fan, Jesper Ø. Nielsen, and Gert F. Pedersen

The paper has been published in the
IEEE Antennas and Wireless Propagation Letters, vol. 13, pp. 349–352, Feb. 2014.

The layout has been revised.

Estimating Discrete Power Angular Spectra in Multi-probe OTA Setups

Wei Fan, Jesper Ø. Nielsen, and Gert F. Pedersen

***Abstract*—The paper discusses over the air (OTA) testing for multiple input multiple output (MIMO) capable terminals with emphasis on estimating discrete power angular spectrum modeled at the receiver (Rx) side in the test zone. Two techniques based on a uniform circular array (UCA) are proposed to obtain accurate direction of arrival estimates as well as power estimates of the impinging signals in the test zone. Simulation results match well with the target, as expected. Measurement results based on a virtual UCA in a practical 3D multi-probe setup further support the simulation results. Possible reasons for the deviations between simulations and measurements are also investigated.**

***Index Terms*—MIMO OTA testing, multi-probe, anechoic chamber, power angular spectrum, antenna array**

I. Introduction

Field tests can fully evaluate mobile devices in a realistic environment. However, they may not be practical due to the high cost and lack of reproducibility of the results. Over the air testing (OTA) in the lab is an alternative to test device performance realistically. The multi-probe anechoic chamber method, due to its capability to physically approximate the realistic multipath environments in a shielded anechoic chamber, has been a promising candidate in standardizations to test multiple-input multiple-output (MIMO) capable terminals [1].

To evaluate the devices equipped with multiple antennas, it is critical to reproduce a specific propagation environment around the device under test (DUT). A continuous power angular spectrum (PAS) is often specified for a channel model at the receiver (Rx) side, see e.g. [2]. It is desirable that with a limited number of probes we should approximate the target continuous PAS. The spatial correlation, which is a statistical measure of the similarity between received signals at different receive (Rx) antennas, has been used to represent the channel spatial characteristics at the Rx side [3], [4]. The spatial correlation is used to determine the test zone size [4].

However, the PAS itself is interesting, not just through its effect on the Rx antenna (i.e. the spatial correlation at the Rx). The PAS of the channel at the Rx side modeled with the multiple probes is discrete, characterized by the angular locations and power weights of the active probes. The discrete PAS directly represent the directivity of the created channels and is preferable to the spatial correlation for certain channel models, e.g. the Rician fading channel models and the constant non-fading channel models. As demonstrated in [5], once the discrete PAS and DUT radiation patterns are known, other interesting parameters, e.g. the spatial correlation accuracy for realistic DUTs, the test zone size, and the reproduced spatial correlation can be easily obtained. In practical multi-probe setups, knowledge on how the channel is emulated in commercial channel emulators is very limited. Estimation of the discrete PAS can be used to verify how well the target channel is implemented in the test area. Furthermore, spatial correlation measurements, which are proposed in [1] to verify the implemented channels would fail for 3D multi-probe setups, as an isotopic antenna does not exist in practice.

Unlike previous work that merely rely on the spatial correlation to model and estimate the channel spatial characteristics created at the Rx side, this paper intends to estimate the discrete PAS using the antenna array theory. While DoA estimation using antenna arrays have been well studied in the literature, the discrete PAS estimation in multi-probe based anechoic chamber setup has not been reported in the literature. The main contributions of this paper lie in three aspects:

- A technique based on a virtual uniform circular array (UCA) to estimate discrete PAS modeled in multi-probe setups is proposed. Simulation results show that the estimated discrete PAS matches well with the target.
- Measurement results based on a virtual UCA in a preliminary 3D multi-probe setup show that the techniques are useful in practice. Previous measurement results were mainly based on 2D multi-probe setups. However, elevation spread can not be ignored in many propagation environments, as demonstrated by measurements. Note that a more complicated practical 3D setup with more probes might be required to have the full flexibility to model arbitrary realistic 3D channel channels [6].
- Possible reasons that introduce deviation between the measurement and simulation results are given.

II. Methods

A. Prefaded signal synthesis technique

The prefaded signal synthesis (PFS) method is a technique proposed for channel emulation in multi-probe based anechoic chamber setups in [4] and it has been implemented in several commercial channel emulators.The basic idea is to transmit Rayleigh or other kinds of fading signals separately from the multiple probes. A cluster is mapped to the multi-probes based on the cluster PAS and probe angular locations. An example is illustrated in Figure 1, where eight power weights for a single Laplacian shaped cluster is shown. Each probe associated with the cluster transmits weighted independent fading sequences with identical statistics. Contributions on obtaining optimal

Wei Fan, Jesper Ø. Nielsen, and Gert F. Pedersen are with the Antennas, Propagation and Radio Networking section at the Department of Electronic Systems, Faculty of Engineering and Science, Aalborg University, Denmark (email: {wfa, jni, gfp}@es.aau.dk).

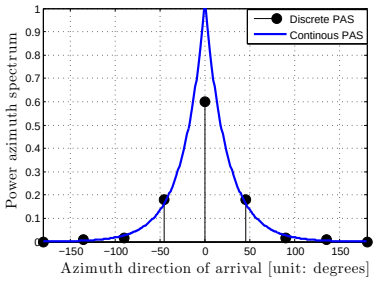

Figure 1. An illustration of the continuous and discrete PAS of a Laplacian shaped cluster with azimuth DoA 0^o and azimuth angle spread 35^o. The discrete angles define the angular locations of the probes.

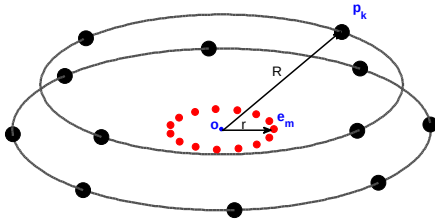

Figure 2. An illustration of the multi-probe setups and the antenna elements on the UCA. The number of probes is K and the number of array elements is M. The radius of the probe sphere R is assumed much larger than the radius of the UCA r.

power weights haven been discussed in [3], [4] and results from [3] are used in Figure 1.

In a practical multi-probe setup, the discrete PAS is generally unknown, as information on the commercial channel emulators is often very limited, and practical setup issues may effectively change the PAS. This paper intends to estimate the discrete PAS modeled in the multi-probe setups using a virtual UCA. The discrete PAS can be used to verify how well the channels are implemented in the lab. For the sake of simplicity, discrete PAS estimation of a single cluster is addressed in this paper. That is, the signals transmitted from the probes are narrowband. This can be easily extended to multiple cluster cases (i.e. wideband channels). Wideband measurements can be performed to detect the multiple delays in the wideband channels and the techniques proposed in the paper can be used to estimate the discrete PAS for each delay.

B. Simulation model

1) Problem formulation: Figure 2 illustrates a multi-probe setup, where $\overrightarrow{op_k}$ is a vector containing the angular location for the kth probe with $k \in [1, K]$. A UCA is used to estimate the discrete PAS, as probes are often placed around the DUT. Uniform linear arrays (ULAs) are not applicable, as two probes at locations symmetric with respect to the line can not be distinguished. $\overrightarrow{oe_m}$ is a vector containing the angular location for the mth UCA element with $m \in [1, M]$.

The baseband model for the received signals at the array elements can be written in a matrix form as follows:

$$\boldsymbol{x}[n] = \mathbf{A}\boldsymbol{s}[n] + \boldsymbol{v}[n] \tag{1}$$

where:

- $\boldsymbol{x}[n] = \{x_m[n]\} \in \mathbb{C}^{M\times 1}$ is a vector containing M received signals at the nth snapshot.
- $\mathbf{A} = \{a_{mk}\} \in \mathbb{C}^{M\times K}$ is a transfer matrix of coefficients from the kth probe to the mth antenna element with

$$a_{mk} = c_{mk} \exp\left[j\frac{2\pi}{\lambda}\frac{\overrightarrow{op_k}\cdot\overrightarrow{oe_m}}{|\overrightarrow{op_k}|}\right] \tag{2}$$

  where $(\cdot)$ is the dot operator and $||$ is the norm operator. c_{mk} is the path loss term from the kth probes to the mth antenna element and it is a constant, as $R \gg r$ is assumed. λ is the wavelength.
- $\boldsymbol{s}[n] = \{s_k[n]\} \in \mathbb{C}^{K\times 1}$ is a vector containing K transmitted signals at the nth snapshot.
- $\boldsymbol{v}[n] = \{v_m[n]\} \in \mathbb{C}^{M\times 1}$ is noise vector. As the study is performed in an anechoic chamber, the noise term is assumed small and neglected.

The auto-covariance matrix $\hat{\mathbf{R}} \in \mathbb{C}^{M\times M}$ of the received signals can be estimated as:

$$\hat{\mathbf{R}} = \frac{1}{N}\sum_{n=1}^{N}\boldsymbol{x}[n]\boldsymbol{x}^{\mathrm{H}}[n] \tag{3}$$

The power weights allocated to the probes depend on the target continuous PAS and probe angular locations, and hence some probes may not be used in synthesizing the channel.

2) DoA estimation: DoA estimation using antenna arrays has long been of research interest given their importance in a great variety of applications and various methods have been proposed [7]. As explained in Sec. II-A, transmit signals from the multiple probes are uncorrelated and narrowband. Two basic DoA estimation algorithms are discussed below.

The mth component of the steering vector $\boldsymbol{a}(\theta,\varphi) = \{a_m(\theta,\varphi)\} \in \mathbb{C}^{M\times 1}$ for a UCA can be expressed as:

$$a_m(\theta,\varphi) = \exp\left[j\frac{2\pi}{\lambda}r\sin\theta\cos(\varphi-\gamma_m)\right] \tag{4}$$

where θ and φ are the elevation and azimuth angle, respectively. $\gamma_m = 2\pi(m-1)/M$ denotes the angular location of the mth element.

a) Beamforming: The beamforming method computes the DOA by measuring the signal power at each possible angle of arrival and selecting the direction of maximum power as the estimate of the angle of arrival [7]. The drawback with the beamforming method is that the spatial resolution is determined by the number of antenna elements and inferior to the high-resolution subspace techniques. The power angular spectrum is given by:

$$P_{beamformer}(\theta,\varphi) = \boldsymbol{a}^H(\theta,\varphi)\hat{\mathbf{R}}\boldsymbol{a}(\theta,\varphi) \tag{5}$$

b) MUSIC method: MUSIC method is a subspace based algorithm, which offers high resolution in DoA estimation [7]. The basic idea is to search through the set of all possible steering vectors and find those that are orthogonal to the noise subspace. The power angular spectrum is given by:

$$P_{music}(\theta,\varphi) = \frac{1}{\boldsymbol{a}^H(\theta,\varphi)\hat{\mathbf{G}}\hat{\mathbf{G}}^H\boldsymbol{a}(\theta,\varphi)} \tag{6}$$

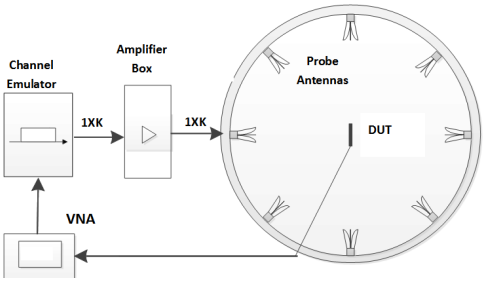

Figure 3. An illustration of the multi-probe based MIMO OTA setup.

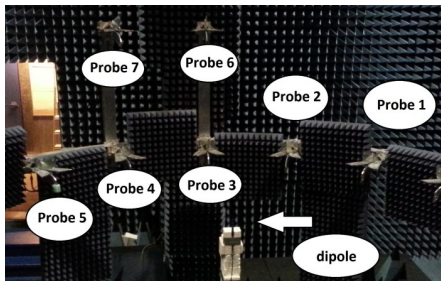

Figure 4. Probe configuration of the 3D practical multi-probe setup used in the measurements. The probe angular locations are detailed in Table I.

where $\hat{\mathbf{G}}$ is the noise subspace eigenvectors, which can be calculated from the auto-covariance matrix $\hat{\mathbf{R}}$ [7]. Note that (6) is a "pseudo-spectrum", as it only checks the orthogonality between steering vectors and the noise space, and hence power estimates in (6) are inconsistent.

3) Signal power estimation: Once the DoA estimates are obtained, we can estimate the average power of signals based on $\hat{\mathbf{R}}$ and the DoA estimates. From (1) and (3), we have

$$\hat{\mathbf{R}} = E[\boldsymbol{x}[n]\boldsymbol{x}^H[n]] = \hat{\mathbf{A}}E[\boldsymbol{s}[n]\boldsymbol{s}^H[n]]\hat{\mathbf{A}}^H = \hat{\mathbf{A}}\hat{\mathbf{P}}\hat{\mathbf{A}}^H \quad (7)$$

where $\hat{\mathbf{A}} = \{a_m(\hat{\theta}_k, \hat{\varphi}_k)\} \in \mathbb{C}^{M\times K}$ is the steering matrix with $\hat{\theta}_k$ and $\hat{\varphi}_k$ the elevation and azimuth angle estimate for the kth signal, respectively. $\hat{\mathbf{P}} \in \mathbb{R}^{K\times K}$ is a diagonal matrix with its kth element on the main diagonal p_k being the power estimate for the kth signal. This least-squared problem can be solved by the pseudo inverse:

$$\hat{\mathbf{P}} = (\hat{\mathbf{A}}^H\hat{\mathbf{A}})^{-1}\hat{\mathbf{A}}^H\hat{\mathbf{R}}(\hat{\mathbf{A}}\hat{\mathbf{A}}^H)^{-1}\hat{\mathbf{A}} \quad (8)$$

III. Simulation and Measurement Results

A. Measurement setup

An illustration of a general multi-probe anechoic chamber setup is shown in Figure 3. The practical 3D probe configuration is shown in Figure 4. The measurement setup is summarized in Table I. θ_i denotes the elevation angle for all the probes on ith elevation ring. φ_{ij} is the azimuth angle of the jth probe on the ith elevation ring. The measurement procedure is detailed in [1]. As a summary, the channel emulator pauses every 10 CIRs to satisfy Nyquist sampling criteria and the field is measured with the network analyzer. The dipole is then moved to next position, and the sweep of the same CIRs is repeated for the new position. This procedure is repeated until all the positions are covered. The virtual UCA is formed by repeating the same CIRs for all the positions.

B. Target models

Based on the preliminary setup, three target discrete PASs are selected, as detailed in Table II. Target model B approximates a single spatial cluster model, while target model C is selected to check the robustness of the virtual UCA for elevation angle estimation. Independent Rayleigh fading sequences with identical statistics are transmitted from the specified probes with known average power values.

Table I
Setup and specifications for the measurements

	Setup and specifications
Channel emulator	10000 channel impulse responses (CIRs) are created and stored. The CIRs are mapped to the OTA probes with known power weights
UCA	A Satimo calibration dipole at 2450MHz is rotated every 24^o with $r = 14$ cm to the center to form a virtual UCA.
Probe angular locations	The probes are organized on two elevation rings. 5 probes on the first ring with $\theta_1 = 90^o$ and $\varphi_{1j} = 135^o + (j-1)\cdot 22.5^o$, $j \in [1, 5]$. 2 probes on the second ring with $\theta_2 = 63.5^o$ and $\varphi_{2j} = 180^o + (j-1)\cdot 22.5^o$, $j \in [1, 2]$.

C. Results and discussions

Estimated DoAs based on simulations and measurements are compared for the three cases. Simulated DoAs match with the target in all cases as expected, see e.g. Figure 5 (left) for case A. The measured and simulated discrete PAS with beamforming technique match very well. With the MUSIC algorithm, deviation of azimuth DoA estimation (e.g. 2.5^o as shown in Figure 5) is mainly caused by calibration error of dipole positions in measurement system and step accuracy of the turntable, since the estimated azimuth DoA match well with the target, with an offset around 2^o for all the azimuth DoAs, as shown in Figure 6. As for the elevation DoA estimate, it is not robust in measurements as the virtual UCA's aperture is small in elevation, and hence the elevation DoA estimate is susceptible to the small noise in the system, as shown in Figure 5, 6, and 7 respectively.

Measured discrete PAS using MUSIC and beamforming algorithms for case B is shown in Figure 6. With the beamforming technique, only 3 probes with high power weights are detected due to the low spatial resolution and high sidelobes. The estimated discrete PAS using MUSIC and beamforming algorithms for the 3D probe configurations in measurements

Table II
Setup and specifications for the measurements

Cases	Discrete PAS
A	Only probe 3 active
B	Probes 1, 2, 3, 4, 5 active with normalized average power shown in Figure 8 (left).
C	Probes 1, 5, 6 active with normalized average power shown in Figure 8 (right).

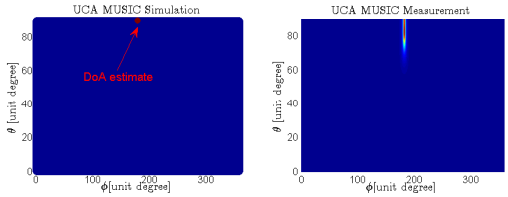

Figure 5. Simulated (left) and measured (right) discrete PAS using the MUSIC algorithm for case A. DOA estimate in the simulation is $[180^o, 90^o]$ and DOA estimate in the measurement is $[182.5^o, 84.5^o]$.

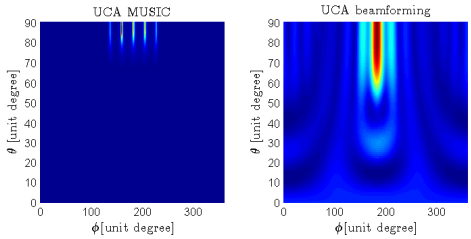

Figure 6. Measured discrete PAS using MUSIC and beamforming algorithms for case B. DOA estimate with MUSIC is $[136.5^o, 88.5^o]$, $[159.5^o, 85^o]$, $[182.5^o, 87.5^o]$, $[205^o, 87^o]$, $[226.5^o, 88.5^o]$, respectively.

are shown in Figure 7 and similar conclusions can be drawn.

Power estimates obtained in simulations using (8) match with the target in all cases, as expected. Power estimates in measurements are shown in Figure 8 for case B and case C, respectively. To demonstrate the impact of elevation angle estimation on the power estimate accuracy, power estimates obtained with the estimated azimuth angles $\hat{\varphi}$ and elevation angles $\hat{\theta}$, are compared with the case where power estimates are obtained with estimated azimuth angles $\hat{\varphi}$ and target elevation angles θ. As shown in Figure 8, the power estimates are robust to elevation angle estimation inaccuracies. The power estimates using (8) generally match well with the target in case B. The power estimates with beamforming are consistent, though with worse accuracy due to the low spatial resolution and sidelobes impact. For case C, the power estimates present around 1dB deviation compared with the target. This might be introduced by the probe calibration inaccuracy.

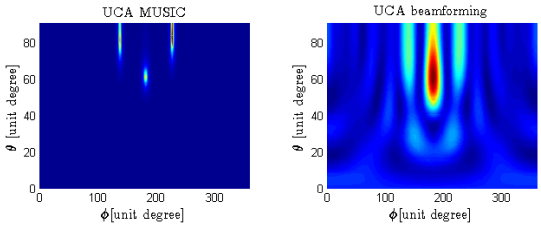

Figure 7. Measured discrete PAS using MUSIC and beamforming algorithms for case C. DOA estimate with MUSIC is $[137.5^o, 83.5^o]$, $[182.5^o, 63^o]$, $[228.5^o, 86.5^o]$, respectively.

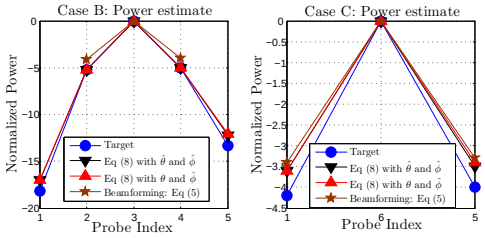

Figure 8. Signal power estimation results based on measurements for case B (left) and case C (right).

IV. Conclusion

We have introduced two techniques to estimate discrete power angular spectrum in the multi-probe based anechoic chamber setups, i.e. the beamforming and the MUSIC technique with power estimation. The beamforming technique provides consistent DoA and power estimates, which are prone to inaccuracy due to low spatial resolution and sidelobes. The MUSIC algorithm presents DoA estimates with high resolution. The power estimates based on DoA estimates match well with the target in the measurements. To improve accuracy and robustness in elevation DoA estimation, a virtual array with large aperture in elevation is suggested in measurements.

Acknowledgment

This work has been supported by the Danish National Advanced Technology Foundation via the 4GMCT project. The authors also appreciate the assistance from Intel Mobile Communications, Denmark in the measurements.

References

[1] "Verification of radiated multi-antenna reception performance of User Equipment," 3GPP, TR 37.977 V1.0.0, Sep. 2013.

[2] D. Baum, J. Hansen, and J. Salo, "An interim channel model for beyond-3G systems: extending the 3GPP spatial channel model (SCM)," in *Proc. IEEE VTC-Spring*, May 2005.

[3] W. Fan, X. de Lisbona, F. Sun, J. Nielsen, M. Knudsen, and G. Pedersen, "Emulating Spatial Characteristics of MIMO Channels for OTA Testing," *Antennas and Propagation, IEEE Transactions on*, vol. 61, no. 8, pp. 4306–4314, 2013.

[4] P. Kyösti, T. Jämsä, and J. Nuutinen, "Channel modelling for multiprobe over-the-air MIMO testing," *International Journal of Antennas and Propagation*, 2012.

[5] W. Fan, J. Nielsen, O. Franek, X. Carreno, J. Ashta, M. Knudsen, and G. Pedersen, "Antenna Pattern Impact on MIMO OTA Testing," *Antennas and Propagation, IEEE Transactions on*, vol. 61, no. 11, pp. 5714–5723, 2013.

[6] W. Fan, F. Sun, P. Kyösti, J. Nielsen, X. Carreño, M. Knudsen, and G. Pedersen, "3D channel emulation in multi-probe setup," *Electronics Letters*, vol. 49, pp. 623–625(2), April 2013.

[7] P. Stoica and R. L. Moses, *Spectral analysis of signals*. Pearson/Prentice Hall Upper Saddle River, NJ, 2005.

Paper G

Channel Spatial Correlation Reconstruction in Flexible Multiprobe Setups

Wei Fan, Istvan Szini, Jesper Ø. Nielsen, and Gert F. Pedersen

The paper has been published in the
IEEE Antennas and Wireless Propagation Letters, Special Cluster on Terminal Antenna Systems for 4G and Beyond, vol. 12, pp. 1724–1727, Jan. 2014.

The layout has been revised.

Channel Spatial Correlation Reconstruction in Flexible Multi-Probe Setups

Wei Fan, Istvan Szini, Jesper Ø. Nielsen, and Gert F. Pedersen

***Abstract*—This paper discusses one aspect of over the air (OTA) testing for multiple input multiple output (MIMO) capable terminals in flexible multi-probe setups. Two techniques to obtain weights as well as angular locations for the OTA probes are proposed for accurate reconstruction of the channel spatial correlation at the receiver side. Examples show that with a small number of probes in a flexible setup, accurate spatial correlation can still be achieved within the test zone.**

***Index Terms*—OTA testing, flexible multi-probe setup, anechoic chamber, multi-antenna terminal**

I. Introduction

Over the air (OTA) testing of multiple input multiple output (MIMO) capable terminals has attracted huge attention in recent years due to the urgent need for testing the radio performance of mobile terminals with multiple antennas [1]. The multi-probe anechoic chamber method is a promising candidate due to its ability to reproduce desired radio channels.

One major challenge with the multi-probe method is the cost of the system and the setup complexity. Each probe is typically connected to an expensive channel emulator. The cost will likely increase dramatically for 3D probe configurations [2]. The fixed multi-probe setup may not be cost effective, as often many probes are not actually used in synthesizing the radio channels. If the probes can be placed according to the channel spatial characteristics in a flexible manner, a larger test area can be created compared with the fixed probe setups with the same number of probes. Hence, a flexible setup mechanism has the potential to save cost of the system, via reducing the number of required active probes and respective hardware.

In one possible installation for the flexible setup, a large number of probes are installed with fixed locations, and a switch box drives a subset of probes based on the target channel models [3]. To reduce mutual coupling and reflection between probes, a minimum separation between probes is required. Fixing the probe locations in the chamber may result in suboptimal probe locations for a given channel model. In this paper, we propose a flexible system arrangement, where the number of probes (consequently the channel emulator output ports) are optimized to the minimum necessary to generate the desirable spatial channel model. An illustration of the setup is shown in Figure 1, where probes are assembled in a movable semi-arc rail. The probe placement is flexible in both the elevation and azimuth angles, enabling the placement on optimal location defined by the proposed algorithm.

Wei Fan, Istvan Szini, Jesper Ø. Nielsen, and Gert F. Pedersen are with the APNET section at the Department of Electronic Systems, Faculty of Engineering and Science, Aalborg University, Denmark (email: {wfa, ijs, jni, gfp}@es.aau.dk).

Istvan Szini is with Motorola Mobility LLC., Libertyville, USA.

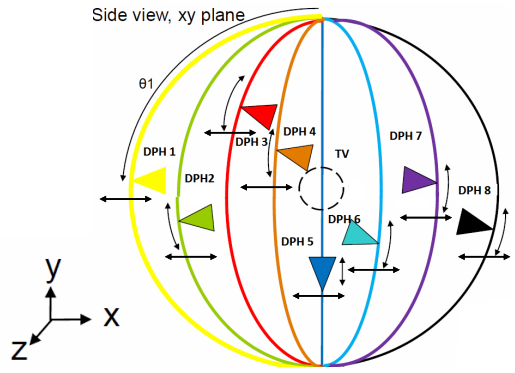

Figure 1. An illustration of the flexible multi-probe setup. DPH denotes dual polarized horn antenna; TV denotes test volume. The elevation and azimuth angle of each probe is to be optimized.

Contributions on the channel emulation techniques have been mainly focused on the fixed multi-probe configurations so far, where the objective is to find the optimum probe weights [2], [4], [5]. Channel emulation for the flexible setup with a small number of probes is more challenging as both the probe weights and the probe angular locations are to be optimized. In this paper, two algorithms, namely the genetic algorithm and the so-called multi-shot algorithm, are proposed to emulate channel spatial correlation in flexible setups. Note that modeling of the other channel parameters, e.g. Doppler power spectrum, power delay profile, etc. in the flexible setups are not addressed in the paper. Modeling of those parameters is addressed in [4] for the fixed setups.

II. Problem Formulation

Channel emulation for fixed multi-probe setups have been detailed in [4], [5], where the focus is on recreating the channel spatial characteristics where the device in located. Spatial correlation is used as a figure of merit to model the channel spatial characteristics. A location pair is used to represent the locations of two spatial samples where two hypothetical isotropic antennas u and v are placed [5]. The spatial correlation for the mth location pair, for a single polarization, is:

$$\rho(m) = \oint \exp(j\beta(\overline{r}_{u,m} - \overline{r}_{v,m}) \cdot \overline{\Omega}) p(\Omega) d\Omega, \qquad (1)$$

where $\overline{r}_{u,m}$ and $\overline{r}_{v,m}$ are vectors containing the position information of antenna u and v at the mth location pair,

respectively. $\overline{\Omega}$ is an unit vector corresponding to the solid angle Ω. β is the wave number. $p(\Omega)$ is spherical power spectrum (SPS) satisfying $\oint p(\Omega)d\Omega = 1$. $(\cdot)$ is the dot product operator. Similar to (1), the emulated spatial correlation for the mth location pair can be calculated as [4], [5]:

$$\hat{\rho}(m, \overline{\mathbf{\Phi}}) = \sum_{n=1}^{N} w_n \exp(j\beta(\overline{r}_{u,m} - \overline{r}_{v,m}) \cdot \overline{\Phi}_n), \qquad (2)$$

where $\boldsymbol{w} = [w_1, ..., w_N]^T$ is a power weighting vector to be optimized. $\overline{\Phi}_n$ is a unit position vector of the nth probe. $\overline{\mathbf{\Phi}} = [\overline{\Phi}_1, ..., \overline{\Phi}_N]^T$ is a matrix that contains the positions of all probes. N is the total number of probes.

To minimize the emulation error over M location pairs, the following objective function is used:

$$\begin{aligned} &\min \ \left\|\hat{\boldsymbol{\rho}}(\boldsymbol{w}, \overline{\mathbf{\Phi}}) - \boldsymbol{\rho}\right\|_2^2, \\ &\text{s.t. } 0 \le w_n \le 1, \ \forall n \in [1, N] \end{aligned} \qquad (3)$$

where $\hat{\boldsymbol{\rho}}$ and $\boldsymbol{\rho}$ are the emulated spatial correlation and the target spatial correlation vectors of size M, respectively, with the mth element described in (2) and (1), respectively. $\hat{\boldsymbol{\rho}} = \mathbf{F_N}\boldsymbol{w}$ with $\mathbf{F_N} \in \mathbb{C}^{M \times N}$ being the transfer matrix for N probes, whose elements are given by:

$$(\mathbf{F_N})_{m,n} = \exp(j\beta(\overline{r}_{u,m} - \overline{r}_{v,m}) \cdot \overline{\Phi}_n), \quad 1 \le m \le M \quad (4)$$

For fixed multi-probe setups (i.e. $\overline{\mathbf{\Phi}}$ fixed), the objective function (3) is a convex optimization problem, which is easily solved in [2], [5]. For flexible multi-probe setups, the objective function (3) is a non-convex optimization problem as both the probe weights and the probe angular locations are to be optimized. The solution for this non-convex problem for the flexible setups is not trivial and more complicated.

In the following, probes are limited to a possibly large set of discrete locations for practical reasons. Let us define $\overline{\mathbf{\Psi}} = [\overline{\Phi}_1, ..., \overline{\Phi}_K]^T$ $(K > N)$ as a matrix that contains the K possible discrete locations for the probes. The channel spatial correlation emulation for flexible setups can be treated in two steps as:

1) Select N locations out of K possible discrete locations for the N probes. The problem formulation for the probe selection is as follows:

$$\begin{aligned} &\min_{\mathbf{c}} \ \|\mathbf{F_K}\mathbf{c} - \boldsymbol{\rho}\|_2^2 \\ &\text{s.t. } \|\mathbf{c}\|_0 = N \end{aligned} \qquad (5)$$

where the norm-0 operation $\|\cdot\|_0$ is defined to be the number of nonzero entries in the vector. $\mathbf{F_K}$ is the transfer matrix for the K possible locations with its element defined in (4). $\boldsymbol{c} = [c_1, ..., c_K]$ is the weighting vector to be optimized.
The problem in (5) is non-convex and NP-hard due to the norm-0 constraint. A brute force method where the optimization is performed for each possible combination of the N locations out of K potential locations can be used, and a total number of combinations is $\begin{pmatrix} K \\ N \end{pmatrix}$. The number of combinations to be tested becomes huge when K is large. Two algorithms are proposed to address the non-convex optimization problem later.
2) After knowing the locations of the N probes, the optimization is simplified to be a convex problem:

$$\min_{\mathbf{c}_{sel}} \|\mathbf{F}\mathbf{c}_{sel} - \boldsymbol{\rho}\|_2^2$$

where $\mathbf{F}$ is the $M \times N$ matrix with N selected columns from $\mathbf{F_K}$, and $\mathbf{c}_{sel}$ is the $N \times 1$ vector with the N selected probe locations.

III. Spatial correlation emulation with flexible setups

A. Genetic algorithm

The genetic algorithm (GA) has been widely used in electromagnetics [6]. The GA is basically a search technique inspired by the principles of genetics and natural selection. A very useful aspect of GA is that it can deal with a large number of variables and it can optimize variables with extremely complex cost surfaces [6]. A limitation is that it can stop in a local optimum, and often, it is not possible to know whether the solution is local or global. We can think of the target channel as the environment and the selected probe locations as the biological species that need to fit in the environment (the channel). The fitness of the probe locations to the environment can be measured by the channel emulation accuracy. In this section, a GA applied to the problem of selecting the optimum probe locations is described. The concept is straightforward: The GA seeks for a set of probe locations that would minimize the channel emulation error. The number of selected probes (N) designates the search space.

A population is the array of chromosomes under examination for the GA. A chromosome contains N variables which represent the N probe locations. Each chromosome will have a cost evaluated by the cost function f, as:

$$f = \min_{\boldsymbol{w}_{GA}} \|\mathbf{F}_{GA}\boldsymbol{w}_{GA} - \boldsymbol{\rho}\|_2^2, \qquad (6)$$

where $\mathbf{F}_{GA}$ and $\boldsymbol{w}_{GA} = [w_1, ..., w_N]^T$ are the transfer matrix and probe weight vector of the chromosome under evaluation. The cost function actually contains a convex optimization process. A flowchart of the GA shown is shown in Figure 2. The description of the employed GA algorithm is given in [6] and is not detailed here. This complexity of GA is:

$$\underbrace{N_{pop}}_{\text{initial population}} + \underbrace{(N_{pop} - 1)}_{\text{cost evaluations per generation}} \times \underbrace{N_g}_{\text{generations}}$$

cost function evaluations.

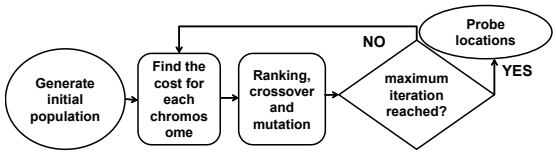

Figure 2. Brief flowchart of the employed GA.

Table I
GA PARAMETER SETUPS

Parameter	maximum number of iterations N_g	population size N_{pop}	selection rate
Value	50	8	50%

B. Multi-shot

One alternative to select the optimum set of probe locations is to use the so-called multi-shot algorithm. The basic idea is that probes with negligible contribution in synthesizing the channels should be removed. Probe locations can be removed in a sequential manner. We denote by k_n the number of potential locations we remove in the nth iteration and we have $K - \sum_{m=0}^{n-1} k_m$ selected locations in the nth iteration. In the multi-shot algorithm, we first perform the optimization for K potential locations. In the nth iteration, based on the individual probe power values $|c_{n,index}|$ $(1 \leq index \leq K)$ in $\mathbf{c}_n$, we remove k_n locations with the least power values. We repeat the location removal process until only $K - \sum_{m=0}^{n-1} k_m = N$ locations are left. In the end, we return both the final probe weights and the corresponding probe locations. The complexity of the multi-shot algorithm is $\frac{K-N}{k} + 1$ convex optimizations if the number of removed locations per iteration is always k.

IV. OPTIMIZATION RESULTS

A. Optimization setups

To illustrate the algorithms, 2D multi-probe setups are considered for simplicity. $K = 360$ uniformly placed locations are defined as possible locations. The parameters for the GA have been chosen through repeated trials, following the guideline in [6]. The number of generations is a tradeoff between the convergence rate and the computational complexity. The parameters used in the GA are summarized in Table I. In the following computations, the number of removed locations per iteration $k_n = 1$ is defined for the multi-shot algorithm.

We examine a set of representative channel models that are used in standardization for the MIMO OTA testing [1]. The models are: a) Single Laplacian shaped spatial cluster with angle of arrival (AoA) 22.5° and azimuth spread (AS) 35°, b) SCME Urban micro (Umi) TDL model (six Laplacian shaped clusters) and c) SCME Urban macro (Uma) TDL model from [7]. Note that a critical single cluster model for the eight probe uniform setup, i.e. the spatial cluster impinging from an angle exactly between two adjacent OTA probes, is selected to show the robustness of the algorithms [5]. A uniform configuration is used for comparison for each considered flexible setup, as detailed in Table II. The eight probe uniform setup is compared with the 3 probe flexible setup, as both of them are able to create a single cluster with an arbitrary AoA without relocation of the probes The idea is to show that with a small number of probes in a flexible setup, accurate spatial correlation can still be achieved.

B. Results

The spatial correlation $|\rho|$ for the single spatial cluster model and correlation error $|\hat{\rho} - \rho|$ are shown in Figure 3. The radius d and polar angle ϕ of each point on the plots correspond to the value at antenna separation d and antenna orientation ϕ [5]. Test area size shown in the optimization results denotes the distance between the two antennas and corresponds to the maximum d in the polar plots. A maximum deviation of 0.15 and 0.3 is achieved over the test area size of 1λ for the flexible setup with 3 probes for the GA and multi-shot algorithm, respectively. In contrast, the correlation error is much larger for the uniform setup with 8 probe. The optimized angle locations for the 3 probes with the two proposed algorithms are shown in Figure 4 (left), where the angular locations are in good agreement with the target single spatial cluster. Figure 5 (left) shows the GA algorithm convergence curve in terms of the minimum and mean cost for each generation for the single cluster model.

Table II
NUMBER OF PROBES AND TEST AREA SIZE FOR THE CONSIDERED SETUPS.

Channel models	Flexible setup	Reference setup	Test area size
Single cluster	$N = 3$	Uniform setup with 8 probe	1λ
SCME Umi TDL	$N = 8$	Uniform setup with 16 probe	1.5λ

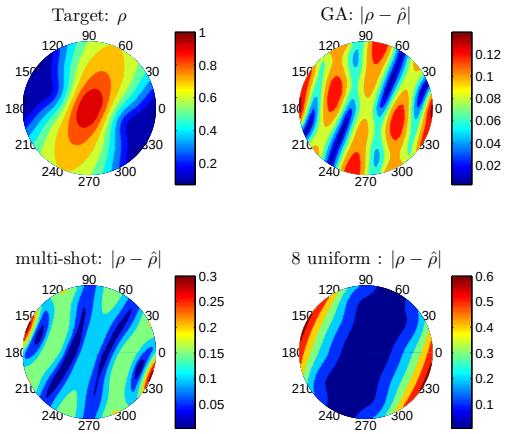

Figure 3. The target spatial correlation $|\rho|$ for the single cluster channel model and the associated correlation error $|\rho - \hat{\rho}|$ for 3 probes with the GA algorithm, 3 probes with the multi-shot algorithm and the uniform probe configuration with 8 probes. Test area size: 1λ.

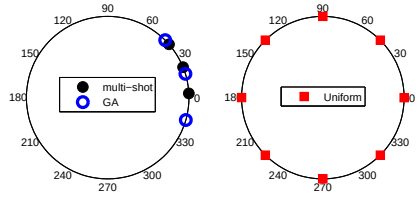

Figure 4. An illustration of the probe configurations detailed in Table II.

The spatial correlation $|\rho|$ for the SCME Umi TDL model and correlation error $|\hat{\rho} - \rho|$ are shown in Figure 6. Narrowband multi-cluster models (with delay information removed) are used to obtain the optimal probe locations. Then each cluster is emulated with the selected probe locations, as described

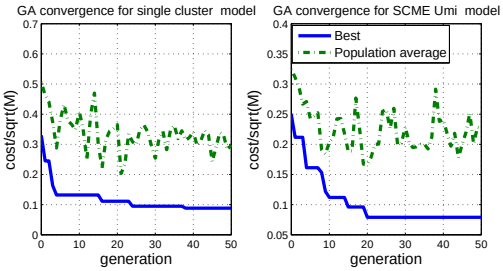

Figure 5. GA convergence curve for the single cluster model (left) and for the SCME Umi TDL model (right).

in [5]. A maximum deviation of 0.12 is achieved over the test area of 1.5λ for the flexible setup with 8 probes for the multi-shot algorithm. The multi-probe algorithm outperforms the GA for the SCME Umi TDL model. Figure 5 (right) shows the GA convergence curve for each generation for the SCME Umi TDL model. The channel emulation accuracy with the 8-probe flexible setup and the multi-shot algorithm offers slightly worse results than the channel emulation accuracy with the 16 uniform probe setup. The optimized angle locations for the 8 probes with the proposed algorithms for the SCME Umi TDL and the SCME Uma TDL models are shown in Figure 7.

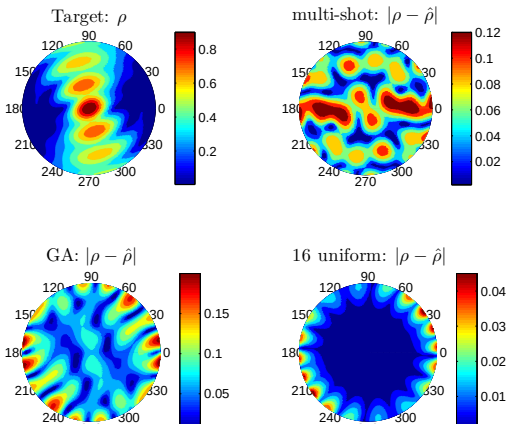

Figure 6. The target spatial correlation $|\rho|$ for the SCME Umi TDL channel model and associated correlation error $|\rho - \hat{\rho}|$ for 8 probes with the multi-shot algorithm, 8 probes with the GA algorithm and uniform probe configuration with 16 probes. Test area size: 1.5λ.

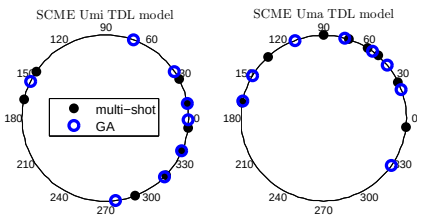

Figure 7. Illustration of optimized locations for SCME Umi TDL (left) and SCME Uma TDL models (right).

The emulation accuracy for the 6 clusters in the SCME Umi TDL model is shown in Table III. Note that the probe locations are selected based on the SPS of the multi-cluster model, so

Table III
ERROR STATISTICS OF CORRELATION ERROR $|\rho - \hat{\rho}|$ FOR THE 6 CLUSTERS IN THE SCME UMI TDL CHANNEL MODEL FOR DIFFERENT ALGORITHMS.

Algorithm	$\lvert\rho - \hat{\rho}\rvert$	1	2	3	4	5	6
multi-shot	max	0.16	0.09	0.44	0.09	0.10	0.15
	rms	0.07	0.05	0.25	0.05	0.05	0.07
GA	max	0.17	0.20	0.65	0.24	0.21	0.18
	rms	0.05	0.06	0.35	0.07	0.06	0.05

the emulation accuracy for each of the clusters might be bad. The correlation error $|\rho - \hat{\rho}|$ for the 3rd cluster is up to 0.44 with the multi-shot algorithm due to the fact that the locations selected are favoring the dominant clusters.

The correlation error $|\hat{\rho} - \rho|$ for the SCME Uma TDL model with the multi-shot and the GA are shown in Figure 8. The GA slightly outperforms the multi-shot algorithm, with correlation error up to 0.25 over the test area of 1.5λ.

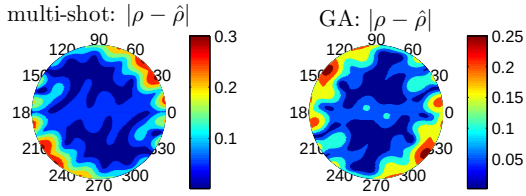

Figure 8. The correlation error $|\rho - \hat{\rho}|$ for 8 probes with the multi-shot algorithm and 8 probes with the GA for the SCME Uma TDL model. Test area size: 1.5λ.

V. CONCLUSIONS

We have introduced two algorithms to determine the weights and angular locations for the probes in flexible setups, i.e. the multi-shot algorithm and the GA. The proposed algorithms offer good spatial correlation accuracy for the flexible setups. The optimization results show that a test area of 1λ can be created for the single cluster channel model with 3 probes, with an spatial correlation error up to 0.14 with the GA. A test area of 1.5λ can be created with 8 probes for the SCME Umi TDL model, with an correlation error up to 0.12 with the multi-shot algorithm, and for the SCME Uma TDL channel model, with an correlation error up to 0.25 with the GA.

REFERENCES

[1] "Verification of radiated multi-antenna reception performance of User Equipment," 3GPP, TR 37.977 V1.0.0, Sep. 2013.

[2] W. Fan, F. Sun, P. Kyosti, J. Nielsen, X. Carreno, M. Knudsen, and G. Pedersen, "3D channel emulation in multi-probe setup," *Electronics Letters*, vol. 49, no. 9, pp. 623–625, 2013.

[3] P. Kyösti, J. Nuutinen, and J. Malm, "Over the air test," Patent US 20 130 059 545 A1, Mar. 7, 2013.

[4] P. Kyösti, T. Jämsä, and J. Nuutinen, "Channel modelling for multiprobe over-the-air MIMO testing," *International Journal of Antennas and Propagation*, 2012.

[5] W. Fan, X. de Lisbona, F. Sun, J. Nielsen, M. Knudsen, and G. Pedersen, "Emulating Spatial Characteristics of MIMO Channels for OTA Testing," *IEEE Transactions on Antennas and Propagation*, vol. 61, no. 8, pp. 4306–4314, 2013.

[6] R. L. Haupt and D. H. Werner, *Genetic algorithms in electromagnetics*. Wiley. com, 2007.

[7] D. Baum, J. Hansen, and J. Salo, "An interim channel model for beyond-3G systems: extending the 3GPP spatial channel model (SCM)," in *Proc. IEEE VTC-Spring*, May 2005.

Paper H

Rician Channel Modeling for Multi-probe Anechoic Chamber Setups

Wei Fan, Pekka Kyösti, Lassi Hentilä, Jesper Ø. Nielsen, and Gert F. Pedersen

The paper has been resubmitted after revision to the
IEEE Antennas and Wireless Propagation Letters, Aug. 2014.

The layout has been revised.

Rician Channel Modeling for Multi-probe Anechoic Chamber Setups

Wei Fan, Pekka Kyösti, Lassi Hentilä, Jesper Ø. Nielsen, and Gert F. Pedersen

***Abstract*—This paper discusses over the air (OTA) testing for multiple input multiple output (MIMO) capable terminals, with emphasis on modeling Rician channel models in the multi-probe anechoic chamber setups. A technique to model Rician channels is proposed. The line-of-sight (LOS) component, with an arbitrary polarization and an arbitrary impinging direction, and non-LOS (NLOS) component, with any impinging power angular spectrum (PAS), can be created. Simulation results show that the emulated Rician channels approximate the target models accurately in terms of field envelope distribution, K factor, Doppler spectrum and spatial correlation at the receiver (Rx) side.**

***Index Terms*—MIMO OTA testing, multi-probe, anechoic chamber, Rician channel modeling, K factor estimation**

I. Introduction

Over the air (OTA) testing of multiple-input multiple-output (MIMO) capable terminals has been actively discussed in standardization recently [1]. Due to its capability to physically synthesize radio propagation environments in a shielded laboratory, the multi-probe anechoic chamber method has attracted great research attention. The radio propagation environment, which is a key factor for MIMO performance, is reproduced as it would be experienced by the device under test (DUT) in the field environment.

As the testing is performed in a shielded anechoic chamber, the reproduced field in the lab is controllable and repeatable. The major challenge with the multi-probe method is to create a realistic multipath environment. Several papers have addressed channel modeling in multi-probe setups, where the goal is to reproduce 2D channel models with accurate spatial characteristics at the receiver (Rx) side, see e.g. [2]. Reference [3] extended the channel emulation technique for 3D channel models with 3D multi-probe setups. However, the work in the literature is limited to model the Rayleigh fading channel models so far. The discussions on channel models in MIMO OTA standards are limited to Rayleigh fading channel models as well [1], e.g. the SCME channel models. However, as shown in numerous contributions in the literature, the Rayleigh fading channel model is not generally valid. Often a specular path exists between the transmitter (Tx) and the Rx. The time varying envelope of the received signal in the multipath environment is often modeled by a Rician distribution, characterized by the K factor [4]. Furthermore, Rician scenarios are expected to be more likely, as future cell sizes will further decrease. To test MIMO capable terminals in realistic environments in the lab, there is a strong need to model Rician channel models in the multi-probe setups.

Very few contributions have addressed modeling Rician fading channels in the multi-probe setups in the literature. An algorithm to model Rician fading models has been implemented in a commercial channel emulator, the Anite Propsim channel emulator. However, a description of the implemented algorithm is not available. In [2], it was briefly mentioned that the prefaded signal synthesis (PFS) technique can support emulating the Rician channel models with the line of sight (LOS) component limited to the directions where one of the probes is located. However, no details were given on how to model Rician fading channels and no results were given. In this paper, a novel technique is proposed to model the Rician fading channel models in the multi-probe setup, where the LOS path with an arbitrary incident direction is possible and a non-LOS (NLOS) component with arbitrary power angular spectrum (PAS) shape can be modeled. More specifically, the specular path is modeled using the so-called plane wave synthesis (PWS) technique, while the scattering NLOS component can be modeled with the PFS technique.

The main contributions of this paper lie in two aspects:

- A technique to create Rician channel models in the multi-probe anechoic chamber setups is proposed.
- A detailed analysis on the reproduced Rician channel models in the multi-probe setup is given, e.g. field envelope distribution, K factor estimation, spatial correlation, Doppler power spectrum, etc. Simulation results have shown that the reproduced Rician channels match very well with the target models.

II. Method

The Rician channel can be decomposed into a specular component for the LOS path and a scattering component for the NLOS path between the Tx and the Rx, where the Rician K-factor is defined as the power ratio of the two. In this section, the multi-probe anechoic chamber setup is first illustrated. After that the target channel models and the techniques to approximate the Rician channel models in the multi-probe setups are detailed.

A. Multi-probe setup and problem statement

An illustration of the multi-probe based anechoic chamber setup is shown in Figure 1. Probe antennas placed around

Wei Fan, Jesper Ø. Nielsen, and Gert F. Pedersen are with the Antennas, Propagation and Radio Networking section at the Department of Electronic Systems, Faculty of Engineering and Science, Aalborg University, Denmark (email: {wfa, jni, gfp}@es.aau.dk).

Pekka Kyösti and Lassi Hentilä are with Anite Telecoms Oy, Oulu, Finland (email: {pekka.kyosti,lassi.hentila}@anite.com).

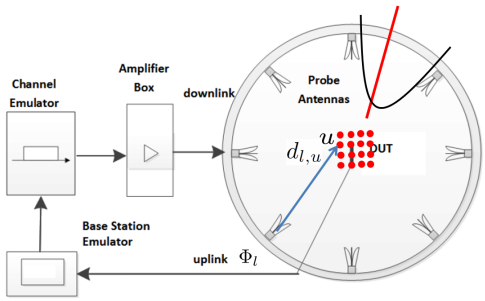

Figure 1. An illustration of the multi-probe based anechoic chamber setup. The red line illustrates the LOS specular component, while the black curve represents the NLOS scattering components. The red dots illustrate the potential locations for the Rx antenna.

the DUT are used as the transmitting antennas to create the multipath channels, with the help of channel emulators.

The LOS path can arrive at the receiver with arbitrary incoming direction. The NLOS scattering multipaths are often modelled by clusters, based on extensive measurements in various scenarios [5]. Typically a cluster consists of a number of rays and has a specifically shaped PAS. Several PAS models have been proposed, see e.g., the truncated Laplacian shape in [5]. It is desirable to enable emulation of Rician channels with an arbitrary impinging direction of the specular LOS components and an arbitrary PAS shape for the NLOS scattering component. An illustration of a target Rician channel model is shown in Figure 1.

The key of the channel emulation in the multi-probe setup is to ensure that the signals emitted from the probes are properly controlled such that the emulated channel seen by the DUT approximate the target channel model.

B. Target channel models

The channel models investigated in this study are geometry-based stochastic channel models (GSCMs), as they are adopted in the MIMO OTA standards [1]. The widely accepted MIMO channel models like SCME, WINNER, and IMT-Advanced models belong to this family [5]. For Tx array with an S elements and an Rx array with U elements, the channel coefficients for one of N multipath components are given by a $U \times S$ matrix of complex amplitudes. The wideband MIMO matrix $\mathbf{H}$ can be written as:

$$\mathbf{H}(t) = \sqrt{\frac{K}{1+K}}\mathbf{H}_{los}(t) + \sqrt{\frac{1}{1+K}}\mathbf{H}_{nlos}(t), \quad (1)$$

where $\mathbf{H}(t) = \{h_{u,s,n}(t)\} \in \mathbb{C}^{U\times S\times N}$. is the instantaneous channel matrix. A detailed description of the channel coefficients can be found in [5]. Note that when Rician K factor approaches infinity, the matrix corresponds to the case of a pure LOS matrix and when $K = 0$, it becomes pure Rayleigh fading matrix. The discussion in this work is limited to single polarized 2D channel models for the sake of simplicity. Note that arbitrarily polarized LOS path can be easily created by synthesizing the horizontally polarized and vertically polarized components independently, with their amplitudes and phases determined by the target arbitrarily polarized field.

1) LOS component: The LOS component can be represented by a time-variant plane wave, with arbitrary impinging direction. The time-evolution of the LOS path is determined by its Doppler frequency, as detailed in [5]. Basically, the parameters of the LOS component include the Tx and Rx antenna array, angle of departure (AoD) and angle of arrival (AoA) for the LOS component, Doppler frequency and delay.

2) NLOS component: The NLOS component consists of one or several clusters, and each cluster is composed by a number of rays. The channel coefficients for the NLOS component are given by the ray based models, as detailed in [5]. For each ray, the AoD/AoA, amplitude, random initial phase and Doppler frequency is defined. The PAS of the cluster is defined by the AoAs/AoDs and magnitudes of the rays within the cluster.

C. Emulated channel models

The emulation of the LOS and NLOS components is described separately below.

1) LOS component: For the LOS component, the goal is to approximate a time-evolving plane wave with an arbitrary impinging direction inside the test area.

As explained in [2], [6], we can approximate a static plane wave with an arbitrary incident direction to the test area, by selecting appropriate complex weights for the probes. Several techniques have been proposed in the literature to obtain the optimal complex weights, see e.g. the optimization methods in [2], [3], the interpolation technique in [6] and the spherical wave expansion technique in [7].

Assuming a uniform probe configuration, the following complex probe weights will create a static plane wave with angle θ [6],

$$g_i = \frac{1}{L}\sum_{l=1}^{L}\cos[\epsilon\cdot(\theta-\Phi_i)],\ i = 1, ..., L \quad (2)$$

where g_i is the weight corresponding to the ith probe with $\epsilon = l - \lceil \frac{L}{2} \rceil$, where $\lceil\rceil$ is the ceiling operator which rounds up the number inside the bracket to the next higher integer. L is the number of OTA probes and Φ_l is the fixed angle of the lth probe.

Introducing a Doppler shift, a time variant radio channel is obtained. The time evolving complex weights are as follows:

$$w_l(t) = g_l \cdot \exp(j2\pi\vartheta t),\ l = 1, ..., L \quad (3)$$

where ϑ is the Doppler frequency of the target LOS component. Then the emulated field at an arbitrary sample location u within the test area is (see Figure 1),

$$E(t,u) = \sum_{l=1}^{L} w_l(t)\cdot\alpha_{l,u} \quad (4)$$

where $\alpha_{l,u}$ is the transfer coefficient from the l-th OTA probe to the sample point u:

$$\alpha_{l,u} = L(d_{l,u})\cdot\exp(-j\frac{2\pi}{\lambda}d_{l,u}) \quad (5)$$

$L(.)$ is the pathloss term and $d_{l,u}$ is the distance from the l-th probe to the sample point u.

2) NLOS component: In the PFS technique, the goal is to approximate the NLOS component for any arbitrary PAS shape. The technique was proposed in [2], and is only outlined here.

Different clusters are modeled independently and each cluster is mapped to the probes, based on the cluster power angular spectrum (PAS) and the angular locations of the probes. The spatial correlation between channels obtained for different Rx locations is used as a figure of merit (FoM) to determine how accurately the spatial characteristics of the cluster at the Rx side (e.g. the impinging PAS shape of the cluster) are reproduced. The target spatial correlation is determined by the target PAS shape, while the emulated spatial correlation depends on the created discrete PAS shape, as omnidirectional DUT antenna patterns are generally assumed in multi-probe anechoic chamber study [3]. The discrete PAS shape is characterized by the discrete angular positions of the probes and the power weights. The optimal power weights for the probes can be obtained by minimizing the deviation between the target and emulated spatial correlation [2].

For the sake of simplicity, the channel coefficients associated with the n-th cluster and the s-th Tx antenna can be denoted as $\boldsymbol{h}(t)$, which is modeled by the ray based model [5]. Assume that the probe weights associated with the n-th cluster are denoted by $\boldsymbol{p} = [p_1, ..., p_L]^T$ and hence the weighted transmitted channel coefficients associated with the n-th cluster can be represented as $[\sqrt{p_1} \cdot \hat{\boldsymbol{h}}_1(t), ..., \sqrt{p_L} \cdot \hat{\boldsymbol{h}}_L(t)]^T$. Note that $\boldsymbol{h}(t)$ and $\hat{\boldsymbol{h}}_l(t)$ with $l \in [1, L]$ are independent and identically distributed complex sequences. The emulated channel coefficients on an arbitrary sample location u within the test area is,

$$\hat{\boldsymbol{h}}(t) = \sum_{l=1}^{L} \sqrt{p_l} \cdot \hat{\boldsymbol{h}}_l(t) \cdot \alpha_{l,u} \tag{6}$$

i.e., a summation of the contributions from each of the L probes. It is easy to check the emulated channel coefficients follow the target channel coefficients in terms of average power, temporal characteristics as well.

III. Simulation Results

A. Simulation scenarios

Key parameters of the simulation setup is detailed in Table I. The target channel consists of a single LOS component with AoA = 22.5^o (i.e. an angle exactly in the middle of two adjacent OTA probes in 8 uniform probe configuration) and a NLOS component, which is modeled by a single spatial cluster. Note that same delay is assumed for the LOS and NLOS component for the sake of simplicity, which is adopted in [5] as well.

B. Simulation results analysis

The objective of this section is to demonstrate how accurately the emulated Rician channel approach the target channel models in terms of field envelope distribution, K factor Doppler power spectrum and spatial correlation at the Rx side.

Table I
Simulation setups

	Details
Probe setup	Eight uniformly distributed antennas on an OTA ring, as shown in Figure 1.
Channel models	• Time samples $N_{ir} = 20000$ • Samples per wavelength: 4 • Center frequency: $f_c = 751$MHz • Direction of travel: 45^o • travel velocity: 30km/h • LOS direction: 22.5^o • K factor: [-100dB, -10dB, 0dB, 10dB, 100dB] • Channel model: The NLOS component is a single spatial cluster with AoA = 0^o and AS = 35^o

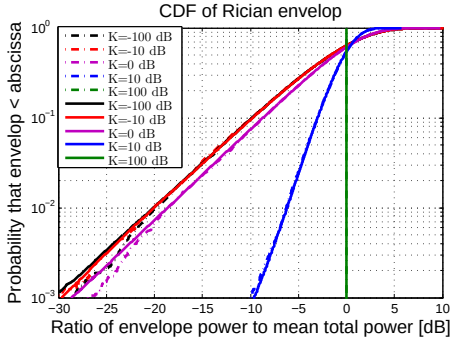

Figure 2. The Rice envelope cdf. The target curves are in solid lines and the emulated curves are in dot lines. Note that the curves for $K = -100$dB and $K = -10$dB lie on top of each other.

1) CDF of the field envelope: The cumulative density functions (CDFs) of the emulated Rician channels with different K factors are shown in Figure 2. The target CDFs are detailed in [8]. For a zero specular component ($K = -100dB$), the CDF distribution is Rayleigh. The CDF approaches Gaussian for a large specular component ($K = 10dB$). As explained in [8], the variance of the Gaussian distribution approaches 0 as the K factor approaches infinity, so the CDF plots approaches a delta function for $K = 100dB$. The CDF plots of the emulated channel generally follows the target very well. The deviations are mainly caused by the insufficient number of samples in the simulated channel.

2) K factor: Moment based estimation method of K factor is adopted [4]. The estimated K of the emulated channel matches very well with the target when K is larger than 0. The deviations when K is small are mainly due to the fact that the LOS component is difficult to detect accurately for small K, and estimation of the K factor is degraded [4], [9].

Table II
K factor estimation.

Target K [dB]	-100	-10	0	10	100
Estimated K [dB]	-6.12	-20.14	0.18	10.06	99.96

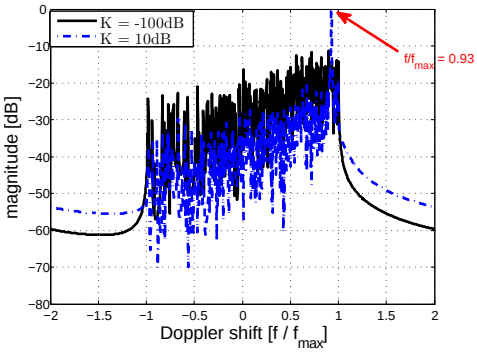

Figure 3. Doppler power spectra of the emulated channels with $K = -100dB$ and $K = 10dB$.

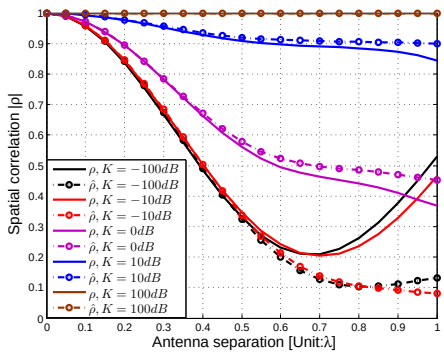

Figure 4. Spatial correlations of the target and emulated channels with different K values.

3) Doppler power spectrum: The Doppler power spectrum of the emulated channels with $K = -100dB$ and $K = 10dB$ are shown in Figure 3. The normalized Doppler frequency for the specular component is 0.93, which matches very well with the target normalized Doppler frequency $f_d^{los} = \cos(45^o - 22.5^o) = 0.92$. The Doppler spectra of the NLOS component for different K values have similar spiky shape, with different power levels.

4) Spatial correlation at the Rx side: Spatial correlation at the Rx side has been used as a measure to assess how accurately the emulated PAS, which is characterized by the probe weights and probe angular locations, match the target PAS. The estimated spatial correlation $\hat{\rho}_{ij}^{Rx}$ between the i-th and the j-th Rx antenna, both from the same 1^{st} Tx antenna is:

$$\hat{\rho}_{ij}^{Rx} = \frac{\sum_{t=1}^{N_{ir}} [h_{1,i,1}(t) \cdot h_{1,j,1}^{*}(t)]}{\sqrt{\sum_{t=1}^{N_{ir}} |h_{1,i,1}(t)|^2 \cdot \sum_{t=1}^{N_{ir}} |h_{1,i,1}(t)|^2}} \quad (7)$$

The target spatial correlation can be calculated, as detailed in [8]:

$$\rho_{ij} = \frac{\int_{-\pi}^{\pi} G_i(\phi) G_j^{\star}(\phi) p(\phi) d\phi}{\sqrt{\int_{-\pi}^{\pi} p(\phi) |G_i(\phi)|^2 d\phi} \sqrt{\int_{-\pi}^{\pi} p(\phi) |G_j(\phi)|^2 d\phi}}, \quad (8)$$

where G_i and G_j are the complex radiation patterns of antenna element i and j , respectively, with a common phase center. $p(\phi)$ is the PAS which satisfy $\int_{-\pi}^{\pi} p(\phi) d\phi = 1$ and it is the combination of the LOS ray and the NLOS PAS.

A uniform linear array (ULA) consists of 21 ideal dipoles with array broadsight 0 degrees are selected as the Rx antennas. The coupling between antenna elements are not considered in this study. The spatial correlations of the target and emulated channels with different K values are shown in Figure 4. The spatial correlation depends highly on the K factors, with correlation 1 among all the antenna elements for a pure LOS ($K = 100dB$). The emulated spatial correlation follows the target curve well up to 0.7λ and deviates after that. This is due to the fact that with eight probes, the created test area size, inside which the channel can be accurately modeled, is limited. Similar conclusions are drawn for Rayleigh fading channel models [2].

IV. Conclusion

A method to create Rician fading channel model with a LOS component with arbitrary polarization and direction is proposed. Both phase and amplitude calibration are required to model the LOS component. Simulation results show that the field envelope distribution, K factor, and Doppler spectrum of the emulated channels match well with the target. The emulated spatial correlation at the Rx side follows the target well up to 0.7λ and deviates after that due to the fact that the test area size, inside which the spatial characteristics of the channel are accurately modeled, is limited with eight probes.

Acknowledgment

The authors appreciate the contributions from colleagues in Anite Telecoms Oy.

References

[1] "Verification of radiated multi-antenna reception performance of User Equipment," 3GPP, TR 37.977 V1.0.0, Sep. 2013.

[2] P. Kyösti, T. Jämsä, and J. Nuutinen, "Channel modelling for multiprobe over-the-air MIMO testing," *International Journal of Antennas and Propagation*, 2012.

[3] W. Fan, F. Sun, P. Kyösti, J. Nielsen, X. Carreño, M. Knudsen, and G. Pedersen, "3D channel emulation in multi-probe setup," *Electronics Letters*, vol. 49, pp. 623–625(2), April 2013.

[4] C. Tepedelenlioglu, A. Abdi, and G. Giannakis, "The Ricean K factor: estimation and performance analysis," *Wireless Communications, IEEE Transactions on*, vol. 2, no. 4, pp. 799–810, July 2003.

[5] "Spatial channel model for Multiple Input Multiple Output (MIMO) simulations (Release 11)," 3GPP/3GPP2, TR 25.996 V11.0.0, Sep. 2012.

[6] W. Fan, J. Nielsen, O. Franek, X. Carreno, J. Ashta, M. Knudsen, and G. Pedersen, "Antenna Pattern Impact on MIMO OTA Testing," *Antennas and Propagation, IEEE Transactions on*, vol. 61, no. 11, pp. 5714–5723, Nov 2013.

[7] J. Toivanen, T. Laitinen, V. Kolmonen, and P. Vainikainen, "Reproduction of Arbitrary Multipath Environments in Laboratory Conditions," *Instrumentation and Measurement, IEEE Transactions on*, vol. 60, no. 1, pp. 275–281, 2011.

[8] R. Vaughan and J. B. Andersen, "Channels, propagation and antennas for mobile communications." Institution of Electrical Engineers, 2003.

[9] P.-Y. Chen and H.-J. Li, "An iterative algorithm for Doppler spread estimation in LOS environments," *Wireless Communications, IEEE Transactions on*, vol. 5, no. 6, pp. 1223–1228, June 2006.

Paper I

Channel Verification Results for the SCME models in a Multi-Probe Based MIMO OTA Setup

Wei Fan, Xavier Carreño, Jagjit S. Ashta, Jesper Ø. Nielsen, Gert F. Pedersen and Mikael B. Knudsen

The paper has been published in the
IEEE 78^{th} *Vehicular Technology Conference (VTC Fall)*, pp. 1–5, Sep. 2013.

The layout has been revised.

Channel Verification of SCME models in a Multi-Probe Based MIMO OTA Setup

Wei Fan[1], Xavier Carreño[2], Jagjit S. Ashta[2], Jesper Ø. Nielsen[1], Gert F. Pedersen[1] and Mikael B. Knudsen[2]
[1]APNet section, Dept. of Elec. Systems, Faculty of Engineering and Science, Aalborg University, Denmark
Email: {wfa, jni, gfp}@es.aau.dk
[2]Intel Mobile Communications, Aalborg, Denmark
Email: {xavier.carreno, jagjitx.singh.ashta, mikael.knudsen}@intel.com

***Abstract*—Multi-input multi-output (MIMO) over the air (OTA) testing methodologies are being intensively investigated by COST IC1004, CTIA and 3GPP, where various MIMO test methods have been proposed which vary widely in how they emulate the propagation channels. Inter-lab/inter-technique OTA performance comparison testing for MIMO devices is ongoing in CTIA, where the focus is on comparing results from various proposed methods. Channel model verification is necessary to ensure that the target channel models are correctly implemented inside the test area. This paper describes the OTA setup at Aalborg University and shows that all the key parameters of the SCME models, i.e., power delay profile, temporal correlation, spatial correlation and cross polarization ratio, can be accurately reproduced in a practical setup.**

I. Introduction

MIMO OTA testing, which is considered a promising solution to evaluate MIMO capable devices in realistic situations, has attracted huge interest from both industry and academia [1]. Standardization work for the development of the MIMO OTA test methods is ongoing in CTIA, 3GPP and IC1004 [5]. Several different MIMO test methods have been proposed which vary widely in how they emulate the propagation channel. Size and cost of the testing system are also quite different for various proposals [2], [3], [4].

The CTIA MIMO OTA Sub Group (MOSG) has been investigating aspects related to MIMO OTA performance evaluation and an inter-lab/inter-technique OTA performance comparison testing campaign has been started since 2012, where the focus is on comparing results of the same methods in different labs and results between different methods [5]. In order to ensure that different MIMO OTA techniques render comparable testing results, test prerequisites are defined in detail. That is, eNodeB configuration, MIMO channel models used for evaluation of MIMO devices, emulated base station (BS) setup, device under test (DUT) and DUT orientation are specified. One prerequisite is that target channel models should be correctly implemented inside the test area for all techniques. And hence channel verification measurements are necessary in the test campaign.

II. Measurement system

An illustration of the multi-probe anechoic chamber setup used for channel verification purpose is shown in Figure 1.

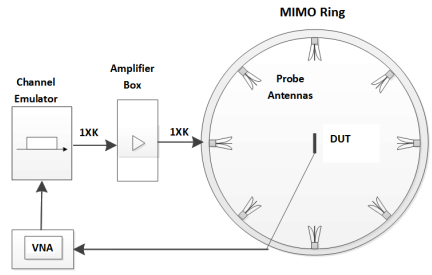

Figure 1. An illustration of the multi-probe based MIMO OTA setup. The main components are a vector network analyzer (VNA), one or several radio channel emulators, an anechoic chamber, OTA probe antennas, power amplifiers (PAs) and the DUT. The spectrum analyzer is used for power Doppler spectrum (PDS) measurements.

Figure 2 shows the practical multi-probe setup used for measurements. 16 dual polarized horn antennas are equally spaced and fixed on an aluminum OTA ring with radius 2 meters. Absorbers are used to cover the metallic ring and the unused probes to alleviate the reflections (as shown in Figure3(a)). Radio channels are generated by the radio channel emulator (as shown in Figure 3(b)) and radiated by the probes into the anechoic chamber. Two Elektrobit F8 channel emulators and 8 dual polarization OTA probes are used to generate the spatial channel model extended (SCME) models. Measurements were performed at 751MHz, which is at the center of LTE frequency band 13 downlink.

A Satimo sleeve dipole and ETS Lingren magnetic loop were used as measurement antennas for channel verification, as shown in Figure 4(a) and Figure 4(b) respectively. Measurement antenna positions were calibrated carefully with a laser positioner before the measurements.

III. SCME channel models

Most parameters in he SCME models are random variables defined by their probability density functions (PDFs). In order to ensure that channel models with the same parameters are implemented in the different labs, SCME tapped delay line (TDL) models are used as target channel models, where a set of values for the power, delays, and angular parameters of the paths are defined, as detailed in [6]. Four channel models, namely SCME Uma TDL, SCME Umi TDL, single cluster SCME Uma TDL and single cluster SCME Umi TDL are

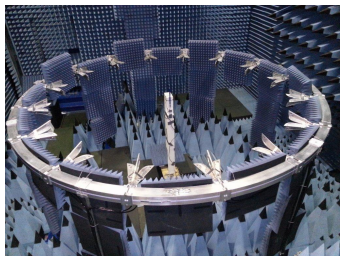

Figure 2. An illustration of the practical anechoic chamber setup in the measurement system.

(a) Absorbers mounted on the OTA ring

(b) Two channel emulator used in the measurement

Figure 3. Absorbers and channel emulator used in the setup.

used in the evaluation of the MIMO OTA performance [5]. Four key parameters of the channel models are required for validation as detailed below:

a) Power delay profile (PDP): All the considered SCME models consist of 6 paths, each associated with a delay and power. Figure 5 illustrates a snapshot of SCME Umi TDL model. The goal of PDP validation is to check whether this PDP in the implemented channels follow that in the target channels. Note that single cluster channel models share the same PDP information as generic models.

b) Doppler Power spectrum (DPS) and temporal correlation function (TCF): PDS and its Fourier transform pair TCF are used to check how channels evolve with time, as shown in Figure 5. The target PDS can be obtained by the power azimuth spectrum (PAS) of the SCME models and we can

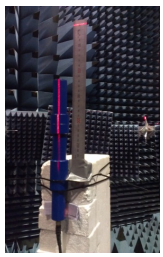

(a) Measurement Antenna for vertical polarization

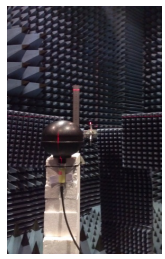

(b) Measurement Antenna for horizontal polarization

Figure 4. Measurement antennas used for channel verification measurements.

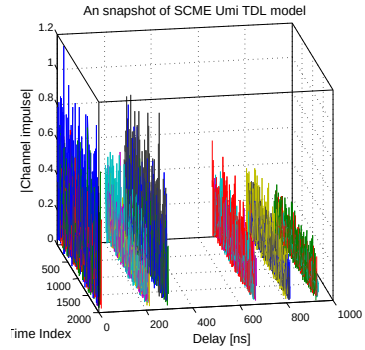

Figure 5. A snapshot of SCME Umi TDL model. The SCME models consist of 6 path (or 18 midpaths).

transform the PDS to a continuous TCF by Fourier transform [7]. Figure 6 shows the TCF functions for all considered SCME TDL models. "Standard" curves denote that the TCFs are calculated based on [8], where 20 subrays are used to discretize the truncated Laplacian shape clusters, while "ideal" curves represent TCFs for ideal PASs. Deviations are caused by insufficient number of subrays to discretize the PAS and truncation of the Laplacian shape. "Ideal" curves are used as target TCFs in this paper.

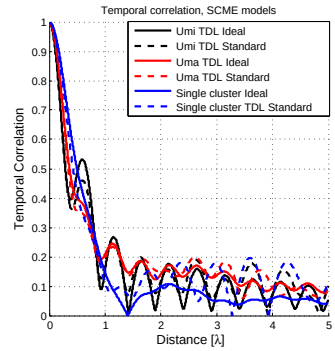

Figure 6. Target TCF for all SCME TDL models. Mobile speed and direction of travel are set according to [5].

c) Spatial correlation : The PAS of SCME models consist of 6 Laplacian shaped clusters, each associated with an angle of arrival (AoA) and azimuth spread (AS). Spatial correlation has been selected as the main figure of merit to characterize the channel spatial information [3]. The goal of the validation is to check whether the implemented channels can reproduce the spatial characteristics of the target SCME models. Target spatial correlation for all SCME TDL models are shown in Figure 7.

d) Cross polarization ratio: The emulated BS antennas are assumed to be dual polarized equal power elements that are uncorrelated and with 45^0 slant [5]. The path power will be modified by the BS antenna pattern according to angle

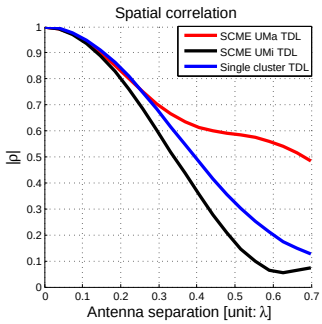

Figure 7. Target spatial correlation for all SCME TDL models. Antenna boresight = 0^o.

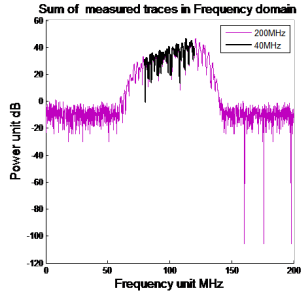

Figure 8. Sum of measured CIRs in frequency domain with VNA span 200MHz and 40MHz.

of departure (AoD) of each path for each polarization. The channel cross polarization ratio (XPR) is assumed to be 9 dB in all the considered channels. Expected XPRs can be calculated according to BS antenna pattern and XPR information in the channel, as listed in Table III for all the considered channels.

IV. Channel Verification Results

In this part, measurement results are compared with the target and simulated results. Target results are explained in Section III and specified in [5], while simulation results are based on CIR files in the channel emulator, which are generated by the SCME engine [9].

A. PDP

The PDP verification measurement was performed following the appendix of [5] with some exceptions as stated below:

- The span of the VNA was initially set to 200MHz to measure PDP according to [5]. Another round of PDP measurements was performed with the VNA span of 40MHz due to the fact that maximum supported bandwidth of the channel emulator is 40MHz. As shown in Figure 8, in the 200MHz measurements, the signal covers around 60MHz, while only the signal within the 40MHz is valid.
- Since the mid-path cannot be differentiated in the measurement with 40MHz bandwidth, the total power of each cluster, which is obtained by linearly summing the powers of the three mid-paths in each cluster is compared with the measurements.

1) Comparison between target and simulated PDP : Comparison results between target PDP and simulated PDP for vertical polarization is shown in Table I. Simulated PDP generally follows the target very well for all scenarios with a maximum deviation within 1dB. There is no difference in delay for all scenarios between target and simulations.

2) Comparison between measured and simulated PDP: One problem of measuring with a VNA span of 200MHz is that aliasing is present in the measurements for the specified number of samples. There are no aliasing issues with the measurement with VNA span of 40MHz. Measurements with 40MHz provide 5 times higher sampling rate than measurements with 200MHz.

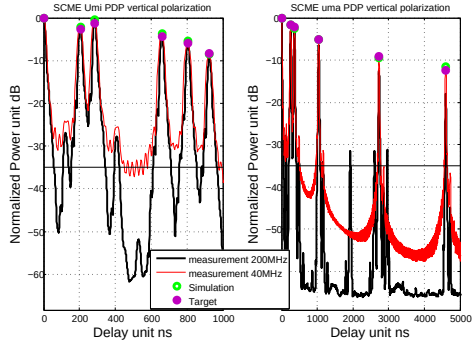

Figure 9. Target, simulated and measured PDPs for SCME Umi TDL and SCME Uma TDL models for vertical polarization.

Comparison between measured (with 40MHz bandwidth) and simulated PDP for all the scenarios for vertical polarization is shown in Table II. Both simulated and target PDP are delta functions in delay domain, while this is not the case in measured PDP. This is due to the bandwidth limitation of the VNA. Deviation between measurement and simulation in terms of delay is within 5ns, which is very accurate. Generally speaking, measurements with a VNA span of 40MHz match very well with simulation, with a deviation of up to 0.7dB for all scenarios, while measurements with VNA span of 200MHz generally present worse match compared with 40MHz measurements, deviation in some scenarios are up to 6.5dB, as shown in Figure 9 (6th path of the SCME Uma TDL model). Measurements with 200MHz bandwidth should not be trusted due to the aliasing issue.

B. PDS and temporal correlation

1) PDS: Raw PDS measurement results with a spectrum analyzer for all the considered scenarios are shown in Figure 10. The measured maximum Doppler frequency f_d matches quite well with the expected f_d in the target channels.

Table I
COMPARISON BETWEEN TARGET (T) AND SIMULATED (S) PDP FOR ALL CHANNELS FOR VERTICAL POLARIZATION. Δ DENOTES THE DEVIATIONS.

Model	Path	Power dB			Model	Power dB			Model	Power dB			Model	Power dB		
		T	S	Δ		T	S	Δ		T	S	Δ		T	S	Δ
Umi	1	0	0	0	Uma	0	0	0	Umi single cluster	0	0	0	Uma single cluster	0	0	0
	2	-2.7	-2.2	0.5		-1.7	-1.6	0.1		-2.7	-2.9	-0.2		-1.7	-1.7	0
	3	-1.3	-0.4	0.9		-2.2	-2.5	-0.3		-1.3	-1.3	0.0		-2.2	-2.2	0
	4	-4.3	-3.7	0.6		-5.2	-5.2	0.1		-4.3	-4.4	-0.1		-5.2	-5.2	0
	5	-6.0	-5.4	0.6		-9.1	-9.5	-0.4		-6.0	-5.9	0.1		-9.1	-9.1	0
	6	-8.4	-8.4	-0.1		-12.5	-11.5	1.0		-8.4	-8.5	-0.1		-12.5	-12.5	0

Table II
COMPARISON BETWEEN MEASURED (M) AND SIMULATED (S) PDP FOR ALL CHANNELS FOR VERTICAL POLARIZATION. Δ DENOTES THE DEVIATIONS.

Model	Path	Power dB			Model	Power dB			Model	Power dB			Model	Power dB		
		S	M	Δ		S	M	Δ		S	M	Δ		S	M	Δ
Umi	1	0	0	0	Uma	0	0	0	Umi single cluster	0	0	0	Uma single cluster	0	0	0
	2	-2.2	-2.2	0		-1.6	-2.2	-0.6		-2.9	-3.2	-0.3		-1.7	-1.8	-0.1
	3	-0.4	-0.7	-0.3		-2.5	-2.7	-0.2		-1.3	-1.2	0.1		-2.2	-1.7	0.4
	4	-3.7	-3.8	-0.1		-5.2	-5.9	-0.7		-4.4	-4.7	-0.3		-5.2	-5.4	-0.2
	5	-5.4	-5.5	0.1		-9.5	-10.1	-0.6		-5.9	-6.2	-0.3		-9.1	-9.0	0.1
	6	-8.4	-8.4	0		-11.5	-11.6	-0.1		-8.5	-8.8	-0.3		-12.5	-12.5	0

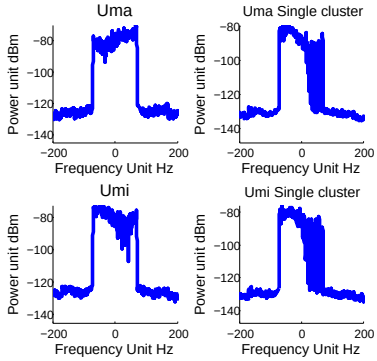

Figure 10. Power Doppler Spectrum for the considered scenarios

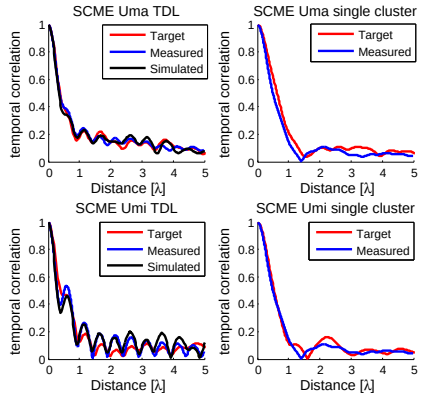

Figure 11. Target, simulated and measured temporal correlations for the considered scenarios.

2) Temporal correlation: It is difficult to directly compare PDS due to fact that channels are created by ray based model in the channel emulator. The measured TCF matches pretty well with the simulated and target TCF, as shown in Figure 11. The deviations are likely caused by the reflections in the chamber.

C. Spatial correlation

The positioner is oriented perpendicular to the AoA= 0^o orientation as specified in [5]. The measurement procedure is different from [5] to decrease measurement time. The dipole is moved to 0.5λ backwards from the center. In this position, the channel emulator is stopped at each CIR position and the field is measured with a VNA for a total of 1000 CIR positions. The dipole is then moved 0.1λ forward, and the sweep over 1000 CIR values is repeated for this new position. This procedure is repeated 11 times until a full wavelength around the center is covered.

We calculated the correlation between the traces measured at first position and at the rest of the positions. Good agreement can be observed between the measured and simulated spatial correlation curves for all scenarios, as shown in Figure 12. In a summarized way, these are the main aspects that we concluded with these results:

- The deviation between the simulated and target spatial correlation is due to the limited number of probes (8 in our measurements) used for channel emulation. The more probes we use, the smaller deviation we should expect. The deviation between simulated and target spatial correlation for different scenarios is different due to the fact that channel emulation accuracy depends on the channel model.
- The deviation between measured and simulated spatial correlation is likely due to the physical limitation of our MIMO OTA multi-probe test setup. In our setup,

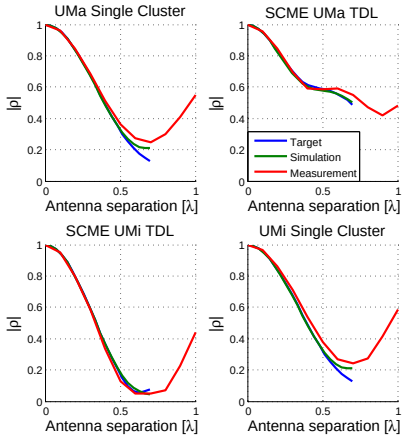

Figure 12. Measured, simulated, and theoretical spatial correlations of the considered scenarios. 0 represents angle of the virtual antenna array bore-sight direction.

the OTA ring of radius 2m is used, while the radius of the test zone is 0.2m. The deviation between the spatial correlation in ideal conditions and the spatial correlation in physically constrained conditions is not negligible in this measurement, as explained in [10].

D. Cross polarization ratio

The measurement procedure for cross polarization ratio is detailed in [5]. In the measurement, the measurement antenna was located at the center of the ring by using a laser positioner. After calibration, equal field response (both power and phase) can be obtained for all the horn antennas. During the measurement, we rotated the receive antenna 360^o for an active horn. The average received power with the magnetic loop and dipole are -29.8dB and -22.5dB, respectively. That is, the antenna gain difference is 7.3dB, which matches well with the value calculated from the antenna specifications.

The measured results for all the target scenarios are illustrated in Table III. As we can see, the measured results after considering the antenna gain difference is around 1dB higher than the target values in all scenarios. The deviations are likely introduced by independent calibrations. Each channel emulator is calibrated with a different antenna, and therefore we have different calibration values. Each calibration value corresponds to the "measurement" antenna being used. The calibration procedure is that it takes the lowest of the outputs, and lowers the rest of the outputs according to this one. If there is 1dB difference in the lowest of the outputs for the horizontal and vertical polarization, we will have 1dB difference.

V. Conclusion

This paper describes the multi-probe anechoic chamber setup used to perform the Inter-lab/inter-technique measurements and presents the channel verification results. Good match between measurements and target has been achieved

Table III
Results for cross polarization measurements for the considered scenarios

	SCME Umi TDL	SCME Umi Single cluster	SCME Uma TDL	SCME Uma Single Cluster
Target	0.83dB	0.83dB	8.13 dB	8.13dB
Simulation	0.76dB	0.68dB	8.12 dB	8.18dB
Raw Measurement	9.73dB	9.0 dB	16.6 dB	16.7dB
Measurement	2.0dB	1.4dB	9.0 dB	9.0dB
Deviation	1.2dB	0.6dB	0.9dB	0.9dB

in terms of PDP, temporal correlation, spatial correlation and cross polarization ratio of the channel. Deviation between measured and simulated PDP in terms of delay is within 5ns, while power deviation of up to 0.7dB is found for all scenarios. The measured TCF matches well with the simulation. The deviations are likely caused by the reflections in the chamber. A good agreement can be observed between the measured spatial correlation curves and theoretical curves for all scenarios. Deviations are mainly due to the physical limitations of the MIMO OTA system. The measured cross polarization ratio is around 1dB higher than the target values in all scenarios. The deviations are likely introduced by separate calibrations for the two polarizations.

References

[1] David A. Sanchez-Hernandez, Moray Rumney, Ryan J. Pirkl, and Markus Herrmann Landmann. MIMO Over-The-Air Research, Development, and Testing. Hindawi Journal of Antenna and Propagation. 9 May 2012.

[2] Ya Jing, Xu Zhao, Hongwei Kong, Steve Duy, and Moray Rumney, Two-Stage Overthe- Air (OTA) Test Method for LTE MIMO Device Performance Evaluation, International Journal of Antennas and Propagation, vol. 2012, Article ID 572419, 6 pages, 2012. doi:10.1155/2012/572419.

[3] Pekka Kyösti, Tommi Jämsä, and Jukka-Pekka Nuutinen, Channel Modelling for Multiprobe Over-the-Air MIMO Testing, International Journal of Antennas and Propagation, vol. 2012, Article ID 615954, 11 pages, 2012. doi:10.1155/2012/615954.

[4] Nabil Arsalane, Moctar Mouhamadou, Cyril Decroze, David Carsenat, Miguel Angel Garcia- Fernandez, and Thierry Monedière, 3GPP Channel Model Emulation with Analysis of MIMOLTE Performances in Reverberation Chamber, International Journal of Antennas and Propagation, vol. 2012, Article ID 239420, 8 pages, 2012. doi:10.1155/2012/239420.

[5] 3GPP TR 37.977 V0.2.0 (2012-05), 3rd Generation Partnership Project; Technical Specification Group Radio Access Networks; Verification of radiated multi-antenna reception performance of User Equipment (Release 11))

[6] D. S. Baum, et al, "An interim channel model for beyond-3G systems: extending the 3GPP spatial channel model (SCM)," in Proceedings of the 61st IEEE Vehicular Technology Conference (VTC '05), vol. 5, pp. 3132– 3136, Stockholm, Sweden, May-June 2005.

[7] R. Vaughan and J. B. Andersen, Channels, Propagation and Antennas forMobile Communications, IET, London, UK, 2003.

[8] "Spatial channel model for multiple input multiple output (MIMO) simulations", 3GPP TR 25.996 V6.1.0, Sep. 2003. [Online]. Available: http://www.3gpp.org/ftp/Specs/html-info/25996.htm

[9] L. Hentilä, P. Kyösti, M. Käske, M. Narandzic , and M. Alatossava. (2007, December.) MATLAB implementation of the WINNER Phase II Channel Model ver1.1 [Online]. Available: https://www.ist-winner.org/phase_2_model.html.

[10] P. Kyösti and L. Hentilä, "Criteria for physical dimensions of MIMO OTA multi-probe test setup," in Proceedings of the 6th European Conference on Antennas and Propagation (EuCAP '12), Prague, Czech Republic, March 2012.

Paper J

Measurement Uncertainty Investigation in the Multi-probe OTA Setups

Wei Fan, Istvan Szini, Michael D. Foegelle, Jesper Ø. Nielsen, Gert F. Pedersen

The paper has been published in the
8^{th} *European Conference on Antennas and Propagation (EuCAP)*, pp. 1–5, April, 2014.

The layout has been revised.

Measurement Uncertainty Investigation in the Multi-probe OTA Setups

Wei Fan[1], Istvan Szini[1,2], Michael D. Foegelle[3], Jesper Ø. Nielsen[1], and Gert F. Pedersen[1]
[1]Department of Electronic Systems, Faculty of Engineering and Science, Aalborg University, Aalborg, Denmark
[wfa, ijs, jni, gfp]@es.aau.dk
[2]Motorola Mobility Inc., Libertyville, USA
[3]ETS-Lindgren, 1301 Arrow Point Drive, Cedar Park, USA

***Abstract*—Extensive efforts are underway to standardize over the air (OTA) testing of the multiple input multiple output (MIMO) capable terminals in COST IC1004, 3GPP RAN4 and CTIA. Due to the ability to reproduce realistic radio propagation environments inside the anechoic chamber and evaluate end user metrics in real world scenarios, the multi-probe based method has attracted huge interest from both industry and academia. This contribution attempts to identify some of the measurement uncertainties of the practical multi-probe setups and provide some guidance to establish the multi-probe anechoic chamber setup. This contribution presents the results of uncertainty measurements carried out in three practical multi-probe setups. Some sources of measurement errors, i.e. cable effect, cable termination, etc. are identified based on the measurement results.**

***Index Terms*—MIMO OTA, multi-probe, anechoic chamber, measurement uncertainty, plane wave synthesis**

I. Introduction

The Multiple Input Multiple Output (MIMO) technique is a promising technology to improve wireless communication systems. Over the air (OTA) testing of MIMO capable terminals has attracted huge attention from both industry and academia [1], where a multi-probe anechoic chamber based method is a promising candidate. Various contributions have addressed issues related to OTA testing of MIMO capable terminals in a multi-probe anechoic chamber, i.e. channel modeling [2]–[4], validation of the implemented channel models [5], [6], end user metrics evaluation [7].

As a mandatory step for standardization, it is required to analyze the sources of errors and uncertainties in the measurements. Very few contributions have addressed the measurement uncertainties in a multi-probe OTA system. In [8], uncertainty analysis in total radiated power (TRP) and total isotropic sensitivity (TRS) is specified. However, the measurement uncertainty analysis defined for OTA testing of single antenna terminals will be not sufficient for the MIMO OTA testing, as the testing system, which includes one or several channel emulators, is more complicated. Furthermore, different figure of merits (FoMs) will be adopted for MIMO OTA testing. In [9], several sources of uncertainties and errors were listed and classified for the multi-probe setup. In recent 3GPP RAN4 meetings, measurement uncertainty evaluation of the multi-probe method has been discussed [10]. In [6], plane wave synthesis (PWS) in a practical setup was investigated and possible reasons for the deviations were briefed. In [11], measurement verification results of two channel emulation techniques, namely PWS and prefaded signal synthesis (PFS) in a practical multi-probe anechoic chamber setup were presented. Possible factors that introduce the measurements inaccuracies were discussed as well. Some deviations existed in the results and the exact causes were missing.

This paper attempts to compare and understand measurement uncertainty levels with different labs, i.e. at Aalborg university (AAU), Denmark, Motorola Mobility (MM), USA and ETS-Lindgren (ETS), USA., thus to show key aspects related to the multi-probe system setup design. Main contributions of this work are:

- Uncertainty measurements in three different practical multi-probe setups are presented. The sources of the errors that exist in the previous contributions are identified.
- Measurement results of the field synthesis for horizontal polarization are reported for the first time in the literature.

II. Multi-probe anechoic chamber setups and testing items

Figure 1 shows a simplified version of the multi-probe setup for testing a device under test (DUT). The DUT is placed on a pedestal in an anechoic chamber and surrounded by multiple probes mounted on an OTA ring. The probes are uniformly distributed located on a horizontally orientated ring with equal spacing in all the setups. The specifications of the three setups are detailed in Table I.

The main testing items of the measurement uncertainty investigations are detailed below:

a) Dipole radiation pattern measurements: The basic idea is to measure the radiation pattern of a calibration dipole which is located at the test area center. Ideally, the measured complex pattern should be constant over orientations. However, due to the system no-idealities, e.g. cable effect, dipole placement, etc. maximum gain and phase variations are up to 2dB and 10 degrees at 900MHz, and up to 1dB and 20 degrees at 2450MHz [11].

b) Turntable stability: The turntable that supports the DUT is not completely static shortly after the turntable rotating and linear sliding. As reported in the turntable stability measurement in the AAU setup in [11], the rotational movement is stable, while the linear slide movement is not stable and 20s of settling time is required. In the MM setup, the linear slide

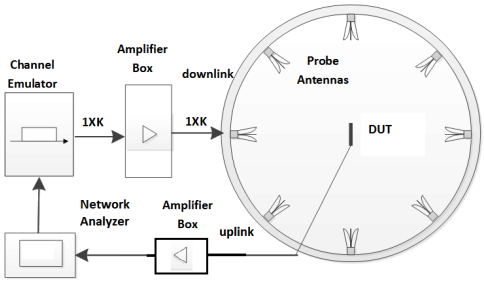

Figure 1. An illustration of the multi-probe based MIMO OTA setup. The main components are a vector network analyzer (VNA) or base station emulator (BSE), one or several radio channel emulators, an anechoic chamber, OTA probe antennas, power amplifiers (PAs) and a DUT.

Table I
SETUP SPECIFICATIONS

	AAU	MM	ETS
Chamber size	10m x 10m x 7m	3m x 3m x 2.4m	4.9m x 4.9m x 3.7m
OTA ring size	An aluminum ring with radius $R = 2$ meters. The ring is partially covered by absorbers, as shown in Fig. 2(a)	Radius $R = 1.2$ meters. Wood masts have been used to support and fix the horn antennas, as shown in Fig. 2(b)	A ring with radius $R = 2$ meters. The ring is fully covered by absorbers. The probes are loaded with absorbers, as shown in Fig. 2(c)
OTA probe	16 dual polarized horn antenna designed by AAU [12], as shown in Fig. 3(a)	8 dual polarized horn antenna designed by AAU, as shown in Fig. 2(b)	16 dual polarized Vivaldi antenna designed by ETS, as shown in Fig. 3(b)
Turntable	Polystyrene placed on top of the turntable to support the DUT, as shown in Fig. 4(a)	As shown in Fig. 4(b)	As shown in Fig. 4(c)
Channel emulator used	Two Anite Propsim F8s	Anite Propsim F16	Anite Propsim FS8 and Spirent VR5
Turntable movement	Rotational and linear slide combined movement supported	Rotational movement supported only	Rotational and linear slide combined movement supported
Cable to DUT	Cable directly connected to DUT	Choke and cartridge at various frequency bands used	Ferrite loaded cable used, as shown in Fig. 4(c)

movement is not supported. In the ETS setup, both movements are supported. The turntable movement in the MM and ETS setups are stable.

c) Channel emulator stability: Signal drifting level of the channel emulator over short term and long term is investigated. Measurements showed that the signal drifting level of different channel emulators over long term and short term is negligible, and the results are not detailed in the paper.

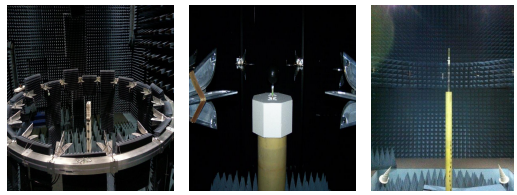

(a) OTA ring at AAU (b) Chamber at MM (c) Chamber at ETS

Figure 2. Anechoic chamber in three setups

(a) Horn antenna (b) Vivaldi antenna

Figure 3. Probe antennas used in AAU/MM (left) and ETS (right).

d) System frequency flatness: Frequency flatness level is investigated in the three setups. Unflat frequency response of the OTA system can be introduced by the channel emulator, termination of the cables (probe antenna) and mismatch between the components.

e) Power Coupling between probes: Power coupling level between probes for both polarizations is investigated in the three setups. Power coupling levels between probes and between polarizations are investigated.

f) Reflection inside the chamber: The reflection level in the three setups is investigated.

g) Plane wave synthesis : Verification results of the PWS technique for vertical polarization with the AAU setup were reported in [6], [11]. In this contribution, better results are achieved with MM and ETS setups as the cable effect and turntable stability issues were addressed. Also, measurement results of the PWS for horizontal polarization are presented.

III. MEASUREMENT RESULTS AND DISCUSSION

A. Dipole radiation pattern measurements

In [11], it is concluded that the inaccurate results of radiation pattern measurements are probably caused by cable

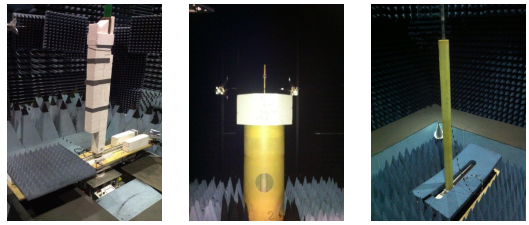

(a) Turntable at AAU (b) Turntable at MM (c) Turntable at ETS

Figure 4. Turntable in different setups

effect or dipole placement error. The position of the calibration dipoles are carefully calibrated with the laser positioner in the three setups. In the MM setup, the cartridges and chokes for various frequency bands are used to connect to the DUT. In the ETS setup, a Ferrite loaded cable is used. Measurement results in the MM and ETS setup are shown in Figure 5 and Figure 6, respectively. Note that the gain patterns are not normalized. Measurements performed in the MM setup were without the channel emulator. The measured gain and phase pattern variation of a calibration dipole are negligible. The gain and phase pattern is quite omnidirectional, as expected. The main reason for the small variation is due to the fact that the dipole is not located in the rotation center (with an offset of around 5mm), as the phase variation follows a sinusoid curve. Measurement result in the ETS setup is shown in Figure 6. The dipole is rotated every 1^o and for every orientation 31 points separated with 1cm are sampled over the test area. The complex radiation pattern results are extracted from the measurements (samples with $r = 0$cm). The gain and phase variation, though rather small, is mainly caused by the position accuracy of the dipole. To sum up, cable effect can be minimized by use of choke and cartridge, or Ferrite loaded cable.

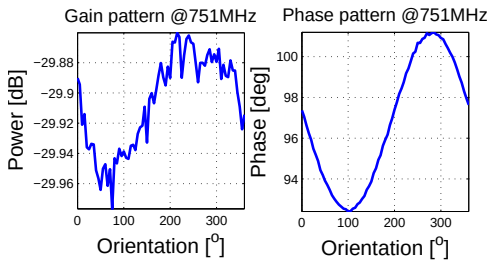

Figure 5. Gain pattern (left) and phase pattern (right) measurement results in MM setup.

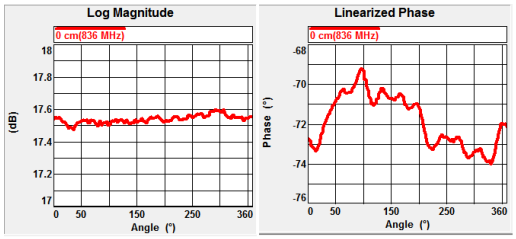

Figure 6. Gain pattern (left) and phase pattern (right) measurement results in ETS setup.

B. Ripples over frequency

In the previous measurements in the AAU setup [13], we investigated the impact of power variation over frequency on spatial correlation. Due to the nonidealities of the channel emulators, the power values are not constant over the LTE band. Also, the cable reflection can cause ripples over frequency band. To show the impact of cable reflection, a measurement was planned in the MM setup. In the first measurement, we measured the S21 of the OTA system (without the channel emulator) with one probe active and the rest terminated with 50Ω loads. In the second measurement, we performed the same measurement with the active probe and the rest non-terminated. The result is shown in Figure 7, where failure to terminate is seen to cause large ripples. The small ripples over frequency with cable terminated might be due to the cable frequency response or the mismatch between components. To investigate the mismatch between components, an additional PA of 20dB and an attenuator of 20dB were added into the system in the measurement in the ETS setup. The ripples caused by mismatch between components are up to around 0.5dB from 600MHz to 7 GHz in the ETS setup.

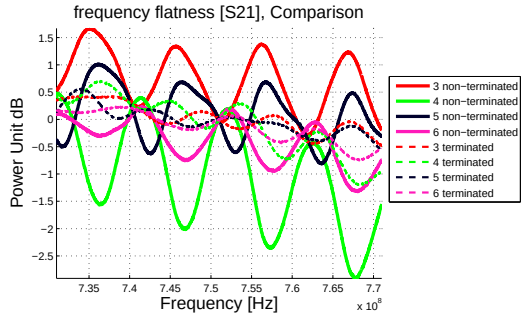

Figure 7. Frequency flatness over 40MHz measured in the MM setup. The number in the legend indicates the active horn index.

C. Power Coupling between probes

Scattering within a multi-probe setup and its impact on measurement uncertainty is investigated in [14]. It is demonstrated that the power coupling level needs to be controlled. In the previous power coupling measurements reported in [6], the cable frequency response and the PA frequency response are not compensated. Different probe antennas are investigated for the OTA systems, e.g. the horn antenna in the AAU and the MM setup, the dual-polarized Vivaldi antenna implemented in a cross form in the ETS setup. The power coupling results in the ETS setup (with cable and PA compensated) are shown in Figure 8 for the vertical polarization. The OTA probe located on the boresight direction of transmitting probe presents the maximum coupling at high frequency. The higher the frequency is, the more directive the Vivaldi antenna becomes. The power coupling will have negligible impact on the synthesized field structure.

D. Reflection inside the chamber

Measurement procedure of the reflection study was detailed in [6]. A wideband horn antenna is located in the middle of the test zone and measurements are performed in frequency domain. The frequency domain data is transformed by an

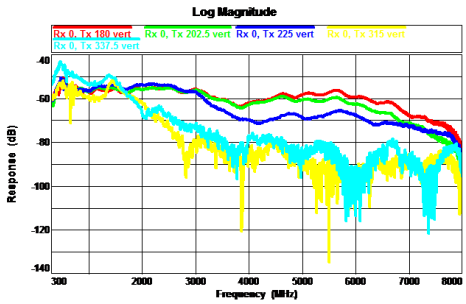

Figure 8. Power coupling between probes for the vertical polarization in the ETS setup. The value in the legend indicates the angular location of the probes.

inverse FFT to yield a time domain signals. Same reflection measurements were repeated in the MM and ETS setup, and no big reflections were identified in the results. To investigate the impact of a intentional reflector on the results. A metallic plate was placed in the chamber in the ETS setup. The result with an intentional reflector is shown in Figure 9. The reflection level is low as the reflector was not placed in the main lobe direction of the receive horn antenna.

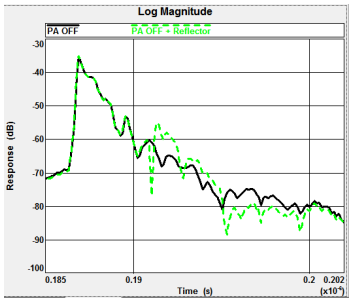

Figure 9. Reflections with/without intentional reflector inside the chamber. Rx antenna: horn

E. Plane wave synthesis

1) Target scenarios and measurement setup: In the previous PWS measurements in the AAU setup, although good agreement was achieved between the measurement and target plane wave (PW), the inaccuracy due to the cable effects, as discussed in Section III-A, was embedded in the results. In the MM setup, as linear slide movement was not supported, the DUT was offset manually with specified radius, as detailed in Table II. Vertically and horizontally polarized static PW with different angle of arrivals (AoAs) are selected as the target scenarios.

2) Results: An example of the measurements in the MM setup is shown in Figure 10. The measured power is normalized to its mean and the simulated phase curve is shifted to match the measured phase. The deviation between the target and emulation is due to the fact that only limited probes are

Table II
PWS MEASUREMENT DETAILS

	MM	ETS
Target scenario	A. Vertically polarized PW with AoA = 0^o	
	B. Vertically polarized PW with AoA = 22.5^o	
	C. Horizontally polarized PW with AoA = 0^o	
	D. Horizontally polarized PW with AoA = 22.5^o	
Rx antenna	Calibration dipole/magnetic loop at 751MHz	Calibration dipole/magnetic loop at 836MHz
Active OTA probes	8 OTA probes are equally spaced and fixed on the OTA ring	
Rx positions	the linear slide is rotated every 5^o with specified offsets to the rotation center ((0cm, 0.25λ, 0.35λ, 0.5λ)	the linear slide is rotated every 1^o and 31 points separated with 1cm are sampled for every orientation.

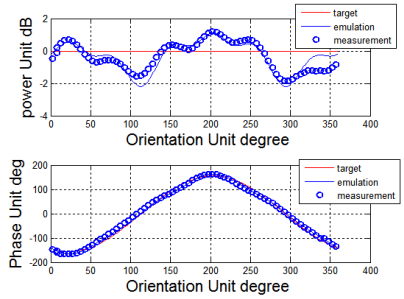

Figure 10. Comparison between the measurement, emulation and target for the power (up) and phase (down) in the MM setup for scenario B.

used. Very good match is achieved between the measurement and emulation.

Results of the PWS measurements performed in the ETS setup are shown from Figure 11 to Figure 14. Overviews of the measured power and phase distribution over the test area for the target scenario A, B, C and D are shown in Figure 11, Figure 12, Figure 13, Figure 14 respectively. Ideally, uniform power and linear phase distribution along propagation direction are expected inside the test area. The measurement generally match with the target very well. The test area performance depends on the target channel models. As a summary, good agreement can be obtained between the measured PW and the target PW both for the vertical and horizontal polarizations.

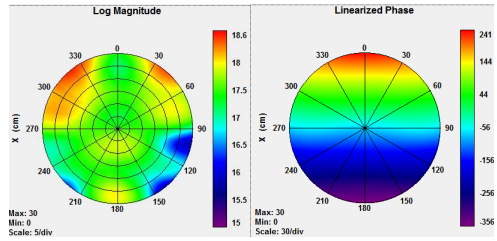

Figure 11. Measured power (left) and phase (right) distribution over test area for the target scenario A.

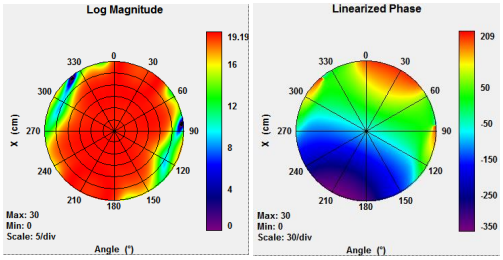

Figure 12. Measured power (left) and phase (right) distribution over test area for the target scenario B.

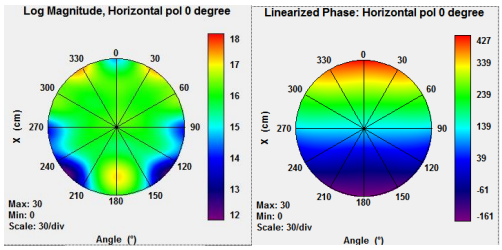

Figure 13. Measured power (left) and phase (right) distribution over test area for the target scenario C.

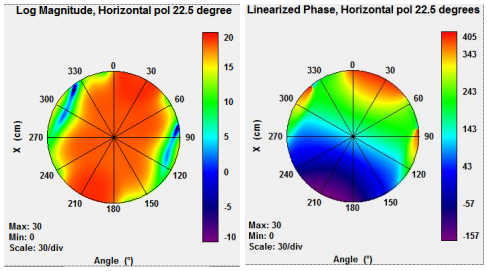

Figure 14. Measured power (left) and phase (right) distribution over test area for the target scenario D.

IV. Conclusion

In this contribution, we presented the uncertainty measurements performed in three different multi-probe setups. Main findings of the work are:

- Cable effect will distort the radiation pattern of the DUT and hence affect the results of the measurements. By use of a choke/cartridge or Ferrite loaded cable, the cable effect can be minimized. Field synthesis measurements demonstrated the improved results with chokes/cartridges and Ferrite loaded cables.
- Polystyrene that used to support the DUT in the AAU setup introduces instability after movement. Turntables used in the MM and ETS setup are more stable.
- Unflat frequency response of the OTA system can be introduced by the channel emulator, termination of the cables (probe antenna) and mismatch between the components.
- Good agreement between the measured plane wave and the target plane wave both for the vertical and horizontal polarizations is obtained in the MM and ETS setup.

Acknowledgment

This work is supported by the COST IC1004 STSM grant.

References

[1] M. Rumney, R. Pirkl, M. H. Landmann, and D. A. Sanchez-Hernandez, "MIMO Over-The-Air Research, Development, and Testing," *International Journal of Antennas and Propagation*, vol. 2012, 2012.

[2] P. Kyösti, T. Jämsä, and J. Nuutinen, "Channel modelling for multiprobe over-the-air MIMO testing," *International Journal of Antennas and Propagation*, 2012.

[3] W. Fan, F. Sun, P. Kyosti, J. Nielsen, X. Carreno, M. Knudsen, and G. Pedersen, "3D channel emulation in multi-probe setup," *Electronics Letters*, vol. 49, no. 9, pp. 623–625, 2013.

[4] W. Fan, X. de Lisbona, F. Sun, J. Nielsen, M. Knudsen, and G. Pedersen, "Emulating Spatial Characteristics of MIMO Channels for OTA Testing," *Antennas and Propagation, IEEE Transactions on*, vol. 61, no. 8, pp. 4306–4314, 2013.

[5] W. Fan, X. Carreño, J. Ø. Nielsen, M. B. Knudsen, and G. F. Pedersen, "Channel Verification Results for the SCME models in a Multi-Probe Based MIMO OTA Setup," in *Vehicular Technology Conference (VTC Fall), 2013 IEEE*. IEEE, 2013, pp. 1–5.

[6] W. Fan, X. Carreño, J. Ø. Nielsen, K. Olesen, M. B. Knudsen, and G. F. Pedersen, "Measurement Verification of Plane Wave Synthesis Technique Based on Multi-probe MIMO-OTA Setup," in *Vehicular Technology Conference (VTC Fall), 2012 IEEE*. IEEE, 2012, pp. 1–5.

[7] X. Carreno, W. Fan, J. O. Nielsen, J. S. Ashta, G. F. Pedersen, and M. B. Knudsen, "Test setup for anechoic room based MIMO OTA testing of LTE terminals," in *Antennas and Propagation (EuCAP), 2013 7th European Conference on*, 2013, pp. 1417–1420.

[8] CTIA, "Test plan for mobile station over the air performance," *CTIA Wireless Association*, 2012.

[9] R4-126702, "Errors and Uncertainties in the MIMO OTA measurements," 2012.

[10] R4-131673, "Measurement uncertainty evaluation of multiprobe method," 2013.

[11] W. Fan, , X. Carreño, J. O. Nielsen, M. B. Knudsen, and G. F. Pedersen, "Verification of Emulated Channels in Multi-Probe Based MIMO OTA Testing Setup," in *Antennas and Propagation (EUCAP), Proceedings of the 7th European Conference on*. IEEE, 2013.

[12] O. Franek and G. F. Pedersen, "Spherical horn array for wideband propagation measurements," *Antennas and Propagation, IEEE Transactions on*, vol. 59, no. 7, pp. 2654–2660, 2011.

[13] W. Fan, J. Nielsen, X. Carreno, J. Ashta, G. Pedersen, and M. Knudsen, "Impact of system non-idealities on spatial correlation emulation in a multi-probe based mimo ota setup," in *Antennas and Propagation (EuCAP), 2013 7th European Conference on*, 2013, pp. 1663–1667.

[14] P. Hallbjorner, "Measurement uncertainty in multipath simulators due to scattering within the antenna array - theoretical model based on mutual coupling," *Antennas and Wireless Propagation Letters, IEEE*, vol. 9, pp. 1103–1106, 2010.